Evaluating the Effect of Aging and Moisture Conditions on the Performance of Bituminous Mixtures

A thesis submitted in Partial Fulfilment of the
Requirements for the Degree of

DOCTOR OF PHILOSOPHY
in Civil Engineering
by

Bhaskar Pratim Das
(Roll no. 156104023)

Department of Civil Engineering

Indian Institute of Technology Guwahati

Guwahati – 781039, India

June 2021

Dedication

Dedicated to my family to whom I shall be ever grateful.

The pursuance of post-graduate studies was possible due to your continuous encouragement and support.

Certificate

This is to certify that the thesis titled "***Evaluating the Effect of Aging and Moisture Conditions on the Performance of Bituminous Mixtures***" submitted by ***Bhaskar Pratim Das*** to the Indian Institute of Technology Guwahati for the award of the degree of Doctor of Philosophy is a record of bonafide research work carried out by him under my supervision and guidance. In my opinion, the thesis work has reached the requisite standard fulfilling the requirement for the degree of Doctor of Philosophy.

The findings presented in this thesis have not been submitted in part or full to any other university or institute for the award of any degree or diploma.

IIT Guwahati
Date:

Dr. Anjan Kumar S.
Assistant professor
Department of Civil Engineering
Indian Institute of Technology Guwahati
Assam - 781039, India

Declaration

I declare that this written submission represents my ideas in my own words, and where other's thoughts and words have been included, I have adequately cited and referenced the original sources. I also declare that I have adhered to all academic honesty and integrity principles and have not misinterpreted or fabricated, or falsified any idea/ data/ fact/ source in my submission. This thesis, in any way, does not purport to endorse any proprietary products or technologies.

IIT Guwahati
Date:

Bhaskar Pratim Das
156104023

Acknowledgments

I owe a profound debt of gratitude to my supervisor Dr. Anjan Kumar S., for his insight and guidance throughout my Ph.D. journey. I remember our first discussion, which ended with you stating, “your day one begins from today, good luck.” I am grateful that I always had the liberty to seek your suggestions for all the challenges this research offered. Above all, I would like to sincerely thank you for teaching me the art of scientific research.

I would also like to extend my heartfelt gratitude to my committee members, Dr. Teiborlang L. Ryntathiang, Dr. C. Mallikarjuna, and Dr. D Pamu. Your opinions and inputs are highly appreciated and helped shaped this thesis.

My gratitude goes to Mr. Nishant Bhargava; without your tremendous amount of support, this research work would have been challenging. My wholehearted thanks go out to Mr. Santanu Pathak and Mr. Supratim Kaushik for your love, encouragement, and beautiful memories to cherish. A special thanks go to Dr. Sanadam Bordoloi for his friendship and support from day one of this journey. Thanks to Mr. Priyesh D Babar, Dr. Ashok Julaganti, Mr. Bibuthi B. Bhardwaj, Mr. Kuldeep Kalita, and Mr. Mrinal Sarmah for your support in the laboratory investigations.

A warm-hearted thanks go to Mrs. Saswati Das for supporting the statistical analysis carried out in this research work. I have enjoyed our discussion over a cup of tea.

I would like to thank the technical staff and the staff members of IITG, who have helped me along the way. I am thankful to the central instruments facility (CIF) of IITG for providing the research facility for the completion of this research work. Thanks to Messers. Larsen and Toubro, IDPL, and Ingevity for the material support provided to carry out this research work.

Last (but certainly not least), I would also like to thank my family for their continuous encouragement, love, and support. My gratitude goes out to my brothers for the motivation that helped me reach my goals. And finally, to my beloved wife for helping me get through the trying times.

Bhaskar Pratim Das

Abstract

Bituminous pavements are exposed to environmental factors such as aging and moisture intrusion. These factors have a significant influence on the performance of the bituminous mixture. Hence, the study's objective was to evaluate the effect of aging and moisture conditions on the performance of bituminous mixtures. In this study, two levels of aging and three levels of moisture conditioning were considered. Hot mix asphalt (HMA) and Warm mix asphalt (WMA) mixtures were produced using two aggregates and unmodified VG 30 binder. A total of 144 specimens were subjected to the indirect tensile strength (ITS) test, 144 specimens for indirect tensile stiffness modulus (ITSM) test, 144 specimens for fatigue tests at 15 °C, and 25 °C. The creep tests were carried out at 40 °C and 45 °C with 117 specimens. Three replicate specimens were used for each test, and results were statistically analysed. In addition, adhesive failure (AF) in moisture conditioned (MC) fractured specimens and the loose mixture was determined using image analysis and photodetection technique. The relations and models considering aging and moisture effects on bituminous mixture adhesion failure, fatigue cracking, and creep resistance were developed.

The cracking resistance parameters such as ITS, fracture energy (FE), fracture work density (FWD), cracking tolerance index (CT_{Index}), and rate-dependent cracking index (RDCI) were estimated from the ITS test data. In general, the values of cracking resistance parameters increased with aging and reduced with moisture conditioning. It was interesting to note that the moisture had a profound effect than aging on cracking resistance. However, the coefficient of variation (CoV) of different cracking parameters increased with the increase in moisture conditioning cycles. In addition, the variation also increased with a reduction in the test temperature. The cracking tolerance index and rate-dependent cracking index parameter showed relatively higher CoV amongst the different parameters compared in this study. A one-way analysis of variance carried out at a significance level (α) of 0.05 showed that ITS, FWD, and FE parameters were sensitive to different aging and moisture conditioning levels evaluated in this study. Furthermore, the cracking resistance parameters indicate that the WMA mixture was relatively moisture-resistant than HMA, attributed to additive characteristics.

The AF was higher at 15 °C when compared to 25 °C. However, both HMA and WMA mixtures exhibited comparable adhesive failure. In conjunction with the tensile strength ratio (TSR), AF was used to classify moisture susceptibility into three zones. These zones are as follows, high resistance (TSR > 80 % & AF < 10 %), moderate resistance (70 % < TSR < 80 % & 10 % < AF < 15 %), and low resistance (TSR < 70 % & AF > 15 %) respectively. The

study highlight that the FE can serve as a measure of cracking resistance in the presence of moisture.

The long-term aged (LTA) mixture had a higher ITSM and fatigue life when compared to the short-term aged (STA) mixture. However, the moisture conditioning reduced the ITSM and fatigue life of both STA and LTA mixtures. The moisture effect on the bituminous mixture's fatigue life increased with the reduction in test temperature, as noticed in AF of the mixtures. The analysis showed that the MC mixture had a higher likelihood of fatigue damage than the unconditioned mixture at different aging levels and test temperatures. The damage-based fatigue life prediction model showed a good coefficient of determination ($0.62 \leq R^2 \leq 0.89$) for the conditions evaluated in this study, with 36 data point at each condition. The damage factor introduced helps compute the fatigue life of bituminous mixtures using cracking resistance parameters estimated using ITS. Further, the Monte Carlo simulation technique was used to simulate the fatigue life of mixtures. The analysis showed that the fatigue life of moisture-resistant mixture increased from STA to LTA condition at each cumulative probability level. The results highlighted that the moisture damage has a dominating effect when compared to the stiffening effect of aging on the fatigue behaviour of mixtures. Also, the effect of aging and moisture was similar for both HMA and WMA mixtures.

The bituminous mixture's creep resistance measured in terms of the flow number obtained from the Francken model showed that the LTA mixture had a higher creep resistance than the STA mixture. The creep behavior of HMA and WMA mixtures was found to be comparable. However, the creep resistance of the MC bituminous mixture was noticed to be inconsistent due to entrapped moisture in the MC specimen for both HMA and WMA. The inconsistency was minimized after removing the entrapped moisture. In contrast to fatigue behaviour, moisture had a lower effect than aging on the creep behaviour of bituminous mixtures.

The study highlights that moisture and aging had a profound effect on the performance of bituminous mixtures. In addition to traffic loading, different aging and moisture damage mechanisms affect the durability aspects of bituminous pavement exposed to the environment. Further studies are required to understand different aging and moisture damage mechanism to control their effects on the performance of bituminous mixtures. Also, the threshold limit for AF in bituminous mixtures requires further refinement and validation with field findings.

Keywords: aging; moisture; adhesion failure; fatigue cracking; creep resistance; warm mix additive; calcareous aggregate; siliceous aggregate.

List of contents

List of tables

List of figures

List of notations

Symbols	Meaning
σ	Stress
ε_t	Tensile strain
$\varepsilon_{d(n,T)}$	Axial strain
Δh	Axial deformation
D	Diameter
D_{MC}	Fatigue damage of moisture conditioned mixture
D_N	Fatigue damage at N^{th} cycle
D_{UC}	Fatigue damage of unconditioned mixture
E	Error
E_0	Initial stiffness modulus
E_N	Stiffness modulus at N^{th} cycle
FE_{MC}	Fracture energy of moisture conditioned mixture
FE_{UC}	Fracture energy of unconditioned mixture
G_f	Fracture energy
h_0	Initial height
l_{65}, l_{75}, & l_{85}	Displacement at 65, 75, and 85 percent of peak load
$\lvert m_{75}\rvert$	Slope
n	Sample size
N_f	Fatigue life
p	Maximum load
P_{65}, P_{75}, & P_{85}	65, 75, and 85 percent of peak load
$P_{t_{peak}}$	Instantaneous power at peak force
S_0	Stiffness modulus
S_a & S_b	Stiffness for cycle a and b
S_t	Indirect tensile strength
t	Thickness
T	Temperature
W_c	Cumulative area
W_f	Fracture work

Glossary of terms

Acronym	Meaning
ACT	Asphalt compatibility tester
AF	Adhesive failure
ANOVA	Analysis of variance
AV	Air voids
CoV	Coefficient of variation
CRI	Cracking resistance index
CT_{Index}	Cracking tolerance index
DR	Damage ratio
FE	Fracture energy
FN	Flow number
FT	Freeze-thaw
FWD	Fracture work density
HMA	Hot mix asphalt
HWB	Hot water bath
ITFT	Indirect tensile fatigue test
ITS	Indirect tensile strength
ITSM	Indirect tensile stiffness modulus
LTA	Long-term aged
MC	Moisture conditioned
MoRT&H	Ministry of road transport and highways
PV	Plateau value
RSC_a	Ratio of stiffness change for cycle a
RDCI	Rate-dependent cracking index
STA	Short-term aged
TSR	Tensile strength ratio
UC	Unconditioned
UUC	Unconfined uniaxial compression
WMA	Warm mix asphalt

Chapter 1

Introduction

1.1 Background

Flexible or bituminous pavement is subjected to numerous vehicular load applications and environmental factors during its service life. Bituminous pavement is designed and constructed to accommodate a specific volume of traffic. However, the effect of environmental factors on pavement performance remains mostly uncertain. The environmental factors of interest are aging and moisture intrusion.

The bituminous mixture undergoes aging in two phases. First, the short-term aging occurs during the mixture production process in the plant and while transportation because of the loss of oily fractions (volatile) and bitumen oxidation. Long-term aging occurs during the service, where the bituminous binder undergoes further aging in the presence of atmospheric oxygen, ultraviolet (UV) radiation, and steric hardening (Newcomb et al., 2015). Petersen (2000) noticed a strong association between the polar functional group formed in a mixture with aging and the cracking observed in bituminous pavements. Reduced cracking resistance of aged bituminous pavement will degrade the fatigue performance of the pavement. With moisture intruding into the voids and cracks of the pavement, the propagation of micro-cracks under the traffic loading will expedite and lead to pavement failure.

Moisture intrusion is detrimental to the bituminous pavement structure. Moisture weakens the adhesive and cohesive bond responsible for holding the bituminous mixture together, which results in distress manifestations like stripping, raveling, and pot-holes (Kiggundu & Roberts, 1988; Sebaaly et al., 2017). Hajj et al. (2011) said that pavement distresses such as fatigue cracking, rutting, and raveling aggravate due to moisture damage. Thus, moisture intrusion reduces the bituminous pavement's durability.

In regions with a wide variation in temperature, rainfall, snowing, and high-altitude regions with very low ambient temperature, the proper construction of pavement become challenging. A warm mix asphalt (WMA) technology can tackle such challenging situations. WMA is a generic term that refers to technologies that allow at least 30 °C reductions in the bituminous mixture's mixing and compaction temperatures (IRC: SP:101, 2014). Different techniques used to reduce the production temperature of the bituminous mixture are: reduction

in the viscosity of bitumen, increase in the binder's volume, and reduction in the surface tension between the aggregates and the bituminous binder (IRC: SP:101, 2014). WMA mixture's advantages include longer hauling distances, reduced bitumen aging, faster turnover to traffic, cold weather paving, reduced wear and tear of mixing plant, better workability, and a healthier working environment for the paving crew. In addition, the reduced production temperature associated with the WMA mixture results in less aging when compared to hot mix asphalt (HMA) mixtures. Thus, a WMA mixture has the potential to offer higher durability compared to the HMA mixture. However, increased moisture susceptibility and weak rutting resistance are the concerns associated with WMA technology (Kim et al., 2012; Rodezno et al., 2015). Thus, a balanced approach towards selecting mixture ingredients, production techniques, and improving mechanical behavior against external factors is continuously evolving, which is very much needed.

1.2 Problem statement

In service, both aging and moisture damage play a critical role in reducing the durability of the bituminous pavement. Therefore, both aging and moisture effects should be considered for performance evaluation to understand the durability issues. The problem statement of this work is to investigate the effect of aging and moisture on the cracking resistance parameters, moisture susceptibility, aggregate-bitumen adhesion properties, fatigue resistance, and creep behavior of bituminous mixtures. The suitability of key parameters such as strength, modulus, or energy-based used to assess the cracking resistance and moisture susceptibility needs to be reevaluated considering the influence of aging and moisture condition levels. With a vast amount of additives/material modification to mitigate the moisture damage, moisture damage still exists in well-processed and constructed bituminous pavements. Hence it will be interesting to investigate the combined aging and moisture effect on the performance of different mixtures such as hot and warm bituminous mixtures with different aggregates.

1.3 Research objective

The main objective of this research work is to understand the effect of aging and moisture conditions on the performance of bituminous mixture. Following tasks were taken up to accomplish the research objective.

- Evaluate test protocol and parameters to assess the moisture damage in a bituminous mixture with different ingredients.

- Determine the impact of aging and moisture on the aggregate-bitumen adhesion characteristics.
- Analyze the impact of aging and moisture on fatigue and creep resistance.
- Develop the relations or models considering aging and moisture effect on bituminous mixtures' fatigue cracking and creep resistance.

1.4 Research scope

The scope of this research work, including test methodologies adopted, the number of specimens per test, and different analytical/ numerical/ statistical methods used to interpret the test results, is presented in Figure 1.1.

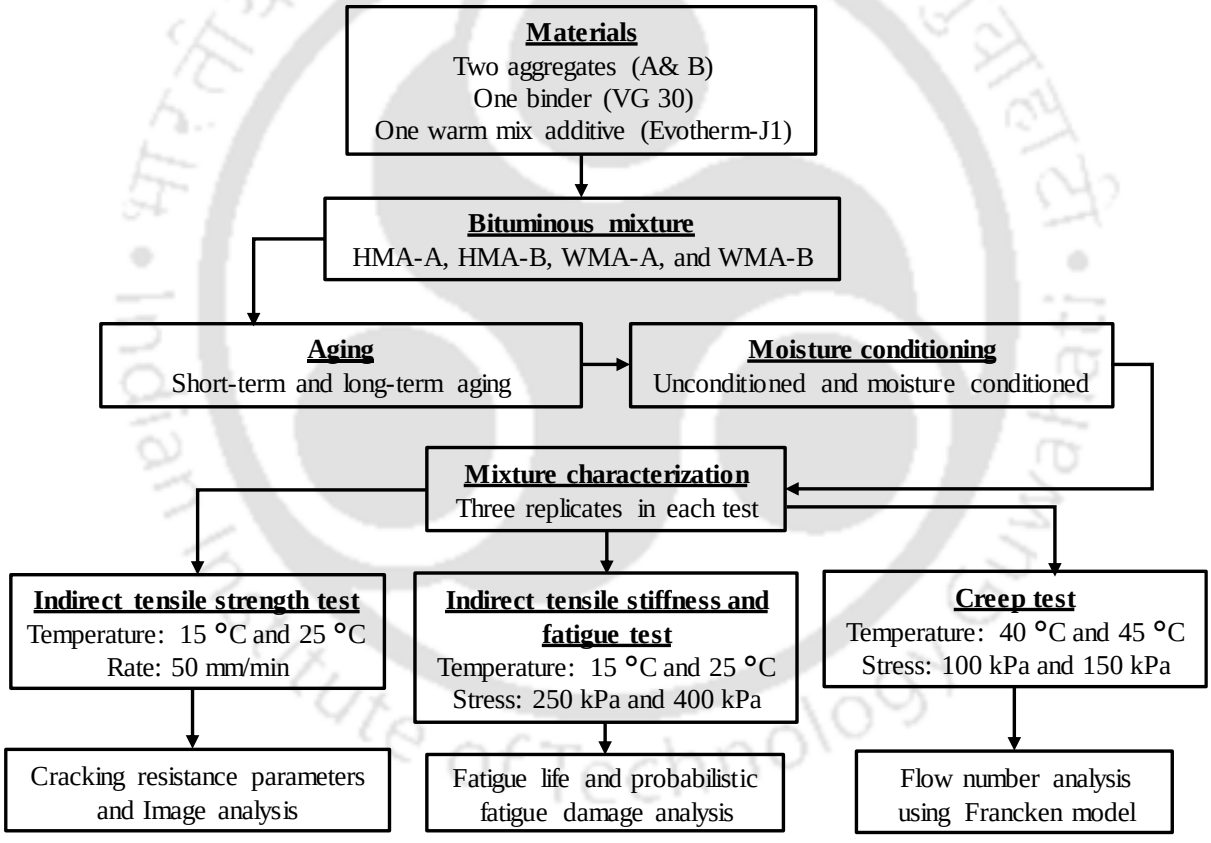

Figure 1.1 Scope of research work

1.5 Organization of the thesis

This thesis consists of eight chapters. Chapter 1 introduces the research area, highlights the research problem and the objectives of the research work. Chapter 2 presents an extensive review of the literature associated with this research work. First, the damage mechanism of aging and moisture was described. Next, the effect of aging and moisture damage on the mechanical behavior of bituminous mixtures was discussed.

Chapter 3 describes the materials used, their properties, test methods and standards, and the research methodology. Bituminous mixtures' cracking resistance using different parameters to identify a suitable cracking resistance parameter was evaluated in Chapter 4.

In chapter 5, the adhesive failure in bituminous mixtures using image processing and analysis techniques was determined. Further, the association of adhesion failure with the tensile strength and fracture energy was summarized.

Chapter 6 shows the resistance of bituminous mixture to fatigue damage, and different fatigue modeling approaches were explored. In chapter 7, the creep resistance of bituminous mixtures and the damping effect of moisture on the creep behavior of mixtures were studied. The summary of findings, salient conclusions, and the way forward of this research work was presented in chapter 8.

Chapter 2

Literature review

2.1 Introduction

A bituminous mixture is a composite of crushed stone aggregates and mineral fillers bounded together by a bituminous binder. A balanced mixture and pavement design, considering the material characteristics, traffic loading, and environmental conditions, are essential to accomplish durability. However, the integrity of the bituminous mixture is affected during service due to complex variation in environmental conditions, traffic loading, and inherent material characteristics, which is reflected as pavement distresses. Different types of distress commonly noticed in bituminous pavement include moisture damage, fatigue cracking, low-temperature cracking, and rutting. The most critical factors which onset the distresses mechanism in bituminous pavements are aging and moisture damage. Aging during production and service contributes to the change in material state (stiffness gain), and moisture contributes to the disintegration of the bitumen-aggregate bond. Thus understanding and evaluating the effect of aging and moisture on the performance of bituminous mixture is continuously evolving.

The aging of bituminous pavements is inevitable. An excessive increase in the stiffness of bituminous mixture with aging can increase the pavement's susceptibility to cracking. Fatigue cracks can initiate due to the repeated application of vehicular loads on an aged pavement. Cracks, once formed, provides a passage for moisture intrusion into the bituminous pavements structure (Kandhal, 1992). Generally, fatigue cracking and rutting are the most common and severe distress associated with the flexible pavement. Rutting or creep is manifested when heavy loads ply on the bituminous pavement at a high temperature. Moisture can accumulate in the depression created by the creep of bituminous pavements. Thus, moisture's presence further aggravates distress manifestation, thereby reducing the service life and increasing the maintenance cost of the pavement.

A detailed review of the literature on the effect of aging and moisture on the performance of the bituminous mixture is presented in this chapter.

2.2 Aging in a bituminous mixture

2.2.1 General

The increase in stiffness of the bituminous binder during its production and in-service is termed aging. Aging during the production of the bituminous mixture is known as short-term aging. The bituminous mixture is produced at an elevated temperature where the thin film of bitumen coating the aggregates undergoes volatilization and oxidation. Aging of the bituminous mixture during service is known as long-term aging. Long-term aging is the progressive oxidation of bitumen in the field due to the interaction with the environment. The polar functional group formed due to oxidation of bituminous binder has a strong molecular association, increasing the bitumen's consistency. The interactions of the chemical functionalities in bitumen usually determine the physical properties and oxidative aging characteristics of the bituminous binder. The influence of oxidative age hardening on excessive pavement cracking was highlighted by Petersen (2009). Thus, the increase in stiffness of bituminous mixture with aging has two effects; either it increases the load-bearing capacity and creep resistance, or it reduces the flexibility of the pavement, making it susceptible to cracking.

2.2.2 Mechanism of aging

Traxler (1963) identified different mechanisms of bitumen aging, as shown in Table 2.1. Out of the fifteen mentioned mechanisms of bitumen aging, Hunter et al. (2015) stated that oxidation, volatilization, steric or physical factors, and extrusion of oils are the most critical factors of bitumen aging, as discussed below.

- **Oxidation**: Oxidation is considered as the most important mechanism of bitumen aging. The oxygen present in the atmosphere oxidizes the bitumen and creates polar oxygen-containing groups. This results in the formation of larger and more complex molecules, which makes bitumen more rigid and less flexible. The degree of oxidation is influenced by the temperature, period of exposure, and bitumen film thickness.
- **Volatilization**: Bitumen loses its volatile components upon exposure to elevated temperature, resulting in the bitumen's hardening. However, the resulting hardening from the evaporation of volatiles in paving grade bitumen is relatively small. The rate of volatilization depends on the diffusion rate and the thickness of the diffusion path.

- **Steric or physical factors**: Steric hardening of bitumen is caused by reorientation or restructuring of molecules within the bitumen and the slow crystallization of waxes. The steric hardening effect is reversible with the application of heat.
- **Extrusion of oils**: Oily components exude from the bitumen into the mineral aggregate, which results in exudative hardening. It is a function of both the exudation tendency of the bitumen and the porosity of the aggregate.

Table 2.1 Mechanisms of bitumen aging (Traxler, 1963)

Factors that influence bitumen aging	**Influenced by**						**Occurring**	
	Time	**Heat**	**Oxygen**	**Sunlight**	**Beta & gamma rays**		**At the surface**	**In the mixture**
Oxidation (in dark)	✓	✓	✓				✓	
Photo-oxidation (direct light)	✓	✓	✓	✓			✓	
Volatilisation	✓	✓					✓	✓
Photo-oxidation (reflected light)	✓	✓	✓	✓			✓	
Photochemical (direct light)	✓	✓		✓			✓	
Photochemical (reflected light)	✓	✓		✓			✓	✓
Polymerisation	✓	✓					✓	✓
Steric or physical	✓						✓	✓
Exudation of oils	✓	✓					✓	
Changes by nuclear energy	✓	✓			✓		✓	✓
Action by water	✓	✓	✓	✓			✓	
Absorption by solid	✓	✓					✓	✓
Absorption of components at a solid surface	✓	✓					✓	
Chemical reactions	✓	✓					✓	✓
Microbiological deterioration	✓	✓	✓				✓	✓

In general, bitumen comprises four broad chemical groups called asphaltenes, saturates, aromatics, and resins (also known as “SARA” fractions). The saturates, aromatics, and resins are collectively called the maltenes. Lu & Isacsson (2002) noticed that the aging of the bituminous binder resulted in an increase in the resins and asphaltenes content and reduced the aromatic content. The authors also measured the corresponding change in the complex modulus of the binder at 25 °C. The authors noticed a two-times increase in the complex modulus of the bituminous binder with aging for different binders evaluated in their study. Yongli et al. (2019) noticed that an increase in the asphaltenes or resins content of a bituminous binder increased

the dynamic modulus of the bituminous mixture and reduced the creep compliance and creep rate of the bituminous mixture. However, with the increase in saturates and aromatics content, the dynamic modulus reduced, the creep compliance increased, and the creep rate also increased.

With the advancement of analytical techniques, detailed information on the chemical functional groups present in bitumen can be extracted. Fourier Transform Infrared spectrometry (FTIR) is an extensively used analytic technique for qualitative and quantitative functional group analysis of a bituminous binder. Petersen (1984) identified carboxylic acids (and their independent salts), anhydrides, ketones, 2-quinolone types, sulfoxides, pyrrolic types, and phenolic types as important polar heteroatom-containing functional groups initially present in the bitumen or formed during oxidative aging. Lu & Isacsson (2002) said that oxidation of the bitumen occurring during the aging process could be quantified by measuring the concentration of the carbonyl (e.g., ketones, carboxylic acids, and anhydrides) and sulfoxide compounds. Liang et al. (2019) studied the effect of pressure aging vessel (PAV) aging on the functional groups of different bituminous binders. The authors noticed that Carbonyl, ether, ester, and sulfoxide components increased with an increase in aging time. However, only the carbonyl component of the binder consistently increased with the long-term aging protocol used in their study. The authors also noticed that the carbonyl area (calculated from the absorbance spectrum obtained from the FTIR test) had a linear relationship with the viscosity of the bitumen. Thus, aging increases the content of functional groups, which, in turn, increases the viscosity of the bitumen.

Ketones and sulfoxides are the primary products formed during oxidative aging. Ketones and sulfoxides are formed more rapidly during the initial stages of oxidation. After this initial oxidation stage, the formation of ketone and sulfoxide takes place at a relatively much slower rate. Researchers have noticed that the amount of ketones formed in bitumen on oxidative aging directly correlates with viscosity. When the concentration of polar functional groups becomes sufficiently high during oxidative aging, the intermolecular association immobilizes an excessive number of molecules. This molecular agglomerate decreases the mobility of molecules to flow past one another under thermal or mechanical stress. The above process results in the bitumen's embrittlement and makes it susceptible to cracking (Petersen, 2009).

2.2.3 Laboratory methods for aging bituminous binder and mixture

An accelerated aging process is carried out in the laboratory to simulate the relative hardening undergone by bituminous binder and mixture during the mixture production process (Short-term aging) and in-service (Long-term aging). There are two types of laboratory aging processes, i.e., aging performed on the bitumen and aging performed on the bituminous mixture. First, the aging performed on the bituminous binder is discussed. A thin film of the bituminous binder is subjected to extended heating in an oven under different conditions in this aging type.

- **Thin film oven test (ASTM D1754):** Thin-film oven test (TFO) simulates the aging experienced by bitumen during the bituminous mixture production stage. In the TFO test, 50 g of bitumen is transferred to a cylindrical pan of 140 mm diameter. This resulted in a bitumen film thickness of approximately 3.2 mm. Two or more pan are placed in a rotating self (5 to 6 rotations per minute). The oven temperature is set to 163 °C, and the aging process is carried out for 5 h. The pans are removed after the aging process was completed and allowed to cool at room temperature. The TFO test's disadvantage is that the lack of binder agitation during the test will result in non-uniform aging of the bitumen film.
- **Rolling thin film oven test (ASTM D2872):** Short-term aging of the bituminous binder is simulated in a rolling thin film oven test (RTFO). The non-uniformed aging of bituminous binder noticed in the case of TFO can be eliminated in the RTFO test by using glass bottles placed in a vertical revolving shelf. Each glass bottle is filled with 35 g of bitumen, which resulted in a film thickness of 1.25 mm. The oven temperature is set to 163 °C, and the airflow is set to 4000 mL/min. RTFO aging process is carried out for 85 min. The continuous movement in the RTFO method ensured that a fresh surface of bitumen is exposed to heat and air continuously.
- **Pressure aging vessel test (ASTM D6521)**: The long-term field aging experienced by bituminous binder is stimulated by the PAV test. In the PAV test, the residue binder obtained after the short-term aging in the RTFO test is further subjected to long-term aging in the PAV. Here, 50 g of RTFO aged binder is poured into a pan of 140 mm in diameter. The resulting thickness of bitumen in the pan is approximately 3.2 mm. The pan is placed horizontally in the PAV chamber, and the aging temperature is maintained

between 90 °C to 110 °C depending on the grade of the bitumen. A pressure of 2.1 MPa is applied for 20 h, and the residue obtained is subjected to a vacuum degassed process.

- **Ultraviolet aging:** The aging resulting from photochemical exposure of solar radiation on bituminous pavements is explored by different researchers (Lopes et al., 2014; Wu et al., 2010). The effect of ultraviolet (UV) rays present in solar radiation on bituminous pavements is not considered in the thermal-oxidative aging process. The impact of UV becomes particularly crucial in simulating the long-term field aging of bituminous pavements. For this purpose, the UV lamps of different intensities and wavelengths (300 to 400 nm) were installed in an oven with a temperature-controlled environment to simulate UV aging.

Next, the laboratory aging methods for the bituminous mixture are discussed. Either loose bituminous mixture or compacted specimens are subjected to an extended heating procedure to simulate the short-term or long-term aged state. The aging temperature and aging duration may vary depending on the research methodology or the referred specification. In general, aging as per the AASHTO R 30 (AASHTO R 30, 2002) protocol is widely used, which recommends three aging levels, as discussed below.

- **Mixture conditioning for volumetric mixture design:** Laboratory prepared loose bituminous mixture is placed in a pan to an even thickness of 25 mm to 50 mm. The pan is then placed in a forced-draft oven at the mixture's compaction temperature for 2 h and stirred after the first hour.
- **Short-term aging:** This conditioning process is like the conditioning process for volumetric mixture design except for the conditioning time. In short-term aging, the mixture is kept in the force draft oven for 4 h at 135 °C to produce a short-term aged (STA) bituminous mixture.
- **Long-term aging:** long-term aging of the bituminous mixture is carried out on compacted specimens of either plant-produced bituminous mixture and laboratory-produced STA bituminous mixture. The compacted specimen is placed in a forced draft oven at 85 °C for 120 h to produce a long-term aged (LTA) specimen.

2.3 Moisture damage of bituminous mixture

2.3.1 General

Moisture has an adverse effect on the durability of the bituminous mixture. The presence of moisture shortens the bituminous pavement's service life by resulting in failures such as thermal cracking, raveling, fatigue, and rutting (Sebaaly et al., 2017). Moisture damage is generally defined as the loss of the system's functional and mechanical properties in the presence of moisture. The moisture damage is defined as the loss of adhesive bond between bitumen and aggregate and/or the loss in the cohesive bond within the bitumen. The loss of adhesive bond between bitumen and aggregate results in the loss of bitumen coating from the aggregate surface, also known as stripping of the bituminous mixture. A comprehensive definition of moisture damage was given by Kiggundu & Roberts (1988) as "*the progressive functional deterioration of a pavement mixture by loss of the adhesive bond between the asphalt cement and the aggregate surface and/or loss of the cohesive resistance within the asphalt cement principally from the action of water.*"

2.3.2 Mechanism of moisture damage

According to Caro et al. (2008a), moisture damage is a two-step process, i.e., moisture transportation and the response of the system. In moisture transportation, moisture infiltrates into the pavement system either in liquid or in a vapour state and reaches the interface between bituminous binder and aggregates. The source of moisture may be rainfall, wet subgrade, humid environment, or incomplete drying of aggregates. Even in a well compacted bituminous mixture, moisture can very slowly work its way between the aggregate surfaces and bituminous binder, weakening or even destroying the bond between aggregate and binder. This results in the loss in strength and load-carrying capacity of the pavement system (Caro et al., 2008a; Kringos et al., 2008). A pictorial representation of the moisture damage process is shown in Figure 2.1.

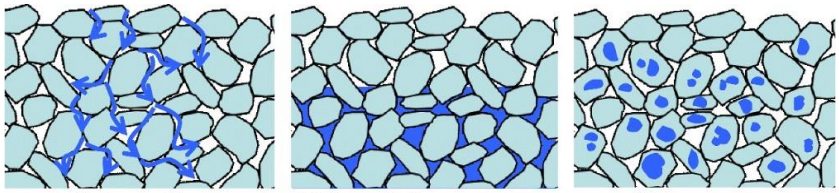

Figure 2.1 Moisture penetration into the bituminous mixture (Kringos et al., 2008)

Researchers have identified six mechanisms responsible for moisture damage in a bituminous mixture (Kiggundu & Roberts, 1988; Little & Jones, 2003). A brief discussion of the different moisture damage mechanisms is presented in Table 2.2, as shown below.

Table 2.2 Mechanisms of moisture damage in a bituminous mixture (Little & Jones, 2003)

Mechanism	Details
Detachment	This mechanism is defined as the microscopic separation of bitumen film from the aggregate surface by a thin layer of moisture with no apparent break in the bitumen film.
Displacement	Displacement is caused by preferential removal of bitumen film from the aggregate surface by moisture due to incomplete coating of the aggregate surface, the presence of a discontinuity or breaks in the bitumen film, such as pinholes and film rupture, where bitumen, aggregate, and moisture are in contact.
Film rapture	Film fissures at sharp aggregate contact or the presence of dust on aggregate surface. Traffic movement or environmental actions such as freeze-thaw (FT) cycles can initiate film rupture. Moisture can access the bitumen-aggregate interface through the broken bitumen film.
Spontaneous emulsification	Spontaneous emulsification is an inverted emulsion of moisture droplets in bitumen. Moisture can diffuse into the bitumen film by the osmosis process in significant quantities, which appears to be the moisture dispersion in the bitumen and is considered an inverted emulsion (for example, water in oil). Once the emulsion formation reaches the aggregate surface, the adhesive bond is broken.
Pore pressure-induced damage	The moisture entrapped in the voids of the bituminous mixture will develop pore pressure under the repeated application of traffic load. The continued buildup in pore pressure will disrupt the bitumen film from the aggregate surface or promote the growth of micro-cracks in the bituminous mixture.
Hydraulic scouring	In a saturated surface under the action of traffic wheels, moisture is sucked under the tires and into the pavement. A capillary tension/compression phenomenon arises, which results in hydraulic scouring of the bituminous mixture.

Little & Jones (2003) further said that the pH of moisture in contact with the bituminous mixture strongly influences the adhesion between the aggregate and bitumen. It is worth

mentioning that adhesive and cohesive failures are the final step in the moisture damage process that begins with different modes of moisture transport, thus initiating the moisture damage process.

2.3.3 Factors influencing moisture susceptibility

The bituminous mixture may experience a loss in adhesive bond strength between aggregate and bitumen and loss in the bitumen's cohesive force in the presence of moisture. Such a bituminous mixture is termed as a moisture susceptible bituminous mixture. The physical and chemical properties of mixture ingredients, i.e., aggregate, bitumen, and additives, will influence the moisture susceptibility of the bituminous mixture. The volumetric properties of the bituminous mixture and environmental factors are other critical factors influencing the moisture susceptibility of a mixture. Different factors influencing the moisture susceptibility of the bituminous mixture are listed in Table 2.3, as shown below.

Table 2.3 Factors affecting bituminous mixture moisture susceptibility (Hunter et al., 2015)

Aggregate	**Bitumen**	**Mixture**	**External**
Mineralogy	Rheology	Void content	Rainfall
Surface texture	Electrical polarity	Permeability	Humidity
Porosity	Constitution	Bitumen content	pH of water
Dust	Surface free energy	Bitumen film thickness	Presence of salts
Durability		Type of filler	Temperature
Surface area		Aggregate gradation	Temperature cycling
Surface free energy		Type of mixture	Traffic
Absorption			Design
Moisture content			Quality
Shape			Drainage
Weathering			

2.3.4 Laboratory tests to assess moisture susceptibility of bituminous mixture

Test on the bituminous mixture's moisture susceptibility can be divided into two categories, i.e., test on loose mixture and test on a compacted specimen. Different methods of loose bituminous mixture testing are available, which differ in how the loose mixture is prepared, subjected to moisture, and evaluated. A brief discussion of the different methods practiced is presented below.

- **Static immersion tests (IS 6241):** In the static immersion test, about 200 g of aggregate particles (20 mm to 12.5 mm) are entirely coated with 5 percent bitumen by the weight

of aggregates. The coated aggregate particles are cooled for 2 h in a 500 ml beaker and immersed completely in distilled water. The beaker is then transferred to a water bath at 40 °C for 24 h. After 24 h of immersion, a visual assessment is made while the mixture is still immersed in the water.

- **Rolling bottle method (BS EN 12697-11)**: About 200 spherical aggregate particles (6.3 mm to 8 mm) are coated with a 0.1 mm bitumen film. The coated aggregate is transferred to a 250 ml flask containing distilled water and a glass rod and rotated at 40 rpm for 72 h. The retained bitumen coating is then visually estimated.
- **Dynamic immersion test (ASTM D3625):** Also known as boiling water test, approximately 250 g of aggregates coated with bitumen is boiled in a container for 10 min. At the end of 10 min, the free bitumen is skimmed off from the water surface and allowed to cool at room temperature. The cooled mixture is transferred into a white paper towel, and visual observation of the retained coating is carried out.
- **Chemical immersion tests:** In this test, the bitumen-coated aggregates are soaked in solutions containing different concentrations of sodium carbonate. Adhesiveness is measured by recording the concentration of the sodium carbonate solution at which stripping is first observed.
- **Net adsorption test (SHRP A-341):** This test was developed as a part of the SHRP A-341 investigation conducted by Curtis et al. (1993). This test works on the principles of adsorption and absorption, where the amount of solute (bitumen) adsorbed from a stock solution of bitumen-toluene onto the adsorbent (aggregate) is measured. For this purpose, the bitumen-toluene solution is prepared by mixing 1 g of bitumen in 1000 ml toluene. 140 ml of bitumen-toluene solution and 50 g of aggregate (passing 4.75 mm sieve) is mixed in a conical flask and agitated for 6.5 h. After 6.5 h, 4 ml of solution is removed to determine the absorbance value using a spectrophotometer. The absorbance value is compared with the stock solution value, and the initial percentage adsorption is determined. Now, 2 ml of water is added into the flask and agitated overnight. Another 4 ml of solution is removed and assessed in a similar manner. This second adsorption value is the percentage net adsorption, which is the amount of bitumen remaining on the aggregates after aqueous desorption.
- **Ultrasonic method** (Vuorinen & Hartikainen, 2001)**:** In this test method, circular-shaped polished aggregate pieces are coated with bitumen and stored at room temperature for 22 h and then soaked in normal water for 6 h. Then the bitumen-covered

face is exposed to ultrasound for 60 s. After this, the test surface is lightly brushed and subjected to oven drying at 110 °C for 2 h. The bitumen stripped to the initial bitumen quantity is expressed in percentage.

Next, the test methods used for evaluating moisture susceptibility of either laboratory-prepared specimens or field cores are discussed.

- **Immersion compression test (ASTM D1075, withdrawn):** This test method measures the loss of compressive strength of the bituminous specimen due to the action of water. For this purpose, at least six 101.6 × 101.6 mm cylindrical specimens will be made and divided into two sets. First, a set of specimens is air-cured at 25 °C for 4 h. The second set of specimens is subjected to moisture conditioning in a hot water bath (HWB) at 60 °C for 24 h or at 49 °C for 4 days and then transferred to a 25 °C water bath 2 h. Both sets of specimens were subjected to a compressive strength test, and the index of retained strength (IRS) is determined. IRS is the ratio of compressive strength of moisture conditioned (MC) specimens to dry specimens.
- **Retained Marshall stability test:** Retained Marshall stability test is carried out following MoRT&H 4th revision recommendations. The bituminous mixture is prepared using 5 percent bitumen of 80/100 grade by weight of aggregates and recommended aggregate gradation. At least 8 standard Marshall specimens with 6 percent air void content are prepared. Specimens are sorted into two groups of similar average specific gravity, with 4 specimens in each group. Specimens belonging to the first group are tested in a dry condition as per the ASTM D1559 specification. Specimen from the second group is subjected to 24 h of soaking in a hot water bath at 60 °C ± 1 °C and then tested as per ASTM D1559 specification. The ratio of the Marshall stability of the conditioned specimens to the standard Marshall stability is termed the 'retained Marshall stability.' A retained Marshall stability value of 75 percent or higher is desirable.
- **Retained stiffness test:** The principle of the retained stiffness test is like the retained Marshall stability test. Here, the indirect tensile stiffness modulus of the bituminous mixture is determined as per BS EN 12697:26 protocol. The moisture conditioning process and testing temperature maybe differ amongst agencies.
- **Modified Lottman procedure (AASHTO T 283):** This is the most widely used protocol for determining the moisture susceptibility of the bituminous mixture. Here,

at least six specimens having an air void of 7 ± 0.5 percent were prepared and divided into two sets. The set of specimens tested dry were wrapped in a leak-proof plastic bag and placed in a water bath at 25 °C for 2 h before testing. The moisture-conditioned set of specimens was first vacuum saturated to 70 to 80 percent and subjected to a freeze-thaw cycle (freezing at -18 °C for 16 h and thawing at 60 °C for 24 h). The moisture-conditioned specimens were then placed in a water bath at 25 °C for 2 h before testing. The indirect tensile strength (ITS) of each specimen was determined, and the average tensile strength of moisture conditioned specimen to dry specimen is expressed as the tensile strength ratio (TSR). ASTM D4867 also has a similar moisture conditioning process and testing protocol for determining moisture susceptibility of the bituminous mixture. Lee & Kim (2014) said that moisture conditioning using freeze-thaw cycles primarily result in the detachment and displacement mechanism of moisture damage.

- **Immersion wheel tracking tests:** The immersion wheel tracking test simulates the traffic action on the bituminous specimen, which was not considered in the above-discussed moisture conditioning protocols. One such approach is the Hamburg wheel tracking test (HWTT) as per the AASHTO T324 protocol. In the HWTT, both cylindrical (150 mm diameter) and slab (300 mm × 250 mm) specimens are tested. After pre-conditioning the specimen in the water bath for 30 min at the selected temperature (25 °C to 70 °C), the wheel action is initiated. The wheel has a width of 47 mm and carries a load of 705 N. Test is stopped when either 20000 wheel passes or 20 mm rut depth was reached. The results can be used to calculate the stripping inflection point, i.e., the onset of stripping in the mixture.
- **Saturation aging tensile stiffness (SATS) test (BS EN 12697-45:2012)**: In this test, a compacted specimen is subjected to both aging and moisture conditioning simultaneously. This mechanism intends to mimic the field moisture damage conditions in a laboratory. The standard SATS procedure involves conditioning five pre-saturated specimens of 100 mm diameter and 60 mm thickness. The pressure in the vessel is set at 0.5 MPa, and the temperature is kept at 85 °C for 24 h. This is followed by a cooling period of 24 h before releasing the air pressure and opening the vessel to remove the specimens for stiffness testing. Airey et al. (2005) noticed that the procedure could successfully reproduce the moisture damage of the bituminous mixture observed in the field.

- **Moisture-induced stress tester (ASMT D7870)**: Bituminous pavements are subjected to dynamics hydrostatic pore pressure and scouring action due to traffic movement over a wet pavement surface. This condition is simulated in the laboratory by a moisture-induced stress tester (MIST). For this purpose, compacted bituminous specimens of 100 mm or 150 mm diameter are placed in the MIST equipment and submerged in water. The temperature is set to 50 °C or 60 °C depending on the high-temperature performance grade of the binder. The number of pressure cycles is set to 3500, and pressure in the chamber is maintained at 275 kPa. After completing the cyclic process, the hot water is drained, and freshwater is introduced to lower the temperature of specimens to 18 to 27 °C. This completes the accelerated cyclic moisture conditioning process. The specimens are then removed and transferred to a water bath at 25 °C for 2 h to 3 h before testing. Finally, the tensile strength or change in other properties such as density, modulus, etc., of the bituminous mixture is determined.

2.4 Cracking resistance of the bituminous mixture

Both aging and moisture intrusion affect the performance of a bituminous mixture. The performance of the bituminous mixture can be defined as the ability to sustain the traffic loading and environmental factors for the designed period. Aging increases the stiffness of the bituminous mixture, and a mixture with excessive stiffness is susceptible to cracking. Therefore, understanding the effect of aging on the bituminous cracking resistance will help identify a mixture with low cracking resistance. Similarly, moisture reduces the durability of the bituminous mixture, which, in turn, will have an adverse effect on the cracking resistance of the bituminous mixture. Thus, there is a need to quantify the cracking resistance of a bituminous mixture under the influence of aging and moisture.

In a laboratory investigation, the cracking resistance of a bituminous mixture can be best estimated by using a repeated load test. However, a repeated load test setup is sophisticated equipment and may require extended testing duration. These may pose limitations to serve as a routine test. On the other hand, a monotonic loading test such as an indirect tensile test (ASTM D6931), semi-circular beam bending (SCB) test (ASTM D8044), etc., be used as a routine test to determine the cracking resistance of bituminous mixture. The load-deformation or the stress-strain curve obtained from a monotonic load test can be utilized to determine parameters like fracture energy (FE), dissipated creep strain energy (DCSE), and elastic energy

(EE). A significant group of researchers has used the indirect tensile testing setup to determine the fracture energy of bituminous mixture (Bahadori et al., 2015; Izadi et al., 2018; Li et al., 2012; Mehrara & Khodaii, 2017; Shu et al., 2008; Wen, 2013; Wen & Kim, 2002).

Fracture energy represents the total energy a material can absorb before failure. FE consists of two components, i.e., the DCSE part, which is lost during testing due to damage formation and heat generation, and the EE part, which is stored during loading and released during the unloaded process. FE is a fundamental material property and captures the complete response of the bituminous mixture, i.e., pre-failure and post-failure under the loading condition. This FE feature becomes particularly useful for delineating brittle bituminous mixture, which does not have a post-failure region of the stress-strain curve. The modulus of the bituminous mixture finds its application in pavement design. The variation in the modulus of the bituminous mixture with aging and moisture is another critical parameter evaluated by researchers. In this section, different parameters used to assess the cracking resistance of the bituminous mixture are presented. The ability of the parameter to capture the effect of aging and moisture on the cracking resistance of the bituminous mixture is also discussed.

2.4.1 Strength-based parameters

Researchers have used the bituminous mixture's tensile strength to evaluate the effect of aging and moisture on the cracking resistance of the mixture. The bituminous mixture's tensile strength can be determined following the ASTM D6931 protocol. The tensile strength ratio or TSR is the most widely used parameter to assess the moisture susceptibility of the bituminous mixture. It can be determined as per ASTM D4867 or AASHTO T 283 protocol. TSR is the ratio of the tensile strength of moisture conditioned to the unconditioned (UC) bituminous specimens.

Researchers have noticed that the mineralogy of aggregate has a significant effect on the moisture susceptibility of the mixture. Praveen & Anand (2012) studied the moisture susceptibility using the TSR of bituminous mixtures produced with quartzite, granite, limestone, and sandstone aggregates. The authors noticed that the TSR of the bituminous mixture with granite, quartzite, and sandstone aggregates was less than 80 percent. However, with the application of an antistripping agent (2 percent lime), the TSR of these bituminous mixtures improved and was higher than 80 percent for most of the cases. In comparison, the TSR of the bituminous mixture with limestone aggregates was higher than 90 percent.

Alataş & Yilmaz (2013) studied the effect of polymeric modification of bitumen on the moisture susceptibility of bituminous mixtures. The authors noticed that the TSR of styrene-butadiene-styrene (SBS) modified mixture was 5.8 %, and ethylene–vinyl-acetate (EVA) modified mixture was 12.7 % higher than the control mixture. Hasan et al. (2013) studied aging's effect on the tensile strength of HMA mixture and WMA (Sasobit and Rheofalt) mixtures. The authors noticed that the mixtures' tensile strength increased with an increase in the level of aging and reached a plateau value with a further rise in aging (extra aged condition). In a similar study, Gao et al. (2017) noticed that the bituminous mixture's tensile strength increased rapidly up to 16 h of aging (aged in an oven at 163 °C for 2 h, 4 h, 8 h, 16 h, and 24 h). However, the increase in the tensile strength at 24 h of aging was not as severe as noticed up to 16 h of aging.

Vargas-Nordcbeck et al. (2016) noticed that the bituminous mixture with a known history of moisture-related distress in the field satisfied the minimum TSR criteria of 0.80 when subjected to only one freeze-thaw cycle. However, with the increase in the freeze-thaw cycles from one to three and six cycles, only bituminous mixtures with antistripping agents satisfied the 0.80 TSR criteria, as shown in Figure 2.2. Thus, more than one freeze-thaw cycle may be necessary to mimic the field moisture damage in laboratory studies.

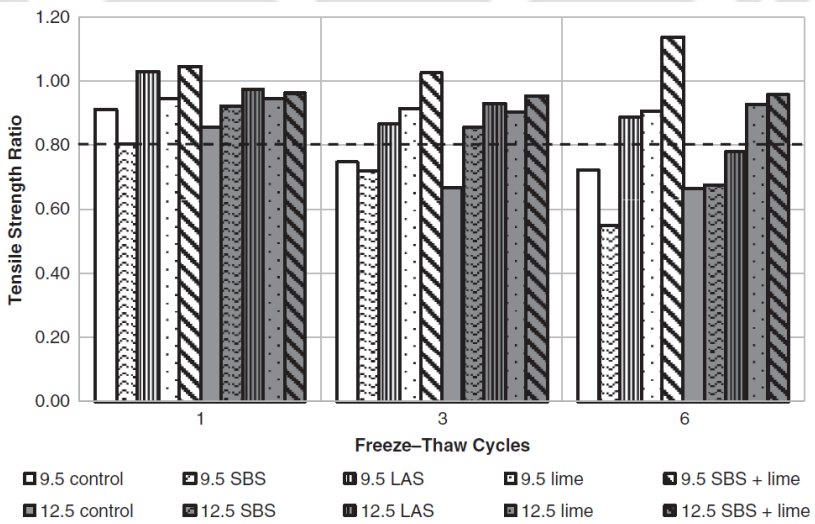

Figure 2.2 TSR results at different F-T cycles (Vargas-Nordcbeck et al., 2016)

Yousif et al. (2018) used a steam cooker to simulated the synergistic effect of aging and moisture on bituminous specimens. Different stages correspond to different numbers of open outlets (stages 1, 2, 3, and 4 represent 2, 1, 3, and 4 open outlets). The authors noticed that the

TSR (as per AASHTO T 283) of the bituminous mixture reduced with an increase in stream aging duration for each stage. The authors also noticed that the mixture's TSR value reduced with the increase in the degree of saturation. The authors recommended a 30 min of steam aging with two outlets opened (stage 1) at 98.8 °C for mimicking the synergistic effect of aging and moisture in the laboratory.

Smith & Howard (2019) compared the tensile strength of laboratory-conditioned specimens with long-term field aged specimens collected from a test section (subjected only to environmental factors). The authors noticed that in terms of the tensile strength of the specimens, 5 days of oven aging at 85 °C was comparable to one to three years of field aging. Compared to unaged specimens, the tensile strength of 5 days oven-aged specimens was 168 kPa higher. When the 5 days aged specimens were further subjected to moisture conditioning (14 days at 64 °C in HWB and 24 h at -22 °C), the tensile strength was only 61 kPa higher than unaged specimens. Thus, aging and moisture conditioning has two opposing effects on the tensile strength of the bituminous mixture.

2.4.2 Application of fracture work and fracture energy

Wen (2013) measured the fatigue cracking in an accelerated load facility subjected to a single-tire of 74 kN load at 19 °C. The author monitored the fatigue cracks appearing at the pavement surface and the associated load repetitions. In addition, cores were collected immediately after construction, and the ITS of the specimens were determined at 19 °C. The authors noticed a good association between the fracture work density (FWD, fracture work by the volume of the specimen) and the number of load repetitions to reach 3 percent fatigue crack.

Zou et al. (2013) subjected bituminous specimens to cyclic pore pressure conditioning (CPPC) using a triaxial cell. In CPPC, bituminous specimens were subjected to 5800 cycles of water pressure ranging from 34.5 kPa to 172.4 kPa. Moisture-conditioned specimens were then soaked for 2 days at 10 °C before testing. The authors noticed that the fracture energy of mixtures reduced with an increase in the aging condition from short-term to long-term aging. The reduction in fracture energy with aging was higher in the case of bituminous mixtures with granite aggregates as compared to limestone aggregate. The fracture energy of mixtures further reduced after subjecting to moisture conditioning. Long-term aged plus CPPC was the most severe condition noticed in their study, which resulted in a 59 % and 18 % reduction in fracture energy of bituminous mixture with granite and limestone aggregate compared to the short-term

aged condition. In addition, the authors found that the fracture energy was more sensitive to the conditions evaluated in their study than the tensile strength of the bituminous mixture.

Similarly, studies noticed that the fracture energy captured the effect of aging and moisture on cracking resistance of bituminous mixture. Saeidi & Aghayan's (2016) study found that aging reduced the fracture energy of the mixture. Whereas, Izadi et al. (2018) noticed that fracture energy of both HMA and WMA mixtures increased with aging. López-Montero & Miró (2016) noticed that moisture conditioning had a minimal impact on the fracture energy of a dense bituminous mixture. These study findings are summarized in Table 2.4.

Table 2.4 Effect of aging and moisture on FE and stiffness

Authors	**Test conditions**	**Findings**
López-Montero & Miró (2016)	Loose mixture oven aging at 85 °C for 7 days. Vacuum saturated specimens (6.7 kPa for 30 min) were placed in an HWB at 40 °C for 72 h.	Aging increases the FE and stiffness of the bituminous mixture. A slight increase in both stiffness and FE of bituminous mixture with MC was noticed. Hot water soaking of the dense bituminous specimen (3 % air voids) with limestone aggregate was insufficient to cause any damage.
Saeidi & Aghayan (2016)	Field cores were collected from the freshly constructed pavement after two and six years of construction.	The authors noticed that the FE of 2 years aged specimen was higher than the FE of a fresh specimen. Insufficient compaction of the bituminous layer during construction may have caused the fresh field cores to have higher air voids and subsequently lower FE than to 2-years. In comparison, the 6-year field aged specimens had considerably lower FE than to 2-year field aged specimens, indicating a reduction in cracking resistance.
Izadi et al. (2018)	AASHTO R30 protocol was followed for long-term aging	The LTA bituminous mixture had higher FE compared to the unaged bituminous mixture. E.g., the RheoFalt modified warm mixture showed a 17 percent increment in FE with aging.

Few researchers have also noticed that fracture energy and fatigue cracking of bituminous mixture are not well co-related. Zhang et al. (2001) noticed that the crack growth rate of bituminous mixtures measured in the laboratory did not correlate with the fracture energy density of the mixtures. Walubita et al. (2013) noticed that the ranking of different bituminous mixtures based on fracture energy was not in agreement with the ranking based on cycles to failure. The authors noticed that with the increase in bitumen content, the peak load

at failure decreases, decreasing the area under the load-displacement curve. However, a bituminous mixture with higher binder content also had relatively higher displacement at failure, and this again increases the area under the load-displacement curve. The two opposing trends in the change in area under the load-displacement curve may compensate for each other. Thus, fracture energy did not capture the effect of change in binder content on the cracking resistance of the bituminous mixture. Table 2.5 summarizes studies showing the association and dissociation between the fracture energy and fatigue life or fatigue cracking of bituminous mixture.

Table 2.5 Correlation of FE and fatigue cracking or fatigue life

Category	Author(s)	Parameters	Remarks
Associated	Wen (2013)	Fracture work density and load repetitions to 3 % fatigue cracking	Fracture work density was highly correlated with 3 % fatigue cracking.
	Bahadori et al. (2015)	Fatigue life and FE	Fatigue life and FE had a correlation of 0.89 to 0.93
	Izadi et al. (2018)	Fracture energy and fatigue life	A correlation (R^2) of 0.80 (approx) was observed between fatigue life and FE
Disassociated	*Zhang et al. (2001)*	Fracture energy density and crack growth rate in bituminous specimens under repeated load	No association between FE and crack growth rate
	Walubita et al. (2013)	FE and fatigue life	The ranking of the bituminous mixture based on FE did not match with the ranking based on fatigue life
	Cao et al. (2019)	Critical fracture energy (CFE) and fatigue life	Poor correlation (R^2=0.30) between CFE and fatigue life

2.4.3 Modulus based parameters

Hasan et al. (2013) studied the effect of the AASHTO R 30 aging process on the resilient modulus and tensile strength of HMA mixture and WMA (Sasobit and Rheofalt) mixtures. The authors noticed that the resilient modulus determined at 25 °C increased for each mixture from unaged to LTA condition. However, the increment in resilient modulus of different mixtures evaluated in the study was comparable. E.g., the control mixture showed a 68 percent increment in resilient modulus with aging. While both warm mixtures, i.e., Sasobit and Rheofalt, showed a 63 percent increment in resilient modulus with aging. Islam & Tarefder (2015) noticed that aging increased the stiffness modulus of the bituminous mixture. The

increment in the stiffness modulus of the bituminous mixture depended on the aging protocol used by the authors. Similarly, Liu et al. (2018) noticed an increase in the complex modulus of mastic specimens with aging. Findings from Islam & Tarefder (2015) and Liu et al. (2018) study is shown in Table 2.6.

Table 2.6 Effect of aging on modulus of bituminous mixture

Authors	Test conditions	Findings
Islam & Tarefder (2015)	Field aging consisted of keeping specimens in the field for 365 days. Laboratory aging: short-term and long-term aging as per AASHTO R30 protocol; specimens maintained at 23 °C inside the laboratory with and without forced air circulation.	The stiffness modulus increased with aging. Laboratory aging found to be severe than field aging. Loose mixture subjected to oven aging resulted in a higher increment of the stiffness modulus than compacted specimens. Stiffness ratio of loose mixture found to increase even after 100 h of aging.
Liu et al. (2018)	Bitumen was aged in an RTFO at a temperature of 163 °C for 30 min, 75 min, 150 min, 225 min, and 300 min for preparing aged mastic specimens	Aging resulted in increased complex modulus and decrease in phase lag which was attributed to increase in asphaltenes.

A bituminous mixture is visco-elastic in nature, and both aging and temperature affect the bituminous mixture's behavior. The effect of aging and a reduction in test temperature on the stiffness bituminous mixture was studied by Botella et al. (2017) using a uniaxial tension-compression strain sweep test. In this study, three types of penetration grade bitumen were used, i.e., 50-70 (unmodified), 35-50 (crumb rubber modified), and 45-80 (SBS modified) for bituminous mixture preparation. Three test temperature, i.e., 10 °C, 3 °C, and -5 °C were used, and the loose bituminous mixture was aged at 85 °C for 7 days in a force draft oven to preparing the LTA specimens. The authors noticed that aging had a higher impact on the complex modulus of the bituminous mixture at lower test temperatures. The LTA bituminous mixtures showed an average increase of 57 %, 51 %, and 43 % in the complex modulus values at 10 °C, 3 °C, and -5 °C, respectively. The authors also noticed that the complex modulus value of unaged bituminous mixtures at 3 °C was comparable to that of aged mixtures at 10 °C. In addition, the authors noticed that a 7 °C reduction in test temperature had the same embrittlement effect on the bituminous mixtures as aging of the mixture.

2.4.4 Parameters developed using a different aspect of the stress-strain curve

Researchers have explored the stress-strain curves to develop new parameters to assess the bituminous mixture's cracking resistance. One such parameter is obtained by normalizing FE with the failure strain. Flexibility Index (FI) is another parameter derived from the Illinois flexibility index test (I-FIT). Here, the fracture energy is normalized by the post-peak slope at the inflection point of the load-displacement curve of the SCB test. A cracking tolerance index (CT_{Index}) utilizes different aspects of the load-displacement curve of the ITS test. A cracking resistance index (CRI) parameter is normalized fracture energy using the peak load. The cracking rate dependency of viscoelastic materials is captured in the rate-dependent cracking index (RDCI) parameter. The application of each parameter to understand a bituminous mixture's behavior under different test conditions is discussed below.

Mehrara & Khodaii (2017) prepared bituminous mixtures using granite and limestone aggregates. One set of specimens were subjected to long-term oven aging at 85 °C for 120 h. Specimens were also subjected to freeze-thaw cycles for moisture conditioning. The authors noticed that aging did not have a significant effect (analysis of variance test, ANOVA) on the FE of the bituminous mixtures. However, both moisture-conditioning and test temperature had a significant effect on the FE of the bituminous mixtures. The authors also noticed that in the case of bituminous mixtures with limestone aggregates, the FE increased with moisture conditioning. This was because moisture-conditioned specimens had higher strain at failure for most cases compared to the dry specimen. A higher failure strain may have compensated for reducing peak load in the moisture-conditioned specimens, resulting in comparable or increased FE with moisture-conditioning than the dry specimens. In this regard, the authors proposed a normalized parameter where the failure strain normalized the fracture energy parameter. The normalized fracture energy of the moisture-conditioned specimens agreed with the stripping noticed in specimens.

Ling et al. (2017) used the FI parameter to evaluate the cracking resistance of bituminous mixtures commonly used in Wisconsin and compared with the fracture energy parameter. Loose bituminous mixtures were subjected to 4 h and 12 h of aging at 135 °C. The authors noticed that the coefficient of variation (CoV) of fracture energy varied from 5 % to 15 %, and FI varied from 8 % to 20 %, respectively. The ANOVA test results showed that aging did not significantly affect the fracture energy but significantly affected post-peak slope and,

therefore, the FI parameter of the mixtures. Aging resulted in an increased post-peak slope and consequently a highly significant reduction in the FI of the bituminous mixtures.

Zhou et al. (2017) proposed a '*cracking test index*' parameter to investigated the sensitivity of the cracking test parameter to reclaimed asphalt pavement (RAP) content, binder type, binder content, and aging duration. The authors noticed that the virgin bituminous mixture's cracking test index was approximately 170, and it was reduced to 40 for the mixture with 20 percent RAP content. Thus, the reduction in cracking resistance of the bituminous mixture with RAP was capture by the parameter. The cracking test index of the bituminous mixture with unmodified PG64-22 binder was 40. In comparison, a bituminous mixture with polymer modified binder showed a higher cracking test index of 80 and 130 for PG64-28 and PG64-32 binder, respectively. Thus, the cracking test parameter captured the positive effect of the polymeric modification. The cracking test index was also sensitive to the change in binder content and air voids.

Further, the authors noticed that the cracking test index reduced with the increase in the aging duration, which indicated a reduction in cracking resistance of bituminous mixtures with aging. For example, the cracking test index of 4 h aged mixture at 135 °C was approximately 360, and 24 h aged mixture at 135 °C aged mixture was 60. In terms of repeatability, the maximum CoV of the cracking test index was 23.5 percent, with most mixtures having a CoV of less than 20 percent. An identical parameter derived from the load-deformation curve of the ITS test and having similar mathematical formulation called the '*cracking tolerance index*, CT_{Index}' is available in ASTM D8225 standard. The CT_{Index} has a similar mathematical formulation with the FI parameter. The CT_{Index} has the potential to substitute the FI parameter since the ITS test is a simple test than the SCB test in terms of sample preparation and requires less time to complete the test.

Kaseer et al. (2018) mentioned a few limitations of the FI parameter. The authors said that no post-peak displacement data is available to calculate the slope parameter for a brittle mixture. Further, in the case of a non-continuous load-displacement curve, accurately determining the inflection point becomes difficult. Hence, The authors proposed the '*CRI*' parameter. The authors explored the sensitivity of CRI and FI to different RAP content and aging conditions. Four aging conditions, i.e., loose mixture aged for 2 h, 1 day, and 2 days at 135 °C, and compacter specimens aged at 85 °C for 5 days. The authors noticed that the bituminous mixtures aged 1 day and 2 days at 135 °C were very brittle, and the FI of the

mixtures could not be determined. However, the CRI successfully ranked mixture with different aging conditions. In terms of the change in RAP content, air voids, and aging level, both CRI and FI results agreed and similarly ranked different mixtures. An increase in the aging or RAP content reduced the CRI and FI parameters, indicating a reduction in the bituminous mixture's cracking resistance. However, the CoV of FI (maximum CoV of approximately 40 %) was relatively higher than the CRI (maximum CoV of about 18 %). In another study, Batioja-Alvarez et al. (2019) also noticed that FI had higher CoV than the CRI parameter. The authors evaluated both laboratories compacted specimens and field cores. The authors noticed that the spread in the boxplot used for representing the CoV of the parameters was much higher in the FI parameter than the CRI parameter.

Nemati et al. (2019) proposed the RDCI parameter to study the cracking resistance of bituminous mixtures. For this purpose, the cumulative work (W_c) as a function of time was used to capture the crack velocity of different bituminous mixtures. A total of 28 different types of bituminous mixtures and aging conditions were used in their study. The authors noticed that the cracking resistance of bituminous mixtures followed a similar trend in terms of FI and RDCI parameters. The ability of RDCI and FI parameter to discriminate the cracking resistance of different mixture was evaluated using a paired *t*-test at 0.05 percent significance level. Paired *t*-test results showed that RDCI discriminated different bituminous mixtures either equally or better as compared to FI. The authors also noticed that the FI parameter had higher CoV compared to the RDCI parameter (as noticed by Kaseer et al., 2018; Batioja-Alvarez et al., 2019).

Sreedhar & Coleri (2020) determined the FI of plant-produced loose bituminous mixture subjected to six different aging levels. The authors noticed that with the increase in aging condition (caused by either an increase in the aging temperature or duration), the FI of the bituminous mixture decreased, indicating lower cracking resistance of the aged bituminous mixture. The authors also noticed that the FI of the bituminous mixture aged at 85 °C for 5 days was almost two times higher than the FI of the bituminous mixture aged at 135 °C for 6 h. Thus, a shorter aging duration at a higher temperature may be ideal for simulating long-term aging in a relatively shorter period.

Thus, researchers have developed and refined different parameters to study the cracking resistance of bituminous mixture from the above discussions. The above-presented parameters also captured the aging and moisture effect on the bituminous mixture cracking resistance. The

mathematical expression of different parameters discussed in section 2.4 is shown in Eq. (2.1) to Eq. (2.10) in Table 2.7.

Table 2.7 Parameters used for assessing the behavior of a bituminous mixture

Expression		Variables	Reference
$S_t = \frac{2000 \times p}{\pi \times t \times D}$	(2.1)	S_t= indirect tensile strength, kPa (termed as ITS in this study) p= maximum load, N t= specimen thickness, mm D= specimen diameter, mm	ASTM D6931
$TSR = \left(\frac{S_{tm}}{S_{td}}\right) \times 100$	(2.2)	TSR= tensile strength ratio, % S_{tm} = average ITS of MC subset, kPa S_{td} = average ITS of dry subset, kPa	ASTM D4867
$W_f = \int_0^u F.du$	(2.3)	W_f= fracture work, J u= load line displacement, mm, F= load, kN.	ASTM D8225
$FWD = \frac{W_f}{volume\ of\ specimen}$	(2.4)	FWD= fracture work density, J/m^3	Wen (2013)
$FE = \frac{W_f}{D \times t} \times 10^6$	(2.5)	FE= fracture energy, J/m^2 D = specimen diameter, mm, t = specimen thickness, mm	ASTM D8225
$FI = A \times \frac{G_f}{\lvert m \rvert}$	(2.6)	FI= flexibility index, G_f= fracture energy, J/m^2 A= calibration coefficient (0.01), $\lvert m \rvert$= slope at the inflection point	Ling et al. (2017)
$CRI = \frac{G_f}{P_{max}}$	(2.7)	CRI= cracking resistance index, G_f= fracture energy, J/m^2, P_{max}= peak load, kN	Kaseer et al. (2018)
$CT_{Index} = \frac{t}{62} \times \frac{l_{75}}{D} \times \frac{G_f}{\lvert m_{75} \rvert}$ $\lvert m_{75} \rvert = \left\lvert \frac{P_{85} - P_{65}}{l_{85} - l_{65}} \right\rvert$	(2.8) (2.9)	CT_{Index}= cracking tolerance index, t= thickness of the specimen, mm, l_{65}, l_{75}, l_{85}= displacement corresponding to 65, 75, and 85 percent of peak load at the post-peak region, mm, P_{65}, p_{85}=65 and 85 percent of peak load, kN, D= diameter of the specimen, mm, m_{75}= slope, N/m.	ASTM D8225
$RDCI = \frac{\int_{t_{peak}}^{t_{0.1}} W_c\, dt}{P_{t_{peak}} \times ligament\ area} \times C$	(2.10)	$RDCI$= rate-dependent cracking index, s^2/m^2, W_c= cumulative area under the cumulative work versus time curve in the post-peak region, J, $P_{t_{peak}}$=instantaneous power at peak force, J/s, $t_{0.1}$, t_{peak}=time at 10 percent and peak load, s, C= unit correction factor set to 0.01	Nemati et al. (2019)

2.5 Adhesive failure in a bituminous mixture

The bond strength between aggregate and bituminous binder governs the strength and stability of the mixture. In the presence of moisture, the bond strength between aggregate and bitumen becomes even more vital. The bituminous mixture's moisture damage is classified either as an adhesive or cohesive failure of the mixture on a micro-level. Adhesive failure occurs at the bitumen-aggregate interface when the bituminous binder is de-bonded or stripped from the aggregate surface. Cohesive failure occurs within the mastic where the bulk of the bitumen flow, tear or is weakened, leading to reduced bituminous mixture's stiffness (Stuart 1990; Little & Jones 2003).

The failure surface noticed by Canestrari et al. (2010) on the aggregate substrate in pneumatic adhesion tensile testing instrument is shown in Figure 2.3. The failure surface may not be purely adhesive or cohesive, and adhesive-cohesive failure may be present, as seen in Figure 2.3 (c). The authors said that if the aggregate surface remains wholly coated with the binder, a cohesive failure occurs inside the bitumen film (Figure 2.3 (a)). When the aggregate surface is clean, adhesive failure has happened at the aggregate-bitumen interface (Figure 2.3 (b)). When the aggregate surface is partially coated with bitumen, a cohesive-adhesive type of loss has occurred (Figure 2.3 (c)). Stripping of the bituminous mixture is distress in bituminous pavement associated with moisture damage. Stuart (1990) defined stripping as "*the displacement of asphalt film from aggregate surfaces that occurs when the aggregate has a greater affinity for water than asphalt*." Studies associated with laboratory assessment of moisture susceptibility of bituminous mixture use both terminologies, i.e., "adhesive failure" and "stripping" interchangeably.

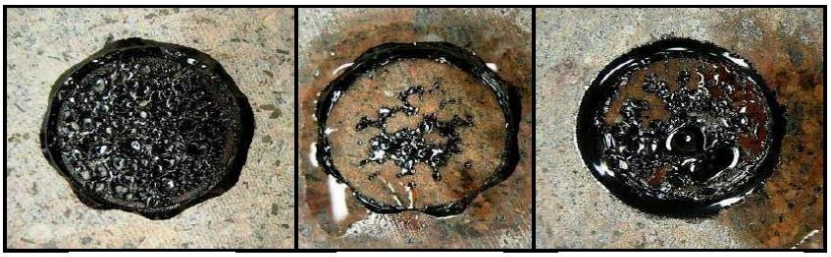

Figure 2.3 Type of failure from a pull-off test (Canestrari et al., 2010)

The bond strength between aggregate and bituminous binder can be determined using a pull-off test. The pull-off test is also known as the bitumen bond strength (BBS) test and pneumatic adhesion tensile testing instrument (PATTI) test. In a pull-off test, the bituminous binder is sandwiched between an aggregate substrate and a metallic pull-stub, and the stub is pulled until failure. Failure occurs when the adhesive strength between aggregate and bitumen or the cohesive strength of bitumen is exceeded. The pull-off tensile strength or bond strength at failure is recorded. In addition, the bond strength of the dry specimen is compared with the bond strength of the moisture-conditioned specimen to quantify the detrimental effect of moisture on the bituminous mixture.

2.5.1 Effect of aging on adhesive failure

Few studies have documented the effect of aging on the adhesive failure of bituminous mixtures. Aguiar-Moya et al. (2015) studied aging's effect on the adhesive bond strength of different aggregate-bitumen combinations using a BBS test. Das et al. (2015) studied the topography of a bitumen subjected to different aging duration using atomic force microscopy (AFM) to quantify the microstructure change with an increase in aging duration. Yuan et al. (2020) studied aging's effect on the adhesive bond strength (BBS test) between one aggregate (basalt) and four different binders subjected to short-term aging (RTFO) and long-term aging (PAV). The results of these studies are summarized in Table 2.8.

Table 2.8 Effect of aging and moisture on adhesive failure

Authors	**Test conditions**	**Findings**
Aguiar-Moya et al. (2015)	RTFO and PAV aging. Specimens were immersed in a water bath at 40 °C for 48 h for MC.	Predominant cohesive failure was noticed in unaged and dry conditions. Adhesion failure was influenced with aggregate type. PAV aged binder had higher AF compared to unaged bitumen. Long-term aging could result in higher AF.
Das et al. (2015)	Bitumen was exposed to air and UV light for 15 and 30 days. The specimens subjected to 30 days of air and UV light aging were	Aging results in reduction of bitumen microstructure. The aging mechanism in a bituminous mixture produces polar products which are soluble in water. Water can dissolve the polar products and remove the polar products from the surface. The bitumen film thickness could reduce with time, and the severity of moisture damage might increase.

Authors	Test conditions	Findings
	MC by washing in distilled water for 5 min.	
Yuan et al. (2020)	PEN 30, PEN 50, PEN 70, and PEN 90 subjected to RTFO and PAV aging	The authors noticed that moderate aging (short-term aging) might contribute to the aggregate-bitumen bond strength. It was also found that severe aging (long-term aging) might not increase the aggregate-bitumen bond strength.

2.5.2 Effect of moisture on adhesive failure

Kanitpong & Bahia (2005) conducted a PATTI test using two aggregates (limestone and granite) and 13 different bitumen types, including neat and modified binders. Binder modification consisted of the application of anti-stripping agents, polymers, air blowing, and chemical treatment. Moisture conditioning was done by submerging specimens in moisture for 24 h at 25 °C and tested at the same temperature. It was noticed that the pull-off strength of specimens with granite aggregate in the dry state was more than specimens with limestone aggregate. The pull-off strength was reduced with moisture conditioning for specimens with both types of aggregate. However, the reduction in pull-off strength was relatively higher in specimens with granite aggregate when compared to limestone aggregate. The failure surface of the specimens revealed a cohesive failure in the dry state. In contrast, failure occurred at the aggregate-bitumen interface (adhesive failure) in the moisture-conditioned specimens. Thus, moisture conditioning transformed the failure type of the specimens, i.e., from cohesive failure to adhesive failure.

Canestrari et al. (2010) used a PATTI test to determine moisture's effect on the aggregate-bitumen bond strength. The authors used two aggregate types (limestone and porphyry) and six different bituminous binders (two unmodified and four modified binders). Specimens were immersed in a distilled water bath at 25 °C and 40 °C for 24 h for moisture-conditioning. The authors noticed that specimens with porphyry aggregates underwent pure adhesive with bond strength in the range of 500 kPa to 1100 kPa. All the specimens tested in dry conditions had a pure cohesive failure. The bond strength associated with pure cohesive failure was between 1200 kPa to 3700 kPa. The authors also noticed a cohesive-adhesive loss

in specimens with both sources of aggregates. In cohesive-adhesive failure, the specimens with limestone aggregates had higher bond strength than porphyry aggregates. The authors suggested a bond strength of 1100 kPa as the limit to separate adhesive failure from cohesive failure.

Apeagyei et al. (2014) sandwiched a 3 mm thick bitumen mastic between two aggregate substrates to conduct a pull-off test at 20 °C. The authors carried out moisture conditioning (1 and 7 days) by submerging the lower aggregate substrate in moisture at 20 °C such that the top 1 to 2 mm of the substrate was exposed to air. The authors used limestone and granite aggregates with one unmodified bitumen (penetration grade 40/60) for mastic and substrate specimen preparation. It was noticed that after 168 h of moisture conditioning, mastics with granite aggregates retained about 10 % of the dry fracture energy. In comparison, mastic with limestone aggregate retained about 80 to 100 % of the dry fracture energy for the same duration of moisture conditioning. The authors also noticed a cohesive-adhesive failure in the dry specimens. Whereas, in the presence of moisture, specimens with granite mastic showed an apparent adhesive failure with complete debonding of mastic from the wet aggregate substrate. On the other hand, no debonding was noticed in the specimens with limestone mastic.

Cui et al. (2014) used a peel test where a peel arm (a flexible aluminum arm of 0.2 mm thickness) is bonded to an aggregate substrate using bitumen as adhesive. The authors used four different types of aggregates (limestone, marble, and two granite aggregates types) and one unmodified binder (penetration grade 40/60) for specimen preparation. Specimens were submerged in distilled water at 20 °C for ten days for moisture-conditioning and tested at 20 °C. The authors noticed a cohesive failure in all specimens tested in dry condition with fracture energy in the range of 540 to 710 J/m^2. The failure surface transformed from cohesive to interfacial (adhesive) in moisture-conditioned specimens. It was noticed that after 7 days of moisture conditioning, specimens with the limestone and marble aggregates had retained 27 % and 96 % of their dry strength. In contrast, specimens with the two granite aggregates retained only 11 % and 5 % of their dry strength after 7 days of moisture conditioning. The basic aggregates (limestone and marble) provided higher resistance against moisture damage than acidic aggregates (granite). Thus, the type of aggregate has an impact on the adhesive and cohesive failure of the bituminous mixture. The effect of aggregate mineralogy on the moisture susceptibility of the bituminous mixture was explained by Abo-Qudais & Al-Shweily (2007), as discussed next.

Abo-Qudais & Al-Shweily (2007) said that limestone and basalt predominantly contain $CaCO_3$ and Al_2O_3 compounds, with basalt having relatively higher silica content than limestone. The SiO_2 content in mineral aggregate is responsible for reducing the bond strength between aggregate and bituminous binder. Further, the positively charged limestone aggregate forms a stronger bond with a bituminous binder (hydrophobic). Basalt, on the other hand, due to the mixed charge present, is hydrophilic in nature.

Zhang et al. (2015) used the PATTI test, peel test, and pull-off test (bitumen sandwiched between two aggregate substrates) to study the effect of moisture on aggregate-bitumen bond strength and evolvement of the failure surface with moisture-conditioning. Two unmodified bituminous binders' types (penetration grade of 40/60 and 70/100) and four aggregate types (two limestones and two granite) were used, and the tests were conducted at 20 °C. Specimens were submerged in moisture at 20 °C for 7 and 14 days for moisture conditioning. All three tests showed similar results in terms of bond strength and failure surface with different specimens. In the case of dry specimens, the effect of aggregate type on the bond strength was minimal, and the bond strength was governed by the stiffness (grade) of the bitumen. This was because, in dry specimens, a cohesive failure occurred within the bulk of the bitumen. Moisture conditioning reduced the aggregate-bitumen bond strength of the specimens in each type of test and transformed the failure surface from cohesive to adhesive failure. The authors noticed that minerals such as arealbite, quartz, k-feldspar, anorthite, and clay increased the moisture susceptibility, while calcite reduced the moisture susceptibility of the bituminous mixture.

It is evident from the above studies that moisture damages the adhesive bond strength of aggregate and bitumen. Furthermore, moisture also transforms the failure surface from cohesive failure to adhesive failure (Cui et al., 2014; Zhang et al., 2015). Thus, the effect of moisture on aggregate-bitumen adhesion can be determined by examining the failure surface of the tested specimen. In this regard, an image processing and analysis tool was used by researchers to quantify the adhesive failure in moisture-conditioned specimens. Image analysis can help to assess the moisture susceptibility of the different bituminous mixture and ascertain the compatibility between different bitumen and aggregate combinations. The advantage of image analysis is that it removes the subjective nature of visual estimation to quantify adhesive failure in the tested specimen. Notably, the association between adhesive failure and different attributes of a bituminous mixture can be further evaluated. A brief discussion of different

image analysis techniques implemented by the researcher to determine the adhesive failure in the bituminous mixture is discussed next.

2.5.3 Application of image analysis to quantify adhesive failure

Merusi et al. (2010) using image analysis to determine the effects of synthetic wax on the stripping of loose bituminous mixtures subjected to boiling water test. The authors classified the surface of moisture conditioned specimen into bitumen covered and stripped surface by using the principal component analysis (PCA) of the red, green, and blue (RGB) radiometric band. The PCA transformed the RGB space into a new image with just one band (intensity). The low-intensity value represents a bitumen-covered area, and the high-intensity values represent the stripped area. Then, image segmentation was performed by selecting a threshold value to quantify the bitumen covered area and stripped area. This process is also known as image classification, where low-intensity pixels are assigned one class, and the higher intensity pixels are assigned to another class. It was noticed that the percent stripping in bituminous mixtures with wax modification was less than the mixture with base bitumen. For example, a bituminous mixture with limestone aggregates and base binder (50/70 penetration grade) showed a 20 % stripping. In comparison, the percent stripping of the same bituminous mixture modified with F-T synthesis wax only 6 %, and for refined fossil wax was 3.2 %, respectively.

Xie et al. (2012) performed image segmentation using a threshold value to identify the percent stripped area present in the fracture face of the bituminous specimens subjected to a direct tension test. The authors assigned low-intensity pixels (bitumen covered area) to one class, i.e., class 0, and high-intensity pixels (stripped area) to another class, i.e., class 1. The authors noticed that temperature had a major influence on the type of failure observed on the fracture surface of the specimens. Specimens tested at 15 °C predominantly had higher adhesive failure as compared to specimens tested at 25 °C. For example, for one type of mixture, the adhesive failure increased from 43 % at 25 °C to 89 % at 15 °C. The authors also noticed an increase in adhesive failure with the increase in strain rate from 0.1 mm/min to 18 mm/min. Thus, the effect of test temperature and loading rate on the adhesive failure of a bituminous mixture can be determined using the image analysis technique.

Lee et al. (2013) presented an elaborate process for determining the stripping in moisture-conditioned bituminous specimens subjected to cyclic direct tension test. Adobe

Photoshop and MATLAB program was used for determining the threshold value and stripping in bituminous specimens. First, in Adobe Photoshop, the cells associated with stripped areas of the image were manually identified and selected. This process is time-consuming and operator-sensitive. The authors used the count function of Adobe Photoshop to determine the percent stripped area of the image. Next, the image was imported to MATLAB and converted into a greyscale image. The threshold value required to segment the greyscale image into a stripped and non-stripped area (cohesive failure region) was determined in MATLAB. This was done by matching the percent stripped area previously determined in Adobe Photoshop and the percent stripped area calculated in MATLAB using different threshold values. In their study, a threshold value of 63 successfully separated the stripped area from the non-stripped area, as shown in Figure 2.4. The authors noticed that percent stripping had a negative relation with predicted fatigue life (R^2 = 0.99) and fatigue life ratio (R^2 = 0.74). Thus, stripping in a moisture-conditioned bituminous mixture may be responsible for reducing the mixture's fatigue life.

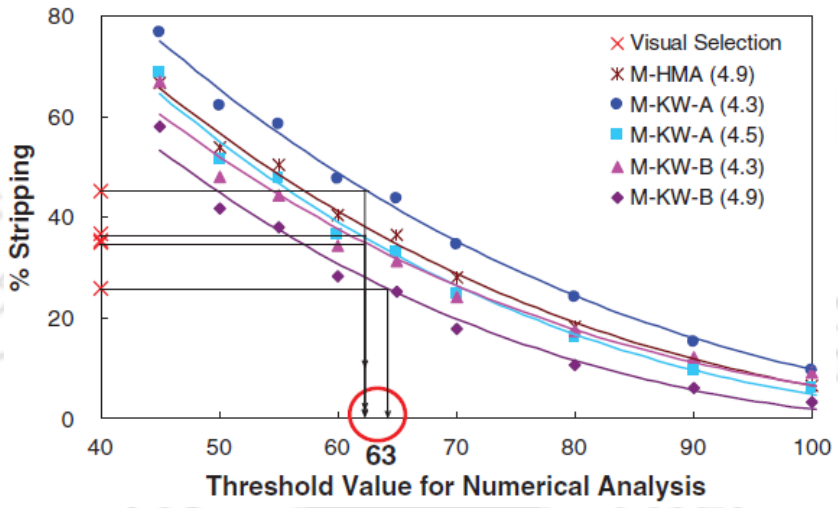

Figure 2.4 Determination of threshold value (Lee et al., 2013)

Lee & Kim (2014) used the same image analysis approach proposed by Lee et al. (2013) to determine the stripping associated with moisture-conditioned specimens of ITS tests, HWTT, and cyclic direct tension (CDT) test. For ITS and CDT, moisture conditioning was carried out by subjecting the saturated specimen (65 % to 80 %) in a HWB at 60 °C for 24 h. While specimen submerged in water at 50 °C was tested in the HWTT test. The authors noticed that the threshold value of 68 for ITS, 85 for HWTT, and 63 for CDT could separate the stripped area present in the test specimen surface from the non-stripped area. The HWTT resulted in

relatively higher stripping in bituminous mixtures, followed by the CDT test and then the ITS test. Also, the HMA mixture had a lower percent stripping value than the WMA mixtures for most cases. It was also noticed that percent stripping determined from ITS had a correlation of R^2 = 0.42 with TSR. Stripping was able to adequately differentiate between various test methods and bituminous mixtures used in their study. Thus, stripping in bituminous mixtures is sensitive to different test methods and types of mixture.

Amelian et al. (2014) used Image pro Plus software to perform image segmentation, detection, and background elimination of the images of bituminous mixtures subjected to boiling water tests. Next, the authors used Image toll software to transform the color image into an 8-bit greyscale image. A threshold value of 65 was used to separate the percent stripped area for the images' total pixel area. The authors noticed that percent stripping identified the moisture susceptibility of different types of bituminous mixtures, the presence of hydrated lime, and the application of Zycosoil warm mix additive, as shown in Table 2.9. Bituminous mixture with limestone aggregate had higher resistance to stripping when compared to Andesite, Quartzite, and Granite. The resistance to stripping of different mixtures also improved with the application of hydrated lime and Zycosoil antistripping agents, as presented in Table 2.9. It was concluded that the image analysis technique was able to objectively quantify stripping in the bituminous mixture as compared to the subjective rating method of quantifying stripping in boiling water test. The authors noticed a correlation of R^2 = 0.90 between stripping obtained from image analysis of boiling water test and stripping present on the fracture face of bituminous specimens subjected to ITS test.

Table 2.9 Results of boiling water test (Amelian et al., 2014)

Mixture type	**Stripping, %**					
	No additive		**Hydrated lime**		**Zycosoil**	
	Average	**SD**	**Average**	**SD***	**Average**	**SD**
Quartzite	40.3	3.37	3.5	0.21	1.4	1.25
Granite	15.8	0.98	1.43	0.1	1.37	0.07
Andesite	86.5	7.2	1.39	0.11	0.82	0.06
Limestone	1.6	0.05	–	–	–	–
Slag–limestone	1.3	0.03	–	–	–	–

*Standard deviation

Hamzah et al. (2014) performed image analysis using MATLAB and Environment for Visualizing Images (ENVI) software to determine the adhesive failure present on the fracture face of bituminous specimens subjected to direct tension test. One and three freeze-thaw cycles

as per ASTM D4867 were used for moisture conditioning. First, image transformation was done using the color transformation function and color lookup tables of MATLAB. Next, two regions of interest (ROI), i.e., stripped and broken aggregates, were identified using ENVI software. Image classification using maximum likelihood and minimum distance method was carried out to calculate the percent adhesive failure present in the tested specimens. The authors noticed that the bituminous mixture with PG 76-grade bitumen had a lower adhesive failure when compared to the mixture with PG 64-grade bitumen. The SBS modifiers used in PG 76 bitumen enhanced the adhesive property at a low-test temperature of 15 °C as compared to unmodified PG 64-grade bitumen. The authors also noticed an increase in adhesive failure with the increase in freeze-thaw cycles for different mixtures evaluated.

Hamzah et al. (2017) used a three-dimensional (3D) imaging technique to quantify the adhesive failure in moisture-conditioned bituminous specimens subjected to a direct tension test at 5 °C, 15 °C, and 25 °C. One freeze-thaw cycle of moisture conditioning was used as per ASTM D4867. The authors captured images of the fractured face of the specimen and generated a 3D model using Autodesk 123-D Catch software. Next, the 3D model was imported into cloud Compare software for further analysis. The RGB model was transformed into a greyscale model, and segmentation was done using a threshold value. Statistical test results showed that mixing temperature and test temperatures significantly affected the adhesive failure of the bituminous specimens. In general, a bituminous mixture produced at higher temperatures had a lower adhesive failure and vice-versa. Also, as the test temperature reduced from 25 °C to 15 °C and 15 °C to 5 °C, the adhesive failure in bituminous mixtures increased. For instance, the percent adhesive failure in specimens with for PG 64 bitumen produced at 120 °C was 16 %, 23 %, and 25 % at 25 °C, 15 °C, and 5 °C, respectively. The authors said that temperature had a substantial impact on the fracture mode of the bituminous mixture.

Zhang et al. (2017) used Image J software to determine the retained bitumen coating (cohesive surface) on the surface of pull-off test specimens subjected to different durations of moisture conditioning. Test specimens were submerged in water at 20 °C for 24 h and 168 h for moisture conditioning. It can be noticed from Figure 2.5 that the retained cohesive surface on limestone (L1) aggregate with both types of bitumen (B1, 40/60 pen and B2, 70/100 pen) was higher as compared to the retained cohesive surface present on the granite aggregates (G1 and G2). The difference in the retained cohesive surface was noticeably higher at 168 h of

moisture conditioning (Figure 2.5). Also, with the increment in conditioning time, the failure surface of the specimens transformed from cohesive to cohesive/adhesive or adhesive failure.

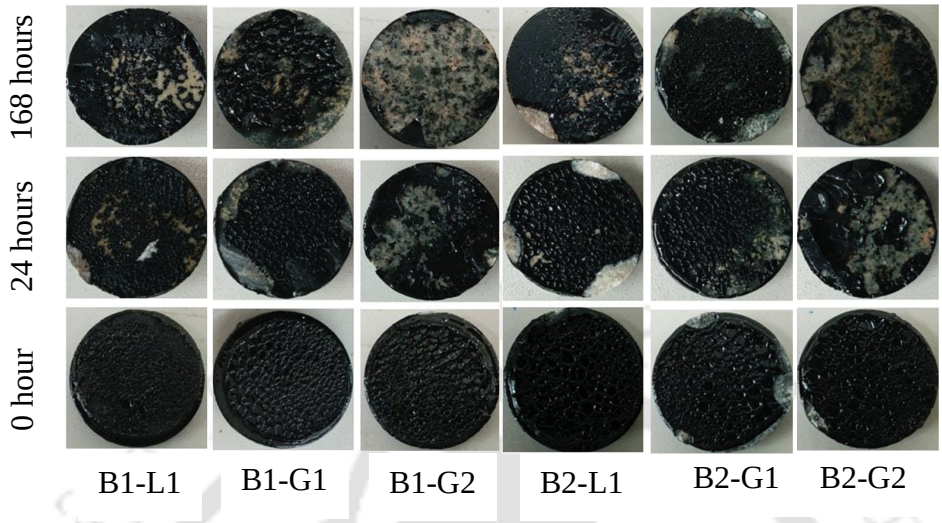

Figure 2.5 Retained cohesive surface after moisture conditioning (Zhang et al., 2017)

Thus, from the above studies, it is understood that adhesive failure can identify moisture susceptible bituminous mixture. Furthermore, adhesive failure was sensitive to different bituminous mixtures, test methods, and test conditions. The factors influencing adhesive failure are listed below.

Factors affecting aggregate-bitumen adhesion in a bituminous mixture are:

- Type of aggregates (Cui et al., 2014; Zhang et al., 2017)
- Type of bitumen and presence of additive (Merusi et al., 2010; Hamzah et al., 2014)
- Production temperature and test temperature (Xie et al., 2012; Hamzah et al., 2017)
- Duration of moisture conditioning (Hamzah et al., 2014; Zhang et al., 2017)
- Test method and production process (Hamzah et al., 2014; Lee & Kim, 2014)

A summary of the literature associated with adhesive failure measurements in a bituminous mixture using image analysis is presented in Table 2.10.

Table 2.10 Image analysis for quantifying adhesive failure in the bituminous mixture

Authors	Type of test (specification)	Moisture conditioning method	Findings*
Merusi et al. (2010)	Loose mixture (EN 12697-11: 2006)	Loose bituminous mixture boiled for 30 minutes in 1250 ml of distilled water in a 2000 ml beaker	The uncoated aggregate surface was lower (2.7 % to 6.3 %) in the mixture with synthetic wax modified binder compared to the mixture with the base binder (17.4 % to 20.4 %).
Xie et al. (2012)	Direct tension test	Not subjected to moisture conditioning	A decrease in the test temperature from 25 °C to 15 °C resulted in an increase in the average value of AF from 43 % at 25 °C to 89 % at 15 °C.
Lee et al. (2013)	Direct tension test	AASHTO T 283	Stripping of the bituminous mixture had a strong association with the fatigue life ratio (R^2 of 0.74) and the predicted fatigue life (R^2 of 0.99).
Amelian et al. (2014)	Boiling water test (ASTM D3625)	250 g of the loose bituminous mixture at 85 to 95 °C was placed in 800 ml distilled boiling water for 10 minutes	Limestone (1.6 %) and slag-limestone (1.3 %) offered higher resistance against moisture damage. Granite mixture had moderate (15.8 %), and quartzite (40.3 %), and andesite (86.5 %) mixture had the least resistance. Percent stripping (ranging from 1.3 to 40.3 %) had an R^2 of 0.70 to 0.93 with the dynamic modulus reduction ratio and an R^2 of 0.38 to 0.58 with retained Marshall stability ratio.
Hamzah, Kakar et al. (2014)	Direct tension test	Vacuum saturated (55 % to 80 %) specimens subjected to FT cycle (16 h at -18 °C and 24 h at 60 °C)	Adhesion failure increased with an increase in moisture conditioning from 1FT to 3FT. HMA mixture had a lower AF compared to the WMA mixture.
Lee & Kim (2014)	ITS, cyclic direct tension test, and HWTT.	AASHTO T 283, saturated specimens (65 % to 80 %)	Recommended percent stripping and aggregate breakage ratio as improved moisture susceptibility parameters compared to TSR of

Authors	Type of test (specification)	Moisture conditioning method	Findings*
		subjected to 60 °C for 24 h, AASHTO T324	the mixture. TSR had an R^2 of 0.42, with percent stripping (from 5 to 25 %).
Hamzah et al. (2017)	Direct tension test	Vacuum saturated (55 % to 80 % in sodium carbonate solution) specimens in subjected to FT cycle (16 h at -18 °C and 24 h at 60 °C)	A reduction in test temperature increased AF. E.g., bituminous mixture with PG-64 binder produced at 120 °C had 16.37 %, 23.05 %, and 25.43 % AF at 25 °C, 15 °C, and 5 °C. Also, a bituminous mixture with higher stiffness had higher AF compared to the mixture with lower stiffness.
Zhang et al. (2017)	Pull-off tensile test	Specimens submerged in water at 20 °C for 24 h and 168 h	Moisture conditioning transformed the failure surface transformed from cohesive to cohesive-adhesive or adhesive, along with a significant reduction in retained tensile strength.
Júnior et al. (2019)	Loose coated aggregates	500 g of loose bituminous mixture submerged at 40 °C for 72 h	Granite aggregates had a higher retained binder (55 %) after moisture conditioning when compared to phonolitic aggregates (30 %).

*value in parenthesis indicated percent stripping or adhesive failure

Thus, from Table 2.10, it can be noticed that researchers have explored image analysis techniques to measure the adhesive failure in the bituminous mixture using different test setups and a wide range of test conditions. Thus, the image analysis technique would help demarcate the effect of different mixture ingredients and test conditions such as temperature, aging, etc.

2.6 Fatigue resistance of the bituminous mixture

Fatigue cracks in the bituminous pavement are distress occurring as interconnected cracks due to repeated vehicular load application. The integrity of bituminous pavement deteriorates with the propagation of fatigue cracks. Crack initiation and crack propagation in materials follow the underlying principles of fracture mechanics. Thus, the fatigue cracking process can be explained with the help of the fracture mechanics approach. According to fracture mechanics, the externally applied load or stress is not uniformly distributed in the body. Due to pre-existing discontinuity, such as internal cracks or notches within the body, the notch acts as a point of stress concentration. The crack growth occurs when enough potential energy is available to overcome the material's surface energy.

In the process of crack formation, the body's potential energy reduces because of the release of stored elastic energy and the work done by the external load. Simultaneously, the body's surface energy increases due to the formation of a new cracked surface, and the energy balance in the body is achieved. Fatigue crack propagation can be described using Paris' law, as shown in Eq. (2.11) (Anderson, 2017). The crack propagation or fracture in a body can occur in three modes. These modes are designated as mode I, mode II, and mode III. In mode I or opening mode of fracture, the fracture plane is perpendicular to the normal force. Mode II or in-plane shear fracture occurs under the action of shear stress, with the fracture propagating in the direction of shear. Mode III or out-of-plane shear fracture is also a shear fracture, but the fracture propagates perpendicular to the shear direction.

$$\frac{dc}{dN} = A \times (\Delta K)^n \tag{2.11}$$

where,

c= crack length,

N= number of loading cycles,

A, n= fracture parameters, and,

ΔK= stress intensity factor (SIF).

2.6.1 Effect of aging

Bhasin et al. (2007) studied the surface free energy to determine the cohesion of the bituminous binders. Bitumen was obtained from different sources and subjected to polymeric modifications (SBS and tire rubber). Two levels of aging were used, i.e., a stirred airflow test (SAFT) was used for short-term aging, and PAV for long-term aging. The authors noticed that, in general, cohesion decreases with short-term and long-term aging when compared to the unaged bitumen. In the case of long-term aged bitumen, five out of the eight bitumen showed a reduction in the work of cohesion. The lower work of cohesion implies that crack propagation would require less work leading to an earlier fracture. This study's findings indicate that the cracking resistance of bituminous mixture may reduce with long-term aging.

Zhu et al. (2009) compared the bituminous mixture's fatigue life subjected to laboratory aging and the natural aging process. AASHTO R30 specification was used for preparing the STA and LTA bituminous mixture. The STA bituminous mixture was compacted, and specimens were placed outdoors for 3, 6, and 9 months to prepare the naturally aged bituminous specimens. A four-point beam bending test was carried out in a strain-controlled mode (200, 300, 500, 700, 900, 1100, and 1300 με) at 15 °C to determine the effect of different aging levels on fatigue life of the bituminous mixture. The authors noticed that at lower strain levels, the STA and unaged bituminous mixture had a much higher fatigue life than LTA and naturally aged mixture. However, at a higher strain level, the fatigue life at different aging levels was comparable, except for LTA bituminous mixture. Thus, with the increase in strain level, the effect of aging on the fatigue life of the bituminous mixture was less noticeable. The authors also measured the cumulative dissipated energy (W_f) of the bituminous mixtures and established fatigue life (N_f) and W_f relations ($N_f = A \times (W_f)^Z$) at different aging levels. The Z parameter signifies the crack growth rate for a condition. The authors noticed that the value of Z increased from unaged (Z =1.00) to STA (Z =1.46) and LTA (Z =1.68) conditions. Whereas the 3, 6, and 9 months aged bituminous mixtures had a Z value of 1.65, 1.80, and 1.86, respectively. Thus, with an increase in the aging level, resistance to crack propagation is also reduced, which reduces fatigue life.

Baek et al. (2012) used a simplified viscoelastic continuum damage approach to construct the damage characteristics of the unaged and aged bituminous mixture. The authors noticed that for the same value of accumulated damage (S), the integrity of the bituminous mixture (the pseudostiffness, C) increased with the increase in the level of aging. Thus, the

bituminous mixture is failing with less evolved damage conditions (less tolerance to damage). The authors also noticed that aging was more noticeable at 19 °C compared to 5 °C and said that the bituminous mixture becomes brittle enough to mitigate the effect of aging at low temperatures.

Arega et al. (2013) compared the fatigue life of five different bituminous mixtures to quantify the relative change in fatigue life with aging. The fatigue life was determined using a dynamic mechanical analysis (DMA) test on the fine aggregate matrix (FAM) specimens at a stress amplitude of 275 kPa. Four WMA mixtures (Sasobit, Advera, Evotherm 3G, and Rediset WMX) and one control HMA mixture was used. The loose bituminous mixture was subjected to oven aging for 4 h at compaction temperature for short-term aging, and compacted FAM specimens were aged for 30 days at 60 °C for long-term aging. The authors noticed that short-term and long-term aged specimens' fatigue life was well related. Furthermore, the relative fatigue cracking resistance of the short-term aged bituminous mixture was comparable with the long-term aged mixture. Thus, to determine the relative fatigue cracking resistance of different bituminous mixtures, short-term aged specimens can be utilized.

A bituminous binder reacts with the oxygen present in the atmosphere to undergo aging. Hernández Noguera et al. (2014) studied the effect of oxygen atoms present in the moisture on a bituminous binder's aging behavior. The authors immersed 2 mm thick sheets of bitumen (penetration grade of 80-100, B1 and 60-70, B2) in distilled water for 12 months. After 12 months of immersion, the authors noticed that the penetration value decreased by 26 % and 34 % for B1 and B2 bitumen. Similarly, an increase in the softening point value and viscosity values was noticed by the authors. The rheological test showed that the shear modulus of bitumen immersed in water for 12 months had a 15 % and 5 % increase in the shear modulus for B1 and B2 bitumen with a decrease in phase angle. In the oxidation process, the oxygen molecules react with bitumen and increase the asphaltenes content. As a result, the bituminous binders’ stiffness increases and offers a higher resistance to flow. From the fractional analysis of bitumen, the authors noticed an increase in the asphaltenes content and a reduction in the aromatics, saturates, and resins content for both types of bitumen after 12 months of immersion in water. A reduction in the ratio between the aromatics and the saturates (*Ar/S*), and the ratio between the resins and the asphaltenes (R/A) denotes the bituminous binder's aging. The authors noticed a reduction of both ratios with 12 months of immersion in water. e.g., in the

case of B2 bitumen, *Ar/S* reduced from 2.61 to 2.57, and *R/A* reduced from 2.67 to 1.41 with 12 months of immersion in water.

Gao et al. (2017) investigated the effect of different aging levels on the bituminous mixtures' fatigue life at 15 °C. An indirect tensile fatigue test (ITFT) was used at a stress level of 0.7 MPa and 10 Hz frequency. The loose bituminous mixture was aged in an oven at 163 °C for 2 h, 4 h, 8 h, 16 h, and 24 h. The authors noticed that the fatigue life of the bituminous mixture increases with the increase in aging time. For e.g., the fatigue life of 8 h, 16 h, and 24 h aged bituminous mixture was approximately 2.2, 2.8, and 3.5 higher than that of the unaged mixture. Aging increases the modulus of the bituminous mixture, which increases the fatigue life of aged specimens in a stress-controlled fatigue test. Further, to study the effect of climate and loading, the elastic modulus of bituminous mixture aged to different levels and subjected to different loading levels (simulated by applying fatigue loading cycles corresponding to 20 % to 80 % of the average fatigue life) was determined. The authors noticed that although both the loading cycle and aging time influenced the elastic modulus of the bituminous mixture, the effect of aging was substantially higher than loading cycles. E.g., the increase in elastic modulus from 2 h to 24 h of aging was more than 60 %, while it changes less than 15 % when the loading repetitions change from 0 % to 80 % of the fatigue life.

Moreno-Navarro et al. (2018) studied the effect of aging on the bituminous binder and compacted specimens. The aged binder (RTFO plus PAV aged) showed a considerably higher complex modulus than the unaged binder. With aging, the ratio of asphaltenes to maltene increases, and the complex modulus of the bituminous binder also increases. The effect of aging on the binder's complex modulus was noticed to be higher at a higher temperature. As the temperature increases, the consistency of lower molecular weight maltene reduces, and asphaltenes govern the bituminous binder's mechanical response. Since aging increases the asphaltene content in the bituminous binder, the effect is more pronounced compared to a lower temperature. In addition to the binder test, compacted specimens were also aged 8 days at 90 °C in an oven and compared with unaged specimens. The authors noticed that micro-cracks were developed at lower dissipated energy in an aged specimen when compared to the unaged specimen. Thus, less energy was required to induce damage in an aged mixture. As noticed in the case of binder testing, the impact of aging on fatigue cracking resistance increased with the increase in test temperature.

Izadi et al. (2018) investigated the effect of long-term aging (as per the AASHTO R30 protocol) on the fatigue behavior of two dense graded hot and warm (Sasobit and RheoFalt) bituminous mixture. Four-point beam bending fatigue and ITS tests were carried out on bituminous mixtures at 25°C. The authors noticed that irrespective of the type of gradation and bituminous mixture used, each mixture showed approximately 75 percent reduction in fatigue life with long-term aging. Further, the association between the FE parameter obtained from ITS and fatigue life was determined. The authors noticed that the FE and fatigue life had a R^2 of approximately 0.80.

2.6.2 Effect of moisture

Kim et al. (2004) compared the fatigue behavior of dry and moisture-conditioned bituminous mastic specimens by performing DMA. Mastic specimens were immersed in distilled water at 25 °C for 1 h for moisture-conditioning, and the DMA was conducted in a strain-controlled mode at 25 °C. The authors noticed that the moisture-conditioned specimen had lower fatigue life and lowered cumulative dissipated pseudostrain energy (DPSE) when compared to the dry specimen. Cumulative DPSE physically indicates the ability of a specimen to accumulated damage before failure. For example, a 36 % reduction in fatigue life and a 28 % reduction in cumulative DPSE with moisture conditioned was noticed in one of the test specimens. Thus, moisture accelerated the fatigue damage and reduced the fatigue life of bituminous mastic specimens.

Khattak & Kyatham (2008) conducted an indirect tensile cyclic fatigue test on dry and moisture conditioned (as per ASTM D4867 protocol) HMA specimens at 25 °C. The authors noticed that specimens with limestone aggregates had considerably higher fatigue life than specimens with granite aggregates, both in the dry and moisture-conditioned states. Moisture had a negative impact on each bituminous mixture's fatigue life. E.g., moisture conditioning reduced the fatigue life of specimens with limestone aggregates by approximately four times. Hydrated lime application improved the resistance to moisture damage of the bituminous mixtures, particularly for the specimens with granite aggregates (approximately six times higher fatigue life). The authors also evaluated the tensile plastic deformation rate (horizontal plastic deformation per cycle) of moisture-conditioned specimens. The authors noticed that the tensile plastic deformation rate was approximately 3.5 times and 8 times higher for moisture-conditioned specimens with limestone and granite aggregate when compared to dry specimens.

Caro et al. (2008b) used the DMA and fracture mechanics model to evaluate bituminous mastic specimens' cracking potential. The crack size index (ΔR), which captures the magnitude of crack growth, was used to assess the effect of moisture on the crack growth of mastic specimens. Moisture conditioning was carried out by vacuum saturating the specimens in distilled water for 1 h. The authors noticed that the moisture conditioned specimens had a higher value of ΔR than dry specimens, indicating more serious damage in moisture conditioned specimens. Further, the probability that the ΔR of moisture conditioned specimen will be higher than the dry specimen was determined. The authors noticed a high probability that the moisture conditioned specimen will have a higher ΔR than the dry specimen, and the likelihood increases with an increase in loading cycles. Thus, moisture has a detrimental effect on the cracking resistance of bituminous mixtures. Also, the probability of $\Delta R_{wet} > \Delta R_{dry}$ of granite specimen was much higher than that of limestone aggregates. Thus, bituminous mixture with moisture susceptible aggregates like granite may result in higher crack growth than aggregates with better resistance against moisture like limestone aggregates in the presence of moisture.

Tong et al. (2013) determined the effect of water vapor diffusion on the crack propagation rate of FAM specimens using a repeated direct tension test. The FAM specimens were placed in a vacuum desiccator with 0 % and 100 % relative humidity (RH) to prepared the dry and moisture-conditioned specimens. The authors found that the crack growth rate of the FAM specimens at 100 % RH was higher than the FAM specimen at 0 % RH. For example, the crack growth rate for one FAM specimen increases by 50 percent when the RH increased from 0 % to 100 %. A higher crack growth rate indicates that a faster crack growth can be expected in specimens with a high RH level. Hence, it could be concluded that deterioration of the bituminous layer in flexible pavement accelerates due to the diffusion of the subsurface water vapor.

The ratio of fatigue life of moisture-conditioned specimens to the unconditioned specimens was used by Moghadas Nejad et al. (2014) to evaluate the effect of moisture on the fatigue life of the HMA mixture. The fatigue life was determined using an ITFT in a stress-controlled mode at 300 kPa, and at a test temperature of 15 °C and 20 °C. Moisture conditioning of the specimen was carried out as per AASHTO T 283 protocol. The authors noticed a fatigue life ratio of 0.60 at 15 °C and 0.57 at 20 °C. Thus, the fatigue life ratio can serve as a simple parameter in assessing moisture's effect in reducing the bituminous mixture's fatigue life.

Garcia Cucalon et al. (2017) evaluated moisture's effect on the crack growth of HMA and WMA mixture. Four different warm mix additives (foaming, Sasobit, Evotherm, and Rediset), two aggregate sources, and two types of binders were used to prepare the FAM specimens. FAM specimens were also aged before moisture conditioning. The loose mixture was subjected to 2 h at 135 °C for the HMA mixture and 116 °C for the WMA mixture for short-term aging. For long-term aging, the compacted specimen was aged at 60 °C for 3 months. Moisture conditioning consisted of vacuum saturating specimen to 70 to 80 percent. The crack growth index parameter (ΔR) at 5000^{th} cycles obtained from the DMA test for the mixtures at different conditions. The authors noticed that ΔR parameter was higher in moisture conditioned specimens as compared to dry specimens. Thus, moisture increases the cracking potential of bituminous mixtures. The effect of aging on the moisture susceptibility of WMA mixtures was much higher when compared to HMA mixtures. In the case of WMA mixtures, resistance to cracking increased with aging, indicating that the WMA mixture's performance might improve with aging. It is worth mentioning here that the authors noticed a sudden failure in aged Sasobit and Evotherm specimens in the presence of moisture, and results could not be compared with other conditions. The investigations highlighted that the difference in the performance of bituminous mixture in the field and the laboratory might be due to the alteration in the aging or curing process involved in the field and laboratory.

Fan et al. (2020) determined the fatigue life of dry and moisture conditioned HMA mixtures at 15 °C using an ITFT at four stress levels (30 %, 40 %, 50 %, and 60 % of the splitting strength). Four saturation levels and six freeze-thaw cycles were used for moisture conditioning. The authors noticed that fatigue life reduced with the increase in the freeze-thaw cycle and saturation level. Further, the fatigue data were fitted to a regression model, i.e., $\log(N_f) = \log(K_1) - K_2 \times \log(\sigma)$. A decrease in the model intercept value corresponds to a decrease in fatigue life. From Figure 2.6 (a), it can be noticed that fatigue life decreased with the increase in saturation level at all freeze-thaw cycles. A gradual reduction in fatigue life with an increase in saturation was noticed for specimens subjected to fewer freeze-thaw cycles (approximately ten cycles). The reduction in fatigue life with an increase in saturation level (up to 20 %) became sharper with the increase in freeze-thaw cycles (beyond ten cycles). Similarly, from Figure 2.6 (b), it can be noticed that fatigue life decreased with the increase in freeze-thaw cycles at all saturation levels. The rate of decrease in fatigue life with an increase in freeze-thaw cycles was relatively higher in specimens with higher saturation levels.

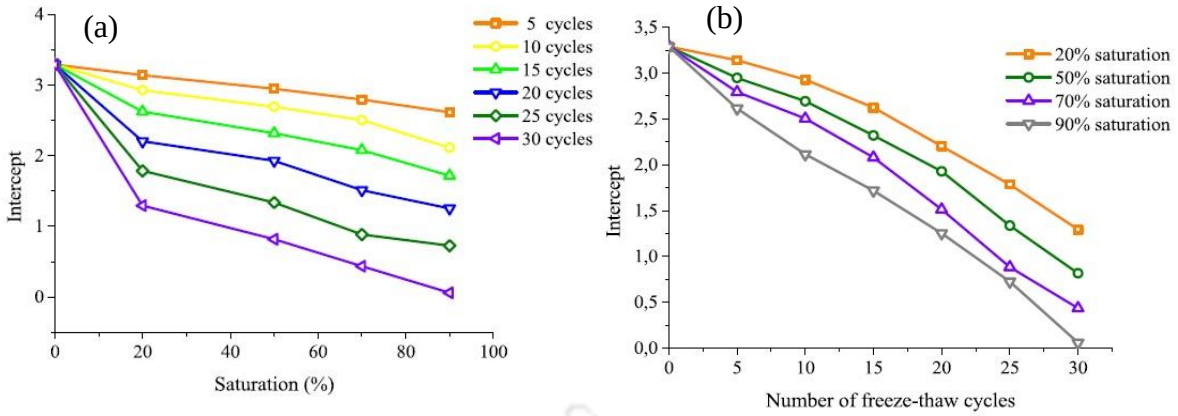

Figure 2.6 Intercept versus: (a) saturation levels; (b) freeze-thaw cycles (Fan et al., 2020)

2.6.3 Effect of test mode on fatigue life of the bituminous mixture

Researchers have noticed that the mode of loading, i.e., stress-controlled or strain-controlled mode, impacts how the effect of aging on the cracking resistance and fatigue life of bituminous mixture is interpreted. The authors noticed that in a stress-controlled mode of testing, an aged bituminous mixture has a higher fatigue life than an unaged bituminous mixture for most of the cases. Di Benedetto et al. (2004) noticed that in the case of a stress-controlled ITFT, in addition to the fatigue damage, the fatigue life of the bituminous mixture is also influenced by the accumulated permanent deformation undergone by the specimen during the testing. The fatigue life of the bituminous mixture decreases with the increase in accumulated permanent deformation and vice-versa.

Baek et al. (2012) evaluated the effect of four aging levels, i.e., short-term aging (loose mixture at 135°C for 4 h, STA), and compacted specimens subjected to 85 °C for 2 days, 4 days, and 8 days (termed as LTA1, LTA2, and LTA3) on fatigue life of the bituminous mixture. The authors noticed that the fatigue life of specimens determined using a stress-controlled fatigue test increased with increasing in aging level. For example, the fatigue life of STA, LTA1, LTA2, and LTA3 at 900 kPa were 44700, 77000, 97200, and 167000. The corresponding initial strain of the specimens were 76, 66, 64, and 52 microstrains, respectively. Thus, a lower strain experienced by the long-termed aged specimen at a constant stress level might have resulted in a higher number of cycles to failure in the long-term aged specimen than the short-term aged specimen.

Gao et al. (2017) noticed that the fatigue life of bituminous mixtures determined using a stress-controlled indirect tensile fatigue test increased with aging duration. The authors noticed that oven aging at 163 °C for 2 h and 4 h resulted in an approximate 50 % and 75 % increase in the fatigue life of bituminous specimens at 15 °C. The authors said that the modulus of the bituminous mixture increases with aging, which makes the mixture stronger and has a longer life in a stress-controlled fatigue test. Previous researchers also observed similar findings (Wang et al., 2019; Akpolat et al., 2020; Goli & Latifi, 2020; Taherkhani & Noorian, 2020; Bharath et al., 2021).

In a strain-controlled mode of fatigue testing, an unaged bituminous mixture has a higher fatigue life than an aged bituminous mixture. Fattah et al. (2016) noticed that the fatigue life of long-term aged bituminous mixture determined using a strain-controlled test was 36 % lower than the short-term aged mixture. Similarly, Izadi et al. (2018) noticed that the fatigue life of bituminous mixtures determined using a strain-controlled four-point bending fatigue beam test reduced significantly with the increase in the aging level for both HMA and WMA mixtures. Thus, researchers have noticed that the fatigue life of bituminous mixture determined in using a strain-controlled test reduced with aging.

Thus, as the stiffness of the bituminous mixture increases with aging, the fatigue life of the bituminous mixture tends to increase in the case of a stress-controlled test. On the contrary, an increase in stiffness has a negative impact on the fatigue life of the bituminous mixture subjected to the strain-controlled test. This implies that a stiffer bituminous mixture may perform better in stress-controlled mode, whereas a softer mixture may perform better in strain-controlled mode. Studies evaluating the effect of aging on bituminous mixture subjected to stress-controlled and strain-controlled testing are shown in Table 2.11 and Table 2.12. Also, a list of factors influencing the stiffness and fatigue behavior of bituminous mixture in a stress-controlled test is presented in Table 2.13.

Table 2.11 Effect of aging in stress-controlled fatigue test

Author(s)	Test details	Test temperature	Replicates	Aging condition	Results
Baek et al. (2012)	900 kPa and 10 Hz, and haversine waveform	5 °C	3	Loose mixture aged at 135 °C for 4 h (STA). Compacted specimen at 85 °C for 2, 4, and 8 days (LTA).	Fatigue life increased with an increase in the aging level
Arega et al. (2013)	275 kPa, 10 Hz, and sinusoidal waveform	23 °C	At least two	Loose mixture aged at compaction (163 °C and 143 °C) for 4 h (STA). Loose mixture aged at 60 °C for 30 days (LTA).	Fatigue life decreased after long-term aging
Gao et al. (2017)	700 kPa, 10 Hz, and half sine waveform	15 °C	6	Loose bituminous mixture aged at 163 °C for 2, 4, 8, 16, and 24 h.	Fatigue life increased with an increase in aging time
Diab et al. (2019)	10 % of ITS was applied at 10 Hz	25 °C	3	Loose bituminous mixture aged at 163 °C for 16 h	Fatigue life decreased after 16 h of aging
Wang et al. (2019)	A minimum of three stress amplitudes at 10 Hz	20 °C	3	Bituminous mixtures aged at 105 °C for 40 h to produce RAP. A replacement of 0, 20, and 40 % RAP in the mixture	Mixture with RAP had higher fatigue life compared to control mixture
Akpolat et al. (2020)	400 kPa	25 °C	3	As per AASHTO R30. 1, 2, 3, and 4 weeks in an oven at 60 °C. Also, 2, 4, 6, 8, and 10 months of aging in the field	Fatigue life increased with an increase in aging time
Goli & Latifi (2020)	1.6 kN load in a haversine waveform. 0.1 s loading and 0.9 s rest period.	25 °C	at least 5	Mixture with 0 % and 40 % RAP content	Mixture with RAP had higher fatigue life compared to control mixture

Author(s)	Test details	Test temperature	Replicates	Aging condition	Results
Taherkhani & Noorian (2020)	100 kPa and 1Hz	25 °C	3	0, 25, 50, and 75 % RAP in mixture	Fatigue life increased with an increase in RAP content and was higher than the control mixture
Bharath et al. (2021)	Four stress levels (2 kN to 8kN). Sinusoidal waveform.	25 °C	4	0, 15, 25, 35, and 45 % RAP n mixture	Mixture with RAP had higher fatigue life compared to control mixture
Enieb et al. (2021)	5 % of ITS was applied at 10 Hz in sinusoidal waveform	25 °C	3	Loose mixture aged at 160 °C for 2 h (STA). Loose mixture aged at 85 °C for 2 days (LTA).	LTA bituminous mixture showed lower fatigue life compared to STA mixture.
Pakenari & Hamedi (2021)	300 kPa, 10 Hz, and sinusoidal waveform	25 °C	---	Loose bituminous mixture aged at 135 °C for 2, 4, and 6 h.	Fatigue life decreased with an increase in the aging

Table 2.12 Effect of aging in strain-controlled fatigue test

Author(s)	Test details	Test temperature	Replicates	Aging condition	Result
Zhu et al. (2009)	200, 300, 500, 700, 900, 1100, and 1300 με at 10 Hz, and sinusoidal waveform	15 °C	3	Loose mixture at 135 °C for 4 h (STA). Compacted specimens at 85 °C for 5 days (LTA). Also, STA specimens were placed outdoors for 3, 6, and 9 months	Aging reduced the fatigue life of bituminous mixtures.
Islam & Tarefder (2015)	600 με at 10 Hz and sinusoidal waveform	20 °C	3	Loose mixture at aged 135 °C for 4 h (STA). Compacted specimens were kept in the field for 335 days for long-term aging.	Aged specimens had shorter fatigue lives as compared to unaged.
Fattah et al. (2016)	300 με at 10 Hz	10 °C, 20 °C, and 30 °C	---	6 days at compaction temperature for long-term aging	Fatigue life decreased after long-term aging
Kakade et al. (2016)	400 με, 500 με, and 600 με at 10 Hz and sinusoidal waveform	25 °C	2	Loose mixture at 135 °C for 4 h (STA). Compacted specimens at 85 °C for 5 days (LTA).	Fatigue life decreased after long-term aging
Izadi et al. (2018)	600 με, 10 Hz, and haversine waveform	25 °C	3	AASHTO R30 for STA. Compacted specimens at 80 °C for 120 h (LTA).	Fatigue life decreased after long-term aging
Mirhosseini et al. (2019)	500 με and 750 με at 10 Hz	20 °C	---	0, 20, 30, and 40 % RAP replacement in mixture	The fatigue life of mixtures reduced with an increase in RAP content.
Crucho et al. (2020)	150, 250, and 350 με at 10 Hz and sinusoidal waveform	20 °C	6	Compacted specimens at 85 °C for 5 days for LTA and Tecnico accelerated aging (TEAGE) condition	The fatigue life of LTA and TEAGE specimens was lower than an unaged specimen.

Author(s)	Test details	Test temperature	Replicates	Aging condition	Result
Daryaee et al. (2020)	500 με and 750 με at 10 Hz	20 °C	3	0, 30 and 50 % RAP replacement in mixture	Bituminous mixtures with RAP had lower fatigue life as compared to the unaged mixture.
Ziari et al. (2020)	500 and 1000 με	20 °C	3	Loose mixture at 135 °C for 4 h (STA). Compacted specimens at 85 °C for 5 days (LTA)	Fatigue life decreased after long-term aging.

Table 2.13 Factors affecting the stiffness and fatigue life in a stress-controlled fatigue test (Tangella et al., 1990; Prowell et al., 2010)

Factors	Change in factor	Effect of change in factor on	
		Stiffness	Fatigue life
Aging	Increase	Increase	Increase
Bitumen content	Increase	Increase[a]	Increase[a]
Aggregate gradation	Open to dense	Increase	Increase
Air void content	Decrease	Increase	Increase
Temperature	Decrease	Increase[b]	Increase

[a] Reaches optimum level above that required by stability considerations
[b] Approaches upper limit at a temperature below freezing

2.6.4 Fatigue life prediction models

Fatigue in the bituminous pavement is caused due to the damage accumulation under the repeated vehicular movements. Roque et al. (2002) said that cracks might initiate as micro-cracks and later merge to form macro-cracks, propagating due to tensile stress or shear stress or combinations of both. Different testing protocols have been developed to measure the fatigue behavior of bituminous mixture in the laboratory. The most popular fatigue testing setup is the beam fatigue test, trapezoidal cantilever beam test, direct tension test, tension-compression test, indirect diametral test, triaxial test, and wheel-track test. Fracture mechanics, continuum damage mechanics, and the energy-based are used to characterize a bituminous mixture's fatigue behavior. This research work focused on the traditional approach for analyzing fatigue behavior of bituminous mixture as discussed below.

In the phenomenological or traditional approach of analyzing fatigue behavior of bituminous mixture, the stress or strain is related to the number of load repetitions till failure. A linear damage accumulation is assumed, and a regression equation relating the fatigue test data to the stress or strain is established. The simplest model in this approach is shown in Eq. (2.12) (Rowe & Bouldin, 2000). For this reason, phenomenological models are also known as regression models. Since bituminous material is viscoelastic, and its behavior is load and temperature-dependent, the bituminous mixture's stiffness is introduced in the model formulation, as shown in Eq. (2.13) (Miner, 1945). Different agencies and organizations have calibrated Eq. (2.13) (Miner, 1945) to their specific pavements and bituminous mixture properties and presented regression models like the Shell pavement design manual model (1978), the asphalt institute model (1982), SHRP A-404 Model (Tayebali et al., 1994), etc. Regressions models have a strong association with the material properties and testing setup used in model development. Considering this, researchers have tried to improve the regression models, either by increasing the number of dependent variables or by introducing variables that can capture fundamental material properties like fracture energy into the model formulation. Table 2.14 presents the regression models proposed in different studies.

$$N_f = K_1\left(\frac{1}{\epsilon_t}\right)^{K_2} \tag{2.12}$$

$$N_f = a\left(\frac{1}{\epsilon_t}\right)^{b}\left(\frac{1}{s_0}\right)^{c} \tag{2.13}$$

where,

N_f = the number of load application to failure,

ϵ_t = applied tensile strain,

s_0 = stiffness modulus of the bituminous mixture, and

a, b, c, K_1, and K_2 = are regression constants.

Table 2.14 Regression models proposed in different studies

Model or Authors	Expression		Variables
Shell pavement design manual model (1978)	$N_f = 4.91 * 10^{-13}(0.86V_b + 1.08)^5 \left(\frac{1}{\epsilon_0}\right)^5 \left(\frac{1}{s_{mix}}\right)^{1.8}$	(2.14)	N_f = fatigue life ϵ_0 = maximum tensile strain in bituminous mixture, (in/in) s_{mix} = dynamic modulus of the bituminous mixture, psi V_b = volume of bitumen in the mixture, percent
The asphalt institute model (1982)	$N_f = 18.4 * C * 4.325 * 10^{-3}(\epsilon_t)^{-3.291}\lvert E^*\rvert^{0.854}$	(2.15)	N_f = number of 18,000 lb equivalent single axle loads ϵ_0 = tensile strain in bituminous layer, (in/in) E^* = bituminous mixture dynamic modulus, psi C = function of the volume of voids and volume of bitumen. V_b *and* V_v = volume of bitumen and air voids, percent.
	$C = 10^M$	(2.16)	
	$M = (\frac{V_b}{V_b + V_v} - 0.69)$	(2.17)	
SHRP A-404 Model (1994)	$N_f = 466.4e^{0.052VFB}(\epsilon_0)^{-3.948}(s_0)^{-2.270}$	(2.18)	ϵ_0 = initial strain, s_0 = initial loss stiffness, and VFB = percentage of voids filled with bitumen.
Nejad et al. (2010)	$N_f = K_1(\frac{1}{\sigma})^{K_2}$	(2.19)	N_f= fatigue life K_1 and K_2= regression coefficient σ = applied stress (30 kPa to 1000 kPa)
Li et al. (2012)	$N_{f50\%} = \frac{1}{a + b\left(\frac{DE_f}{DE_{IDT}}\right)^c}$	(2.20)	N_f= fatigue life, DE_f = initial dissipated energy density obtained from beam fatigue test, DE_{IDT} = total dissipated creep strain energy density at failure obtained from ITS test, a, b, and c= regression coefficient

Model or Authors	Expression		Variables
Wen (2013)	$N_f = \alpha_1 \left(\frac{1}{\epsilon_t}\right)^{\alpha_2} (FWD)^{\alpha_3} h^{\alpha_4}$	(2.21)	N_f = fatigue life ϵ_t = strain amplitude FWD = fracture work density of bituminous mixture α_1, α_2, α_3, and α_4= regression coefficient h = thickness of bituminous layer
Bahadori et al. (2015)	$N_f = 10^{37.89} \left(\frac{1}{\epsilon_t}\right)^{4.13} (F.E.)^{14.126}$	(2.22)	N_f = fatigue life ϵ_t = strain amplitude $F.E.$ = fracture energy density of bituminous mixture
Meena et al. (2016)	$N_f = 0.5161 * C * 10^{-4} \left(\frac{1}{\epsilon_t}\right)^{3.89} \left(\frac{1}{M_r}\right)^{0.854}$ C is the same as Eq. (2.16)	(2.23)	N_f= fatigue life M_r = resilient modulus ϵ_t = maximum tensile strain at the bottom of the bituminous layer
Fan et al. (2020)	$\log(N_f) = \log(K_1) - K_2 \times \log(\sigma)$	(2.24)	N_f= fatigue life K_1 and K_2= regression coefficient σ = applied stress

Regression models cannot explain the damage accumulation mechanisms, which is a noteworthy disadvantage of this model. The effect of aging and moisture on the bituminous mixture's damage accumulation can be studied using the decay in the stiffness modulus of the bituminous mixture under repeated loading. The stiffness decay curve has three distinct phases, as shown in Figure 2.7. In phase I, heating and thixotropic cause a rapid reduction in bituminous mixture stiffness with load repetition. In phase II, a network of diffused micro-crack begins, and stiffness reduces in a linear manner. Coalesce of micro-cracks causes a rapid decrease in stiffness of bituminous mixture, which marks the beginning of phase III. The transition from phase II to phase III is considered critical damage and is used by researchers to study the cracking resistance of bituminous mixture (Baaj et al., 2005; Tapsoba et al., 2013, Corradini & Cerni, 2020). Whereas, Saha & Biligiri (2019) considered the transition point from phase I to phase II (crack initiation) as a critical parameter and noticed that crack initiation had a fair correlation (R^2 > 0.72) with fracture toughness and dynamic modulus of the bituminous mixture. The damage at failure can be determined using the stiffness degradation model used by Perraton et al. (2015), as shown in Eq. (2.25).

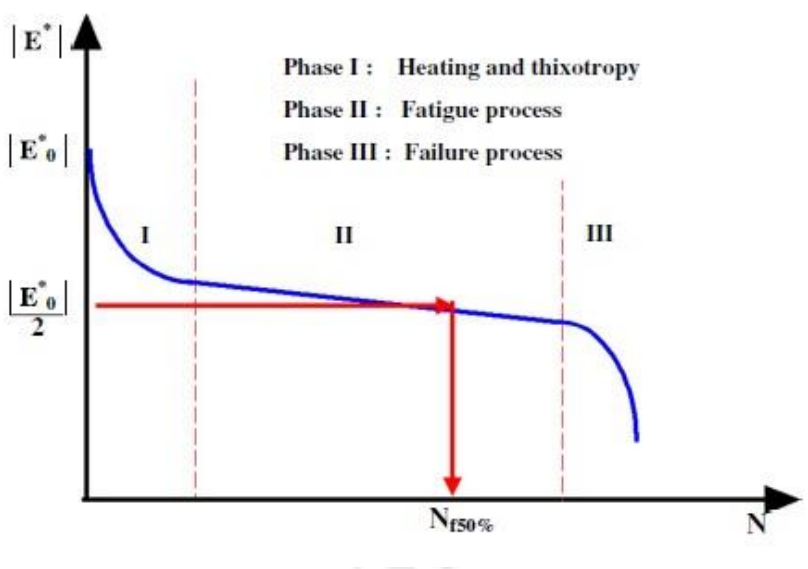

Figure 2.7 Evolution of stiffness with number of cycles (Perraton et al., 2015)

$$D_n = 1 - \frac{E_n}{E_0} \qquad (2.25)$$

where,

D_n= fatigue damage at n^{th} cycle,

E_0 = initial stiffness modulus (modulus value at 100^{th} cycle), MPa, and

E_n = stiffness modulus at n^{th} cycle, MPa

Researchers have explored an energy-based approach to characterize the fatigue behavior of bituminous mixtures. During the loading cycle of the fatigue damage process, the energy input can be measured using the area under the stress-strain curve. In viscoelastic material like a bituminous mixture, the loading and unloading path does not overlap. A hysteresis loop is created that represents the energy dissipated during the process. A portion of the dissipated energy is absorbed in performing mechanical work. In this regard, the ratio of dissipated energy change (RDEC), i.e., the ratio of the amount of dissipated energy change between different loading cycles, represents the true damage in the bituminous mixture with each loading cycle. The expression used to calculate the RDEC is shown in Eq. (2.26) (Modarres & Aloogar, 2017). Researchers have noticed that RDEC versus loading cycle plot has three distinct stages. The second stage representing a constant percentage of input energy converted into damage is of particular interest to the researchers. The plateau value (PV) is the RDEC value corresponding to a 50 percent stiffness reduction in the initial stiffness. Shen et al. (2006) subjected different bituminous mixtures to stress-controlled and strained controlled four-point bending beam fatigue tests at 10 Hz and 20 °C. The authors noticed that the constant value of PV obtained from the RDEC approach is a unique parameter for fatigue damage analysis regardless of the type of materials and loading mode used. Wu et al. (2014) also noticed that the PV and fatigue life relations obtained from the RDEC approach using three different types of tests, i.e., the flexural beam fatigue test (strain-controlled test), the direct tension (stress-controlled test), and loaded wheel fatigue tests (stress-controlled test) agreed with each other.

$$RDEC_a = \frac{DE_a - DE_b}{(b-a) \times DE_a} \tag{2.26}$$

where,

$RDEC_a$= ratio of dissipated energy change for cycle a,

DE_a and DE_a= dissipated energy associated with cycles a and b, J/m^3.

Maggiore et al. (2014) used a 2-point beam bending test in a controlled strain mode at 20 °C and two frequencies, i.e.,15 Hz and 25 Hz, to determine the dissipated energy of the bituminous mixtures. The authors noticed a good association ($R^2$of 0.96) between PV and fatigue life. Modarres & Aloogar (2017) used the RDCE approach to compare the fatigue life of HMA and WMA mixtures subjected to different strain levels. The authors noticed that at each strain level, the WMA mixtures had a lower PV and higher fatigue life as compared to HMA mixtures. This was due to the reduced mixing and compaction temperatures in WMA mixtures, which resulted in less aging of the bituminous binder in WMA mixtures and had beneficial effects on the fatigue behavior of the WMA mixtures. Thus, PV and fatigue life has a unique relationship and is independent of the mode of testing and material property.

Regression-based fatigue modeling approaches are deterministic, i.e., it accounts for the averaged values of the input parameter and fatigue life. However, fatigue damage in a bituminous mixture is a stochastic process with considerable variability and randomness caused by material properties (inherent material property variation and construction variation) and imposed environmental conditions. In this regard, researchers use probabilistic approaches to capture the randomness in fatigue data, as discussed below.

Studies have widely used Weibull distribution and lognormal distribution to model the scatter in the fatigue life of the bituminous mixture. Caro et al. (2008b) determined the crack size index (ΔR) of wet and dry specimens using fracture mechanics. The crack size index followed a lognormal distribution, and the probability of ΔR of a wet specimen being higher than a dry specimen was noticed. The authors also noticed that the bituminous mixture with granite aggregates had a higher probability value (ΔR of a wet specimen being higher than a dry specimen) when compared to the mixture with limestone indicating higher moisture susceptibility. Singh & Swamy (2017) constructed the probabilistic damage characteristics (PDC) curve of the damage parameter used in the viscoelastic continuum damage approach. A Weibull distribution was used to construct the PDC curves corresponding to different reliability levels. It was noticed that with the increase in reliability level, the numerical value of the damage parameter reduced. Bala & Napiah (2020) used survival analysis to compare the fatigue life of different bituminous mixtures using hazard function. Fatigue life data followed a two-parameter Weibull distribution, and the authors noticed that at any level of reliability, a bituminous mixture modified using polypropylene (PP) had higher fatigue life compared to the mixture with polyethylene (PE).

Thus, researchers have used different approaches for analyzing and modeling the fatigue behavior of bituminous mixture. The regression-based fatigue models have a relatively simple formulation but fail to explain the damage propagation in the bituminous mixture. On the other hand, the damage propagation in a bituminous mixture can be addressed with the help of a stiffness degradation model. Further, the variability and scatter associated with a fatigue test can be captured using a probabilistic fatigue modeling approach.

2.7 The creep resistance of the bituminous mixture

Creep in a bituminous pavement is caused due to repeated heavy traffic loading on the wheel path. There are three stages associated with the creep in bituminous mixtures, i.e., the primary, secondary and tertiary stages. Zhou & Scullion (2002) discussed the damage mechanism associated with the three different creep stages of a bituminous mixture. In the primary stage, the motion of dislocation or strain hardening occurs, which results in the densification of the bituminous mixture under repeated loading. However, the mobility of dislocation reduces as the number of simultaneous dislocations increases. Thus, the creep strain per cycle gradually decreases despite an increase in the bituminous mixture's accumulated creep strain (total plastic strain). The accumulation of creep strain reaches a point where micro cracks initiate. The occurrence of microcracking results in more dislocations to develop by providing space for the mobility of dislocation. The occurrence of a microcrack is a work-softening process. In the secondary stage, the rate of work-hardening is dynamically equal to that of work-softening, which results in the linear accumulation of creep strain with loading cycles. As the loading progresses, the micro-cracks gradually propagate and coalesce to form a macro crack. The initiation and propagation of macro cracks accelerate the rate of work-softening, and creep strain per cycle rapidly increases, which marks the beginning of the tertiary stage

2.7.1 Effect of aging

Said (2005) collected field cores from the test section, which were 1, 12, and 24 months old, and conducted a repeated load creep test to determine the effect of field aging on the creep resistance of the bituminous mixture. The authors noticed that creep resistance increased with an increase in field aging duration. Interestingly, creep resistance increased considerably during

the 1st year of service, suggesting that a bituminous pavement is more susceptible to creep deformation in the initial years of service.

Azaria & Mohseni (2013) developed an incremental repeated load permanent deformation (iRLPD) testing protocol to measure the effect of aging on the creep resistance of bituminous mixtures. For STA condition, loose mixtures were kept in an oven at 135 °C for 0 h to 6 h, in 1 h interval. For the LTA condition, the STA mixture was compacted, and the specimen was subjected to 2 and 5 days at 85 °C. The iRLPD test was carried out at four stress levels, i.e., 200 kPa, 400 kPa, 600 kPa, and 800 kPa. The minimum strain rate (MSR) at the end of each stress increment was recorded, and an MSR relation was developed using a power-law relation ($MSR = 0.001 \times TP^b$, where TP is the product of temperature and deviatoric stress). E.g., from MSR relation for 3 h STA bituminous mixture subjected to different LTA conditions, it was noticed that the coefficient "*b*" reduced from 2.68 for no LTA condition to 2.48 and 2.37 for 2 days and 5 days of LTA conditions. A reduction in "*b*" parameter indicates an increase in the creep resistance of the bituminous mixtures. The authors also noticed that the MSR of the LTA mixtures in some cases was significantly affected by the duration of short-term aging. This study pointed out the importance of the duration of short-term aging of bituminous mixtures for the accurate prediction of long-term creep prediction in a bituminous mixture.

Othman & Omranian (2015) prepared bituminous specimens from loose bituminous mixture collected from both plant and field (10 km away from mixing plant). The creep resistance characteristics were determined at a temperature of 40 °C. One batch of the loose mixture was aged in the laboratory for 2 h and 4 h in an oven at 135 °C. The authors noticed that plant-produced specimens had the lowest creep resistance, followed by field, 2h, and then 4 h aged lab specimens. Therefore, the creep resistance of the bituminous mixture will increase with the increase in the duration of aging.

Fernández-Gómez et al. (2016) studied the effect of four different aging treatments on the creep resistance of the bituminous mixture. Aging treatments considered were, i.e., unaged, UV aged (100, 200, and 500 h in UV chamber), PAV aged (5, 20, and 50 h in the pressure aging vessel), and field cores (collected after 1.5, 3, 5, 8, and 11 years from construction). Results of the creep test carried out at 60 °C showed that the creep resistance of the bituminous mixtures increases with the increase in exposer to UV radiation and PAV aging time. However, PAV aging resulted in a more significant increment in the bituminous mixtures' creep resistance

than UV aging. Comparing the creep resistance of field aged and PAV aged specimens, it was noticed that the creep resistance of 20 h and 50 h PAV aged specimens was similar to that of 8 years and 11 years of field aged specimens.

Yin et al. (2017) collected field cores during construction and after 8 to 22 months of service. In addition, the loose bituminous mixture was collected during construction for laboratory aging studies. Bituminous mixtures were subjected to short-term aging in an oven aging at 135 °C for 4h and then compacted. Compacted specimens were placed in an oven at 85 °C for 3 days and 5 days and at 60 °C for 14 days to simulate LTA condition. The number of days with a daily maximum temperature higher than 32 °F (termed as cumulative degree days, CDD) was recorded to evaluate the effect of aging on the creep resistance of field cores collected. The rutting resistance parameter (RRP) ratio obtained from the HWTT of different specimens was determined. The RRP ratio was defined as the ratio of the RRP of specimens collected during construction (STA specimens) to the RRP of specimens collected during service (LTA specimens). It was noticed that the RRP ratio increase with an increase in field aging days. Thus, the creep resistance of bituminous mixtures increased with the increase in field aging. The authors also noticed that the RRP of 14 days at 60 °C was equivalent to 10,000 CDD and 5 days at 85 °C was equivalent to 19,000 CDD. Thus, in the laboratory aging process, the aging temperature may have a higher impact on the creep resistance of bituminous mixtures than the duration of aging.

2.7.2 Effect of moisture

Cheng et al. (2003) studied the effect of moisture conditioning on the creep resistance of bituminous mixtures prepared with granite and limestone aggregates. For moisture conditioning, saturated specimens were soaked in a water bath for 8 h. The authors noticed that wet specimens were more susceptible to creep deformation and had higher creep microstrain. Also, specimens with granite aggregates were more vulnerable to creep deformation under the action of moisture than specimens with limestone aggregates. The authors calculated the Gibbs free energy per unit mass of aggregate from surface energy measurements of aggregates and bitumen to understand the higher creep noticed in bituminous mixtures with granite aggregates. The Gibbs free energy per unit mass of aggregate is the energy required to detach the bitumen film from the unit mass of aggregate. The average Gibbs free energy of limestone aggregates was 7.752×10^5 erg/g, and granite aggregates were 1.82×10^5 erg/g, respectively. Thus, a bituminous mixture with limestone aggregates will require more energy to strip off the bitumen

coating from the aggregate surface in the presence of moisture compared to mixtures with granite aggregates. This supports the higher creep resistance noticed in the bituminous mixture with limestone aggregates in the presence of moisture compared to mixture granite aggregates.

A specimen undergoes creep deformation and stripping simultaneously in the HWTT. Kanitpong & Bahia (2005) evaluated the relation of the HWTT parameter with the adhesive and cohesive bond strength obtained from the pull-off and tack test. The HWTT parameters considered were cycles to the onset of stripping, cycles to 12.5 mm rut depth, and cycles to failure. It was noticed that cycles to failure had a comparatively better correlation with mixtures adhesive and cohesive properties. Thus, the bituminous mixture's adhesive and cohesive properties may influence the creep resistance of the bituminous mixture in the presence of moisture.

The amount of air void present in the bituminous specimen also impacts the creep resistance of the bituminous mixture. To consider the effect of air void on the creep resistance of bituminous mixture, Rahman et al. (2010) compared the creep strain rate of HMA specimens subjected to moisture conditioning with the dry specimens. The specimens were compacted to 4 % and 8 % air voids. The authors noticed that at 4 % air voids, moisture conditioned specimens' strain rate was approximately two times higher than dry specimens. With the increase in air voids to 8 %, moisture conditioned and dry specimens had comparable strain rates.

Mehrara & Khodaii (2011) analyzed the creep resistance curves of dry and moisture conditioned specimens to determine moisture's effect on the creep behaviour of bituminous mixtures. The authors noticed that at the 200 kPa stress level, the rate of creep deformation and creep strain of the specimens subjected to moisture conditioning was remarkably higher than the dry specimens at both 40 °C and 50 °C. However, at 40 °C, the moisture-conditioned specimens reach the tertiary stage of the creep deformation in a lower number of cycles when compared to the dry specimens. At 50 °C, both moisture-conditioned and dry specimens reached the tertiary stage at comparable cycles. Thus, the effect of moisture on the creep resistance of the bituminous mixture was more prominent at 40 °C compared to 50 °C when subjected to a higher stress level of 200 kPa. The mechanical behavior of bituminous mixtures at higher temperatures was predominantly influenced by the temperature compared to moisture.

For specimens tested at 100 kPa, it was noticed that the moisture-conditioned specimens showed higher resistance to creep than the dry specimens at 40 °C. However, at a higher test temperature of 50 °C, the moisture conditioned specimen tested a 100 kPa also showed a higher creep strain than the dry specimen. The authors said that moisture might act as a damper in the bituminous specimens if it cannot reduce the adhesive and cohesive bond in the specimen. As a result, the rate of permanent deformation reduces, and reduced creep in bitumen specimens is observed. Findings from this study suggest that it will be appropriate to conduct a creep test on moisture-conditioned specimens at higher stress levels and/or higher test temperatures to observe meaningful results.

Bennert et al. (2011) blended pre-wetted aggregates with dry aggregates in an HMA and WMA mixture to introduce the effect of entrapped moisture during the production process. The target moisture content of the aggregate blend was fixed at 0 %, 3 %, and 6 %, respectively. An HWTT was conducted at 50 °C until a creep deformation of 12.5 mm or 20000 cycles, whichever was achieved earlier. It was noticed that as the moisture content increased, the bituminous mixtures reached stripping inflection point in fewer cycles, and the creep deformation also increased. For example, the stripping inflection point of the bituminous mixture with gravel aggregate was 6343, 3610, and 3335 at 0 %, 3 %, and 6 % moisture content. And the corresponding creep deformation was 8.67 mm, more than 12.5 mm, and 12.22 mm, respectively. Thus, the initial moisture content present on the aggregates will have a noticeable impact on the bituminous mixture's creep resistance.

Fang et al. (2017) conducted a creep test on bituminous mixtures at two stress levels (0.7 MPa and 0.9 MPa) and two test temperatures (60 °C and 70 °C). The authors noticed that dry specimens showed the first two stages of creep behavior, i.e., primary and secondary stages. Whereas the moisture conditioned specimens reached the tertiary stage. Further, the creep deformation sharply increased in moisture-conditioned specimens with an increase in either the test temperature or the stress level. Range analysis of the dynamic stability index showed that temperature had the most noteworthy effect on the creep of the bituminous mixture, followed by moisture and then the applied stress level.

Wang et al. (2018) developed a multi-physics repeated loading permanent deformation (MRLPD) test to simulate the dry, rainfall onset, ongoing rainfall, and rainfall end conditions in porous asphalt (PA) mixture with 18.5 % air voids. The test was conducted at 45 °C, 50 °C, and 55 °C. The authors noticed that the creep deformation of the specimens under rainfall onset

and ongoing conditions was higher than the dry specimens. The development of pore pressure and moisture penetration into the aggregate surface with increased moisture exposure resulted in higher permanent deformation. The higher permanent deformation of ongoing than the onset of rainfall was because, during the ongoing condition, the specimen was saturated, which reduced the resistance to the permanent deformation of the specimen. The specimen's resistance under rainfall end condition was higher than dry because pore pressure developed may help in absorbing a part of the wheel load. It was noticed that the temperature change had a higher impact on the bituminous mixture's creep resistance compared to the influence of moisture. The authors concluded that the moisture damage is accelerated at high temperatures, and in turn, there is an increase in the rutting of the bituminous mixture.

From section 2.7.1 and section 2.7.2, it can be noticed that researchers have evaluated the creep behavior of bituminous at different aging and moisture conditioning levels. Aging increased the creep resistance of the bituminous mixture, whereas the moisture reduced the creep resistance. Aging changes the chemical properties and rheological behavior of bituminous binders, e.g., aging alters the carbonyl and sulfoxide content of the binder, which in turn affects the creep behavior of the bituminous mixture. On the other hand, moisture reduces the integrity of the bituminous mixture in two ways: loss of bitumen-aggregate adhesion and a reduction in the cohesive strength and stiffness of the bituminous mixture. Thus, both aging and moisture may change the creep resistance of the bituminous mixture.

2.7.3 Creep resistance models

Creep in bituminous pavements occurs due to the accumulation of small permanent deformations in the pavement layers or at the subgrade due to the vehicle's repeated stress. The mechanism involves densification and shear deformation depending on the factors like the grade of bitumen, bitumen content, mixture type, load levels, the temperature of the pavement, initial compacted density, etc. Among different test methods used to assess the creep resistance of bituminous mixture, wheel tracking test, static creep test, and dynamic creep test are most widely used. The bituminous mixture's behavior in a dynamic or repeated load creep test is studied by plotting the specimens' permanent strain versus loading cycles, also known as the creep curve. This creep curve obtained from a dynamic creep test is shown in Figure 2.8. The creep resistance of different bituminous mixtures can be analyzed and compared using the mixture's creep curve.

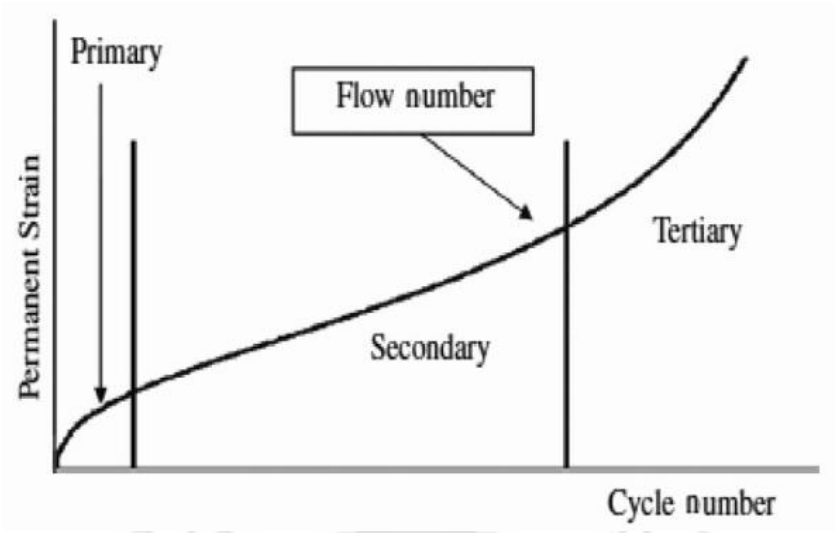

Figure 2.8 Three phases of permanent deformation curve (Nejad et al., 2014)

The creep curve is divided into three zones, i.e., primary, secondary, and tertiary. In the creep curve's primary zone, the strain rate decreases nonlinearly with load repetition due to the compaction of the mixture. In the second phase, the strain rate remains constant with the loading cycle. In the tertiary stage, the strain rate increases with an increase in loading cycles. The cycle number at which tertiary flow starts is referred to as the "flow number (FN)' and is considered crucial as it is an indication of the start of shear deformations (Witczak et al., 2002).

Generally, power models are used to model the secondary (linear) phase of the creep curve ($\epsilon_p = aN^b$). The regression parameters 'a' and 'b' obtained from a regression analysis of the linear portion of the curve ignore the creep curve's tertiary zone. Regression models are also dependent on the combination of materials and test conditions used. A higher value of parameters a and b implies a reduction in the bituminous mixture's creep resistance. A semi-log and a power-law model can be used to capture the primary stage of the curve. In comparison, the exponential model will capture the tertiary stage of the creep curve. In Table 2.15, different models used to capture the bituminous mixture's creep behavior are presented (Zhou et al., 2004; Biligiri et al., 2007).

Table 2.15 Models used to study the creep resistance in a bituminous mixture

Author	Permanent Deformation Model		Variables
Semi-log model (Barksdale, 1972)	$\varepsilon_p = a_1 + b_1 \log N$ $\varepsilon_{pn} = \frac{b_1}{N}$ (N > 1)	(2.27) (2.28)	ε_p = accumulated permanent strain ε_{pn} = permanent strain at the N^{th} load application a_1 and b_1 = positive regression constants
Power law model (Monismith et al., 1975)	$\varepsilon_p(\mathrm{N}) = \mathrm{aN}^b$	(2.29)	$\varepsilon_p(\mathrm{N})$ = accumulated permanent strain *a*, *b* = regression constants *N*= number of load repetition
Francken (1977)	$\varepsilon_p(N) = AN^B + C(e^{DN} - 1)$	(2.30)	*N*= number of load repetition ϵ_p = permanent axial strain, µm, and, *A*, *B*, *C*, and *D* = regression constants
VESYS model (Kenis 1977)	$\varepsilon_{\mathrm{pn}} = \mu\, \varepsilon_r\, \mathrm{N}^{-a}$	(2.31)	ε_{pn} = permanent strain at the N^{th} application ε_r = resilient strain µ = constant of proportionality between permanent strain and elastic strain α = 1-b = rate of decrease in incremental permanent deformation with increase in *N* *N*= number of load repetition
Brown & Bell (1979)	$\varepsilon_p = (q/a)^b(N)$	(2.32)	ε_p = permanent strain *q* = deviator stress *a*, *b* = constants *N*=number of load repetition
Ohio State model (Majidzadeh et al., 1980)	$\varepsilon_p = \mathrm{aN}^{1-\mathrm{m}}$	(2.33)	ε_p = accumulated permanent strain; a and m = regression constants *N*= number of load repetition
Huschek (1985)	$e_{irr} = c * \sigma t^A$	(2.34)	e_{irr}= permanent deformation *c* and *A* = constant and consolidation characteristic σ and *t* = stress level and loading time

Author	Permanent Deformation Model		Variables
Khedr (1986)	$\varepsilon_p/N = A_a N^{-m}$	(2.35)	ε_p = permanent strain; A_a= function of resilient modulus and applied stress m = material parameter
Tseng and Lytton's model (1989)	$\varepsilon_a = \varepsilon_0 e^{-\left(\frac{\rho}{N}\right)^b}$	(2.36)	ε_a = permanent strain ε_0, b and ρ = regression constants
Superpave model (Lytton et al., 1993)	$\log \varepsilon_p = log\, \varepsilon_p(1) + S\ \log N$	(2.37)	ε_p = accumulated permanent strain $\varepsilon_p(1)$ = permanent strain at first load application S = positive regression constants N=number of load repetition
Monismith et al. (1994)	$\varepsilon_z^p = [\delta(T) N^{\alpha} \sigma^{n-1} t] * \left[\sigma_z - 0.5(\sigma_x + \sigma_y)\right]$	(2.38)	ε_z^p= vertical permanent deformation $\delta(T)$ = function of temperature α = coefficient determined experimentally σ and t = equivalent stress and loading time N= number of stress repetition
AASHTO 2002 model (Witczak et al., 2002)	$\log \frac{\varepsilon_p}{\varepsilon_r} = log\, C + 0.4262\ \log N$ $C = T^{2.02755}/5615.391$	(2.39) (2.40)	ε_p = accumulated permanent strain; ε_r = resilient strain N= number of load repetition
Zhou et al. (2004)	$\varepsilon_p = aN^b;\ N < N_{PS}$ $\varepsilon_p = \varepsilon_{ps} + c(N - N_{PS});\ N_{PS} \leq N < N_{ST}$ $\varepsilon_p = \varepsilon_{ST} + d\left(e^{f(N-N_{ST})} - 1\right);\ N \geq N_{ST}$	(2.41) (2.42) (2.43)	N_{ps}, N_{st} = load repetitions corresponding to the initiation of the secondary and tertiary stage. ϵ_{ps}, ϵ_{st}= permanent strain corresponding to the initiation of the secondary and tertiary stage ϵ_p= permanent strain at the end of N cycles. a, b, c, d, and f = material constant

2.8 Effect of warm mix additives on a bituminous mixture

From section 2.4 to section 2.7, it can be noticed that researchers have evaluated the properties of bituminous mixture modified with different types of additives. Warm mix additive is one such additive that facilitates the reduction in the mixture's production temperature compared to the hot bituminous mixture. A reduced production also means that a bituminous mixture will undergo less aging during the production process. In this section, the effect of a warm mix additive on the mechanical behavior of the bituminous mixture is discussed, as shown in Table 2.16.

Table 2.16 Mechanical behavior of a warm bituminous mixture

Authors	WMA additive	Properties studied	Remarks
Haggag et al. (2011)	Advera, Evotherm 3G, Sasobit	Dynamic modulus and fatigue cracking resistance	No significant difference in dynamic modulus and fatigue crack resistance of the HMA and WMA was noticed.
Nazzal et al. (2011)	Aspha-min, Evotherm, Sasobit	Rut depth recorded in the test section of the accelerated pavement loading facility	During the first 1000 passes, test sections with WMA mixture had higher rut depth. However, the rut depth during the 3000 to 10000 cycles of both HMA and WMA mixtures was comparable.
Ghabchi et al. (2013)	Sasobit, Advera, and Evotherm	Work of adhesion and TSR	The addition of a warm mix additive resulted in an increase in the work of adhesion between binder and different types of aggregates used. However, only Evotherm resulted in a significant increase in work of adhesion with granite aggregate. HMA mixture had higher (0.93) TSR as compared to Advera (0.71) and Evotherm (0.66) mixtures.
Hill et al. (2013)	Sasobit, Advera, Evotherm 3G, and Rediset LQ	TSR and passes to reach 12.5 mm rut depth	Only the mixture with Evotherm 3G satisfied the 80 % TSR requirement. HMA and mixture with Sasobit sustained higher wheel passage (approximately 40 % higher) than mixture with Evotherm 3G, Advera, and Rediset LQ.
Xie et al. (2014)	Sasobit, Evotherm, and Rediset	TSR and bending strain at failure.	Each bituminous mixture had TSR higher than 80 %. Compared to the HMA mixture, each WMA mixture had a lower bending strain at failure, indicating reduced resistance to cracking at low temperatures (-10 °C).
Sebaaly et al. (2015)	Advera, Evotherm, Foaming	Wet and dry ITS, TSR, resistance to rutting	HMA and WMA mixtures satisfied the minimum 80 % TSR requirement. For a selected aggregate source, the rut depth was not influenced by the type of warm mix additive.

Authors	WMA additive	Properties studied	Remarks
Lu & Saleh (2016)	Evotherm 3G and Sylvaroad	TSR and fatigue life	Only the WMA mixture with Evotherm 3G had TSR higher than 80 %. Bituminous mixture with Evother 3G warm mix additive had significantly lower numbers of cycles to failure compared to HMA mixture.
Kassem et al. (2018)	Sasobit, Evotherm, and Rediset	Cohesive and adhesive bond energy	WMA additives reduced the cohesive bond energy of bituminous binder, which resulted in better coating with aggregates. The addition of warm mix additives also improved the adhesive bond energy between aggregate and binders.
Abd El-Hakim et al. (2019)	Foaming and Evotherm DAT	Resilient modulus, TSR, Hamburg wheel tracking test	Bituminous mixture with Evotherm additive had lower resilient modulus as compared to HMA and Foaming technology at different laboratory conditioning (oven aging time and temperature). WMA mixtures subjected to 5 days aging at 85 °C satisfied the 80 % TSR requirement. The rut depth of WMA mixtures after 10,000 wheel pass was higher than HMA at different conditions

The nature of warm mix additive, i.e., chemical package or wax-based or foaming, etc., also influences the behaviour of a bituminous mixture, as shown in Table 2.17.

Table 2.17 Effect of warm mix additive properties on a bituminous mixture

Authors	Binder	Warm mix additive		Mixture properties	
		Type	Nature		
Mogawer et al. (2011)	PG64-22	Not used	HMA	Stripping inflection point (cycles); loss in pull-off tensile strength (%)	12600; 37.7
		Advera	Foaming		9700; 45.5
		Evotherm M1	Chemical package		14200; 46.1
		Sasobit	Wax based		13700; 41.6
		SonneWarmix	Wax based		10300; 38.1
Leng et al. (2014)	PG64-22	Not used	HMA	ITS (MPa); Fracture energy (J/m2)	0.68; 900
		Evotherm 3G	Chemical package (surfactant and antistripping agent)		0.60; 1100
		Rediset LQ-1106	Chemical package with antistripping agent		0.78; 950
Lu & Saleh (2016)	Penetration grade 80/100	Not used	HMA	ITS (kPa); Fatigue life (cycles)	630; 5.9×10^5
		Evotherm 3G	Chemical package		520; 2×10^5
		Sylvaroad	Enhance coating and workability		410; 8.8×10^5

2.9 Statistical analysis

Studies have used statistical tools to quantify the effect of different factors like aging, moisture, type of additive, aggregate gradation, aggregate and bitumen types, test temperatures, etc., on the mechanical behavior of bituminous mixtures. A few commonly used statistical tools are listed in Table 2.18.

Table 2.18 Commonly used statistical analysis tools

Author	Statistical analysis tool	Parameters	Replicates
Mohammad et al. (2012)	A student's t-test at 0.05 significance level	Rut depth at 50 °C TSR at 25 °C SCB at 25 °C	3-SCB 3-ITS 2-LWT
Punith et al. (2012)	A student's t-test at 0.05 significance level	ITS, toughness, and deformation calculated from ITS test at 25 °C	4
Bayekolaei et al. (2016)	ANOVA Tukey pairwise comparisons	Marshall stability RM at 25 ℃ and 40 ℃ Rut depth at 60 °C	3
Cucalon et al. (2016)	ANOVA Tukey pairwise comparisons	ITS & TSR at 25 °C HWTT at 50 °C	3-ITS 2-HWTT
Kaseer et al. (2018)	ANOVA Tukey pairwise comparisons	FI at 25 ℃ CRI at 25 ℃	4
Nemati et al. (2019)	A student's t-test at 0.05 significance level	RDCI at 25 ℃ FI at 25 ℃	3, 4, and 24 (based on quantity collected from HMA plant)
Amani et al. (2020)	ANOVA	SCB at −20 ℃ SCB at 25 ℃ ITS at 25 ℃	3
Akentuna et al. (2020)	ANOVA Tukey pairwise comparisons	ITS LWT SCB	3 – IDT 4 – LWT 4 – SCB
Jahanbakhsh et al. (2020)	ANOVA Tukey pairwise comparisons	Marshall stability and flow IDT test SCB test	3
Al-Asi & Asi (2021)	ANOVA	ITS Dynamic creep Resilient Modulus Fatigue Life	3
Gupta et al. (2021)	Anderson Darling normality test If following normal distribution - two sampled student tests; Otherwise - Mann-Whitney U test	Air voids (AV) Cantabro tests (CB) Permeability (PM) ITS test	3 – AV 3 – CB 4 – PM 4 – ITS

Author	Statistical analysis tool	Parameters	Replicates
Phan et al. (2021)	Tukey-Kramer	CT_{index} Flow number Overlay testing (Cyclic fatigue)	3

2.10 Chapter summary: Research gaps

This chapter presented a comprehensive literature review on the influence of aging and moisture on the bituminous mixture's performance. The literature summary is present in section 2.10.1, and the research gap is presented in section 2.10.2.

2.10.1 Chapter summary

The literature study is summarized in different sub-section below.

A. Cracking resistance of the bituminous mixture

Researchers have explored different test processes and parameters to capture the cracking resistance of bituminous mixture. A monotonic loading test such as an indirect tensile test (ASTM D6931) or a semi-circular beam bending test (ASTM D8044) is used to evaluate the bituminous mixture's cracking resistance. The stiffness and resilient modulus of the bituminous mixture also quantify the mixture's cracking resistance. Researchers noticed that the tensile strength and modulus of the bituminous mixture increased with an increase in aging and reduced with the increase in moisture conditioning cycles. The tensile strength of the bituminous mixture increased at a higher rate during the initial aging period and reached a plateau after a specific duration of aging. The tensile strength ratio is widely used to assess moisture's effect on a bituminous mixture's cracking resistance.

Researchers have utilized the load-deformation curve generated from a monotonic test to determine parameters like fracture energy, dissipated creep strain energy, and elastic energy. Fracture energy of the bituminous mixture reduced with aging, indicating a reduction in the cracking resistance of the mixture. Whereas, few studied have also noticed that fracture energy increased aging. Few researchers noticed that fracture energy and fatigue cracking of bituminous mixture are not well co-related. The fracture energy parameter was more sensitive to different test conditions as compared to the tensile strength parameter. Recently parameters like the flexibility index, cracking tolerance index, cracking resistance index, and the rate-

dependent cracking index parameters was developed utilizing different aspects of the stress-strain curve. Researchers have noticed that the CRI parameter had a lower coefficient of variation than the FI parameter.

B. Adhesive failure in the bituminous mixture

Studies carried out a visual observation to quantify or rate the extent of adhesive failure in loose bituminous mixtures or compacted specimens subjected to moisture conditioning. The biased nature of visual estimation to quantify adhesive failure was replaced with image analysis techniques. The extent of adhesive failure in bituminous mixture increased with the increase in moisture conditioning cycles or duration. The adhesive failure was also noticed to increase with the reduction in test temperature. Furthermore, researchers explored the effect of aging on adhesive failure. The authors noticed that the level of aging also influences the adhesive failure in the bituminous mixture. A moderate aging level (e.g., short-term aging) may positively contribute to the adhesive bond strength between aggregate and bitumen. However, in a longer duration, moisture intrusion can remove/dissolve the polar compounds formed during aging (e.g., long-term aging) and increase the extent of adhesive failure in the bituminous mixture. Researchers have also noticed that the aggregate mineralogy significantly influences the bituminous mixture's adhesive failure. Basic aggregates tend to offer higher resistance against adhesive failure as compared to acidic aggregates.

C. Fatigue resistance in the bituminous mixture

Researchers have noticed that in the case of a stress-controlled fatigue test, the fatigue life of the bituminous mixture increases with the increase in the duration of aging. Laboratory estimated fatigue life depended on the test temperature with higher fatigue life at lower test temperature and vice-versa. At a higher test temperature, the impact of aging on the fatigue life of the bituminous mixture was noticed to be more significant. Researchers noticed that in an aged bituminous binder, a crack requires less work to propagate than an unaged bitumen. This may be due to the decrease in the work of cohesion with aging in the bituminous binder. In bituminous mixtures, the crack initiates at a lower dissipated energy value in an aged mixture. Therefore, it propagates at a higher rate in the long-term aged bituminous mixture than the short-term aged and unaged bituminous mixture. Researchers have noticed that moisture also accelerated the crack growth in the bituminous mixture. Moisture reduces the cumulative dissipated pseudo strain energy (a measure of the damage accumulation before failure) in a

bituminous mixture. The crack size index (ΔR) of moisture-conditioned specimens was higher than the dry specimen, indicating more serious fatigue damage in moisture-conditioned specimens.

Researchers also explored different approaches to model the fatigue life of the bituminous mixture. For example, regression models developed to determine a bituminous mixture's fatigue life can't explain the damage accumulation mechanisms in a mixture. However, researchers noticed that fracture energy had a good association with the fatigue life, and including fracture energy in the regression model may improve the model. In addition, a stochastic modeling approach considers the associated variabilities like inherent material property variation, construction variation, and variation imposed by a change in environmental conditions.

D. Creep resistance of the bituminous mixture

Researchers noticed that the level of aging influences the creep resistance of bituminous mixture. The bituminous mixture's creep resistance increased with the increase in aging duration. The increment in creep resistance rate with aging in the bituminous mixture was much higher during the initial aging period. The long-term creep resistance of the bituminous mixture was influenced by the degree of short-term aging. The laboratory mixture aging temperature also influenced the creep behavior in the bituminous mixture. A higher creep resistance was noticed in mixtures subjected to higher aging temperature and vice-versa. Compared to aging duration, the aging temperature might have a higher influence on the creep resistance of the bituminous mixture. Moisture reduced the creep resistance of the bituminous mixture. Research showed that a higher stress level might better assess the creep resistance of a bituminous mixture conditioned with moisture when compared to a lower stress level. Further, moisture's negative impact on the bituminous mixture's creep resistance may be prominent at higher test temperatures. Research also showed that the effect of temperature, followed by moisture, followed by the stress level, is the order of significance on the bituminous mixture's creep behaviour.

2.10.2 Research gap

Amongst the different parameters developed by researchers, there is a need to identify a suitable parameter that can capture the influence of aging and moisture conditions on the

cracking resistance of bituminous mixture. The adhesive failure in the bituminous mixture has the potential to screen moisture susceptible mixture. The severity of adhesive failure in a bituminous mixture also depends on moisture conditioning and the extent of bitumen aging. In this regard, limits or threshold values of adhesive failure are required to categorize bituminous mixture into different zones based on their moisture susceptibility. Further, the association of adhesive failure with the indirect tensile strength and fracture energy of the bituminous mixture may help understand the effect of moisture on the cracking resistance of the mixture. Evaluating the fatigue behavior of a bituminous mixture is important, especially when the mixtures are exposed to both aging and moisture conditioning. Most of the test protocols consider only mimicking aging during laboratory characterization of bituminous mixtures. A study on the synergistic effect of aging and moisture conditions on fatigue and creep damage resistance will aid in developing an understanding of performance and help design a durable bituminous mixture. A probabilistic fatigue damage modeling approach may be better suited to account for the variability and scatter in the fatigue data resulting from different aging and moisture conditioning levels. Both aging and moisture influence the creep resistance of the bituminous mixture. Thus, knowledge on the influence of test conditions such as the magnitude of stress and test temperature on the creep resistance of moisture-conditioned bituminous mixture is required.

Chapter 3

Materials, Test Methods, and Research Methodology

3.1 Introduction

This chapter discusses the physical and engineering properties of materials used in the research work. The test procedures to investigate the bituminous mixture's performance regarding resistance to moisture damage, resistance to creep, and fatigue life of mixtures are highlighted. The criterion considered for different test conditions based on the review of previous works (Chapter 2) is presented in Table 3.1. The research methodology associated with each task and the experimental program to accomplish the research work tasks is shown next.

Table 3.1 Criterion considered for different test conditions

Category		Selected levels	Reasons	Reference
Materials	Aggregate	Two sources, i.e., calcareous and siliceous	Calcareous aggregates have good resistance against moisture damage, and siliceous aggregates have low resistance against moisture damage	Airey et al. (2008); Cui et al. (2014)
	Bitumen and warm mix additive	VG30 (PG 64-xx) and Evotherm-J1	VG 30 is used for most of the paving operations in India. The application of Evotherm-J1 does not require any modification to the standard specimen production equipment. Also, it contains adhesion promoters.	IRC: 111-2009; Ingevity, North Charleston, SC
Test temperature	Tensile strength	15 °C and 25 °C	Specifications recommend 25 °C. Researchers predominantly use 15 °C	ASTM D6931; Gao et al. (2017)
	Fatigue	15 °C and 25 °C	Selected based on the range of test temperatures predominantly used by researchers	Moghadas Nejad et al. (2014); Diab et al. (2019)
	Creep	40 °C and 45 °C		Bennert et al. (2011); Pouranian et al. (2020)

Category		Selected levels	Reasons	Reference
Stress level	Fatigue	250 kPa at 25 °C and 400 kPa at 15 °C	Stress levels were selected to maintain strain range in the range of 100 με to 400 με	BS EN 12697-24: 2012
	Creep	100 kPa and 150 kPa	100 kPa is recommended by standard. 150 kPa was recommended for moisture conditioned specimen	BS DD 226: 1996; Mehrara and Khodaii, (2011)
Aging		STA and LTA	As per AASHTO R 30 and NCHRP 815 recommendation	AASHTO R30; Newcomb et al. (2015)
Moisture		UC, 1 FT, and 3FT cycles. Loose mixture boiling water test	More than one FT cycle may be required for better evaluation	ASTM D3625; AASHTO T 283; Vargas-Nordcbeck et al. (2016)

3.2 Research methodology

The nomenclature of the materials, parameters, test conditions and equipment used in this study is shown in Table 3.2. The materials, parameters, test conditions, and equipment presented in Table 3.2 is discussed in details in Section 3.3 to 3.7 respectively.

Table 3.2 Materials, parameters, test conditions, and equipment used in this study

Materials/Parameters/Test conditions/ Equipment	Name/Acronym
Aggregate	Source A, Source B
Bitumen	VG 30
Bitumen additive	Evotherm-J1
Aging	STA, LTA, T-283
Moisture	UC, 1 FT, 3FT, boiling water test
Equipment	ITS, ITSM,ITFT, Creep, Asphalt compatibility tester (ACT)

The research methodology used in this study is shown in Figure 3.1. Four critical tasks were formulated to achieve the objective. The experimental framework associated with each task is shown in Figure 3.2 to Figure 3.6.

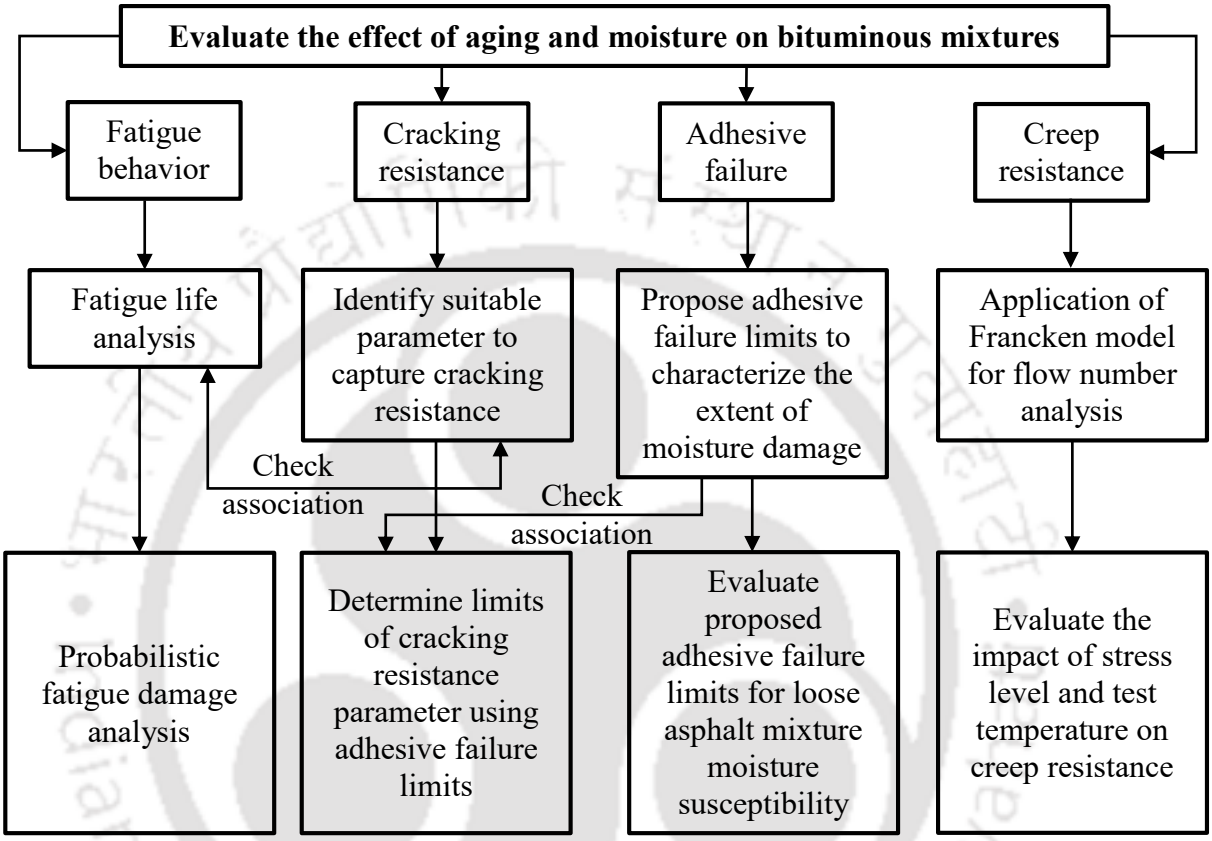

Figure 3.1 Research methodology of this study

3.2.1 Task 1: Identification of cracking index

The research framework used for determining a suitable cracking resistance of bituminous mixtures subjected to aging and moisture conditioning is shown in Figure 3.2.

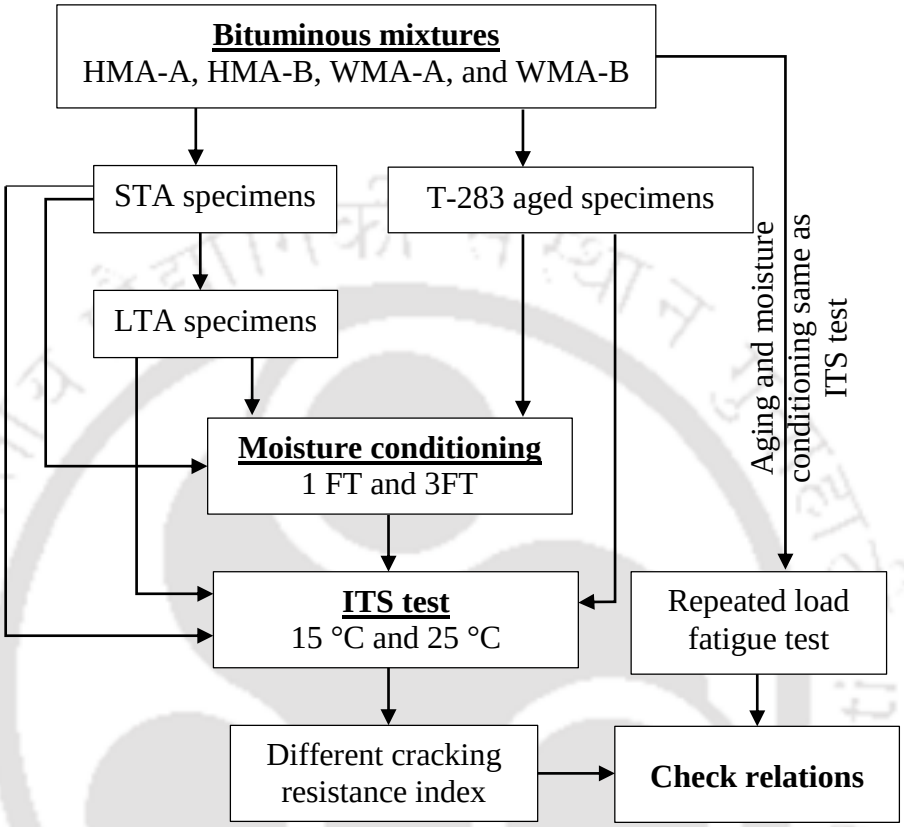

Figure 3.2 Framework to identifying suitable cracking index parameter

3.2.2 Task 2: Adhesive failure in bituminous mixtures

The image analysis process begins with image acquisition, and a digital camera (Nikon D3400, 24 megapixels) was used for capturing the images. The color digital image was converted into a greyscale image for further processing. The region coated with bitumen, the region of adhesive failure, and the region of broken aggregates need to be identified in the greyscale image. This can be done by establishing two threshold values that will separate one region from the other. In this study, two methods were used. In Method 1, threshold values were directly determined from different fractions of crushed aggregates. In Method 2, the procedure established by Lee et al. (2013) was used. This threshold value (T_1) will separate the region with broken aggregates from the specimen, as shown in Figure 3.3. The percent pixel area associated with T_1 threshold value was designated as P_1. Then, the percent pixel area of broken aggregates was determined by subtracting the P_1 from the total percent pixel area (100 percent area) as shown in Eq. (3.1) (Lee & Kim, 2014). Next, the threshold value associated with aggregates completely coated with bitumen was determined using a process like Method 1. This threshold value (T_2) will separate the region coated with bitumen from the specimen. The percent pixel area associated with T_2 threshold value was designated as P_2. For determining the percent, adhesive failure Eq. (3.2) (Lee & Kim, 2014) was used. The research framework used for determining the adhesive failure in the bituminous mixtures subjected to aging and moisture conditioning is shown in Figure 3.4.

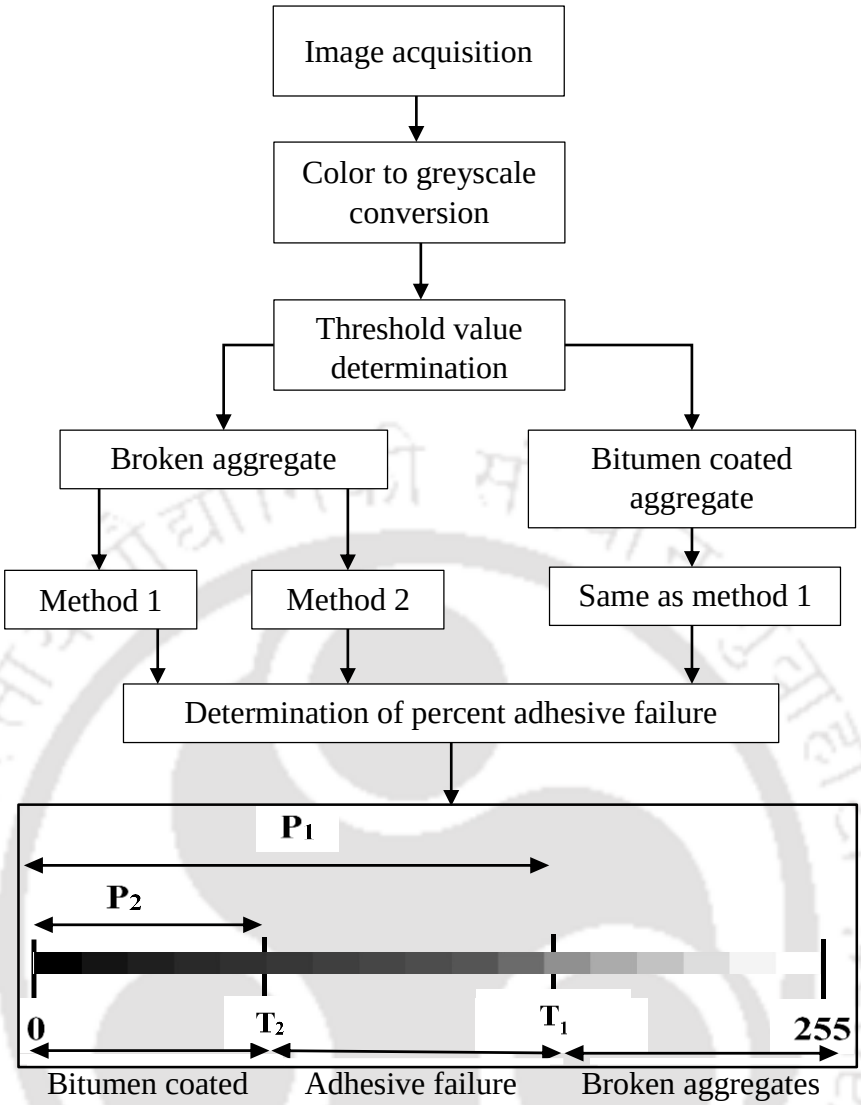

Figure 3.3 Image analysis methodology

$$Broken\ Aggregates, BA\ (\%) = 100 - P_1 \quad (3.1)$$

$$Adhesive\ Failure, AF\ (\%) = 100 - (BA + P_2) \quad (3.2)$$

where,

P_1= pixel area associated with the threshold value of T_1, %

P_2= pixel area associated with the threshold value of T_2, %.

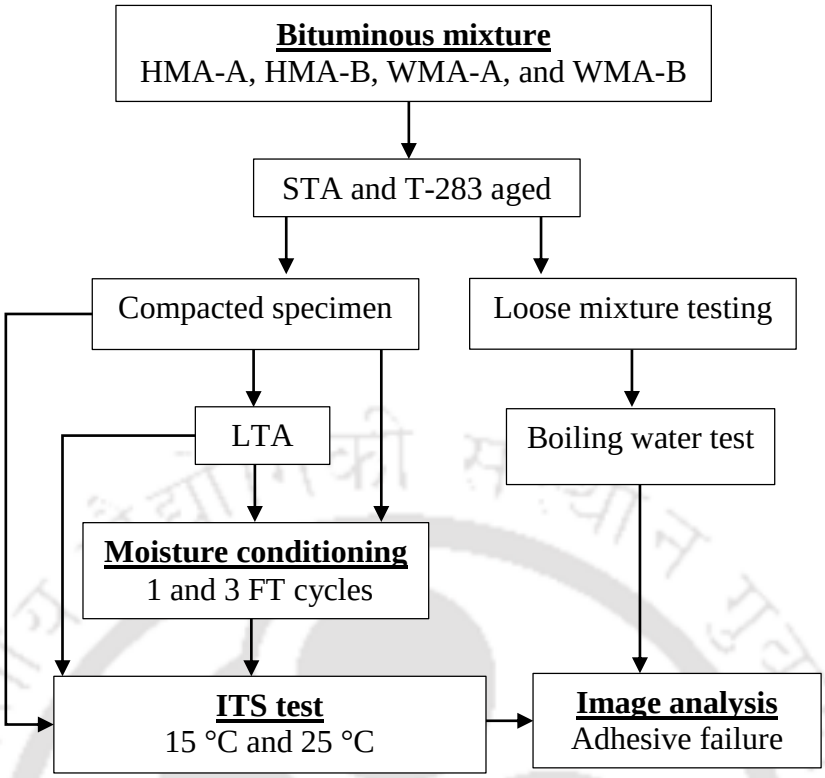

Figure 3.4 Framework to understand adhesive failure in a bituminous mixture

3.2.3 Task 3: Fatigue performance of the bituminous mixture

The research framework used for understanding the fatigue behavior of bituminous mixtures subjected to aging and moisture conditioning is shown in Figure 3.5.

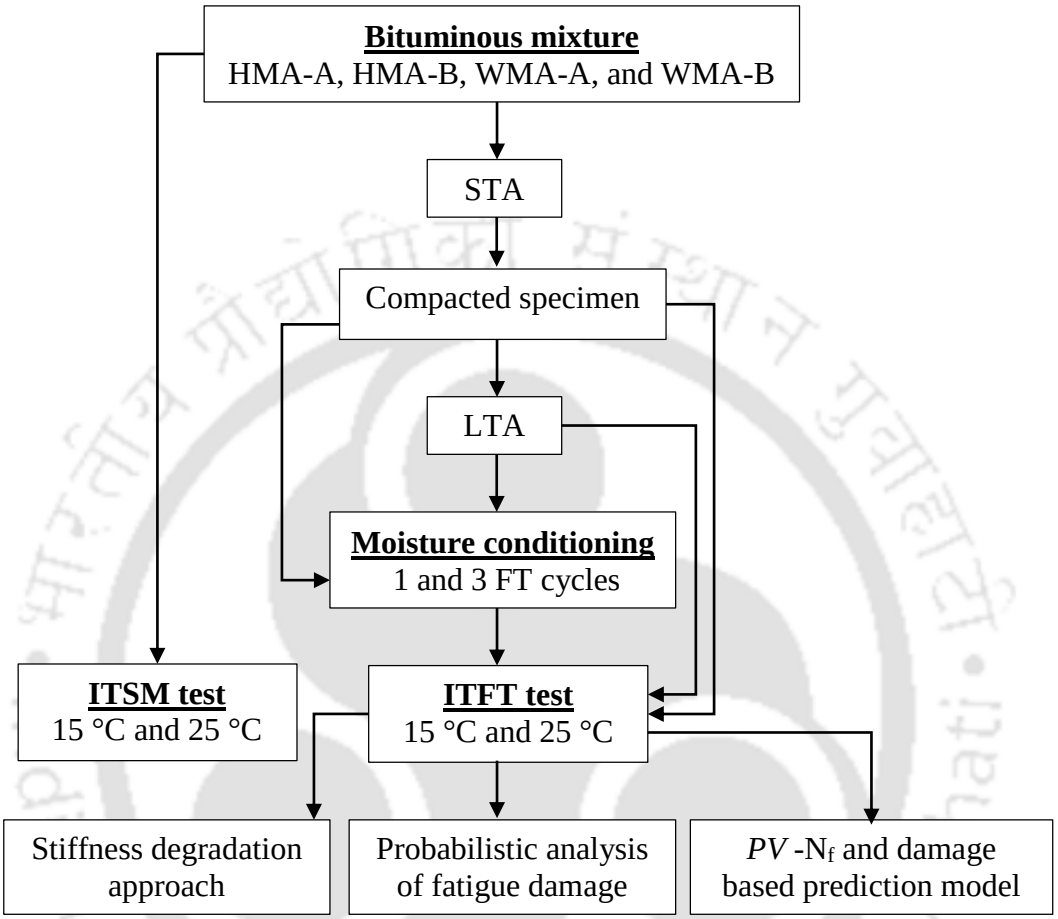

Figure 3.5 Framework to determine the fatigue behavior of a bituminous mixture

3.2.4 Task 4: Creep resistance of bituminous mixtures

The research framework used for understanding the creep behavior of bituminous mixtures subjected to aging and moisture conditioning is shown in Figure 3.6

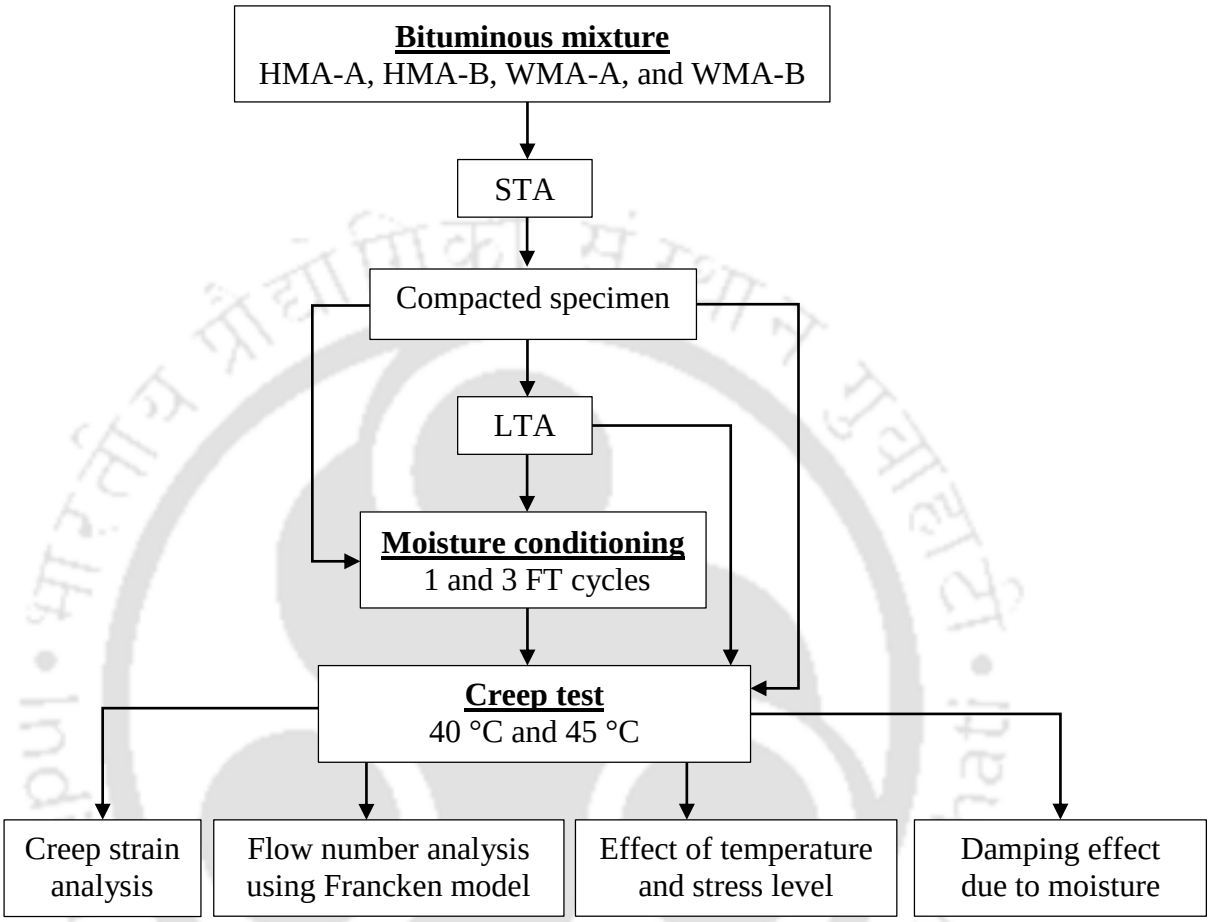

Figure 3.6 Framework to determine the creep behavior of a bituminous mixture

3.3 Materials

3.3.1 Bitumen and warm mix additive

Bitumen is the binding agent in the bituminous mixture. The climatic conditions and traffic volume are taken into consideration while selecting the grade of the bituminous binder. MoRT&H (2013) recommends using a viscosity grade VG-30 binder for Indian conditions with the highest daily mean air temperature of 30 °C or more and the lowest daily mean air temperature of -10 °C or less. Also, VG-30 grade bituminous binder is most widely used in

Indian for bituminous road constructions. In this study, one unmodified viscosity grade VG-30 binder was used to produce the bituminous mixtures. The effect of aging and moisture on a bituminous mixture produced at a relatively lower production temperature was also evaluated in this study. For this purpose, Evotherm-J1 (Ingevity, North Charleston, SC) warm mix additive was used for producing the warm mix asphalt (WMA) mixtures. The Evotherm-J1 is a chemical package that contains adhesion promoters, improves the coating, workability, and compaction of the bituminous mixture. The VG-30 binder was heated to 125 ± 5 °C, and the Evotherm-J1 warm mix additive was added at a rate of 0.4 % by weight of binder for preparing the WMA mixture, as per the manufacturer's recommendation. The physical properties of the VG-30 binder and VG-30 binder modified with the Evotherm-J1 warm mix additive are shown in Table 3.3.

Table 3.3 Properties of bitumen

Properties	**Test specification**	**Specification limit**	**Result**	
			VG 30	**VG 30 with Evotherm-J1**
Specific Gravity	IS: 1202-1978	-	1.03	1.03
Penetration at 25 °C, 100 g, 5 s, 0.1 mm	IS: 1203-1978	min. 45	51	52
Kinematic viscosity at 135 °C, cSt	ASTM D4402	min 350	585	504
Softening point, °C	IS: 1205-1978	min 47	51	50
Ductility at 25 °C, cm	IS: 1208-1978	min 40	91	92
$\lvert G^* \rvert / \sin(\delta)$ @ 64 °C (unaged)	ASTM D7175	1 kPa	1.78	1.59
$\lvert G^* \rvert / \sin(\delta)$@ 64 °C (STA)	ASTM D7175	1 kPa	4.65	2.92

3.3.2 Aggregate

Mineral aggregates form the bulk of the bituminous mixture and contribute to about 92 to 96 percent of the volume. Aggregates also contribute to the compressive strength of the mixture. From the literature, it is well understood that the mineralogical composition of aggregate affects bituminous mixtures' moisture susceptibility. Aggregates that are calcareous have a good resistance against moisture damage, and siliceous aggregates have low resistance against moisture damage (Airey et al., 2008; Cui et al., 2014). Thus, one calcareous and one siliceous source of aggregates termed as "source A" and "source B" were used in this study. MoRT&H (2013) requirements for aggregates used for the bituminous mixture were checked for each aggregate source, as shown in Table 3.4. The engineering properties are shown in Table 3.4, and it could be noticed that both aggregate sources are different from each other.

Source A aggregates are relatively stronger, rounded, and have less water absorption value as compared to source B aggregates.

Another important aspect is the mineralogical composition of the aggregate sources. The mineralogical composition of the aggregates used in this study was determined using X-ray diffraction (XRD). The material passing 75 μ sieve was scanned using copper Kα radiation with a wavelength of the incident X-ray equal to 1.54 Å. The diffractometer was running at 50 kV and 100 mA. The step widths were 0.03° from 10° to 90° 2-theta with a scan step time of 1s per step. Elemental composition was determined using Field Emission Scanning Electron Microscope (FESEM) coupled with energy dispersive X-ray (EDX) spectroscopy. The backscattered electron images in the FESEM display compositional contrast resulting from different atomic number elements and their distribution. EDX allows one to identify the elements and their relative percentage.

Table 3.4 Properties of aggregates

Properties (test)	**Test specification**	**Specification limit**	**Result**	
			Source A	**Source B**
Cleanliness (grain size analysis)	IS: 2386 part I	Max. 5 % passing 75 μ	1.18%	1.23%
Particle shape (combined flakiness and elongation index)	IS: 2386 part I	Max. 35 %	29.4	35.4
Angularity number	IS: 2386 part I	-	4	7
Strength (aggregate Impact Value)	IS: 2386 part IV	Max. 24 %	20	24.6
Water Absorption, max 2 %	IS: 2386 part III	Max. 2 %	0.87	1.21
Specific gravity (coarse aggregate)	IS: 2386 part III	-	2.749	2.671
Specific gravity (fine aggregate)	IS: 2386 part III	-	2.754	2.601
Specific gravity (filler)	IS: 2386 part III	-	2.794	2.746
Mineralogical composition	-	-	Calcareous	Siliceous

The raw data obtained from XRD was quantitatively analyzed using match software. Aggregates source A consisted of Calcium carbonate (47.2 %), Dolomite (41.9 %), and silicon dioxide (10.9 %), while source B consisted primarily of Quartz (77.3 %) and Anorthite (22.7 %), respectively. The morphology and atomic percentages of aggregates source A and source B are shown in Figure 3.7. From FESEM images (Figure 3.7), it could be noticed that particles in source A aggregates are uniform-like in shape (sub-rounded to angular shaped). In contrast, source B aggregates are irregular-like in shape (flat and elongated). The atomic percentages obtained from EDX of source A and source B are also shown in Figure 3.7. Furthermore, it

could be noticed that source A predominantly consists of calcium elements, while source B consists of a silicon element. Hence, mineral aggregates source A would be calcareous (basic) in nature, while aggregates in source B would be siliceous (acidic) in nature. Thus, it is believed that source A aggregates would exhibit higher resistance to moisture damage when compared to source B. In line with the above observation, source B aggregates had a higher affinity to moisture than source A aggregates (as shown in Table 3.4).

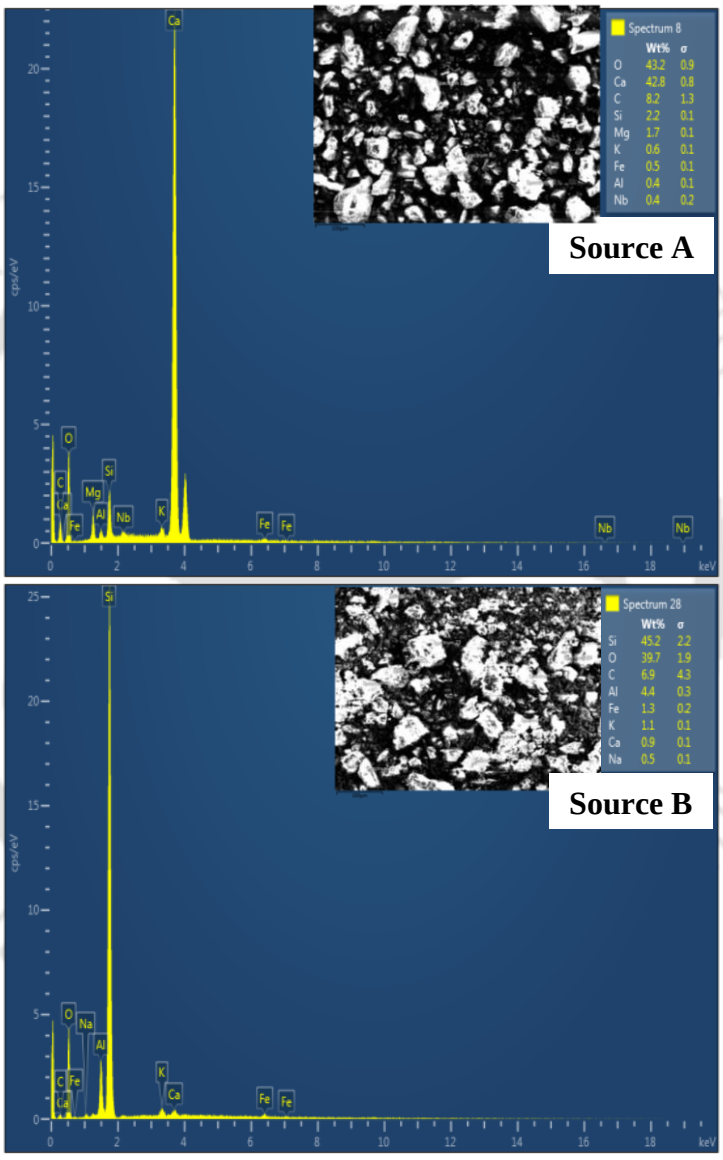

Figure 3.7 Mineralogy of source A and Source B aggregates

Bituminous concrete (BC) aggregate gradation with a nominal maximum aggregate size of 13.2 mm is the most commonly used aggregate gradation for the surface course on Indian highways. In this study, BC grade-2 (BC-2) aggregate gradation was used for preparing the

bituminous mixtures. A mid-point gradation was adopted for specimen preparation, as shown in Figure 3.8, as per MoRT&H (2013) recommendation.

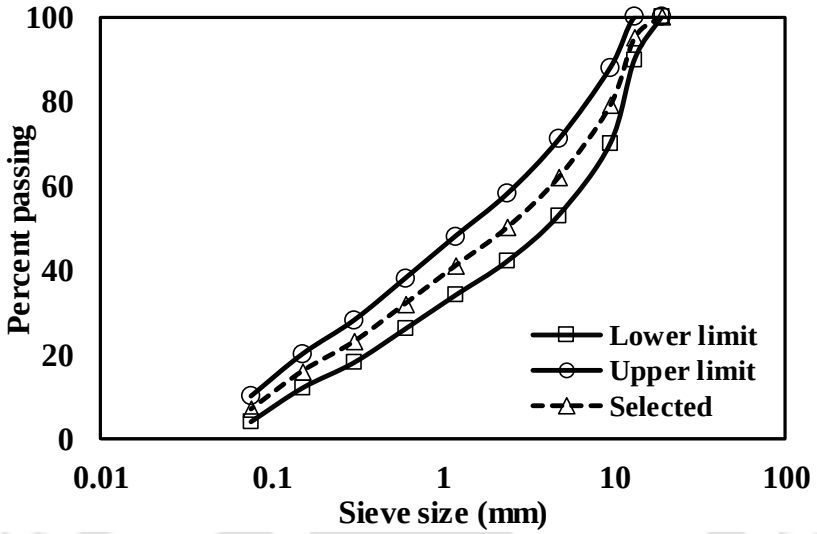

Figure 3.8 Aggregate gradation used for specimen preparation (BC-2)

3.4 Bituminous mix design

Marshall method of mixture design was used for bituminous mixture design following the Asphalt Institute manual series 2 guidelines. As mentioned in sections 3.3.1 and 3.3.2, one unmodified VG-30 unmodified bituminous binder and two aggregate sources (termed A and B) were used. The HMA mixture with aggregate source A was termed as HMA-A, and with aggregate source B was termed as HMA-B mixture. Similarly, mixtures produced with Evotherm-J1 warm mix additive were termed as WMA-A and WMA-B, respectively. In this study, a mix design was performed on the HMA-A mixture, and the same optimum binder content (OBC) was used for preparing the remaining mixtures, i.e., HMA-B, WMA-A, and WMA-B. The application of the same binder content for different mixtures will eliminate the effect of binder content variation on the performance of the bituminous mixture.

After selecting the ingredients, the first step in the mix design is to determine the working temperatures. The bituminous mixture should have adequate workability during the mixing and compaction process. The viscosity of bitumen in a range of 0.17 ± 0.02 Pa.s and 0.28 ± 0.03 Pa.s is recommended to mix and compact the bituminous mixture (Asphalt Institute MS-2). The viscosity of the VG-30 binder was determined at 135 °C and 165 °C using a rotational viscometer as per ASTM D4402 protocol. A plot of temperature versus viscosity was produced, as shown in Figure 3.9. The temperature corresponding to 0.17 ± 0.02 Pa.s for mixing and 0.28

± 0.03 Pa.s for compaction was determined, as shown in Table 3.5. For WMA mixtures, the mixing and compaction temperature recommended by the manufacture was adopted for preparing specimens, as shown in Table 3.5. The IRC recommended mixing and compaction temperature is also shown in Table 3.5. The mixing and compaction temperatures for HMA and WMA mixture adopted in this study satisfied the IRC requirements (see Table 3.5).

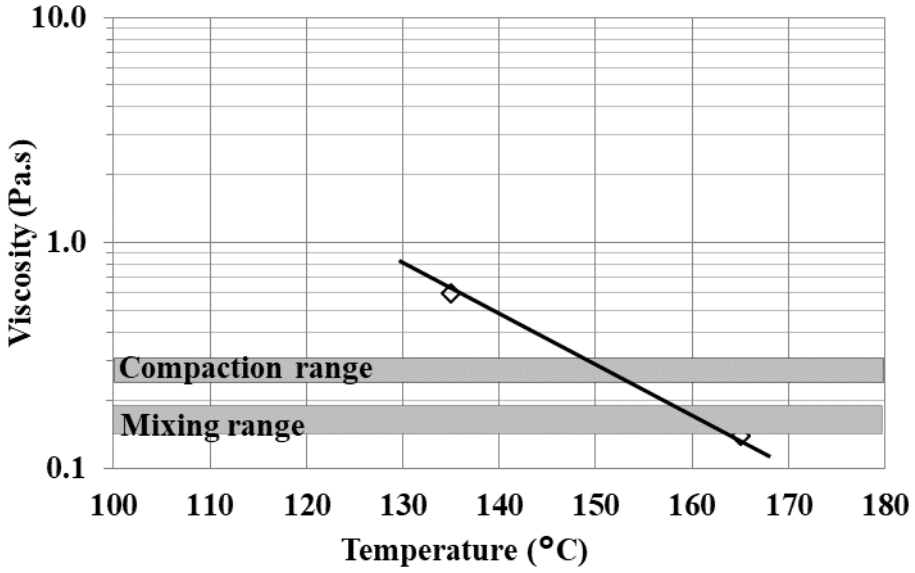

Figure 3.9 Mixing and compaction temperature chart

Table 3.5 Mixing and compaction temperature

Process	Viscosity, Pa.s	HMA		WMA	
		Adopted, °C	IRC:111 requirement, °C	Adopted, °C	IRC: SP:101 requirement, °C
Mixing	0.17 ± 0.02	160 ± 3	150-165	130 ± 3	Max. 130
Compaction	0.28 ± 0.03	153 ± 3	Min. 140	116 ± 3	Min. 115

For optimum binder content determination of the bituminous mixture, three specimens were prepared at each binder content as per Asphalt Institute MS-2 guideline. From density-void analysis and stability-flow analysis, a binder content of 5.4 % was noticed to satisfy the IRC:111 requirements, as shown in Table 3.6. The binder content of 5.4 % was selected as the optimum bitumen content (OBC) for the HMA-A mixture. As mentioned, HMA-B, WMA-A, and WMA-B mixtures were also prepared at 5.4% binder content and checked against the IRC:111 requirements. Each mixture was found to satisfy the specification requirements, as shown in Table 3.6. Further, a one-way ANOVA was carried out at a 5 percent significance

level on the volumetric properties, i.e., air voids, VMA, and VFB of the bituminous mixtures. It can be noticed from Table 3.7 that the volumetric properties of all four mixtures were not significantly different.

Table 3.6 Mix design results of different mixtures

Properties	**Limits**	**HMA-A**	**HMA-B**	**WMA-A**	**WMA-B**
Optimum binder content (OBC), %	Min 5.4	5.4			
Marshall stability at 60 °C, kN	Min. 9	15.16	13.91	13.14	9.87
Flow value, mm	2 – 4	3.96	2.78	3.44	2.84
Air voids, %	3 – 5	3.57	3.47	4.09	4.04
Voids in mineral aggregate (VMA), %	Min. 14	14.02	14.5	14.19	14.97
Voids filled with bitumen (VFB), %	65 – 75	74.54	74.19	71.18	72.99
Marshall quotient (MQ)	2 – 5	3.83	5	3.82	3.47

Table 3.7 One-way ANOVA of volumetric properties

Parameter		**Sum of squares**	**df**	**Mean square**	**F value**	**p-value**
Air voids	Between groups	0.8805	3	0.294	2.368	0.147
	Within groups	0.99139	8	0.124		
	Total	1.87189	11			
VMA	Between groups	0.92421	3	0.308	3.123	0.088
	Within groups	0.78925	8	0.099		
	Total	1.71345	11			
VFB	Between groups	24.0048	3	8.002	2.431	0.140
	Within groups	26.3366	8	3.292		
	Total	50.3414	11			

3.5 Aging of bituminous mixtures

In this study, the AASHTO R30 protocol was followed for aging different bituminous mixtures. However, the changes recommended in NCHRP 815 (Newcomb et al., 2015) document was incorporated into the AASHTO R30 aging protocol. For producing STA bituminous mixtures, loose bituminous mixtures were kept in a forced-draft oven for 2 h ± 5 min at compaction temperature (135 ± 3 °C for HMA and 116 ± 3 °C for WMA). The STA mixtures were compacted to 7 ± 1 % air voids for mechanical testing. The compaction effort (the number of hammer drops) required to achieve the target 7 ± 1 % air voids was determined using a few trail mixtures. Each specimen had a diameter of 100 ± 1 mm and a height of 63.5

± 2.5 mm. One set of STA compacted specimens were further aged in an oven at 85 ± 3 °C for 120 ± 0.5 h to produce the LTA specimens. Another set of bituminous mixtures was aged as per AASHTO T 283 specification and termed as "T-283" for all subsequent references. As per AASHTO T 283 aging protocol, the loose mixture was aged for 16 ± 0.5 h at 60 ± 3 °C followed by 2 h at compaction temperature. One set of T-283 aged loose mixtures were also compacted to 7 ± 1 % air voids. The aging process used in this study is shown in Figure 3.10.

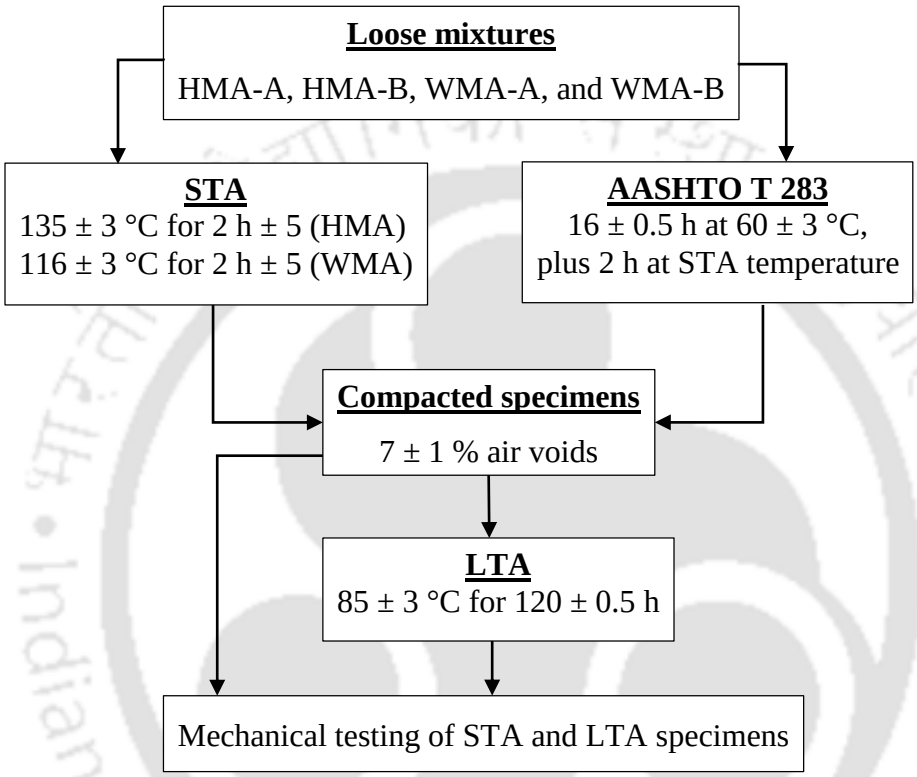

Figure 3.10 Different levels of aging used in this study

3.6 Moisture conditioning of bituminous mixtures

In this study, both loose bituminous mixtures and compacted specimens were subjected to moisture conditioning. In the case of loose mixture moisture conditioning, STA and T-283 aged loose mixtures were subjected to the boiling water test (as per ASTM D3625 protocol) for a boiling time of 10 min. Each 1200 g batch of the loose mixture was sub-divided into batches of 250 g each and subject to boiling water test, as shown in Figure 3.11 (a). In the case of compacted specimens, each specimen was saturated to 70 to 80 percent degree of saturation by applying a partial vacuum (ASTM D4867), as shown in Figure 3.11 (b). The specimens were then subjected to freeze and thaw cycles. For the freezing cycle, specimens wrapped in the plastic film were kept in a freezer at -18 ± 3 °C for 16 ± 1 h. Next, the specimens were

removed from the freezer and subjected to a thawing cycle of 24 ± 1 h in a hot water bath at 60 ± 1 °C, as shown in Figure 3.11 (c) & (d). One and three freeze-thaw (FT) cycles were used for moisture conditioning.

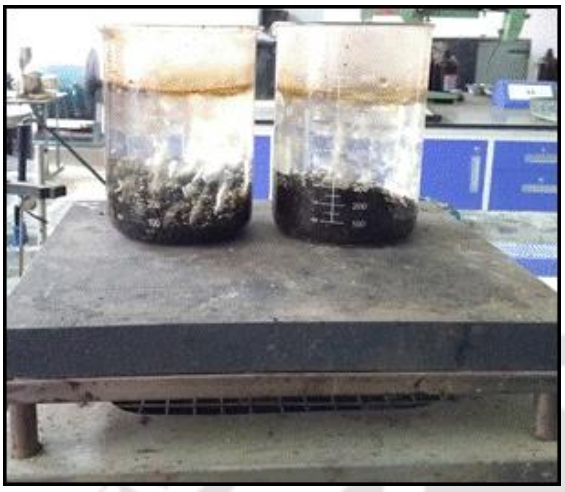

(a) Boiling water test

(b) Vacuum saturation

(c) Freezing at -18 °C ± 3 °C

(d) Thawing at 60 °C ± 1 °C

Figure 3.11 Moisture conditioning process used in this study

3.7 Testing equipment and protocols

Different testing equipment and test protocols used in this work are briefly explained below.

3.7.1 Asphalt compatibility tester

Moisture damage in the loose bituminous mixtures was assessed in terms of percent loss measured by the asphalt compatibility tester (ACT) equipment. The ACT measures the reflected light from the loose bituminous mixture's surface using a photodetector. An increase

in the measured reflected light is recorded as an increase in the percent loss of bituminous binder coating in the mixture. Before initiating the test sequence, the ACT was calibrated for each type of bituminous mixture as per InstroTek manual guidelines. First, each batch of moisture conditioned loose bituminous mixture weighing approximately 1200 g was dried using a hot air gun, as shown in Figure 3.12. Next, approximately 400 ± 20 g of the dried loose bituminous mixture was placed in the pan of the ACT instrument to measure the percent loss of the bituminous mixtures. The percent loss measured by the ACT was recorded for further analysis, as shown in Figure 3.13. Three replicate specimens were used for percent loss measurement using ACT at different conditions.

Figure 3.12 Loose mixture drying process

Figure 3.13 ACT equipment used for loose mixture testing

3.7.2 Indirect tensile stiffness modulus test

The indirect tensile stiffness modulus (ITSM) of the bituminous mixture was determined in an indirect tension mode as per BS EN 12697-26 specification at 15 °C and 25 °C. The specimens were pre-conditioned at 15 °C and 25 °C in the environmental chamber for 5 ± 0.5 h before testing. The test consists of applying repeated haversine waveform load pulses with rest periods. The load pulse applied is adjusted to achieve a 5 ± 2 µm transient peak horizontal deformation, and the ITSM value is calculated using Eq. (3.3) (BS EN 12697-26). Further, to evaluate the moisture susceptibility of the different bituminous mixtures at different aging and moisture conditioning levels, the ratio of moisture conditioned ITSM to unconditioned was determined, as shown in Eq. (3.4). The test setup is shown in Figure 3.14. For data extraction and stiffness modulus calculation, the universal report generator software provided by Cooper was used, as shown in Figure 3.15. Three replicate specimens were used for the ITSM test at different conditions.

$$ITSM = \frac{F \times (\mu + 0.27)}{z \times h} \tag{3.3}$$

$$ITSMR = \frac{ITSM_c}{ITSM_u} \times 100 \tag{3.4}$$

where,

$ITSM$ = indirect tensile stiffness modulus, MPa,

F = peak vertical load, N,

µ = Poisson's ratio,

z= horizontal deformation of the loading cycle, mm,

h= thickness of the specimen, mm.

$ITMS_c$= average *ITSM* of the conditioned, MPa, and,

$ITSM_u$ = average *ITSM* of the unconditioned specimen, MPa.

Figure 3.14 ITSM test setup

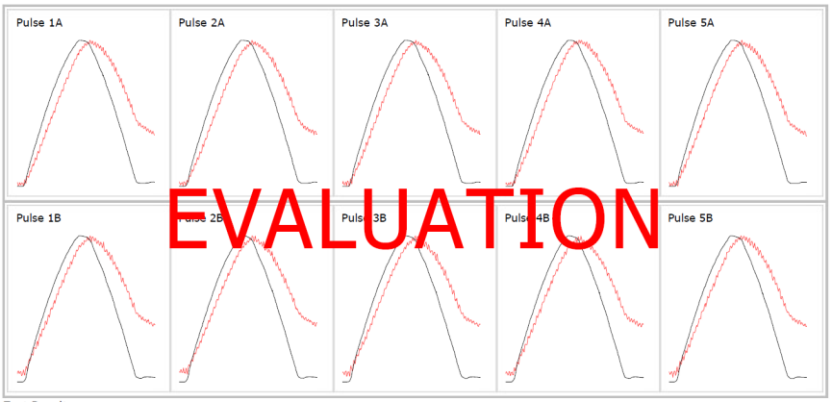

Test Results

	1A	2A	3A	4A	5A	Mean A	1B	2B	3B	4B	5B	Mean B	Mean A&B
Load Peak to Peak (kN)	3.02	3.03	3.03	3.03	3.03	3.03	3.58	3.57	3.58	3.58	3.59	3.58	**3.30**
Horizontal Stress (kPa)	279.2	279.6	280.0	279.8	279.9	279.7	330.4	329.8	330.2	330.7	331.1	330.4	**305.1**
Load-Area Factor	0.60	0.60	0.60	0.60	0.60	0.60	0.59	0.60	0.60	0.60	0.60	0.60	**0.60**
Horizontal Deformation (um)	5.5	5.5	5.5	5.5	5.5	5.5	5.0	5.0	5.0	5.0	5.0	5.0	**5.2**
Load Rise Time (ms)	137	137	137	137	137	137	128	127	126	127	127	127	**132**
Measured Stiffness (MPa)	5985	5926	5929	5994	5925	5952	5573	5556	5600	5584	5671	5597	**5774**
Adjusted Stiffness Modulus (MPa)	5975	5919	5918	5982	5913	5942	5554	5552	5608	5577	5665	5591	**5766**

Figure 3.15 ITSM results generated by the universal report generator

3.7.3 Indirect tensile strength test

The ITS test was carried at 15 °C and 25 °C as per the ASTM D6931 protocol. The ITS test was carried out by applying a compressive load at the rate of 50 mm/min along the specimen's vertical diametric plane until failure, as shown in Figure 3.16. The maximum load at failure was used to determine the ITS of the specimen using Eq. (2.1) (ASTM D6931). The tensile strength ratio (TSR) of moisture-conditioned and unconditioned specimens was determined using Eq. (2.2) (ASTM D4867). Researchers have also utilized the load-deformation data or the stress-strain data obtained from the ITS test to determine the fracture work density and fracture energy of the bituminous mixture (Huang et al., 2010; Wen, 2013). The complete load-deformation curve was considered in this study because it accounts for both peak load and post-peak behavior of the load-deformation curve. Due to equipment constraints, the test stopped once the load was reduced to approximately 20 percent of peak load. Thus, the data acquisition system of the equipment recorded up to 20 percent post-peak load-deformation data, as shown in Figure 3.17. In this study, the fracture work was determined using the MATLAB tool (see Eq. (2.3), as per ASTM D8225). Fracture work was converted into fracture work density by dividing the fracture work by the volume of the specimen, as shown in Eq. (2.4) (Wen, 2013). Next, the fracture energy of the specimen was determined using Eq. (2.5) (ASTM D8225). Three replicate specimens were used for the ITS test at different conditions.

Figure 3.16 ITS test setup

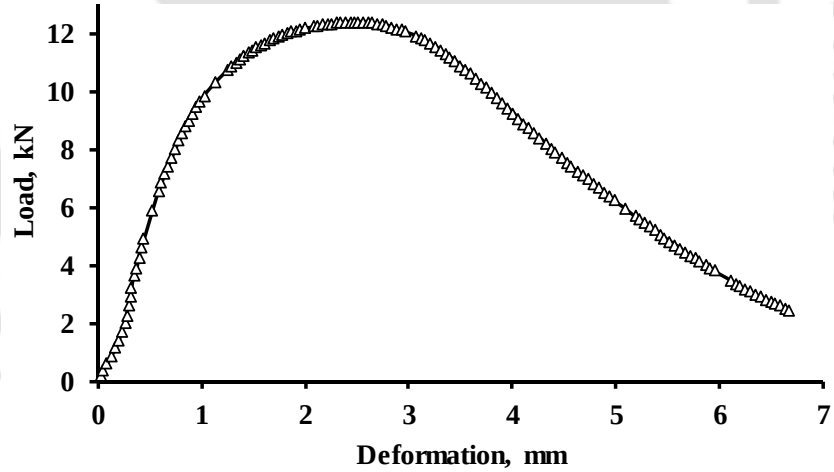

Figure 3.17 Load-deformation curve in ITS test

3.7.4 Indirect tensile fatigue test

The fatigue life of the bituminous mixture was determined under constant repeated stress (stress-controlled test) using indirect tensile loading mode (Indirect Tensile Fatigue Test, ITFT) as per BS EN 12697:24 specifications. The specimens were pre-conditioned at 15 °C and 25 °C in the environmental chamber for 6 ± 0.5 h before testing. A haversine loading waveform with 0.1 s loading and 0.4 s rest period was adopted. The stress level of 400 kPa at

15 °C and 250 kPa at 25 °C were used. The stress levels were selected to keep the initial strain amplitude of unconditioned specimens around 120 με. The test was terminated with the complete fracture of the specimen, and the number of cycles at failure was recorded as the fatigue life (N_f) of the specimen. The test setup is shown in Figure 3.18, and a representative test output is shown in Figure 3.19. Three replicate specimens were used for the ITFT test at different conditions.

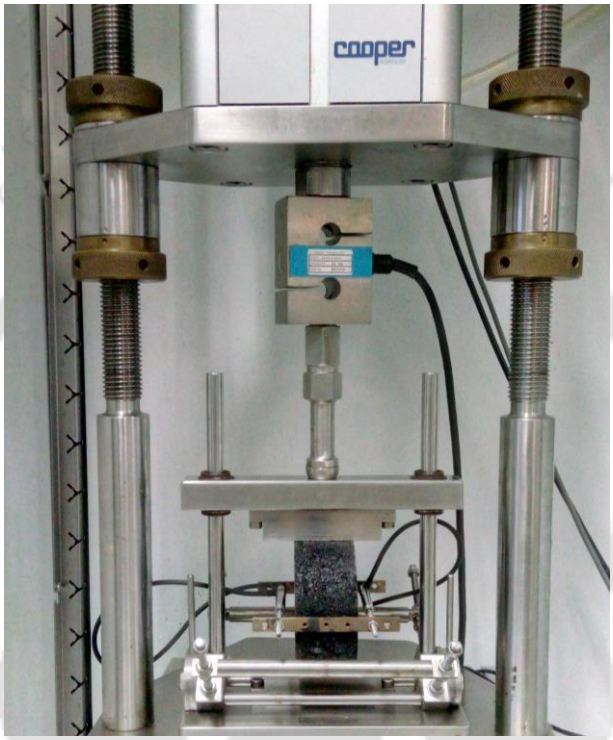

Figure 3.18 Fatigue test setup

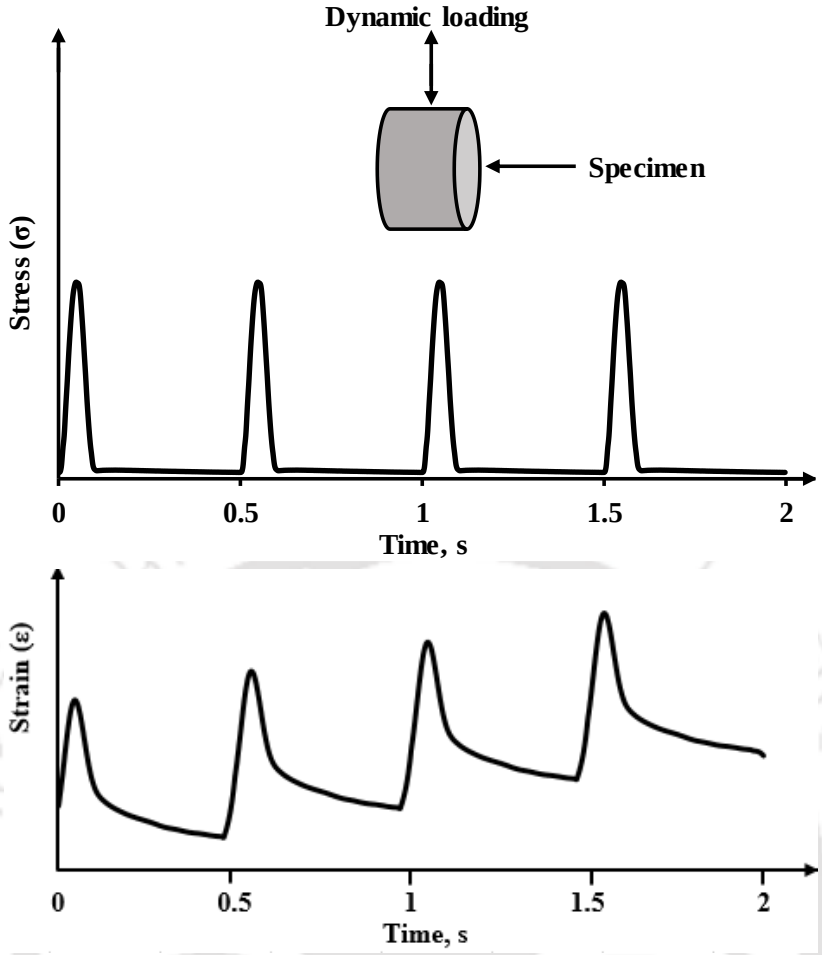

Figure 3.19 Representative output from the fatigue test

3.7.5 Creep test

The bituminous mixture's resistance to permanent deformation was determined using an unconfined uniaxial compression (UUC) test as per BS DD 226-1996 standard. The test was conducted at two temperatures, i.e., 40 °C and 45 °C, and two stress levels, i.e., 100 kPa and 150 kPa. The specimens were pre-conditioned at 40 °C and 45 °C in the environmental chamber for 5 ± 0.5 h before testing. The testing protocol includes a preloading stage where the specimen was loaded with static stress of 10 ± 1 kPa for 600 ± 6 s. Next, in the second stage, the stress of 2 kPa was applied for 20 ± 0.5 s. The third stage was the testing stage, in which the specimen was subjected to a square waveform with a frequency of 0.5 Hz (loading and rest period of 1 sec each). The test was conducted until 10,000 cycles or specimen failure, whichever occurred sooner. Failure was defined as the deformation of more than 10 mm (LVDT range). The axial strain at the end of the rest period immediately after application of load was determined using the relation shown in Eq. (3.5) (BS DD 226-1996). The test setup used in this study is shown

in Figure 3.20, and a representative test output is shown in Figure 3.21. Three replicate specimens were used for the creep test at different conditions.

$$\varepsilon_{d(n,T)} = \frac{\Delta h}{h_0} \tag{3.5}$$

where:

$\varepsilon_{d(n,T)}$= axial strain at T (°C) temperature after n load applications,

Δh= axial deformation of the specimen, mm, and

h_0 = initial height of the sample after preloading, mm.

Figure 3.20 Unconfined uniaxial creep test setup

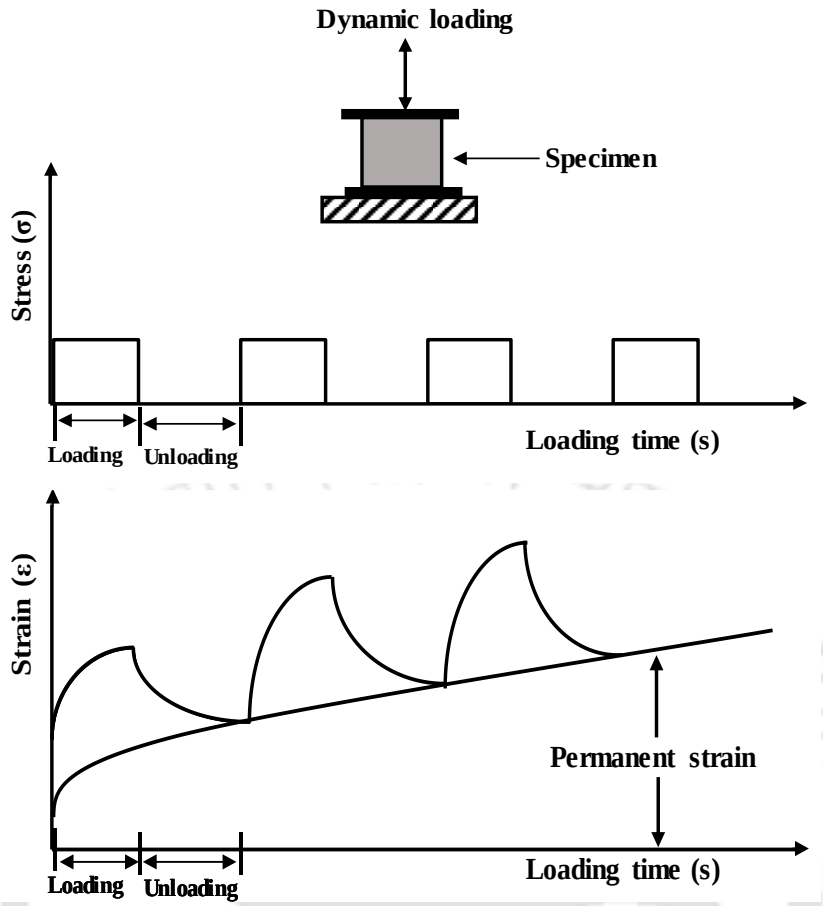

Figure 3.21 Representative output from creep test

Chapter 4

Identification of cracking resistance parameter

4.1 Introduction

In this chapter, the load-deformation data obtained from the ITS test was utilized to derive parameters listed in Table 4.1. First, the variability associated with each parameter was studied. Next, the parameter response to aging and moisture conditioning was evaluated. A statistical analysis (ANOVA at a significance level of 0.05) was carried out for each cracking resistance parameter to determine the significance of aging and moisture. The effect of the warm mix additive on the ITS and FE parameter was determined. Finally, limits on CoV and standard deviation of ITS and FE were proposed.

4.2 Details of the experimental matrix

The experimental details associated with this chapter are shown in Table 4.1. The cracking resistance of four different bituminous mixtures was evaluated at two test temperatures, i.e., 15 °C and 25 °C. A total of 144 specimens were subjected to the ITS test. Bituminous mixtures were subjected to both short-term and long-term aging conditions. For the moisture conditioned bituminous mixture, one and three freeze-thaw cycles of moisture conditioning were used. Different cracking resistance parameters calculated are shown in Table 4.1. The expressions used to determine different parameters used in this chapter were already discussed in section 2.4 of chapter 2 and presented in Table 2.7. The association of the identified cracking resistance parameter with the bituminous mixture's fatigue life was further evaluated in chapter 6 (see section 6.3.3).

Table 4.1 Details of test conditions used to evaluate cracking resistance index

Mixtures	Test temperature	Aging condition	Moisture condition	Tests	Parameters
Four types (HMA-A, HMA-B, WMA-A, and WMA-B)	Two levels (15 °C and 25 °C)	Two levels (STA and LTA)	Three levels (UC, 1FT, and 3FT)	ITS test	ITS, FWD, FE, CRI, CT_{Index}, RDCI

This study evaluated the suitability of different parameters based on the following criteria (Zhou et al., 2017).

- A suitable parameter that can be computed using the output of simple test equipment. The test configuration in the ITS test does not require any cutting, gluing, drilling, or notching of the specimen before testing. Thus, the ITS test can be considered a relatively simple test. In addition, the testing time in the ITS test is usually less than a minute, making it a convenient routine test.
- A suitable parameter should have minimum variation at different test conditions, i.e., the CoV of the parameter should be lower with the change in aging levels or moisture conditioning levels.
- A suitable parameter should be sensitive to test conditions, i.e., the change in the test condition, e.g., a change in aging or moisture conditioning levels, should be appropriately reflected by the change in the parameter's value. A statistical test like ANOVA can be used to evaluate whether the change in aging or moisture conditioning levels has a significant effect on the parameter's mean value.
- The parameter should have a good association with the fatigue life of the bituminous mixture determined using a repeated load testing setup.

4.3 Results and discussion

4.3.1 Variability associated with different parameters

The ITS of different mixtures was determined at each condition, and the load-deformation data of the ITS test was used to calculate the FWD, FE, CRI, CT_{Index}, and RDCI parameters. The CoV of the parameters was determined and presented using a boxplot. The impact of different aging and moisture levels on the CoV of different parameters was the primary concern. For this purpose, this study combined bituminous mixtures at a given aging and moisture conditioned state. Parameters determined at 15 °C are shown in Figure 4.1, and the parameters determined at 25 °C are shown in Figure 4.2. It could be noticed from Figure 4.1 and Figure 4.2 that aging had a mixed effect on the CoV of bituminous mixtures. For most of the cases, the CoV of parameters at the LTA condition was comparable to the CoV of the parameter at STA condition.

However, moisture conditioning increased the CoV of different parameters evaluated in this study. The range of CoV of parameters subjected to moisture conditioning was also higher than the CoV of parameters of the unconditioned bituminous mixture, as seen in Figure 4.1 and Figure 4.2. Thus, moisture conditioning might result in higher variation in the strength and stiffness parameters of the bituminous mixtures. In few cases, it was also noticed that the CoV of bituminous mixtures subjected to 3FT cycles was not higher than mixtures subjected to 1FT cycles. This may be due to the fact that moisture damage (dry-wet-dry cycles) in bituminous mixtures is a physical phenomenon with a different source of variability, which may increase the overall variability of the experimental results (Manrique-Sanchez et al., 2020). The other possible reason could be higher moisture damage with 3FT cycles. The CoV of different parameters was also influenced by the test temperature. The CoV was noticed to be much higher at 15 °C as compared to 25 °C. At lower temperatures, the variation in the strength of the bituminous mixture might also increase. Thus, an increase in moisture conditioning and reduction in temperature might result in an increase in the variability of a test parameter.

In comparison, Fakhri & Ahmadi (2017) noticed that the CoV of the FI parameter increased with both long-term aging and moisture conditioning. For example., it was noticed that the CoV of the FI parameter increased from 6 % at STA (loose mixtures at compaction temperature for 4 h) to 9 % at LTA (compacted specimens at 120 h at 85 °C) condition. The authors also noticed an increase in CoV of FI parameter from 8 % for the unconditioned mixture to 14 % for mixtures subjected to 5 FT cycles. Similarly, Manrique-Sanchez et al. (2020) also noticed that the CoV of FI parameter and CRI parameter increased from 33.2 % and 18.7 % at dry state to 63.2 % and 22.3 % at the third moisture conditioned cycle. Thus, it can be said that aging can also increase the variation in the strength properties of the bituminous mixtures.

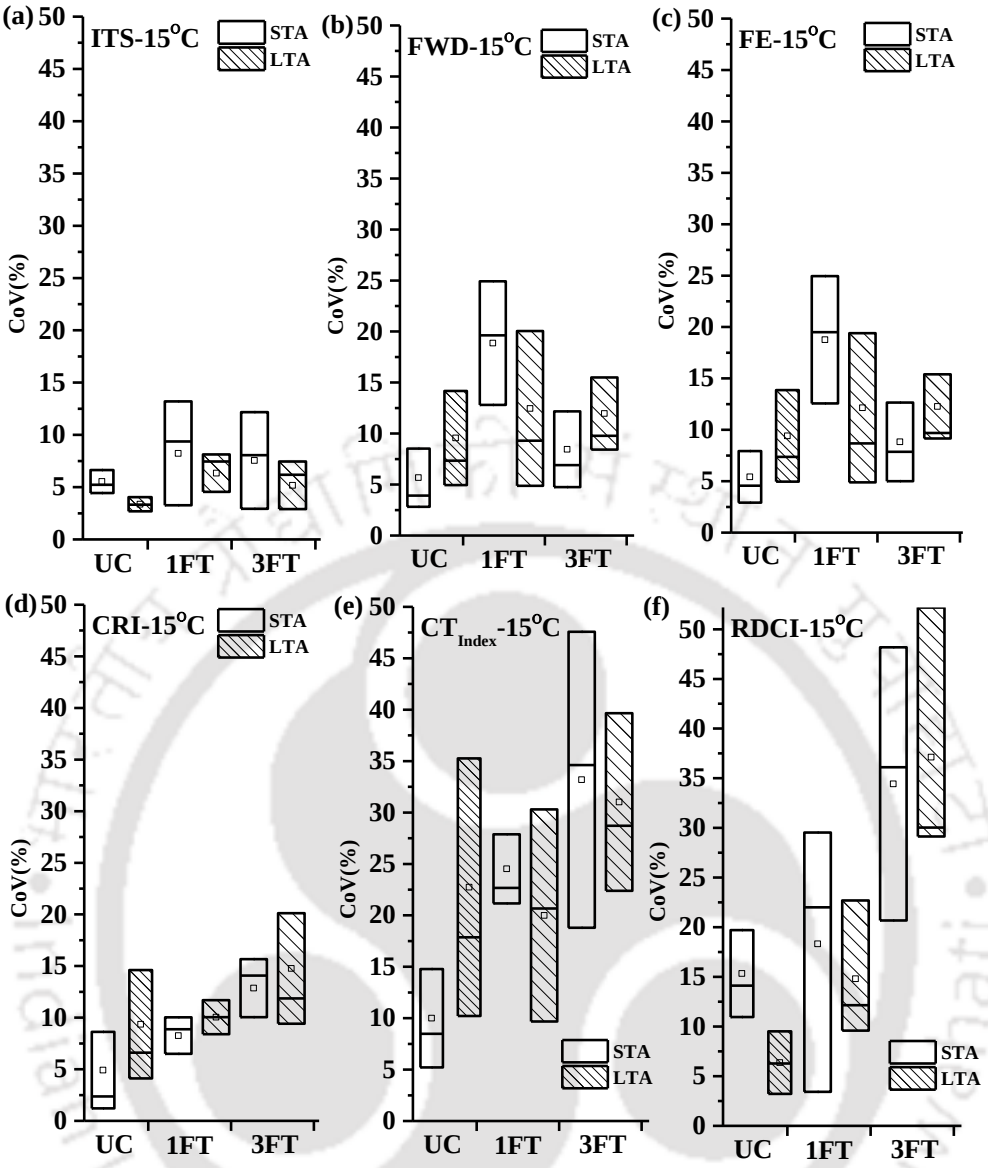

Figure 4.1 CoV of different parameters at 15 °C

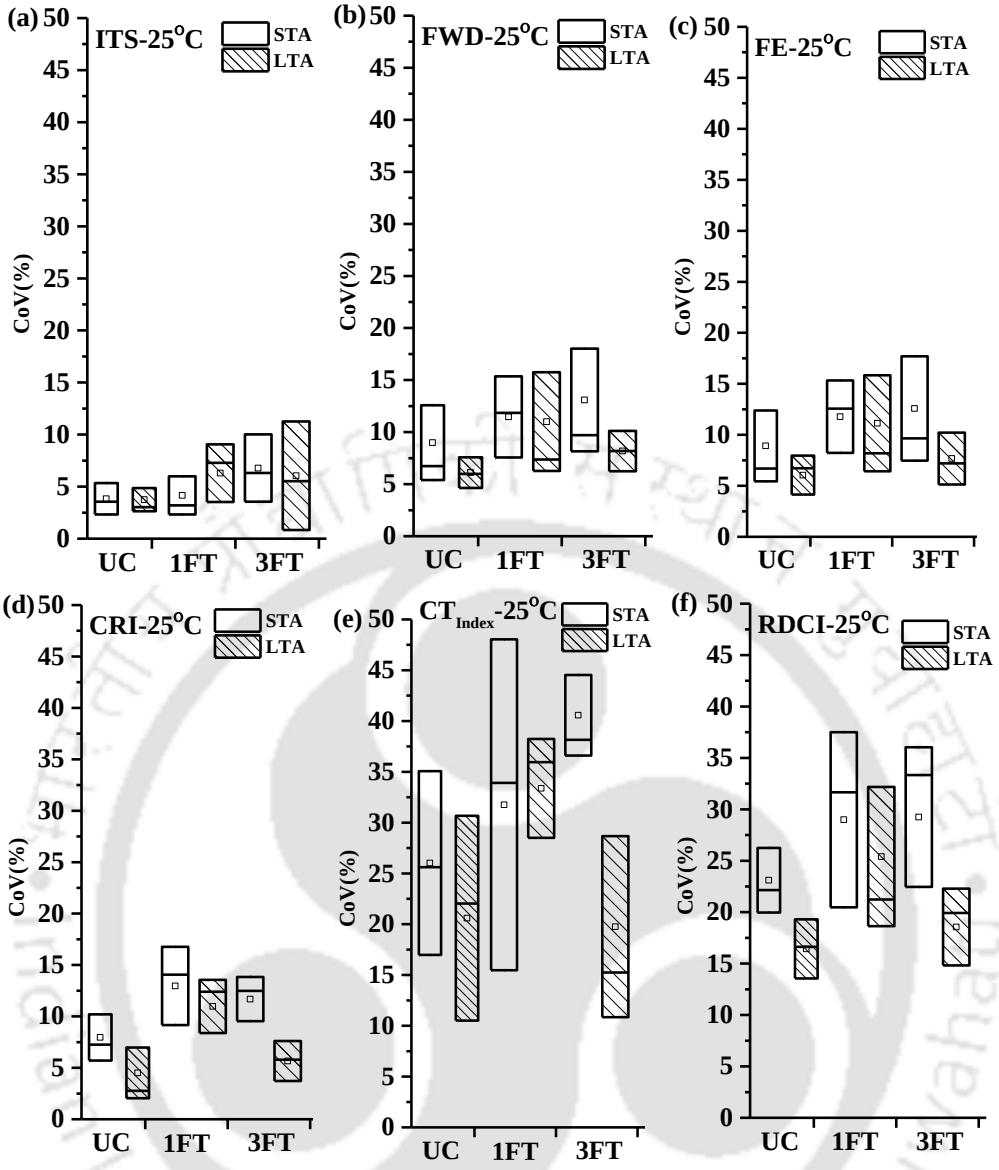

Figure 4.2 CoV of different parameters at 25 °C

The effect of moisture on the CoV of CT_{Index} and RDCI parameter was noticed to be higher than other parameters evaluated in this study (see Figure 4.1 and Figure 4.2). This can be attributed to the variability in the slope component used in the mathematical formulation of both CT_{Index} and RDCI parameter, which was influenced by moisture conditioning (elaborated in section 4.3.3). Also, the CT_{Index} and RDCI parameter had a higher CoV compared to other parameters. The maximum CoV of CT_{Index} of unconditioned and moisture conditioned bituminous mixtures was close to 35 % and 50 %. In comparison, the CoV of ITS, FWD, FE, CRI parameters for unconditioned and moisture-conditioned bituminous mixtures was less than 15 % and 20 % respectively.

The CoV of parameters noticed in this study were comparable with previous research work. Kaseer et al. (2018) noticed that the CRI parameter had a maximum CoV of 20 %. Researchers have also noticed that FI had a CoV of approximately 35 % or higher (Batioja-Alvarez et al., 2019; Kaseer et al., 2018). The CoV of the RDCI parameter, as noticed by Nemati et al. (2019), ranged from 10 % to 30 %, which was comparable to the CoV of the unconditioned bituminous mixture noticed in this study (see Figure 4.1 and Figure 4.2).

4.3.2 Identification of parameter sensitive to different conditions

Effect of aging

Different parameters determined for each mixture at 15 °C and 25 °C are shown in Figure 4.3 to Figure 4.10. The parameters for HMA-A mixtures at 15 °C are shown in Figure 4.3, and at 25 °C are shown in Figure 4.4. The error bars represent one standard division (SD). The ITS, FWD, and FE of the HMA-A mixture are shown in Figure 4.3 (a)-(c) and Figure 4.4 (a)-(c). It could be noticed that the ITS of the bituminous mixture increased from STA to LTA condition. For example, the ITS of the unconditioned HMA-A mixture at 25 °C increased from 1228 kPa at STA to 1295 kPa at LTA conditions. Whereas the FWD and FE of the bituminous mixture showed a mixed trend with aging. It could be noticed from Figure 4.4 (c), that the FE of the HMA-A mixture at 25 °C reduced from 0.77 kJ/m^2 at the STA condition to 0.67 kJ/m^2 at the LTA condition. However, the FE of the unconditioned HMA-B mixture at 15 °C increased with aging (see Figure 4.5 (c)). Thus, aging increased the tensile strength and had a mixed effect on the resistance to fracture in bituminous mixtures. Since the change in the FE of the unconditioned bituminous mixture from STA condition to LTA condition was not significant (see Table 4.5 and Table 4.6), the FE of STA and LTA bituminous mixtures can be considered comparable.

The CRI, CT_{Index}, and RDCI parameters reduced from STA to LTA condition. For example, Figure 4.4 (d) presents the CRI parameter of the HMA-A mixture at 25 °C. In the unconditioned state, the CRI of the HMA-A mixture was 620 at the STA condition and 525 at the LTA condition. Similarly, the CTI and RDCI parameters also reduced with aging from 79 and 28 at STA condition to 47 and 18 at LTA condition at 25 °C (see Figure 4.4 (f) & (e)) respectively.

Previous studies by Yilmaz et al. (2013) noticed that ITS of the bituminous mixture increased from 840 kPa at STA (4 h at 135 °C) condition to 996 kPa at LTA (120 h at 85 °C)

condition. Diab et al. (2019) noticed that the ITS increased from approximately 900 kPa to 1200 kPa as the aging time of the loose bituminous mixture increased from 2 h to 16 h. Manrique-Sanchez et al. (2020) also noticed that the FE of the STA (loose mixture at 160 °C for 2 h) specimen reduced from 0.79 kJ/m^2 to 0.65 kJ/m^2 at LTA (loose mixture at 95 °C for 10 days) condition. Whereas, Izadi et al. (2018) noticed that FE of STA (AASHTO R30) mixture increased from 7.045 J/m to 8.035 J/m at LTA (compacted specimens at 80 °C for 5 days) condition. Kaseer et al. (2018) noticed that short-term aged bituminous mixtures had a CRI of 430, and long-term aged bituminous mixtures had a CRI of 290. Nemati et al. (2019) noticed that RDCI of a bituminous mixture reduced from 22 at STA condition to 16 at the long-term aged condition and tested at 25 °C.

Effect of moisture

The ITS, FWD, and FE of both STA and LTA bituminous mixtures were reduced with moisture conditioning. For example, from Figure 4.4 (a)-(c), it could be noticed that the STA HMA-A mixture showed a 32 % and 66 % reduction in the ITS value at 1FT and 3FT conditions than the unconditioned mixture. Interestingly, both FWD and FE showed a reduction of 23 % and 65 % at 1FT and 3FT conditions than the unconditioned STA HMA-A mixture. However, the CRI was noticed to be either comparable or increased with an increase in moisture conditioning level. Similarly, from Figure 4.4 (e) & (f), an increase in CT_{Index} and RDCI parameter with the increase in moisture conditioned cycle was noticed for most of the cases. From the literature, it is well understood that the cracking resistance of bituminous mixture reduces in the presence of moisture (Sebaaly et al., 2017; Tong et al., 2015). Thus, CRI, CT_{Index}, and RDCI might not be suitable parameters for evaluating the effect of moisture on the cracking resistance of bituminous mixture.

A similar decrease in ITS and FE of the bituminous mixture was also reported in the literature. Cong et al. (2020) noticed an approximate reduction of 17.5 % and 23 % in ITS value of bituminous mixture at 1FT and 3FT cycle as compared to unconditioned bituminous mixture tested at 25 °C. Chen & Huang (2008) noticed an average reduction of 20 % at 25 °C in the FE of the bituminous mixture subjected to the 1FT cycle of moisture conditioning.

Different parameters determined for HMA-B, WMA-A, and WMA-B mixture at 15 °C and 25 °C (Figure 4.5 to Figure 4.10) followed a similar trend as noticed in the case of the HMA-A mixture. Also, a summary table (Table 4.2) is presented to corroborate the findings of

this study with existing literature. Thus, only ITS, FWD, and FE were selected for further analysis.

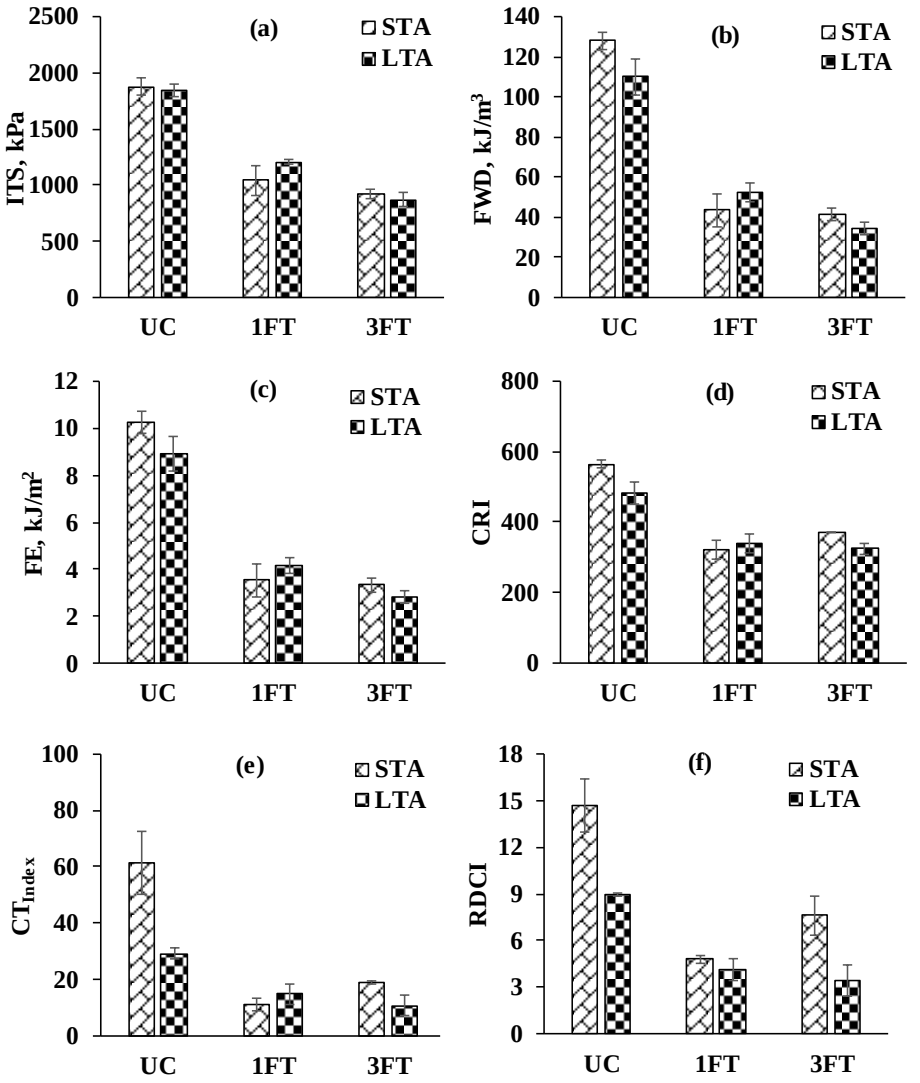

Figure 4.3 Different parameters determined for HMA-A mixture at 15 °C

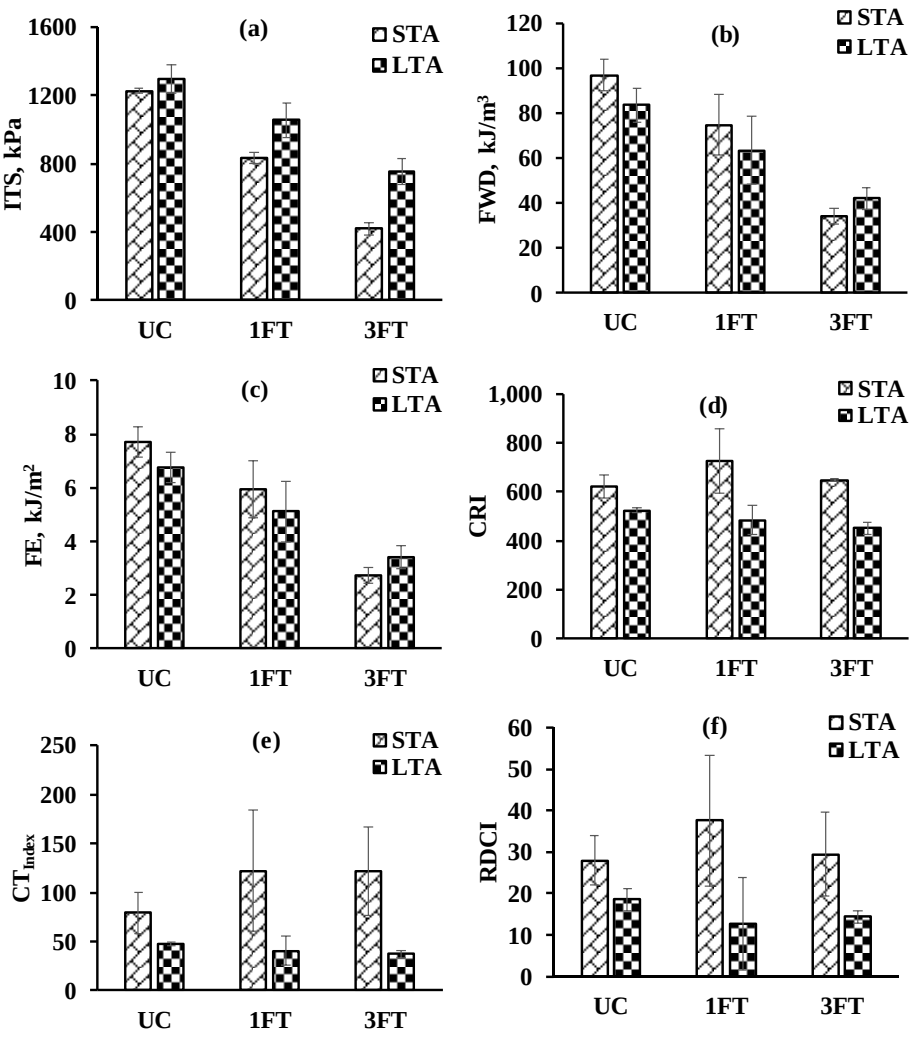

Figure 4.4 Different parameters determined for HMA-A mixture at 25 °C

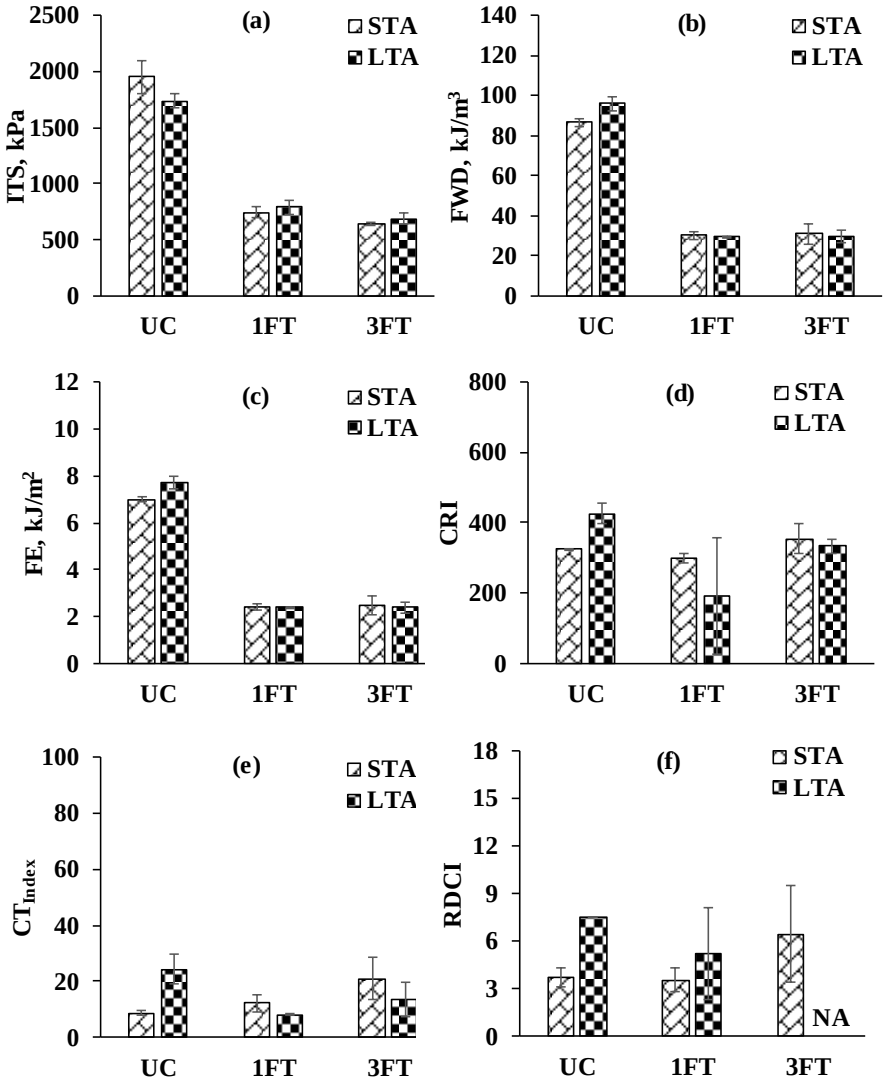

Figure 4.5 Different parameters determined for HMA-B mixture at 15 °C

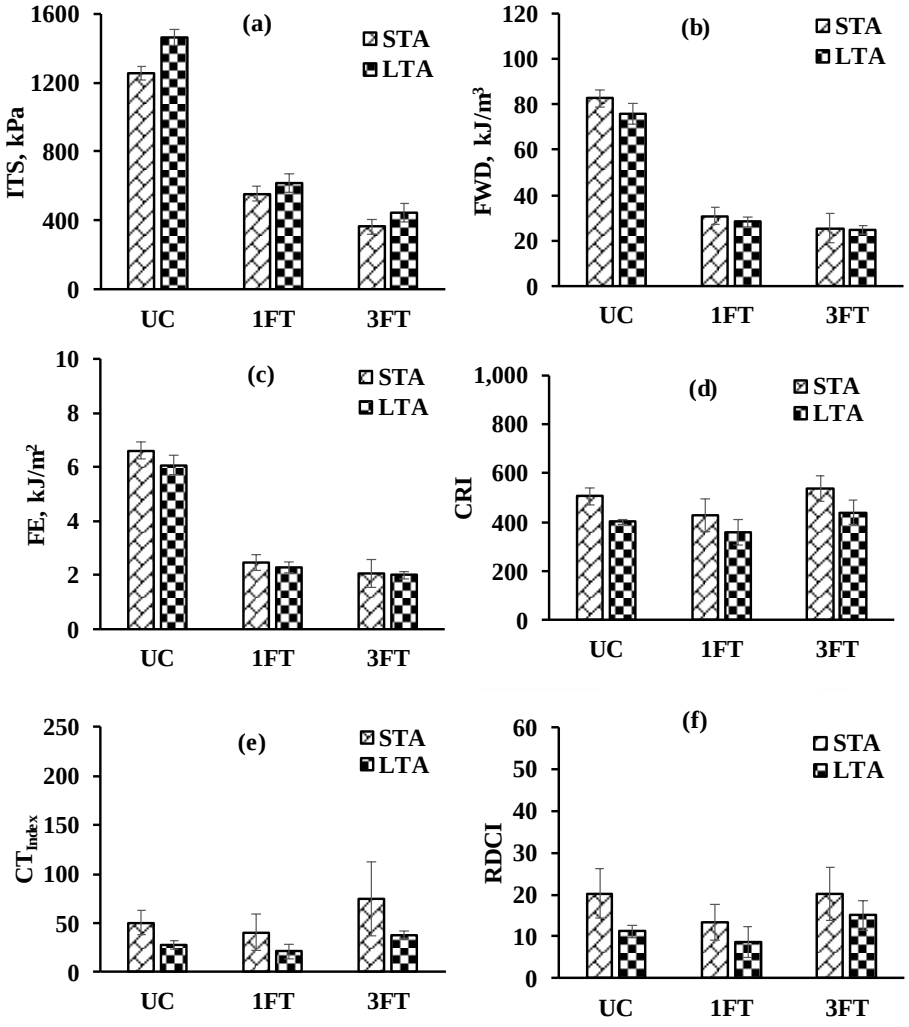

Figure 4.6 Different parameters determined for HMA-B mixture at 25 °C

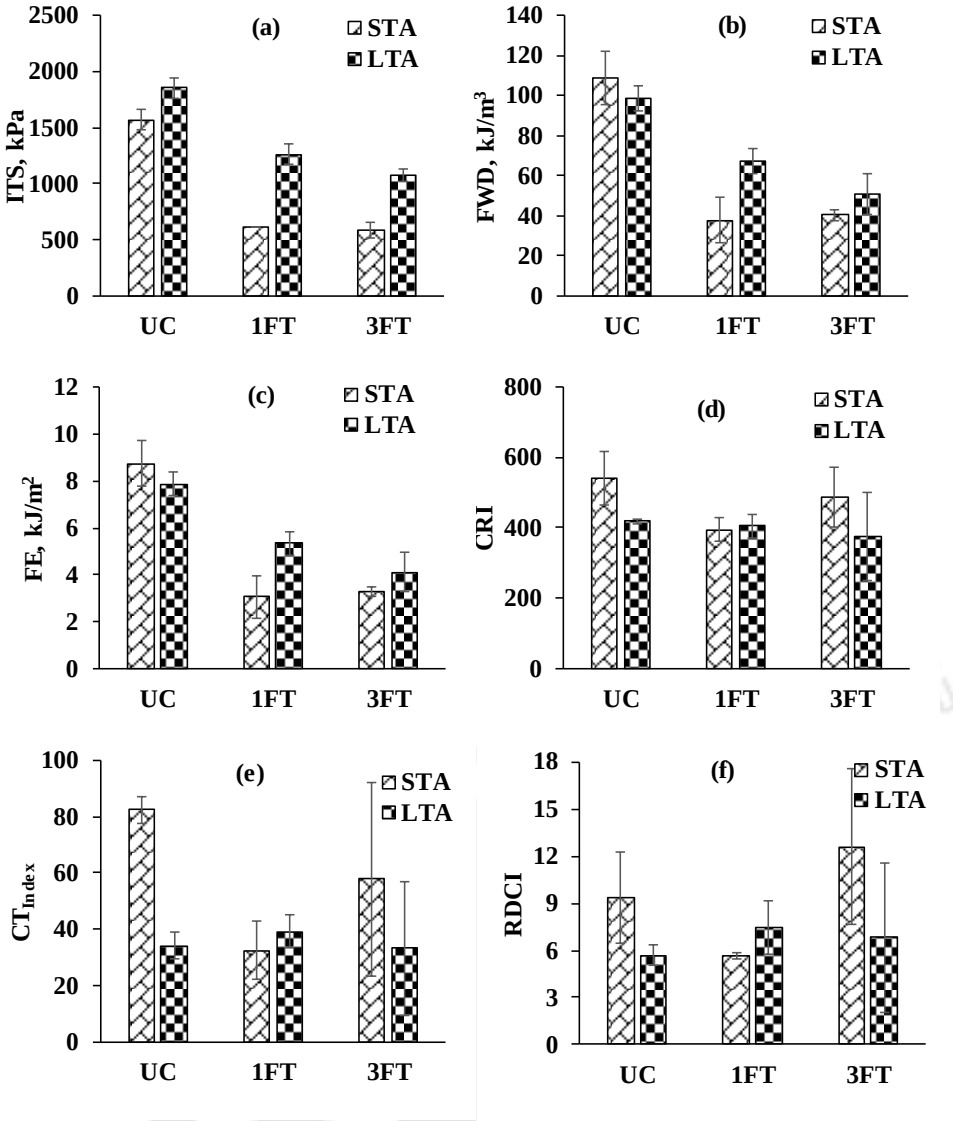

Figure 4.7 Different parameters determined for WMA-A mixture at 15 °C

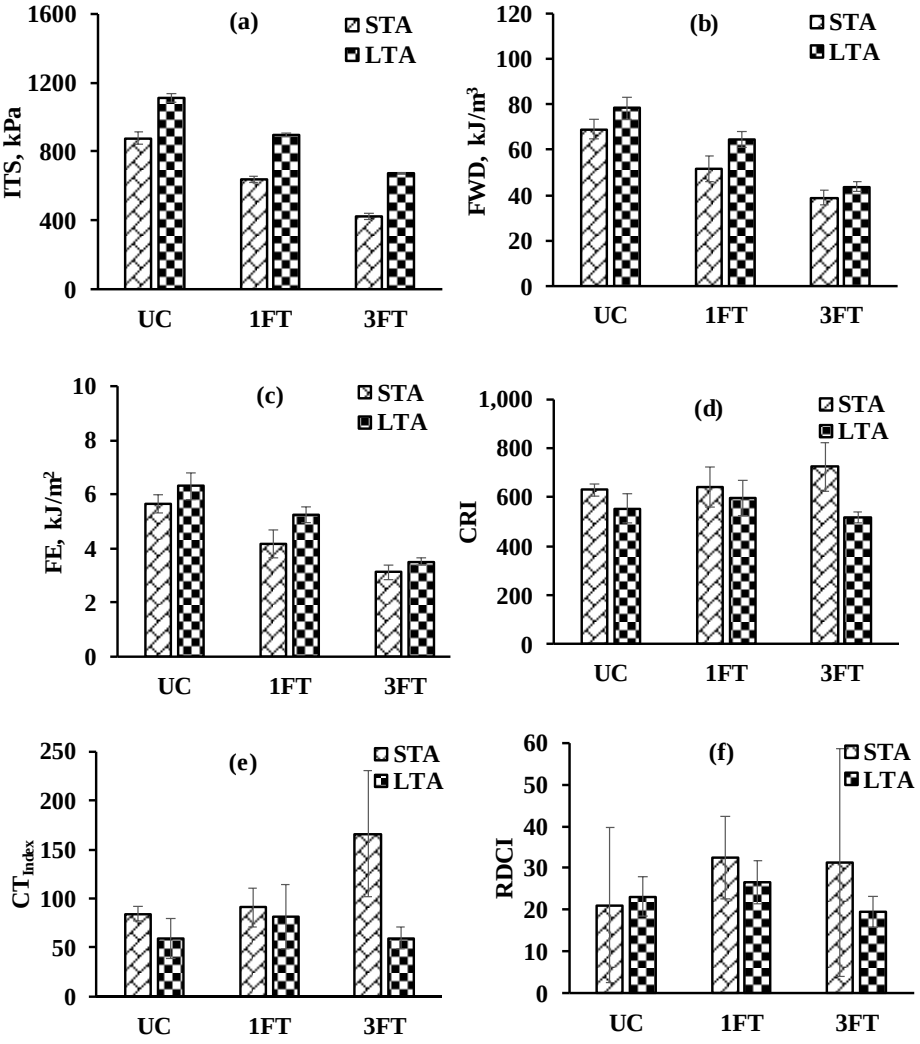

Figure 4.8 Different parameters determined for WMA-A mixture at 25 °C

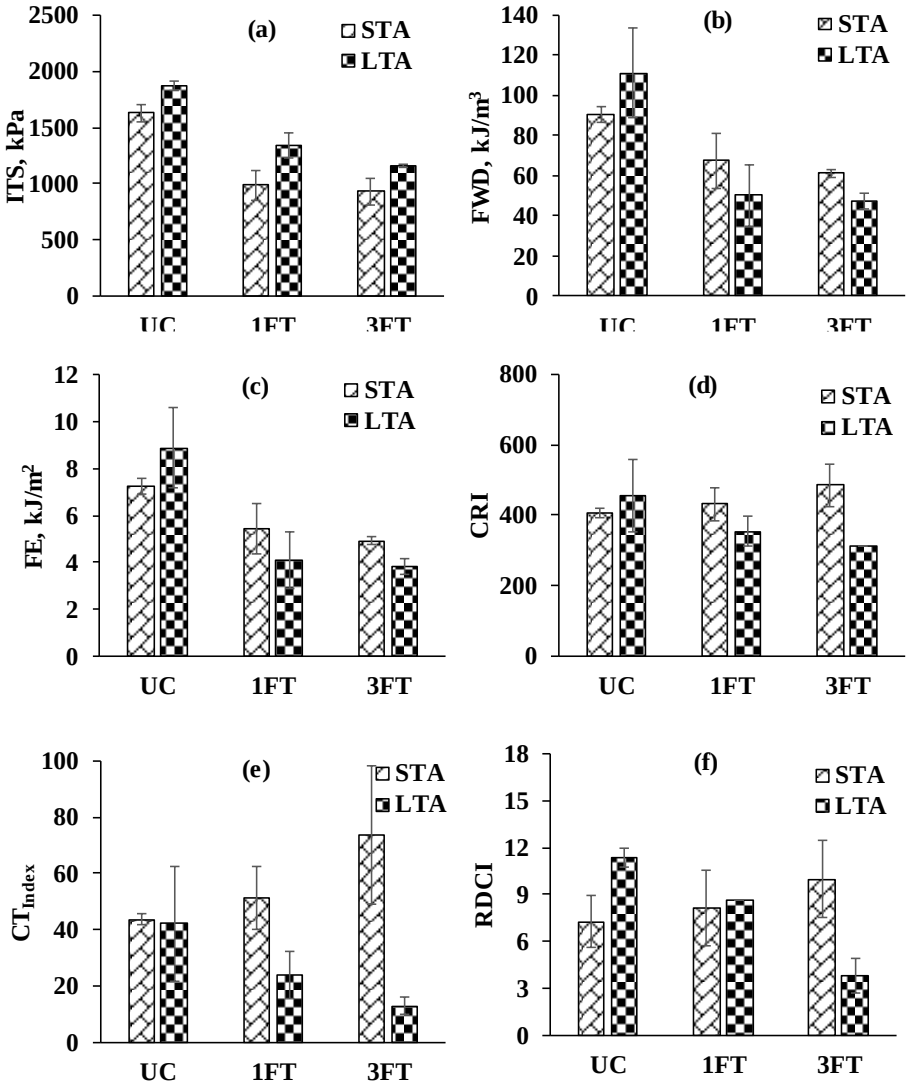

Figure 4.9 Different parameters determined for WMA-B mixture at 15 °C

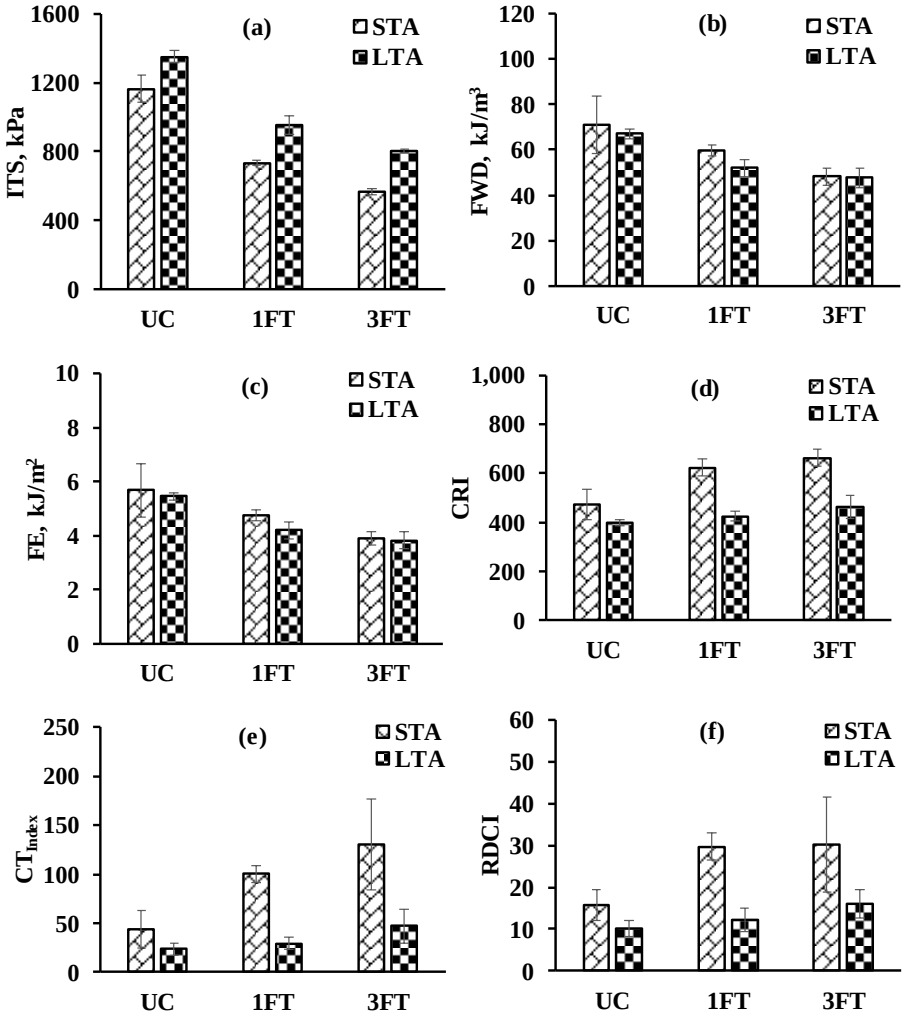

Figure 4.10 Different parameters determined for WMA-B mixture at 25 °C

Table 4.2 Corroborating results of this study with previous literature

Factor	Findings of this study	Previous studies	Remarks
Measure of variability in terms of CoV	CoV increased with an increase in moisture conditioning cycles.	CoV increased with an increase in moisture conditioning cycles (Fakhri & Ahmadi, 2017; Manrique-Sanchez et al., 2020)	Moisture damage (dry-wet-dry cycles) is a physical phenomenon with a different source of variability, which increases the overall variability of the experimental results.
	The CT_{Index} and RDCI parameters have relatively higher CoV (maximum value of 35 %) as compared to ITS, FWD, FE, and CRI.	CT_{Index} and RDCI parameters have CoV close to 30 % (Batioja-Alvarez et al., 2019; Kaseer et al., 2018).	The slope parameter used for determining the CT_{Index} and RDCI had relatively higher variability, which increased the variability of both parameters.
Effect of aging	For most of the cases, the ITS increased with an increase in the aging level.	The ITS increased with an increase in aging level (Yilmaz et al., 2013; Diab et al., 2019)	The bitumen constituent composition varies due to aging imparting hardness and hence increases the ITS of the mixture.
	FE of STA and LTA mixtures were comparable. The CRI and RDCI parameter reduce with aging.	FE showed a mixed trend with an increase in aging level. (Izadi et al., 2018; Manrique-Sanchez et al., 2020). CRI and RDCI parameter reduce with aging (Kaseer et al., 2018; Nemati et al., 2019)	When the aged specimen had a more brittle fracture behavior compared to the unaged specimen, the FE (area under the load-deformation curve) of the aged specimen was reduced.
Effect of moisture	For most of the cases, ITS and FE were reduced with increase moisture conditioning levels.	ITS and FE reduced with increase moisture conditioning level (Chen & Huang, 2008; Cong et al., 2020)	With the increase of moisture conditioning cycles, moisture diffused into the specimen and reduced the bond strength between binder and aggregates, which reduced ITS and FE of the mixture.
	The CT_{Index} of moisture-conditioned specimen increases compared to the unconditioned specimen.	Similar observations were made by Chen et al. (2020).	The post-peak slope (the denominator in CT_{Index}) decreases with an increase in the moisture conditioning cycle. This increased the CT_{Index} value of the moisture-conditioned specimen.

4.3.3 *Complications with CT_{index}, CRI and RDCI*

To understand the variability associated with CT_{index}, the slope values of different mixtures tested at 25 °C is plotted against its corresponding CT_{Index} as shown in Figure 4.11. It could be seen from Figure 4.11 that the slope values decrease considerably with the increase in moisture conditioning level from UC to 1FT and from 1FT to 3FT cycle. Since, FE of moisture conditioned specimen is divided by a much smaller slope value compared to unconditioned specimen, the CT_{Index} of moisture conditioned specimen increases compared to the unconditioned specimen. Similar observations were made by Chen et al. (2020). CRI and RDCI has mathematical formulation like CT_{Index} and a similar increase in the parameter with moisture conditioning was expected.

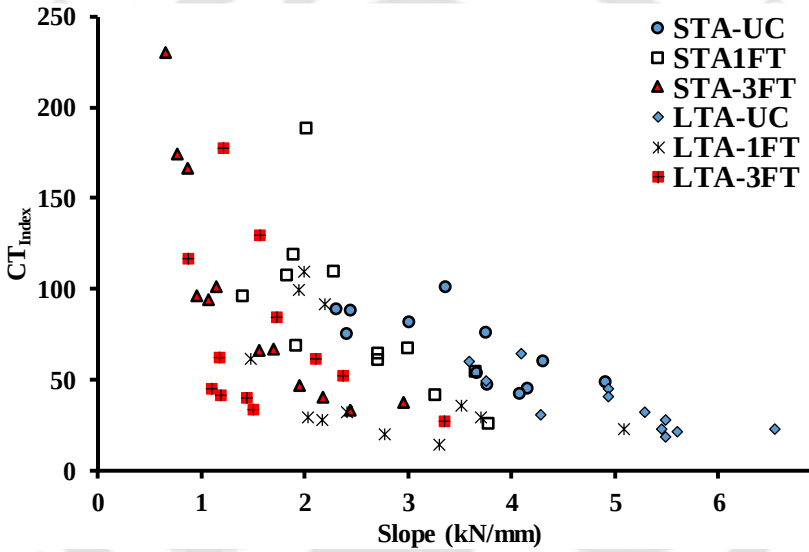

Figure 4.11 Slope versus CT_{Index} at 25 °C

4.3.4 *Statistical interpretation of the parameters*

The mean value of cracking resistance parameters is expected to change when it is subjected to different conditions. Therefore, it is essential to know that the changes observed are statistically significant. For this purpose, one-way ANOVA at a significance level (α) of 0.05 was carried out for each cracking resistance parameter considering six different conditions (STA-UC, STA-1FT, STA-3FT, LTA-UC, LTA-1FT, and LTA-3FT). The null hypothesis assumed was that the mean value of a parameter was the same at all six conditions. The ANOVA test performed for ITS, FWD, and FE of bituminous mixtures tested at 15 °C is shown in Table 4.3. A *p*-value smaller than 0.05 was noticed for ITS, FWD, and FE for different mixtures, and the null hypothesis was rejected. Thus, the change in the value of different

parameters with the change in conditions was statistically significant. Similarly, from Table 4.4, it could be noticed that the ITS, FWD, and FE of the bituminous mixtures at 25 °C were significantly affected by the change in the aging and moisture conditioning levels.

Table 4.3 One-way ANOVA results at 15 °C

Mixture	Dependent variable		Sum of Squares	df	Mean Square	F-value	p-value
HMA-A	ITS	Between groups	3.1E+06	5	6.2E+05	111	1.3E-09
		Within groups	6.7E+04	12	5.6E+03		
		Total	3.2E+06	17			
	FWD	Between groups	2.4E+10	5	4.8E+09	140	3.3E-10
		Within groups	4.1E+08	12	3.4E+07		
		Total	2.5E+10	17			
	FE	Between groups	1.6E+08	5	3.1E+07	125	6.5E-10
		Within groups	3.0E+06	12	2.5E+05		
		Total	1.6E+08	17			
HMA-B	ITS	Between groups	5.2E+06	5	1.0E+06	182	7.1E-11
		Within groups	6.9E+04	12	5.8E+03		
		Total	5.3E+06	17			
	FWD	Between groups	1.3E+10	5	2.7E+09	248	3.8E-10
		Within groups	1.1E+08	10	1.1E+07		
		Total	1.4E+10	15			
	FE	Between groups	8.7E+07	5	1.7E+07	272	2.4E-10
		Within groups	6.4E+05	10	6.4E+04		
		Total	8.7E+07	15			
WMA-A	ITS	Between groups	3.9E+06	5	7.7E+05	148	2.4E-10
		Within groups	6.3E+04	12	5.2E+03		
		Total	3.9E+06	17			
	FWD	Between groups	1.3E+10	5	2.6E+09	29	5.1E-06
		Within groups	9.5E+08	11	8.7E+07		
		Total	1.4E+10	16			
	FE	Between groups	8.0E+07	5	1.6E+07	30	4.8E-06
		Within groups	5.9E+06	11	5.4E+05		
		Total	8.6E+07	16			
WMA-B	ITS	Between groups	2.1E+06	5	4.1E+05	49	1.4E-07
		Within groups	1.0E+05	12	8.4E+03		
		Total	2.2E+06	17			
	FWD	Between groups	7.6E+09	5	1.5E+09	12	4.2E-04
		Within groups	1.4E+09	11	1.3E+08		
		Total	9.0E+09	16			
	FE	Between groups	4.7E+07	5	9.5E+06	12	3.5E-04
		Within groups	8.6E+06	11	7.8E+05		
		Total	5.6E+07	16			

Table 4.4 One-way ANOVA results at 25 °C

Mixture	Dependent variable		Sum of Squares	df	Mean Square	F-value	p-value
HMA-A	ITS	Between groups	1.6E+06	5	3.2E+05	77	1.1E-08
		Within groups	5.1E+04	12	4.2E+03		
		Total	1.7E+06	17			
	FWD	Between groups	8.8E+09	5	1.8E+09	19	2.4E-05
		Within groups	1.1E+09	12	9.2E+07		
		Total	9.9E+09	17			
	FE	Between groups	5.6E+07	5	1.1E+07	20	1.9E-05
		Within groups	6.7E+06	12	5.6E+05		
		Total	6.3E+07	17			
HMA-B	ITS	Between groups	3.2E+06	5	6.4E+05	279	5.6E-12
		Within groups	2.7E+04	12	2.3E+03		
		Total	3.2E+06	17			
	FWD	Between groups	1.1E+10	5	2.2E+09	132	4.7E-10
		Within groups	2.0E+08	12	1.7E+07		
		Total	1.1E+10	17			
	FE	Between groups	6.9E+07	5	1.4E+07	132	4.6E-10
		Within groups	1.3E+06	12	1.0E+05		
		Total	7.0E+07	17			
WMA-A	ITS	Between groups	8.8E+05	5	1.8E+05	408	5.8E-13
		Within groups	5.2E+03	12	4.3E+02		
		Total	8.8E+05	17			
	FWD	Between groups	3.6E+09	5	7.1E+08	42	3.4E-07
		Within groups	2.0E+08	12	1.7E+07		
		Total	3.8E+09	17			
	FE	Between groups	1.5E+07	5	3.1E+06	12	2.7E-04
		Within groups	3.1E+06	12	2.6E+05		
		Total	1.8E+07	17			
WMA-B	ITS	Between groups	1.3E+06	5	2.5E+05	132	4.6E-10
		Within groups	2.3E+04	12	1.9E+03		
		Total	1.3E+06	17			
	FWD	Between groups	1.5E+09	5	3.0E+08	8	1.4E-03
		Within groups	4.3E+08	12	3.6E+07		
		Total	1.9E+09	17			
	FE	Between groups	1.8E+07	5	3.5E+06	39	5.2E-07
		Within groups	1.1E+06	12	9.1E+04		
		Total	1.9E+07	17			

Further, Tukey's post-hoc test was carried out to determine each test condition's significance on the ITS, FWD, and FE of the bituminous mixtures. The STA-UC is considered as the base condition, and other conditions, i.e., STA-1FT, STA-3FT, LTA-UC, LTA-1FT, and LTA-3FT, were compared with the STA-UC condition. Results of Tukey's post-hoc test carried

out for ITS, FWD, and FE parameter at 15 °C is shown in Table 4.5, and at 25 °C is shown in Table 4.6. As seen from Table 4.5 and Table 4.6, the ITS, FWD, and FE at different conditions used in this study were significantly different from the STA-UC condition, except for a few cases. The STA-UC condition was not significantly different from the LTA-UC condition in terms of the FWD and FE parameters. Since all three parameters showed comparable sensitivity to change in condition, selecting a parameter becomes difficult. Thus, the association of the cracking resistance parameters with fatigue life (number of cycles till fracture in a repeated test) was carried out. Only ITS and FE were considered for further analysis.

Table 4.5 Tukey's post-hoc test results at 15 °C

Mixture	Condition (i)	Condition (j)	ITS		FWD		FE	
			p-value	Sig.	p-value	Sig.	p-value	Sig.
HMA-A	STA-UC	STA-1FT	1.4E-07	Y*	7.4E-09	Y	1.6E-08	Y
		STA-3FT	3.0E-08	Y	5.5E-09	Y	1.1E-08	Y
		LTA-UC	9.9E-01	N+	2.5E-02	Y	5.1E-02	N
		LTA-1FT	1.6E-06	Y	2.5E-08	Y	4.9E-08	Y
		LTA-3FT	1.5E-08	Y	2.3E-09	Y	4.8E-09	Y
HMA-B	STA-UC	STA-1FT	2.2E-09	Y	4.3E-08	Y	2.6E-08	Y
		STA-3FT	8.3E-10	Y	4.9E-08	Y	3.1E-08	Y
		LTA-UC	3.9E-02	Y	8.7E-02	N	8.1E-02	N
		LTA-1FT	3.4E-09	Y	9.3E-08	Y	5.9E-08	Y
		LTA-3FT	1.3E-09	Y	3.9E-08	Y	2.4E-08	Y
WMA-A	STA-UC	STA-1FT	2.0E-08	Y	1.6E-05	Y	1.4E-05	Y
		STA-3FT	1.4E-08	Y	2.3E-05	Y	2.0E-05	Y
		LTA-UC	4.6E-03	Y	8.2E-01	N	7.7E-01	N
		LTA-1FT	2.2E-03	Y	1.9E-03	Y	1.5E-03	Y
		LTA-3FT	2.6E-05	Y	1.1E-04	Y	1.0E-04	Y
WMA-B	STA-UC	STA-1FT	2.1E-05	Y	2.1E-01	N	2.1E-01	N
		STA-3FT	8.5E-06	Y	7.8E-02	N	6.7E-02	N
		LTA-UC	5.9E-02	N	4.1E-01	N	3.7E-01	N
		LTA-1FT	2.2E-02	Y	1.2E-02	Y	1.1E-02	Y
		LTA-3FT	4.4E-04	Y	7.0E-03	Y	6.4E-03	Y

*Yes; +No

Table 4.6 Tukey's post-hoc test results at 25 °C

Mixture	Condition (i)	Condition (j)	ITS		FWD		FE	
			p-value	Sig.	p-value	Sig.	p-value	Sig.
HMA-A	STA-UC	STA-1FT	8.8E-05	Y*	1.2E-01	N+	1.1E-01	N
		STA-3FT	3.8E-08	Y	4.1E-05	Y	3.5E-05	Y
		LTA-UC	7.9E-01	N	5.5E-01	N	6.3E-01	N
		LTA-1FT	5.9E-02	N	1.1E-02	Y	1.1E-02	Y
		LTA-3FT	1.3E-05	Y	1.6E-04	Y	1.5E-04	Y
HMA-B	STA-UC	STA-1FT	5.8E-09	Y	2.9E-08	Y	2.8E-08	Y
		STA-3FT	3.5E-10	Y	9.6E-09	Y	9.9E-09	Y
		LTA-UC	1.8E-03	Y	3.8E-01	N	3.9E-01	N
		LTA-1FT	1.7E-08	Y	1.8E-08	Y	1.8E-08	Y
		LTA-3FT	1.0E-09	Y	8.5E-09	Y	8.4E-09	Y
WMA-A	STA-UC	STA-1FT	9.3E-08	Y	2.8E-03	Y	3.8E-02	Y
		STA-3FT	5.4E-11	Y	1.4E-05	Y	6.2E-04	Y
		LTA-UC	1.1E-07	Y	1.3E-01	N	1.0E+00	N
		LTA-1FT	8.3E-01	N	7.8E-01	N	3.3E-01	N
		LTA-3FT	5.7E-07	Y	7.7E-05	Y	1.3E-02	Y
WMA-B	STA-UC	STA-1FT	5.8E-07	Y	2.5E-01	N	9.1E-03	Y
		STA-3FT	1.3E-08	Y	5.8E-03	Y	1.0E-06	Y
		LTA-UC	2.0E-03	Y	9.6E-01	N	4.0E-02	Y
		LTA-1FT	8.3E-04	Y	2.0E-02	Y	2.0E-05	Y
		LTA-3FT	3.8E-06	Y	4.7E-03	Y	3.8E-06	Y

*Yes; +No

4.3.5 Effect of warm mix additive on ITS and FE

As mentioned in Section 1.2 and section 3.3.1, the effect of reduced production temperature on the moisture susceptibility of a warm bituminous mixture was investigated in this study. Figure 4.12 and Figure 4.13 presents the ratio of moisture conditioned (MC) ITS to unconditioned (UC) ITS of bituminous mixtures. Similarly, Figure 4.14 and Figure 4.15 present the ratio of moisture conditioned FE to unconditioned FE of bituminous mixtures. It could be noticed from Figure 4.12 to Figure 4.15 that the MC/UC ratio of ITS and FE of WMA mixtures is higher than the HMA mixture for most of the cases. Thus, a bituminous mixture with Evotherm-J1 warm mix additive may have higher resistance to moisture damage. The adhesion promoter present in warm mix additive may have resulted in higher ITS and FE ratios.

Further, the statistical significance test using t-test ($\alpha = 0.05$) and Cohen's d-value was used to compare the ITS and FE values of HMA and WMA mixture. Results are summarized in Table C.1 to Table C.4 in Appendix C. It was also noticed that the ITS of short-term and long-term aged HMA and WMA mixtures were significantly different under moisture

conditioned state at 15 °C and at 25 °C. However, no significant difference in the FE values of HMA and WMA mixtures was noticed for most of the cases.

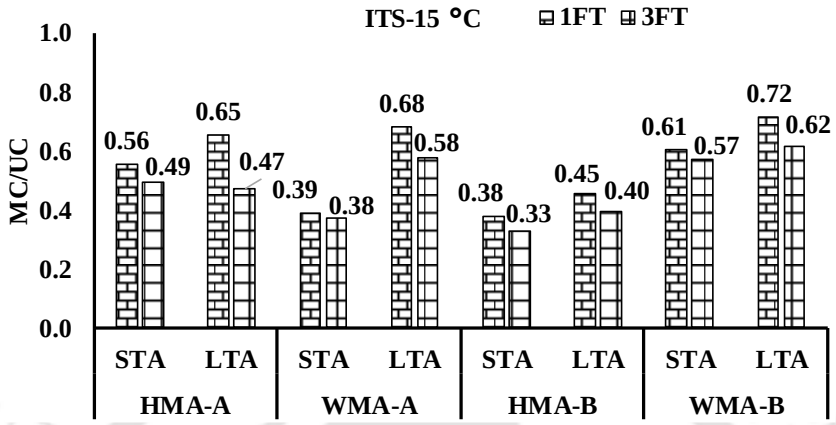

Figure 4.12 Ratio of MC to UC values of ITS of a bituminous mixture at 15 °C

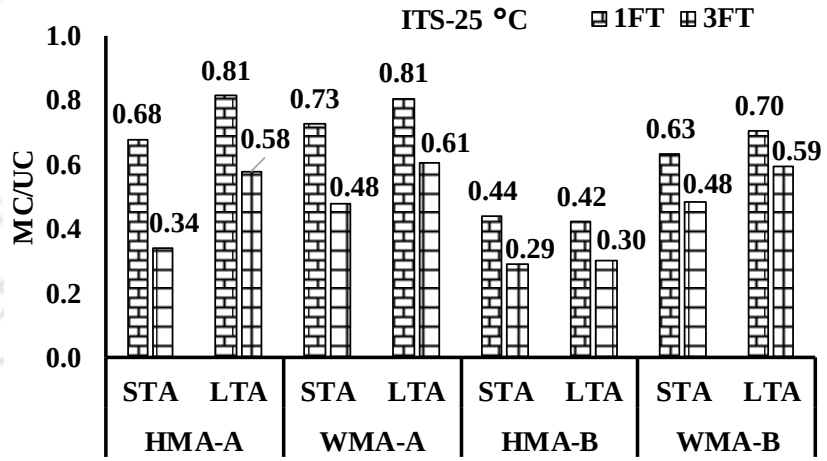

Figure 4.13 Ratio of MC to UC values of ITS of a bituminous mixture at 25 °C

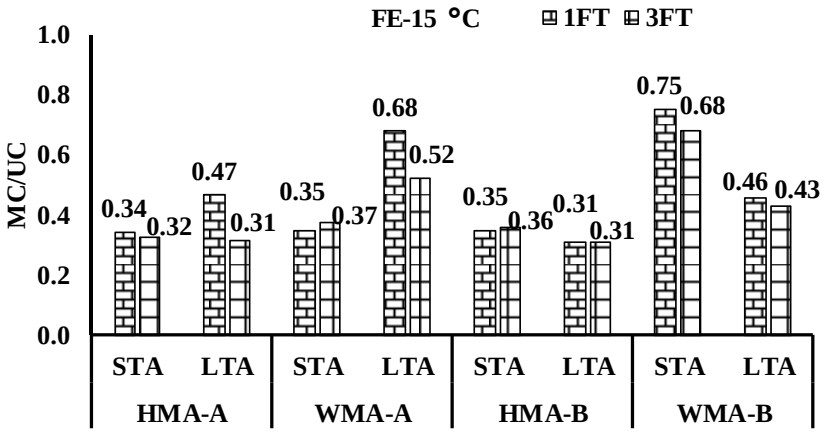

Figure 4.14 Ratio of MC to UC values of FE of a bituminous mixture at 15 °C

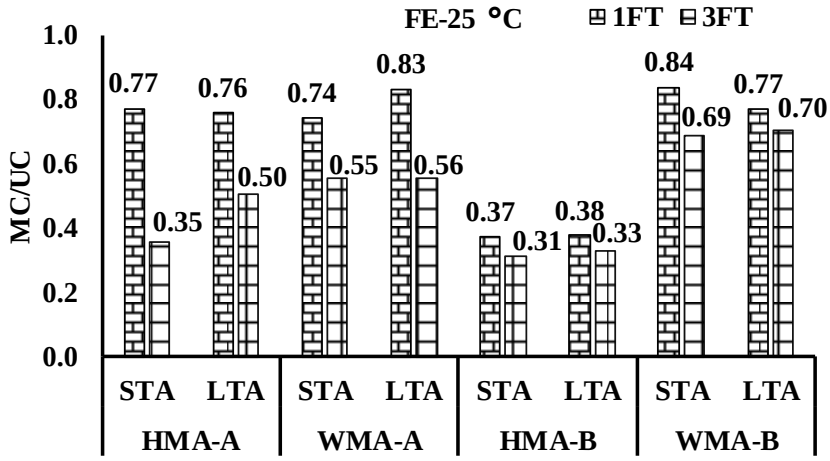

Figure 4.15 Ratio of MC to UC values of FE of a bituminous mixture at 25 °C

4.3.6 Threshold limits of the CoV

ASTM D4867 suggested that the standard deviation of ITS of the bituminous mixture should not exceed 55 kPa for dry or moisture-conditioned specimens. Therefore, a standard deviation of 55 kPa for the ITS values of bituminous mixtures was selected as the threshold. The association between the standard deviation and CoV of the ITS of different mixtures was determined, as shown in Figure 4.16. It could be noticed from Figure 4.16 that for specimens with a standard deviation of 55 kPa or less, the corresponding CoV was less than 10 %, except for one case. Thus, a CoV of 10 % could be used as a threshold value to determine the quality of the test parameter. Next, the standard deviation and CoV of FE of different mixtures were determined and plotted, as shown in Figure 4.17. With the 10 % CoV as a threshold value, it

could be noticed from Figure 4.17 that for most of the cases, the standard deviation of FE was less than 400 J/m^2. Similarly, the standard deviation of different cracking resistance parameters could be determined. However, the 10 % threshold value of CoV established in this study further needs to be verified using different types of bituminous mixtures and additives.

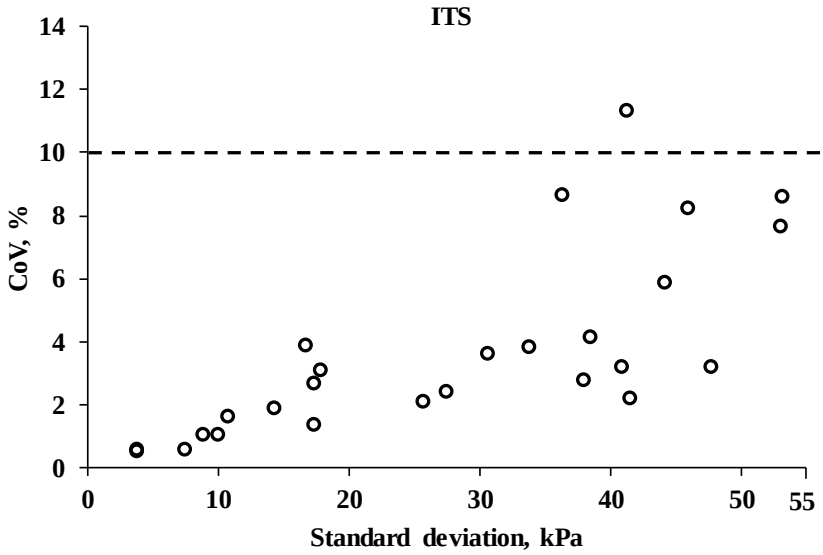

Figure 4.16 Association of standard deviation and CoV of ITS

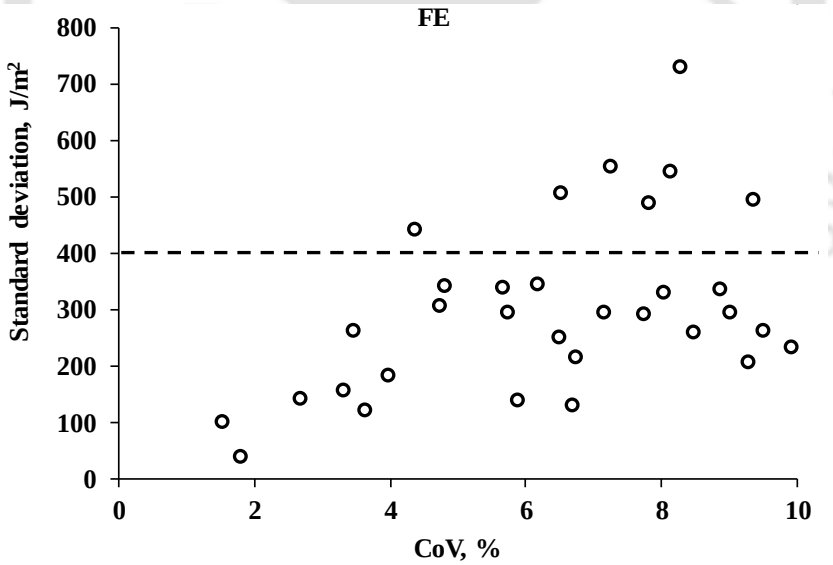

Figure 4.17 Association of standard deviation and CoV of FE

4.4 Summary

In this chapter, different parameters used to evaluate the bituminous mixtures' cracking resistance were examined by comparing the behavior under static loading. Various parameters were explored to benchmark the cracking resistance behavior under the influence of aging and moisture conditioning. Amongst different parameters compared, the ITS, FE, and FWD had a comparatively lower CoV. The value of ITS, FE, and FWD parameters reduced with an increase in moisture conditioning levels. However, CRI, CT_{Index}, and RDCI did not decrease with an increase in moisture conditioning levels. The statistical analysis showed that ITS, FE, and FWD were sensitive to different aging and moisture conditioning levels evaluated. Considering that FE considers both peak load and post-peak behavior of the load-deformation curve, FE might be better suited to assess the cracking resistance of mixtures exhibiting brittle-like behavior. The use of ITS in such mixtures as a cracking resistance parameter might pose limitations. The ratio of moisture conditioned to unconditioned ITS and FE of bituminous mixtures showed that a bituminous mixture with Evotherm-J1 warm mix additive might have higher resistance to moisture damage. The results of this study showed that the standard deviation in FE should be less than 400 J/m^2 with a CoV less than 10 %.

Chapter 5

Adhesive failure in bituminous mixtures

5.1 Introduction

In this chapter, the effect of moisture on the adhesive failure of the bituminous mixture was evaluated using the image analysis technique. A method to determine the threshold values of crushed aggregates and aggregates coated with bitumen was proposed. The association between TSR and adhesive failure of the bituminous mixture was used to determine the limits of adhesive failure. Further, the association between adhesive failure and fracture energy was evaluated to propose a threshold of fracture energy that will help screen bituminous mixture susceptible to undergo cracking in the presence of moisture.

5.2 Experimental program

The experimental detail associated with this chapter is shown in Table 5.1. Bituminous mixtures were subjected to three aging levels, i.e., short-term, long-term, and T-283 aging conditions. Compacted specimens were moisture conditioned using one and three freeze-thaw cycles as per the ASTM D4867 protocol. In the case of loose bituminous mixture testing, moisture conditioning was carried out using a boiling water test as per the ASTM D3625 protocol. The bituminous mixtures' tensile strength was determined at 15 °C and 25 °C using the ITS test as per ASTM D6931 protocol.

Table 5.1 Experimental matrix used for adhesive failure analysis

Mixtures	Test temperature	Aging condition	Moisture condition	Tests	Parameters
HMA-A, HMA-B, WMA-A, and WMA-B	15 °C and 25 °C	STA, LTA, and T-283	Freeze-thaw (UC, 1FT, and 3FT) and boiling water test	ITS and ACT	ITS, TSR, FE, and adhesive failure

Next, the adhesive failure in moisture-conditioned compacted specimens and loose mixtures were measured. The adhesive failure present in the fractured face of the ITS specimen was measured using a digital image processing and analysis technique. Details of the image analysis technique are presented in section 5.3. Adhesive failure also was measured using ACT equipment, which measures the percent loss (synonymous with adhesive failure) in moisture-conditioned loose bituminous mixtures. The ACT measures the percent loss present on the surface of the loose bituminous mixtures. Multiple readings were taken by reshuffling the loose bituminous mixtures to capture the entire sample's moisture damage. For this purpose, the required sample size was calculated using Eq. (5.1) as suggested by Montgomery & Runger (2010). The standard deviation value of one and the error of 0.5 were assumed. A sample size of 16 was selected.

$$n = \left(\frac{Z_{\alpha/2} \times \sigma}{E}\right)^2 \quad (5.1)$$

where,

n= is the sample size,

$Z_{\alpha/2}$=1.96 (95 percent confidence interval of a normal distribution, assumed),

σ= standard deviation, and

E= error.

5.3 Digital image processing and analysis

5.3.1 Image acquisition and image analysis process

Digital image processing and analysis technique was used to determine the adhesive failure present in the ITS specimen's fractured face. The split test specimens subjected to moisture conditioning were dried overnight at room temperature before capturing the image. A digital camera (Nikon D3400, 24 megapixels) was used to capture the split specimens' images. A constant level of illumination was created using two 20 watts LED light sources. The light sources were covered with a transparent paper sheet, which allowed diffused light to reach the specimen surface and minimize reflection. The setup fabricated for capturing images is shown in Figure 5.1.

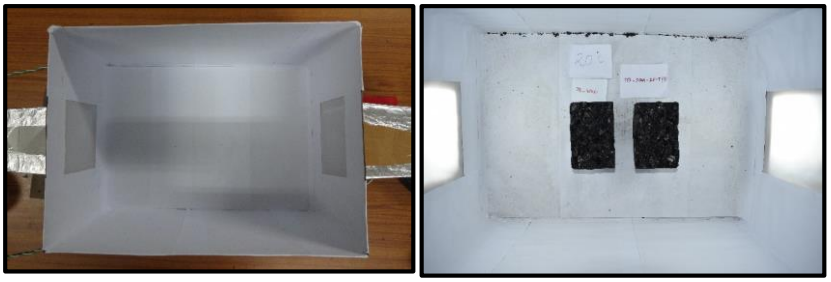

(a) Setup before switching on

(b) Setup during capturing image

Figure 5.1 Setup used for capturing images

The image analysis process begins with converting the RGB (color) image to a greyscale image. A grayscale image has 256 different grey-level shades with 0 for perfect black and 255 for ideal white. Next, the broken aggregates present in the specimens need to be eliminated from the total surface to determine the region with adhesive failure. This was done by selecting the threshold value, which denotes the greyscale boundary separating broken aggregate, adhesive failure region, and bitumen coated region from each other. In this study, a method was proposed to directly determine the required threshold values from crushed aggregates and bitumen-coated loose mixture, as explained in Section 5.3.2. This process of determining the threshold value of aggregate and the corresponding adhesive failure in the bituminous mixtures is designated as 'Method 1'. Results obtained from Method 1 were then compared with the results obtained using the mesh selection method (termed as Method 2) suggested by Lee et al. (2013).

5.3.2 Determination of the threshold value of aggregate

Method 1

In the first method, i.e., Method-1, to determine the threshold value of crushed aggregates, representative aggregates retained on sieve size of 13.2 mm, 9.5 mm, and 4.75 mm from each source of aggregates were selected. The sample size for each aggregate size was estimated using Eq. (5.1) (Montgomery & Runger, 2010). A sample size of 30 was used to determine the threshold value. First, the image of each aggregate face was cropped out and imported to Image J software. The RGB image was then converted to an 8-bit grayscale image, and the threshold value was systematically varied. The threshold value that completely captured the aggregate face was recorded. A pictorial representation of the process is shown in

Figure 5.2. For the case presented in Figure 5.2, the threshold value was found to be 142. Similarly, the process was repeated for all 30 aggregates of different sizes and sources. The average threshold value for aggregates source A was 119, and aggregate source B was 126, as shown in Table 5.2.

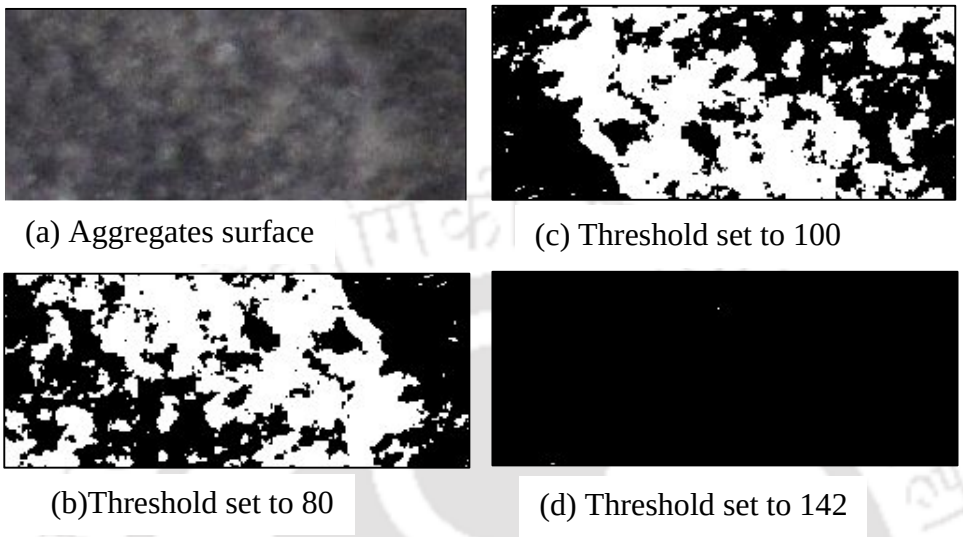

(a) Aggregates surface (c) Threshold set to 100

(b)Threshold set to 80 (d) Threshold set to 142

Figure 5.2 Selection of aggregate threshold value using Method 1

Table 5.2 Threshold values of aggregate using Method 1

Aggregate size, mm	Source A threshold		Source B threshold		Paired t-test (α=0.05)		
	Avg.	COV, %	Avg.	COV, %	Between source A and B	Within source	
13.2	119	15	128	18	p = 0.06	For source A	For source B
9.5	122	11	131	16	p = 0.06	13.2~9.5 (p= 0.36)	13.2~9.5 (p=0.55)
4.75	117	21	117	22	p = 1.00	9.5~4.75 (p=0.35)	9.5~4.75 (p=0.02)
Avg.	119		126				

Method 2

Lee et al. (2013) used a mesh selection method by visual estimation to determine the threshold value of aggregates, which was adopted as the second method, i.e., Method 2, in the study. In Method 2, first, 30 representative images of the fractured face of specimens were selected from each aggregate source. Next, the RGB image was imported to Adobe Photoshop for calculating the percent area of broken aggregates present in the image of the fractured face of the specimen (see Figure 5.3 (a)). Using the grid tool in Adobe Photoshop, fine mesh or grids of 2 mm × 2 mm each was overlapped on the fractured face of the specimen, as shown in Figure 5.3 (b). Next, the grids enclosing broken aggregates were manually identified by visual identification. The total number of such grids was recorded using the count tool, as shown in Figure 5.3 (b). The percentage of broken aggregates was calculated as the ratio of grids containing broken aggregates to the total number of grids present on the specimen's fractured face. The same process was repeated for all 30 specimens for each aggregate source, and the corresponding percent broken aggregates were recorded.

To determine the threshold values of the aggregate, first, the image used in the mesh selection process was imported into Image J software. Next, the RGB image was transformed into an 8-bit grayscale image. Then, the threshold value was systematically varied from 50 to 140 for generating different percent broken aggregate values corresponding to each threshold value. A representative image of the process is shown in Figure 5.4. The threshold values at which the percent broken aggregate value matched the percent broken aggregate calculated from the mesh selection process was recorded. This process was repeated for all 30 specimens and for both sources of aggregates. The threshold values corresponding to the different sources of aggregates are shown in Table 5.3. The average threshold value for aggregates source A was 98, and aggregate source B was 101, respectively. Lee & Kim (2014) used a threshold value of 111 to identify the broken aggregate in their study.

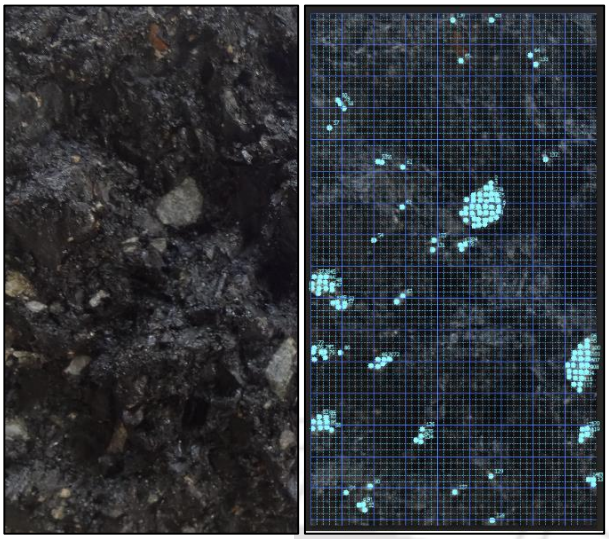

(a) Original image (b) Image with grid

Figure 5.3 Representative image of mesh selection method by visual estimation

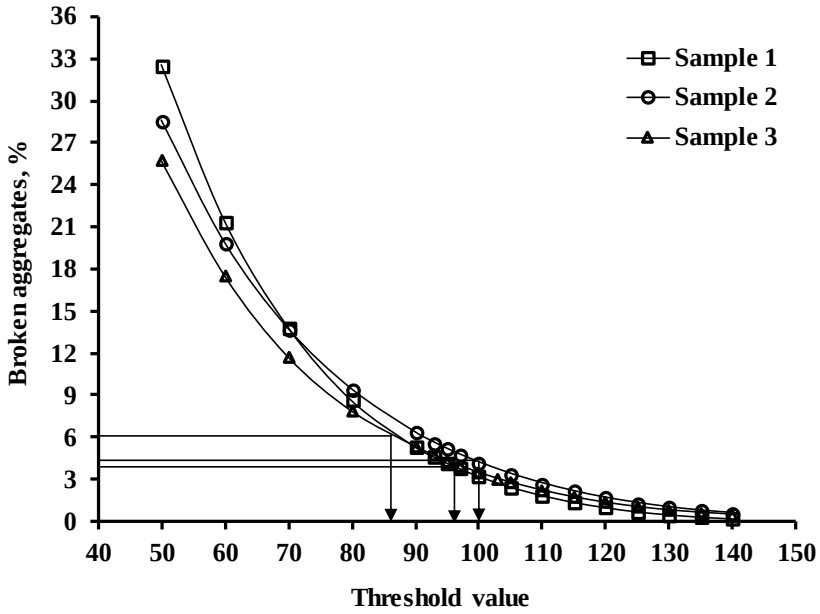

Figure 5.4 Aggregate threshold value using Method 2

Table 5.3 Threshold values of aggregate using Method 2

Source A threshold		Source B threshold		Paired t-test between source A and B (α=0.05)
Average	CoV, %	Average	CoV, %	
98	11	101	13	p = 0.205

5.3.3 Determination of threshold value of aggregate coated with bitumen

Next, the threshold value associated with aggregates completely coated with bitumen was determined following a similar process to determine the aggregate threshold value in Method 1. First, the loose bituminous mixture was prepared, as shown in Figure 5.5 (a). Then, the region of interest (ROI) was selected, cropped, and transformed into a greyscale image, as shown in Figure 5.5 (b). Next, the threshold value was systematically varied until the complete ROI is captured, as shown in Figure 5.5 (c) & (d). Three specimens were used, and a threshold value of 65 was noticed to capture the region of aggregates completely coated with bitumen in each case.

(a) Import the image to Image J software and select the ROI

(b) Crop and transform RGB image into 8-bit greyscale image

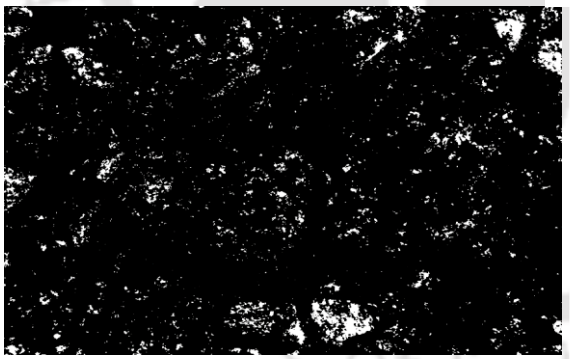

(c) Change threshold value until entire ROI is captured (e.g. threshold set to 40)

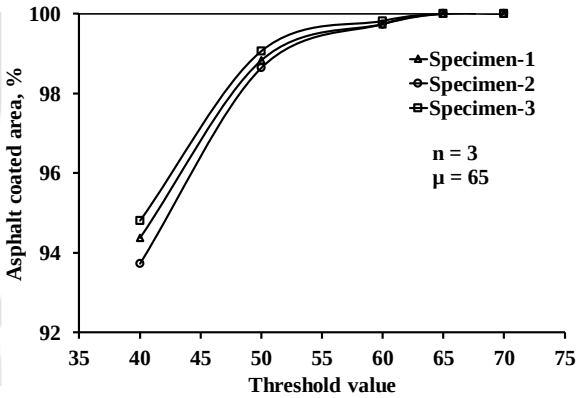

(d) Threshold selection from different specimens

Figure 5.5 Threshold value of bitumen coated aggregate

Researchers like Lee et al. (2013) used a threshold of 63, Amelian et al. (2014) also used a threshold of 65, and Lee & Kim (2014) used a threshold value of 68 to separate adhesive failure and bitumen coated aggregate in their studies. Thus, the threshold value determined in this study was comparable to previous research findings. The region associated with a threshold

value higher than 65 and lower than the aggregate threshold value (119 or 126 for Method 1 and 98 or 101 for Method 2) represents the region with adhesive failure.

5.3.4 Determination of percent adhesive failure

The threshold values established earlier (section 5.3.2 and section 5.3.3) for different sources of aggregates were utilized to calculate the percent broken aggregates and percentage adhesive failure of the specimen. The RGB image was imported to Image J software and converted into 8-bit images, as shown in Figure 5.6. The ROI was specified using the polygon selection method. The threshold value was set to 119 (Method 1) or 98 (Method 2) in the case of specimens with source A aggregates and 126 (Method 1) or 101 (Method 2) for specimens with source B aggregates to determine the percent broken aggregate. The measure tool of Image J was used to determine the percent pixel area associated with the set threshold value and designated as P_1. Then, the percent pixel area of broken aggregates was determined by subtracting the P_1 from the total percent pixel area (100 percent area), as shown in Eq. (5.2) (Lee & Kim, 2014). Similarly, for determining the percent adhesive failure, the threshold value was set to 65, and the corresponding percent pixel area (designated as P_2) was determined using the measure tool. Then, the percent broken aggregates and percent pixel area P_2 were subtracted from the total percent pixel area to obtain the specimens' adhesive failure, as shown in Eq. (5.3) (Lee & Kim, 2014). A pictorial representation of the process, along with the flowchart, is shown in Figure 5.6.

$$Broken\ Aggregates, BA\ (\%) = 100 - P_1 \tag{5.2}$$

$$Adhesive\ Failure, AF\ (\%) = 100 - (BA + P_2) \tag{5.3}$$

where,

P_1= pixel area associated with the threshold value of 119 or 126 for Method 1 and 98 or 101 for Method 2, %

P_2= pixel area associated with the threshold value of 65, %.

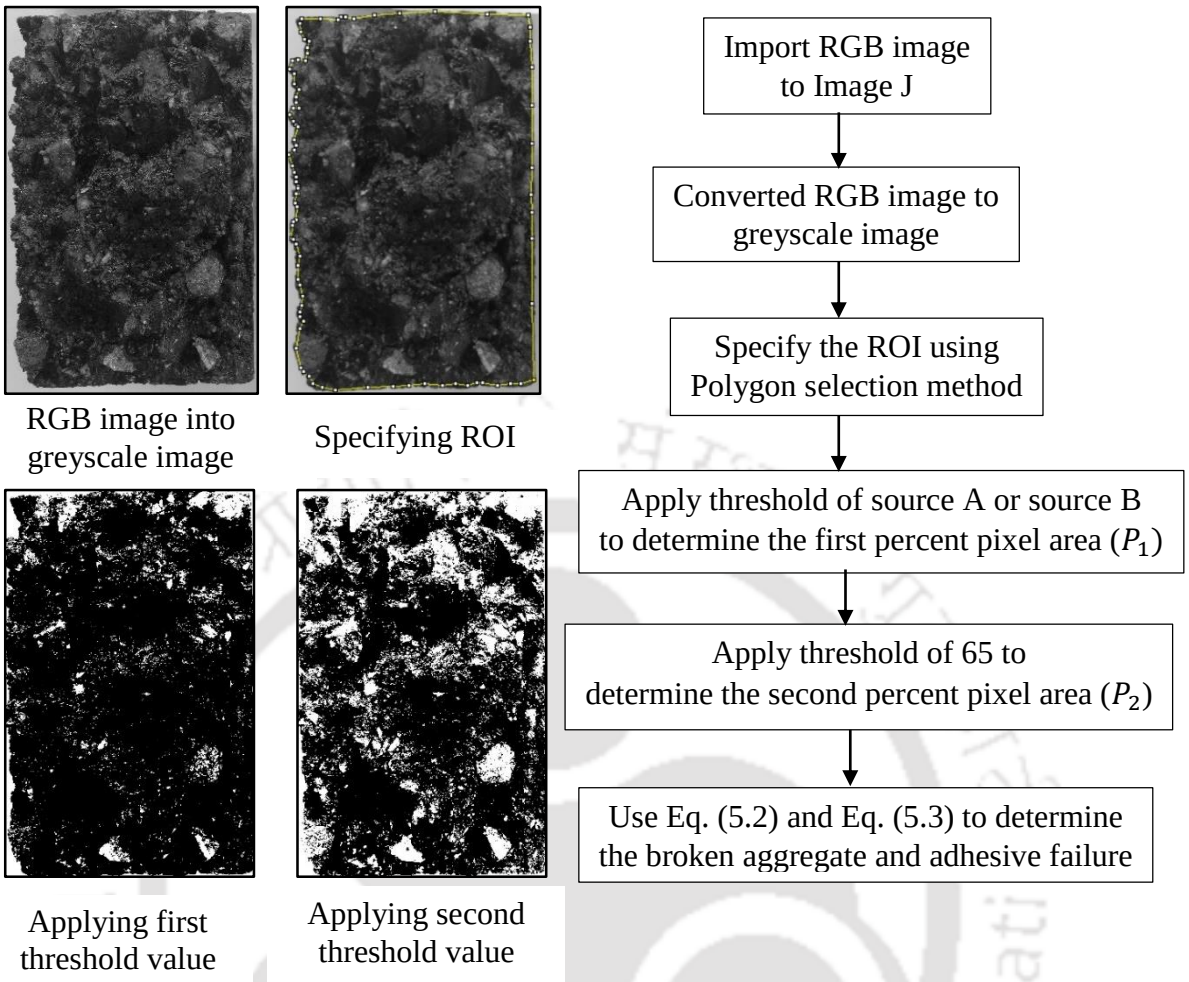

Figure 5.6 Determination of percent adhesive failure

5.4 Results and discussion

5.4.1 Assessment of moisture susceptibility using TSR parameter

Paving agencies widely use the TSR parameter to assess the moisture susceptibility of bituminous mixtures. Researchers, agencies, and highway officials consider a bituminous mixture with a minimum TSR of 80 percent as safe against moisture damage. Most widely, the TSR of the bituminous mixture is determined using by following the AASHTO T 283 standard. AASHTO T 283 protocol requires subjecting a loose bituminous mixture to an oven aging at 60 °C for 16 h and then another 2 h at the mixture's compaction temperature. On the other hand, to evaluate bituminous mixtures' mechanical performance, researchers subject either a loose bituminous mixture or compacted specimen to a short-term aging and long-term aging process. Thus, the aging conditions used for moisture susceptibility tests and performance tests

may not be the same in many cases. Therefore, in this study, a comparison was made between the TSR values of STA, LTA, and T-283 aged bituminous mixtures, as shown in Figure 5.7.

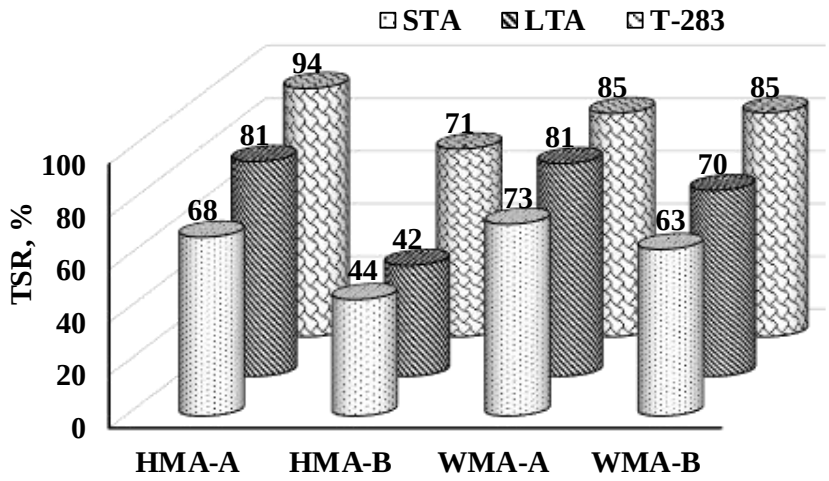

Figure 5.7 TSR of bituminous mixtures at different aging levels

From Figure 5.7, it can be noticed that in the case of T-283 aged bituminous mixtures, except for the HMA-B mixture, all other bituminous mixtures satisfied the 80 percent TSR requirement. Bituminous mixture with source B aggregates (siliceous aggregates) was appropriately identified as a moisture susceptible mixture (TSR < 80 %). However, with the warm mix additive application with the adhesion promoter, the WMA-B mixture showed a TSR value of 85 percent. Based on the bituminous mixtures' TSR values, it could be said that the HMA-A mixture may offer higher resistance against moisture damage compared to other mixtures used in this study. It could be noticed from Figure 5.7 that the TSR of bituminous mixtures increased from STA to LTA and from LTA to T-283 aged condition. It also becomes clear that when a bituminous mixture is subjected to AASHTO T 283 aging process, it will result in higher TSR values as compared to the STA and the LTA aging conditions. Thus, the aging method substantially affects the TSR of the bituminous mixture. Airey et al. (2005) also noticed that with the increase in the aging level, the retained stiffness modulus ratio (stiffness modulus of a conditioned mixture divided by the stiffness modulus of the unconditioned mixture) increased. An ANOVA test was carried out at a 5 percent significance level to understand the statistical significance of aging on the TSR of bituminous mixtures. It could be noticed from Table 5.4 that the TSR of the bituminous mixtures significantly changed with the change in aging conditions. Further, the Tukey post-hoc test showed that in most cases, a change in the aging condition had a significant effect on the TSR of the bituminous mixture

(see Table 5.5). Thus, the aging protocol used may significantly impact the moisture susceptibility of the bituminous mixture.

Table 5.4 One-way ANOVA results of TSR

Mixture		Sum of Squares	df	Mean Square	F-value	p-value
HMA-A	Between groups	1036	2	518	21	2.1E-03
	Within groups	151	6	25		
	Total	1187	8			
HMA-B	Between groups	1582	2	791	81	4.5E-05
	Within groups	59	6	10		
	Total	1640	8			
WMA-A	Between groups	220	2	110	10	1.1E-02
	Within groups	63	6	11		
	Total	283	8			
WMA-B	Between groups	734	2	367	37	4.2E-04
	Within groups	59	6	10		
	Total	794	8			

Table 5.5 Tukeys post-hoc test results of TSR

Mixture	Condition	p-value	Sig.
HMA-A	STA~LTA	3.7E-02	Yes
	STA~T283	1.6E-03	Yes
	T283~LTA	4.8E-02	Yes
HMA-B	STA~LTA	7.1E-01	No
	STA~T283	1.0E-04	Yes
	T283~LTA	6.7E-05	Yes
WMA-A	STA~LTA	5.5E-02	No
	STA~T283	9.9E-03	Yes
	T283~LTA	3.6E-01	No
WMA-B	STA~LTA	6.6E-02	No
	STA~T283	3.7E-04	Yes
	T283~LTA	3.3E-03	Yes

5.4.2 Percent of adhesive failure

In this study, two different methods were used to determine the adhesive failure in bituminous mixtures. First, the percent adhesive failure values obtained from both ways were compared. For this purpose, the adhesive failure values were grouped as follows, AF of STA mixtures at 15 °C (15 °C-STA), AF of LTA mixtures at 15 °C (15 °C-LTA), AF of STA

mixtures at 25 °C (25 °C-STA), and AF of LTA mixtures at 25 °C (25 °C-LTA). Next, the best-fit probability distribution for the adhesive failure of bituminous mixtures in the four different groups was determined using a statistical test (Anderson-Darling). It could be noticed from Table 5.6 that with a change in test conditions, the best-fit probability distribution also changes. The probability density at different adhesive failure values for both methods and different test conditions was determined using the best-fit distribution, as shown in Figure 5.8 and Figure 5.9. Figure 5.8 and Figure 5.9 show that the adhesive failure values determined using Method-1was relatively higher than the adhesive failure values determined using Method-2. A paired *t*-test at a 5 percent significance level was conducted to see if the adhesive failure values obtained using both methods were significantly different. It could be seen from Table 5.7 that the difference in the adhesive failure values obtained using the two methods was significantly different for most of the cases. Thus, it could be said that the image analysis process adopted has a significant effect on the adhesive failure values determined in bituminous mixtures. Comparing both Method-1 and Method-2, the image analysis process used in Method-1 was straightforward and didn't involve any manual identification steps as required in Method-2. Also, the adhesive failure values obtained using Method-1 were relatively higher than Method-2. Thus, image analysis using Method -1 will result in more conservative adhesive failure values. Based on the above discussions, the adhesive failure obtained using Method -1 was selected for further analysis. It could also be noticed from Figure 5.8 and Figure 5.9 that the adhesive failure at 15 °C was higher than 25 °C, irrespective of the test method used. Thus, a bituminous mixture might undergo higher adhesive failure at a lower test temperature than a higher test temperature (Xie et al., 2012).

Table 5.6 Best fit probability distributions for AF

Condition	Method	Anderson-Darling statistics			Best fit distribution
		Normal	Lognormal	Weibull	
15 °C-STA	Method-1	0.66	0.30	0.91	Lognormal
	Method-2	0.78	0.35	1.06	Lognormal
15 °C -LTA	Method-1	0.19	0.47	0.21	Normal
	Method-2	0.26	0.51	0.27	Normal
25 °C -STA	Method-1	0.69	2.02	0.86	Normal
	Method-2	0.52	1.61	0.65	Normal
25 °C -LTA	Method-1	0.36	0.35	0.25	Weibull
	Method-2	0.28	0.42	0.23	Weibull

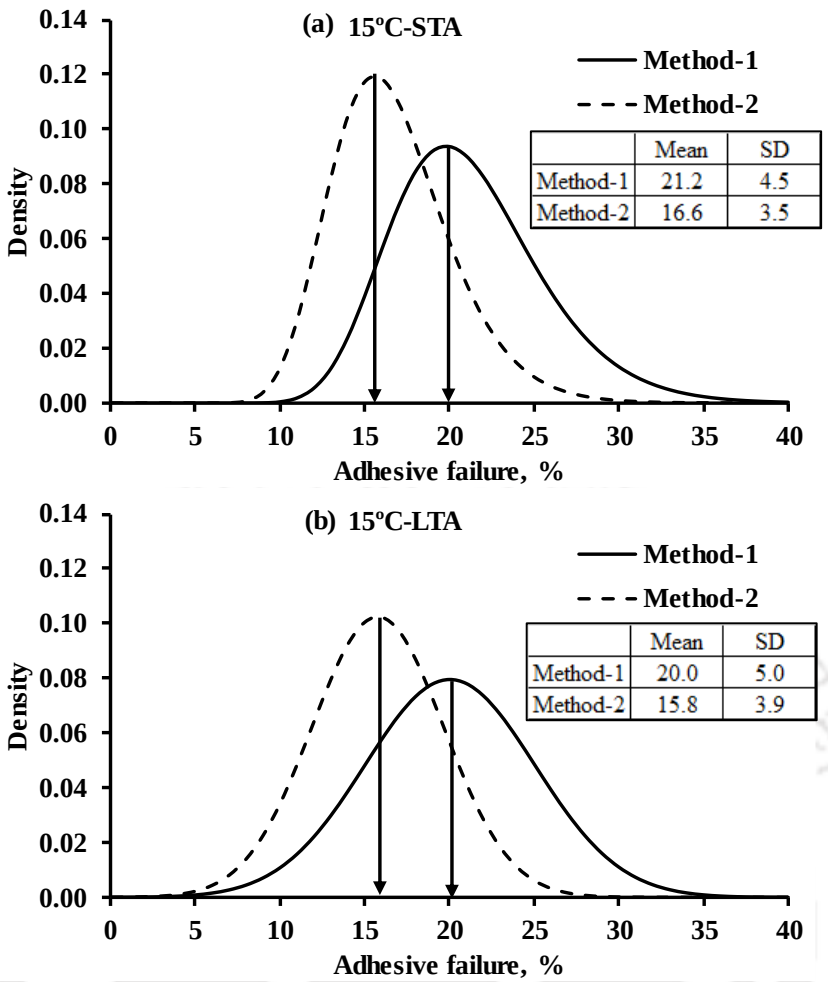

Figure 5.8 Adhesive failure at 15 °C: (a) STA; (b) LTA

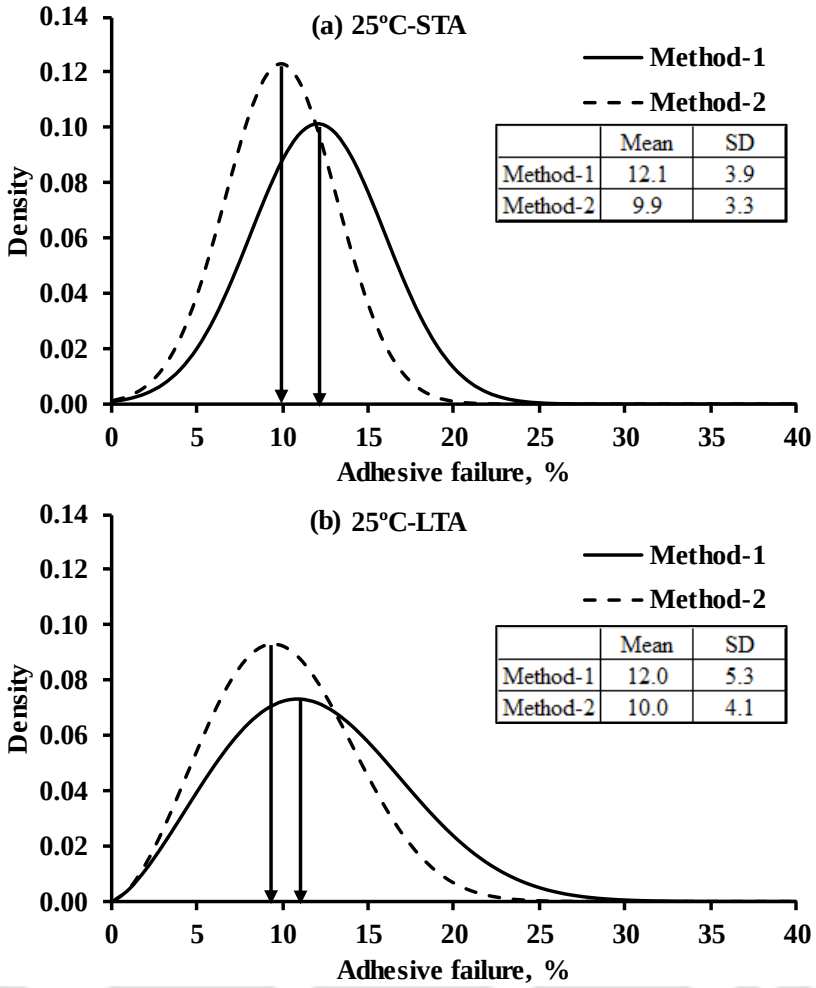

Figure 5.9 Adhesive failure at 25 °C: (a) STA; (b) LTA

Table 5.7 Paired t-test of adhesive failure determined using Method 1 and Method 2

Mixture	Aging	Moisture	15 °C		25 °C	
			p-value	Significant	p-value	Significant
HMA-A	STA	1FT	0.01	Yes	0.00	Yes
		3FT	0.02	Yes	0.06	No
	LTA	1FT	0.06	No	0.04	Yes
		3FT	0.01	Yes	0.01	Yes
HMA-B	STA	1FT	0.01	Yes	0.07	No
		3FT	0.03	Yes	0.02	Yes
	LTA	1FT	0.01	Yes	0.19	No
		3FT	0.01	Yes	0.26	No
WMA-A	STA	1FT	0.00	Yes	0.15	No
		3FT	0.01	Yes	0.01	Yes
	LTA	1FT	0.01	Yes	0.45	No
		3FT	0.06	No	0.03	Yes
WMA-B	STA	1FT	0.03	Yes	0.01	Yes
		3FT	0.00	Yes	0.00	Yes

Mixture	Aging	Moisture	15 °C		25 °C	
			p-value	Significant	p-value	Significant
	LTA	1FT	0.02	Yes	0.06	No
		3FT	0.02	Yes	0.06	No

5.4.3 Association of adhesive failure and TSR parameter

In this study, the different combinations of aggregates, production process (HMA and WMA), aging, moisture conditioning, and test temperature were selected to obtain a comprehensive experimental matrix that will result in a wide range of TSR and its associated adhesive failure values. It could be noticed from Figure 5.10 (a) that the TSR value of bituminous mixtures varied from as low as 20 percent to 100 percent. Similarly, a wide range of adhesive failures of different bituminous mixtures could be noticed in Figure 5.10 (b). Lee & Kim (2014) used one HMA mixture and five WMA mixtures (Evotherm-3G, a chemical additive, a foaming technology, and two different organic additives) to determine the adhesive failure and associated TSR values. The authors noticed that the TSR of moisture conditioned bituminous mixture (as per AASHTO T 283) varied from approximately 40 percent to 100 percent. The corresponding adhesive failure values changed from roughly 5 percent to 15 percent, respectively. Further, from the statistical test (Anderson-Darling), it was noticed that the best fit distribution for TSR and AF was a lognormal and normal distribution. The distribution parameters, i.e., mean (μ) and standard deviation (σ), are also presented in Figure 5.10.

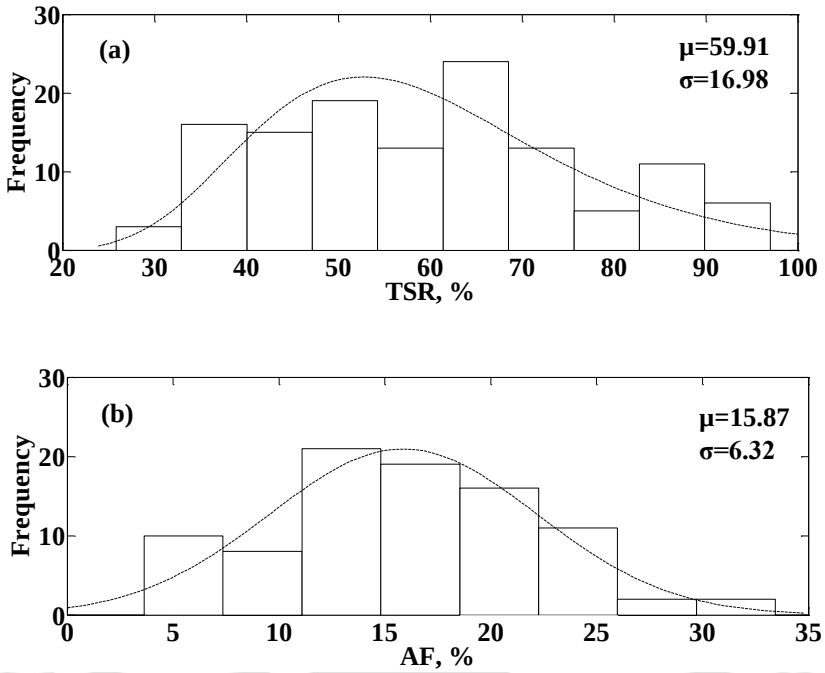

Figure 5.10 Histogram: (a) TSR; (b) adhesive failure

Studies suggest that a TSR value of 70 to 80 percent or higher is considered resistant to moisture damage (Radhakrishnan *et al.*, 2020; Tanzadeh *et al.*, 2020). Thus, bituminous mixtures having a TSR value higher than 80 percent were grouped. Similarly, bituminous mixtures were also grouped into a TSR value of 80 to 70, 70 to 60, 60 to 50, and less than 50. The corresponding adhesive failure of the bituminous mixtures in different groups is shown in Figure 5.11. In general, it could be seen from Figure 5.11 that as the moisture susceptibility of bituminous mixtures increases (reduction in TSR), the adhesive failure also increases. A bimodal distribution of adhesive failure was noticed in bituminous mixtures with TSR higher than 80 percent. The spread in the distribution of adhesive failure values increased, and skewness reduced with an increase in moisture susceptibility. It was also interesting to notice the demarcation of moisture susceptibility in bituminous mixtures based on adhesive failure. It was seen that for bituminous mixtures with a TSR value of 80 percent or higher, adhesive failure was less than 10 percent. Thus, bituminous mixtures with 10 percent or less adhesive failure could be considered to exhibit higher resistance against moisture damage.

Similarly, Lee & Kim (2014) noticed that bituminous mixtures with TSR values higher than 80 percent had a percent adhesive failure of less than 10 percent. Tayebali *et al.* (2018) noticed that for bituminous mixtures with adhesive failure (results obtained from boiling water test), less than 10 percent satisfied the TSR requirement of 85 percent. Thus, 10 percent of

adhesive failure could be considered the threshold value that could delineate bituminous mixtures with high resistance against moisture damage.

Bituminous mixtures with TSR values between 70 to 80 percent had an adhesive failure range of 5 to 14 percent with a median value higher than 10 percent. The literature review suggested 70 percent TSR as the lower acceptable limit. Thus, a corresponding value of 15 percent adhesive failure could be proposed to identify bituminous mixtures with moderate resistance against moisture damage. Thus, bituminous mixtures having an adhesive failure between 10 to 15 percent could be considered to offer moderate resistance against moisture damage. It is important to notice from Figure 5.11that for bituminous mixtures having TSR less than 70 percent, adhesive failure's median value was higher than 15 percent. Thus, adhesive failure of 15 percent or higher could identify bituminous mixtures with low resistance against moisture damage. Therefore, based on the adhesive failure of 10 percent or less, 10 to 15 percent, and more than 15 percent, three zones of bituminous mixtures were identified. Three zones were classified as high, moderate, and low resistance against moisture damage.

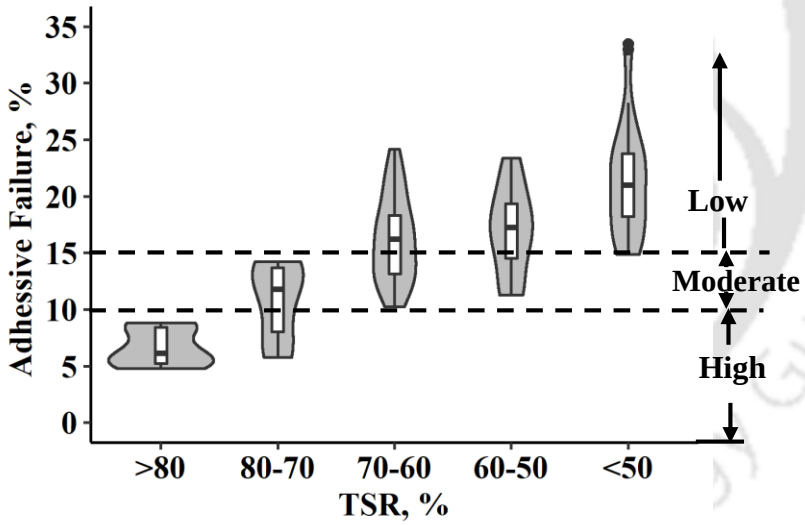

Figure 5.11 Association of adhesive failure with TSR

A multilinear regression model was developed using the adhesive failure (AF) as the response variable and ITS, air voids (AV), saturation (S), and test temperature (T) as predictor variables. In this model, variable ‘ T’ was used as a categorical variable which takes the value of ‘0’ for observation at $T = 15\,°C$, and ‘1’ for observation at $T = 25\,°C$. The model formulation is shown in Eq. (5.4). The model parameters of Eq. (5.4) are shown in Table 5.8. It could be noticed from Table 5.8 that saturation (70 to 80 %) did not have a significant (p-

value (0.85) >0.05) effect on the response variable. Thus, the model formulation was revised, as shown in Eq. (5.5), and the model parameters are shown in Table 5.9. It could be noticed from Table 5.9 that the model and model parameters were statistically significant at a significance level of α =0.05. The adhesive failure of bituminous mixtures tested at 15 °C can be determined using Eq. (5.6), and mixtures tested at 25 °C can be determined using Eq. (5.7). The relations presented in Eq.(5.6) and Eq. (5.7) further need to be improved by incorporating different types of bituminous mixtures and test conditions.

$$AF = a_1 + a_2 \times ITS + a_3 \times \mathrm{AV} + a_4 \times \mathrm{S} + a_5 \times \mathrm{T} \quad (5.4)$$

$$AF = a_1 + a_2 \times ITS + a_3 \times \mathrm{AV} + a_4 \times \mathrm{T} \quad (5.5)$$

$$AF = 19.62 - 0.01 \times ITS + 1.45 \times \mathrm{AV} \quad (5.6)$$

$$AF = 8.84 - 0.01 \times ITS + 1.45 \times \mathrm{AV} \quad (5.7)$$

where,

$a_1, a_2, a_3, a_4, and\ a_5$= regression coefficients

Table 5.8 Regression parameters of adhesive failure model for Eq. (5.4)

Coefficients	Estimates	pValue	Adjusted R-square	Model p-value
a_1	21.65	6.73E-02	0.64	3.09E-17
a_2	-0.01	5.99E-07		
a_3	1.49	2.62E-02		
a_4	-0.03	8.48E-01		
a_5	-10.83	1.23E-17		

Table 5.9 Regression parameters of adhesive failure model for Eq. (5.5)

Coefficients	Estimates	pValue	Adjusted R-square	Model p-value
a_1	19.62	1.71E-04	0.64	4.06E-18
a_2	-0.010	4.76E-07		
a_3	1.45	2.20E-02		
a_4	-10.78	2.13E-18		

5.4.4 Fracture energy for screening moisture susceptible bituminous mixtures

In section 5.4.3, the bituminous mixtures were categorized into three zones based on adhesive failure. The fracture energy (FE) of the bituminous mixtures in the corresponding zones was determined using Eq. (2.5) as per ASTM D8225, as shown in Figure 5.12. First, the effect of loss of adhesion between bituminous binder and aggregate on fracture energy of mixtures was studied. It could be noticed from Figure 5.12 that the FE value of bituminous mixtures reduces with the increase in adhesive failure value. The average percent reduction in FE of moisture-conditioned bituminous mixtures with respect to unconditioned mixtures for each zone of adhesive failure is also presented in Figure 5.12. An adhesive failure of 10 percent or less resulted in an average reduction of 28 percent in FE of the bituminous mixture. Similarly, adhesive failure of 10 to 15 percent and more than 15 percent resulted in a 42 percent and 54 percent reduction in FE of bituminous mixtures, respectively.

It is interesting to notice that an approximately 5 percent increase in adhesive failure (from 10 % to 15 %) reduced the FE of bituminous mixtures by almost twice (from 28 % to 54 %). Thus, adhesive failure has a strong influence on the FE of bituminous mixtures. This also points out that the FE is a potential parameter to delineate poor-performing bituminous mixtures against moisture damage. Similar observations was also noticed by Apeagyei et al. (2015).

Fracture energy is also a measure of the cracking resistance of a bituminous mixture. The average fracture energy of bituminous mixtures with high, moderate, and low resistance against moisture damage could be explored using adhesive failure values. Figure 5.12 shows that the average FE value of bituminous mixtures corresponding to the group with AF less than 10 percent is 5200 J/m^2. Thus, bituminous mixtures with a fracture energy value of 5200 J/m^2 or higher could be considered highly resistant to moisture damage. Similarly, the average FE value of bituminous mixtures in the low resistant zone was found to be 3300 J/m^2 or less. Thus, bituminous mixtures with FE between 5200 J/m^2 and 3300 J/m^2 could be considered to offer moderate resistance against moisture damage. Bituminous mixtures with FE values lower than 3300 J/m^2 were found to offer low resistance against moisture damage measured in terms of the bituminous mixtures' adhesive failure. Further, adhesive failure and corresponding FE values of a wide range of bituminous mixtures and field cores could be used to establish FE threshold values of bituminous mixtures to screen moisture susceptible bituminous mixtures.

In this study, approximately 80 data points were used to arrive at the limits of adhesive failure and fracture energy.

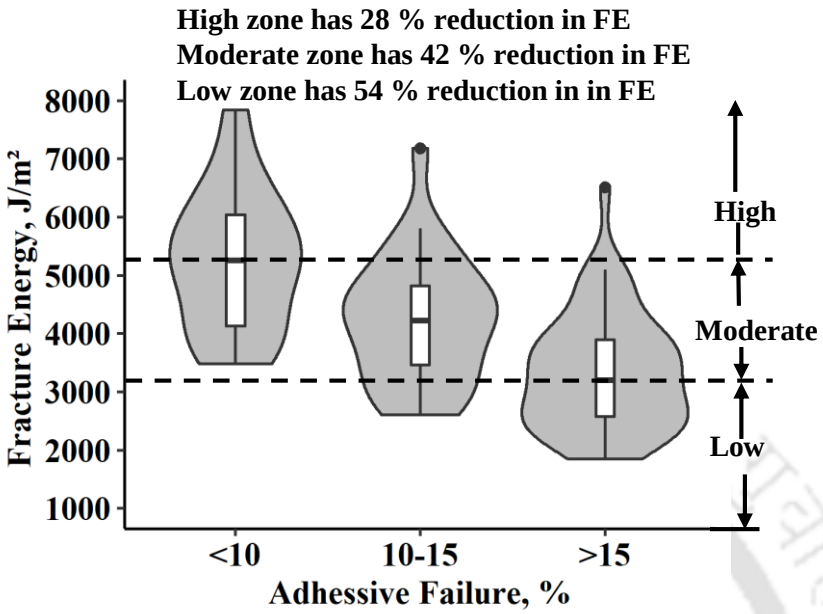

Figure 5.12 Determining fracture energy limits

5.4.5 Adhesive failure of loose bituminous mixtures

From section 5.4.3, it could be noticed that bituminous mixtures with adhesive failure of less than 10 percent had high resistance against moisture damage. The 10 percent adhesion failure limit was further used to determine the bituminous mixture's moisture susceptibility using a boiling water test. For this purpose, ACT was used to measures the percent loss (synonymous with adhesive failure) in moisture-conditioned loose bituminous mixtures. The percent loss for STA and T-283 aged bituminous mixtures is shown in Figure 5.13 (a). It could be noticed from Figure 5.13 (a) that the percent loss in the case of HMA-B mixtures was higher than 10 percent and substantially higher than the other bituminous mixtures used in this study. Aggregate source A was calcareous, while aggregate source B was siliceous. Bituminous mixtures with basic or calcareous aggregates are more resistant to moisture damage than acidic or siliceous aggregates (Cui et al., 2014). Thus, the threshold of 10 percent loss appropriately identified the HMA-B mixture as poor resistance against moisture damage. At the same time, WMA-B mixtures had a percent loss lower than 10 percent. The Evotherm-J1 warm mix additive is a chemical package that also includes adhesion promoters, which resulted in a marked decrease in the percent loss of the WMA-B mixtures (Al-Qadi et al., 2012; Wang et

al., 2013). Thus, the limits on adhesion failure proposed in this study could also be applied to test the moisture susceptibility of the bituminous mixture during the production stage.

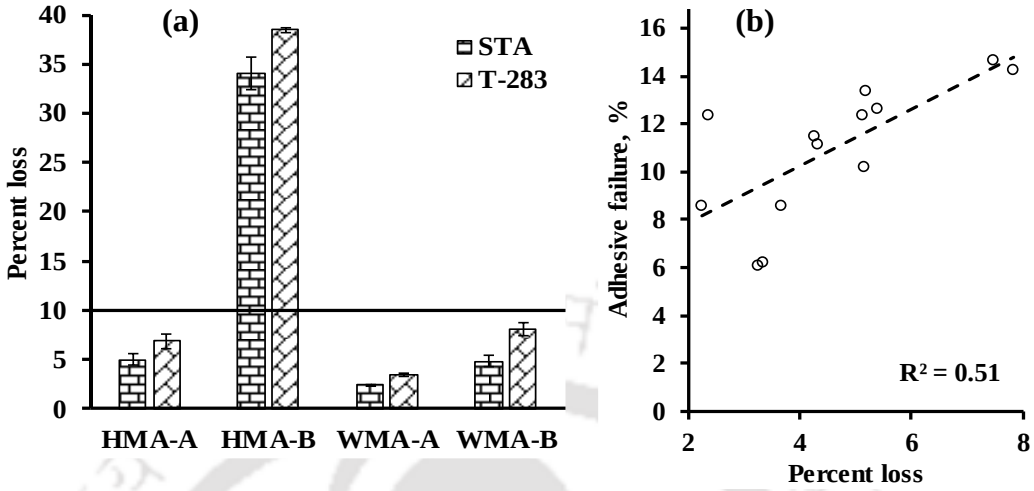

Figure 5.13 Boiling test results: (a) percent loss; (b) association of percent loss with AF

The association between adhesive failure measured using two different techniques, i.e., percent loss measured from the loose mixture using ACT and the adhesive failure measured using image analysis from compacted specimens, was determined, as shown in Figure 5.13 (b). It could be noticed from Figure 5.13 (b) that the R^2 value was close to 0.50. Considering that the moisture conditioning and adhesive failure evaluation process was different in compacted specimens and loose bituminous mixtures, an R^2 close to 0.50 could be regarded as a fair association. Manrique-Sanchez et al. (2020) said that the dry-wet-dry moisture conditioning cycle is a physical phenomenon with different sources of uncertainty which increases the total variability of the experimental results. This might result in a lower R^2 value of moisture-conditioned specimens. Lee & Kim (2014) also noticed lower R^2 value of 0.32 between the adhesive failure determined from the cyclic direct tension test and the HWTT. It is worth mentioning that the association between percent loss and the adhesive failure evaluated in this study was based on the results of four bituminous mixtures. Additional experimental results are required to understand the association of adhesive failure measured from different types of tests.

5.4.6 Effect of warm mix additive on adhesive failure

Figure 5.14 and Figure 5.15 presents the adhesive failure in bituminous mixtures at different aging levels and test temperatures. It could be noticed that from Figure 5.14 and

Figure 5.15 that bituminous mixtures with aggregate source B had relatively higher adhesive failure as compared to mixtures with aggregate source A. The relatively higher silica content in aggregate source B may have resulted in higher adhesive failure. Comparing HMA and WMA mixtures, it could be noticed that in the case of bituminous mixture with aggregate source B, WMA mixture had relatively lower adhesive failure compared to HMA mixture (see Figure 5.14 and Figure 5.15). However, bituminous mixtures with aggregate source A showed a mixed trend. The warm mix additive used in this study may have better compatibility with the bituminous mixture produced with siliceous aggregates than calcareous aggregates. Similarly, Hurley & Prowell (2006) noticed that WMA mixtures (Evotherm additive) with granite aggregates had higher TSR (0.96 with PG64-22 and 0.84 with 76-22) as compared to WMA mixture with limestone aggregates (0.62 with PG64-22 and 0.66 with PG76-22). From visual estimation, the authors noticed that only the WMA mixture with limestone aggregate showed adhesive failure.

A paired t-test ($\alpha = 0.05$) and Cohen's d-value was used to compare the adhesive failure values of HMA and WMA mixture and results are summarized in Table C.5 and Table C.6 in appendix C. No significant difference between the adhesive failure values of WMA and HMA mixtures was noticed at different aging level and test temperature.

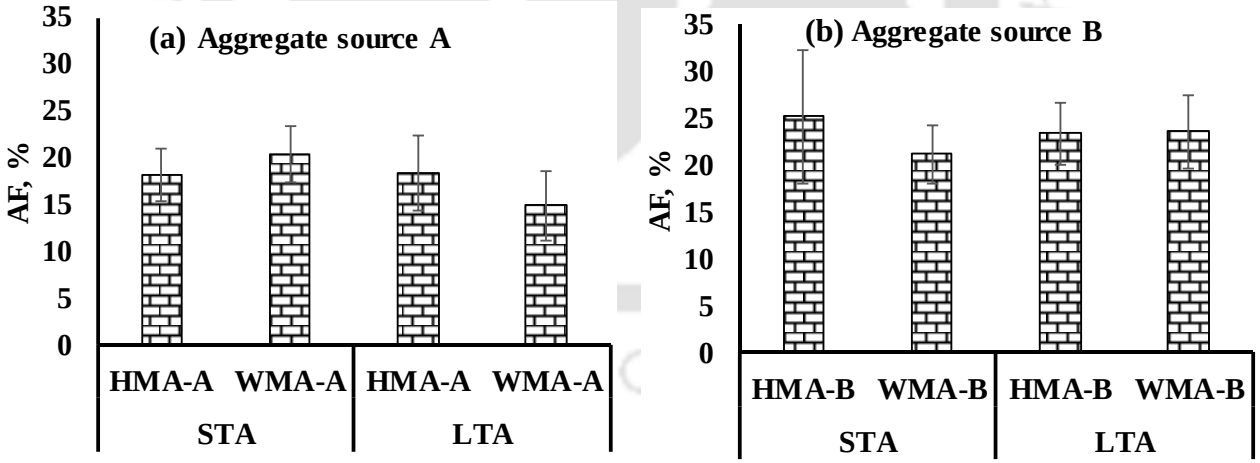

Figure 5.14 Adhesive failure of a bituminous mixture at 15 °C: (a) source A; (b) source B

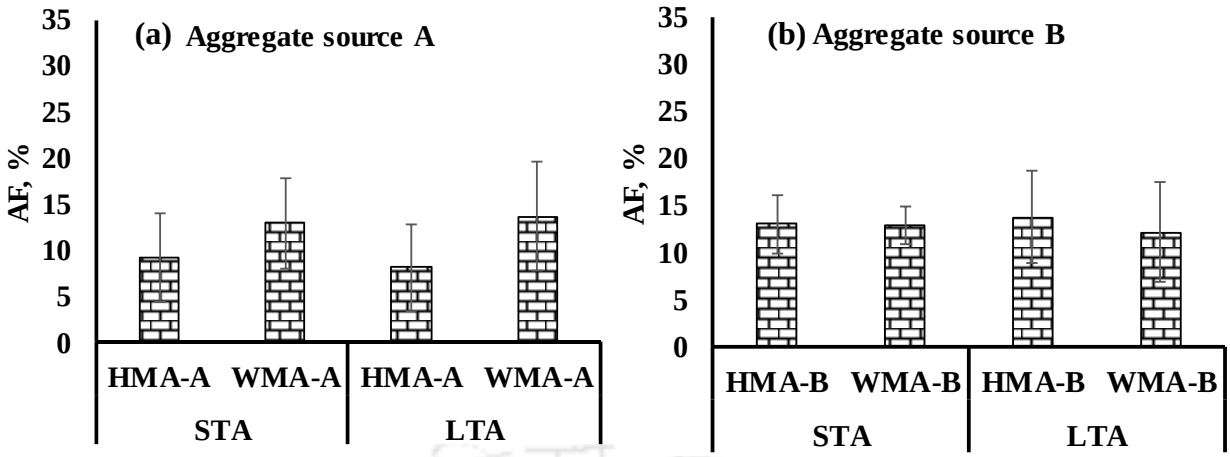

Figure 5.15 Adhesive failure of a bituminous mixture at 25 °C: (a) source A; (b) source B

5.5 Summary

In this chapter, the association between adhesive failure, tensile strength ratio, and fracture energy of bituminous mixtures at different aging levels, moisture conditioning, and test temperature was evaluated. It was noticed that the image analysis process has a significant effect on the adhesive failure values of bituminous mixtures. The image analysis process proposed in this study was more conservative when compared to the existing image analysis process. A high adhesive failure value was associated with a low tensile strength ratio and vice versa. This indicate adhesive failure as a factor of detachment and displacement mechanism to quantify moisture damage in bituminous mixtures. The proposed image analysis process will help to identify bituminous mixtures susceptible to undergo adhesive failure in the presence of moisture. The range of adhesive failure in bituminous mixtures was determined to categorize bituminous mixtures into high, moderate, and low resistant bituminous mixtures based on the tensile strength ratio. Three zones based on adhesive failure values of 10 % or less, 10 to 15 %, and higher than 15 % were identified as zones of high, moderate, and low resistance against moisture damage. The proposed adhesive failure ranges were used to determine the values of fracture energy to screen moisture susceptible bituminous mixtures. The fracture energy associated with the three zones could serve as a measure of high, moderate, and low cracking resistance of bituminous mixtures in the presence of moisture. Also, the association of adhesive failure of loose bituminous mixtures and compacted specimens was studied. A fair correlation between the compacted specimen's adhesive failure and the percent loss of loose bituminous

mixtures was noticed. The adhesive failure noticed in WMA mixtures was not significantly different from the HMA mixtures used in this study.

Chapter 6

Effect of Aging and Moisture on Fatigue of Bituminous Mixtures

6.1 Introduction

This chapter investigates the fatigue behavior of bituminous mixtures subjected to aging (STA & LTA) and moisture conditioning. First, the effect of different test conditions on the stiffness modulus of bituminous mixtures was evaluated. Next, variation in the fatigue life with change in aging and moisture conditioning state was studied. The association of fatigue life with the cracking resistance parameter was evaluated. A probabilistic stiffness degradation approach was used to analyze the fatigue damage in bituminous mixtures. Next, a ratio of stiffness change and a damage-based fatigue life prediction model was proposed to determine the fatigue life of bituminous mixtures. Also, the effect of warm mix additive on mixture's fatigue life was discussed.

6.2 Experimental program

The experimental matrix used for fatigue analysis of bituminous mixtures is shown in Table 6.1. Bituminous mixtures were subjected to two aging levels, i.e., short-term and long-term aging. Moisture conditioning was carried out using one and three freeze-thaw cycles as per the ASTM D4867 protocol. A stress-controlled repeated load fatigue test was carried out by applying stress of 400 kPa at 15 °C and 250 kPa at 25 °C. A complete fracture of the specimen marked the specimen's fatigue failure, and the number of cycles at failure was recorded as the fatigue life (N_f) of the specimen. Also, an ITSM test was conducted at the same test temperatures as ITFT. A total of 144 specimens were used.

Table 6.1 Experimental matrix used for failure analysis

Mixtures	Test temperature	Aging condition	Moisture condition	Tests	Parameters
HMA-A, HMA-B, WMA-A, and WMA-B	15 °C and 25 °C	STA and LTA	UC and freeze-thaw (1 and 3 cycles)	ITSM and ITFT	Fatigue life, fatigue damage, ITSM, the ratio of stiffness change, plateau value

6.3 Results and discussion

6.3.1 Stiffness modulus of bituminous mixtures

The variation in stiffness modulus of bituminous mixtures with mixture type and different test conditions are discussed in this section.

Effect of aging

The stiffness modulus of unconditioned bituminous mixtures subjected to STA and LTA conditions are shown in Figure 6.1. The error bar represents one standard deviation. It could be noticed from Figure 6.1 that the stiffness modulus of LTA bituminous mixtures was higher than the STA bituminous mixtures both at 15 °C and 25 °C. It is because aging increases the hardness of the bituminous binder, which increased the stiffness modulus of bituminous mixtures. The percent increase in the stiffness modulus from STA to LTA condition was higher for specimens tested at 25 °C as compared to specimens tested at 15 °C. Thus, the effect of aging on the stiffness of bituminous mixtures was relatively more at an intermediate temperature. A one-way ANOVA test at a 5 % significance level was carried out to determine the statistical significance of aging on stiffness modulus of bituminous mixtures, as shown in Table 6.2. It could be noticed from Table 6.2 that aging significantly increased the stiffness modulus of bituminous mixtures at both 15 °C and 25 °C. Islam & Tarefder (2015) also noticed that the stiffness modulus of the bituminous mixture increased with an increase in the duration of aging. The LTA specimen showed a 1.2 times higher stiffness modulus than the STA specimen.

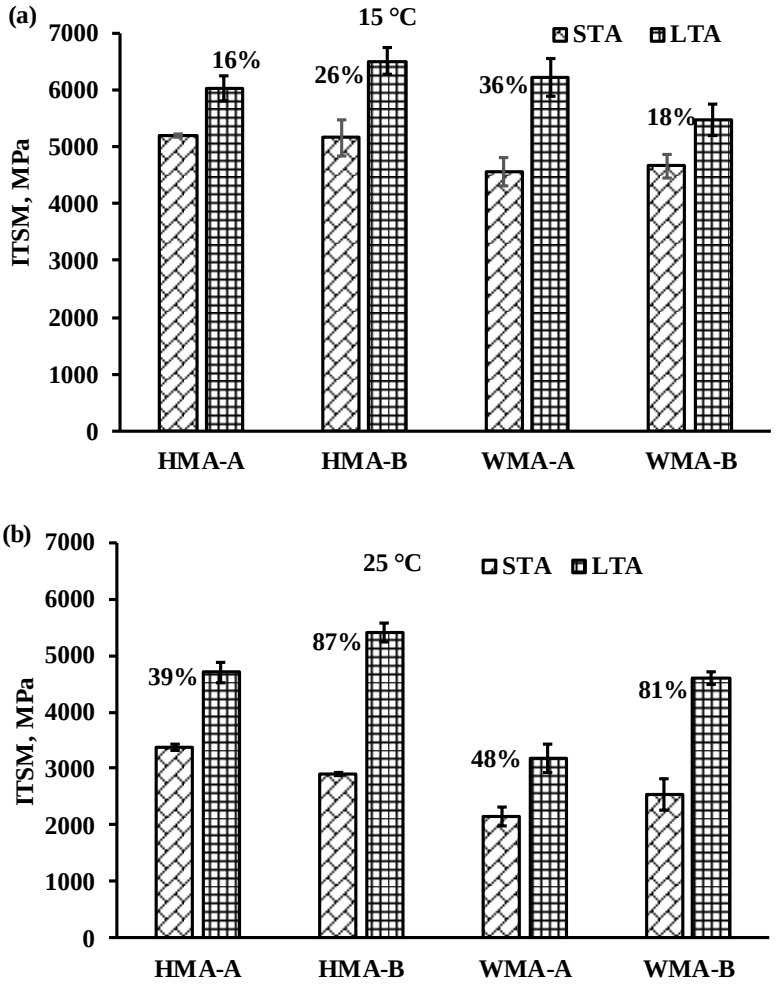

Figure 6.1 Stiffness modulus of UC bituminous mixtures: (a) 15 °C; (b) 25 °C

Table 6.2 One-way ANOVA test on ITSM of UC bituminous mixtures

Mixture	15 °C		25 °C	
	p-value	Significant	p-value	Significant
HMA-A	1.0E-02	Yes	2.1E-05	Yes
HMA-B	1.6E-04	Yes	2.4E-07	Yes
WMA-A	2.1E-04	Yes	2.3E-05	Yes
WMA-B	2.0E-02	Yes	9.8E-07	Yes

Effect of moisture

The stiffness modulus reduced with moisture conditioning for STA bituminous mixtures, as noticed in Figure 6.2. As expected, bituminous mixtures subjected to 3FT cycles of moisture conditioning experienced a higher reduction in stiffness modulus than the 1FT cycle of moisture conditioning. Furthermore, the percent reduction in the stiffness modulus

with an increase in moisture conditioning cycles was relatively higher at 25 °C as compared to 15 °C. Thus, moisture might have a higher negative impact on bituminous mixtures' stiffness modulus at higher test temperatures. The negative effects of moisture on the stiffness modulus of the bituminous mixture are also reported by researchers (Airey et al., 2005).

From Figure 6.2, it could be noticed that the HMA-B mixture had a higher reduction in stiffness modulus at 1FT and 3FT conditions compared to other bituminous mixtures, irrespective of the test temperature. It might be due to the siliceous nature of source B aggregates, which are more susceptible to moisture damage. However, the WMA-B mixture showed a relatively lower reduction in stiffness modulus with moisture conditioning as compared to HMA-B mixtures. For example, the WMA-B mixture tested at 15 °C had 13 % and 16 % higher stiffness modulus at 1FT and 3FT conditions than the HMA-B mixture. This might be due to the presence of adhesion promoter in the warm mix additive, which reduced the moisture susceptibility of WMA-B mixtures (Al-Qadi et al., 2012).

It could be noticed from Figure 6.3 that the effect of moisture on the stiffness modulus of LTA bituminous mixtures was similar, as noticed in the case of STA bituminous mixtures. To statistically infer the effect of moisture, the stiffness modulus at UC, 1FT, and 3FT conditions were compared using one-way ANOVA at a 5 % significance level. Furthermore, it could be noticed from Table 6.3 and Table 6.4 that the reduction in stiffness modulus of the bituminous mixture with moisture conditioning was significant at both STA and LTA conditions for most of the cases. Further, it could be noticed from Figure 6.1 to Figure 6.3 that the stiffness modulus of bituminous mixtures decreased with the increase in test temperature from 15 °C to 25 °C.

Further, the statistical significance testing using t-test and Cohen’s d-value showed that the ITSM of short-term aged HMA and WMA mixtures was not significantly different at 15 ^{o}C and 25 ^{o}C for most cases. However, at 25 ^{o}C, the ITSM of long-term aged HMA and WMA mixtures were statistically different for most cases, including the moisture conditioned state (analysis presented in Table C.7 and Table C.8 in appendix C).

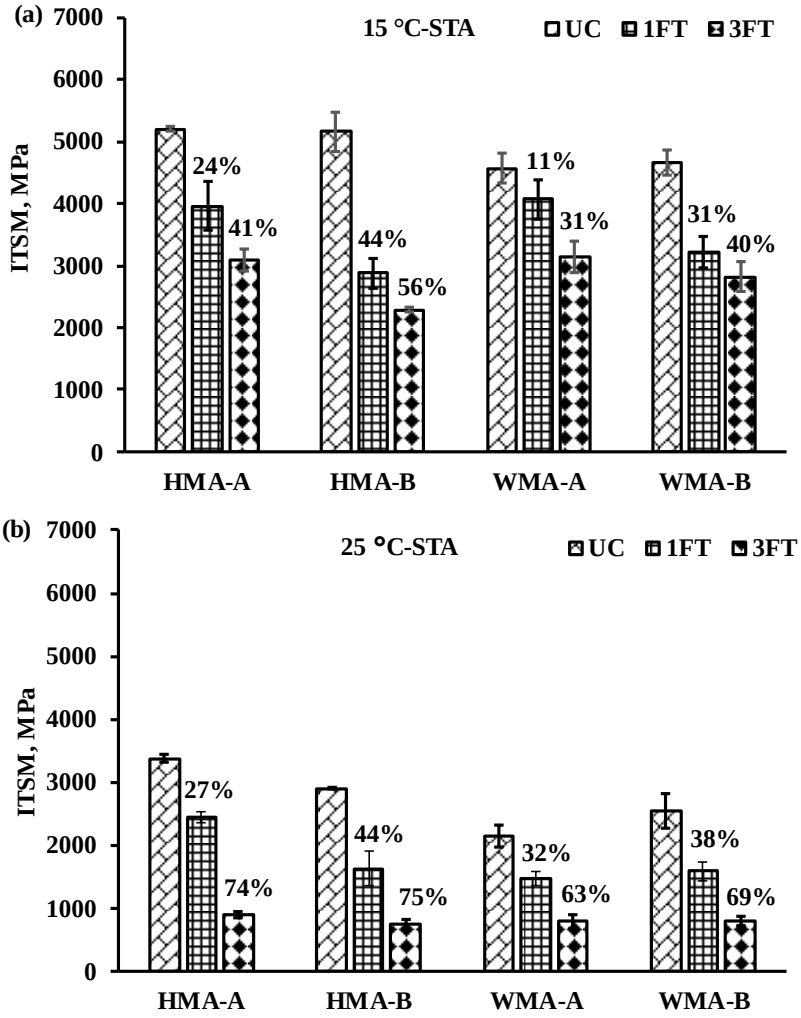

Figure 6.2 Stiffness modulus of the bituminous mixture at STA: (a) 15 °C; (b) 25 °C

Table 6.3 One-way ANOVA test on ITSM of STA mixtures

Mixture	Condition	15 °C		25 °C	
		p-value	Significant	p-value	Significant
HMA-A	UC~1FT	3.3E-04	Yes	7.2E-04	Yes
	UC~3FT	1.3E-06	Yes	1.0E-06	Yes
	1FT~3FT	6.5E-03	Yes	4.0E-06	Yes
HMA-B	UC~1FT	5.6E-07	Yes	1.4E-05	Yes
	UC~3FT	2.6E-07	Yes	9.6E-07	Yes
	1FT~3FT	7.6E-02	No	4.7E-04	Yes
WMA-A	UC~1FT	3.7E-01	No	1.3E-03	Yes
	UC~3FT	8.1E-04	Yes	1.2E-06	Yes
	1FT~3FT	2.3E-02	Yes	1.3E-03	Yes
WMA-B	UC~1FT	2.1E-04	Yes	1.2E-04	Yes
	UC~3FT	1.7E-05	Yes	2.1E-07	Yes
	1FT~3FT	4.3E-01	No	7.2E-04	Yes

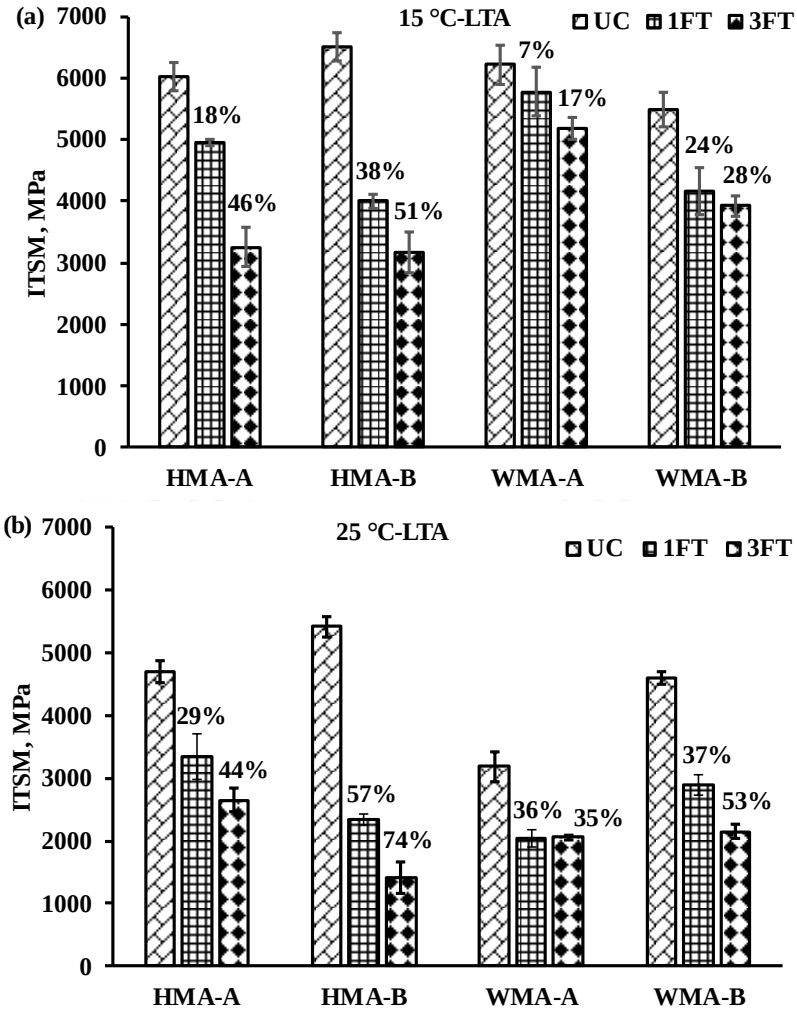

Figure 6.3 Stiffness modulus of the bituminous mixture at LTA: (a) 15 °C; (b) 25 °C

Table 6.4 One-way ANOVA test on ITSM of LTA mixtures

Mixture	Condition	15 °C		25 °C	
		p-value	Significant	p-value	Significant
HMA-A	UC~1FT	1.2E-03	Yes	1.8E-05	Yes
	UC~3FT	2.5E-07	Yes	2.0E-07	Yes
	1FT~3FT	1.6E-05	Yes	6.9E-03	Yes
HMA-B	UC~1FT	2.4E-07	Yes	0.0E+00	Yes
	UC~3FT	2.4E-07	Yes	0.0E+00	Yes
	1FT~3FT	9.7E-03	Yes	2.8E-04	Yes
WMA-A	UC~1FT	5.0E-01	No	8.3E-06	Yes
	UC~3FT	1.1E-02	Yes	9.4E-06	Yes
	1FT~3FT	2.1E-01	No	1.0E+00	No
WMA-B	UC~1FT	4.6E-04	Yes	2.6E-07	Yes
	UC~3FT	9.4E-05	Yes	0.0E+00	Yes
	1FT~3FT	8.5E-01	No	1.2E-03	Yes

6.3.2 Fatigue life analysis

The variation in bituminous mixtures' fatigue life with mixture type and different test conditions are discussed in this section.

Effect of aging

The fatigue life of unconditioned bituminous mixtures at 15 °C and 25 °C is presented in Figure 6.4. It could be noticed from Figure 6.4 that the fatigue life of bituminous mixtures increased with a change in aging level. Furthermore, it could be noticed that the fatigue life reduced with the increase in test temperature from 15 °C to 25 °C. For example, an average reduction of 92 percent for STA bituminous mixtures and 84 percent for LTA bituminous mixtures was noticed with the increase in test temperature from 15 °C to 25 °C. In comparison, Al-Khateeb & Ghuzlan (2014) also noticed that fatigue life is approximately reduced by 95 to 99 percent, with the increase in test temperature from 20 °C to 30 °C. Hence as temperature increases, mixtures become more susceptible to plastic flow, which will reduce the fatigue life of bituminous mixtures (Safaei & Castorena, 2016).

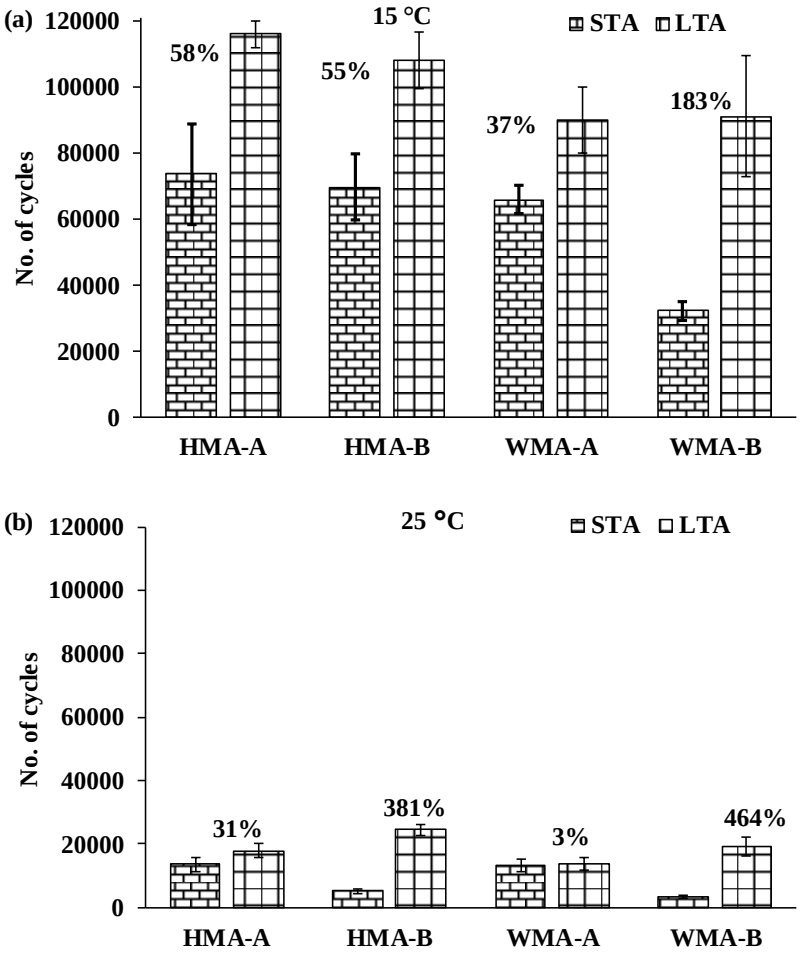

Figure 6.4 Fatigue life of UC bituminous mixtures: (a) 15 °C; (b) 25 °C

The gain in stiffness of bituminous mixture with aging (as noticed in Figure 6.1) increased the fatigue life determined using a stress-controlled setup. As discussed in section 2.6.3, researchers have noticed that in a stress-controlled mode of fatigue testing, an aged bituminous mixture has a higher fatigue life than unaged mixtures. A comparison of strain experienced by the STA and the LTA specimen at 400 kPa and 15 °C is shown in Figure 6.5. It could be seen from Figure 6.5 that the strain experienced by the STA specimen was higher than the LTA specimen for applied stress of 400 kPa at 15 °C. On average, the LTA specimen experienced a 16 % lower initial strain than the STA specimens. Thus, a lower strain experienced by the LTA specimens at a constant stress level resulted in a higher number of cycles to failure in the LTA specimen than the STA specimen (Baek et al., 2012).

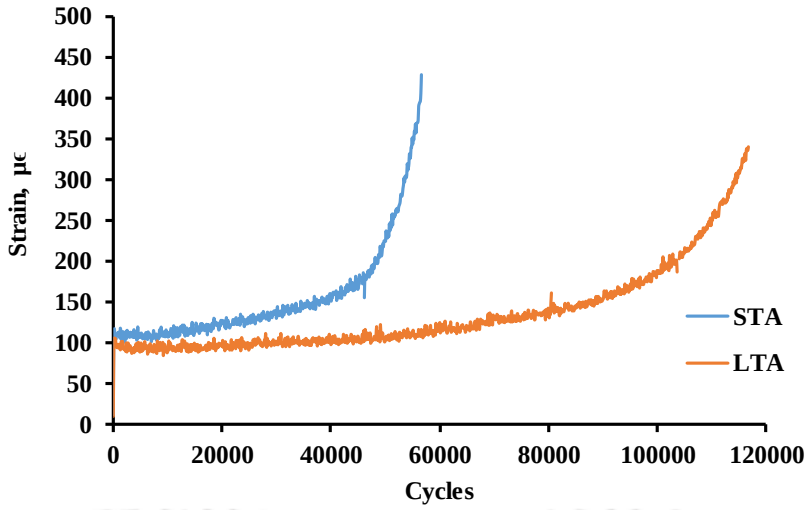

Figure 6.5 Strain experienced by STA and LTA specimen at 400 kPa and 15 °C

This study noticed that the STA specimens had relatively higher accumulated permanent deformation than the LTA specimen due to higher stiffness as also noticed by Di Benedetto et al. (2004). Comparison for specimen tested at STA and LTA condition at 400 kPa, and 15 °C is shown in Figure 6.6. It could be noticed from Figure 6.6 that the STA specimen had higher permanent deformation than the LTA specimen, which might have resulted in lower fatigue life of the STA specimen when compared to the LTA specimen.

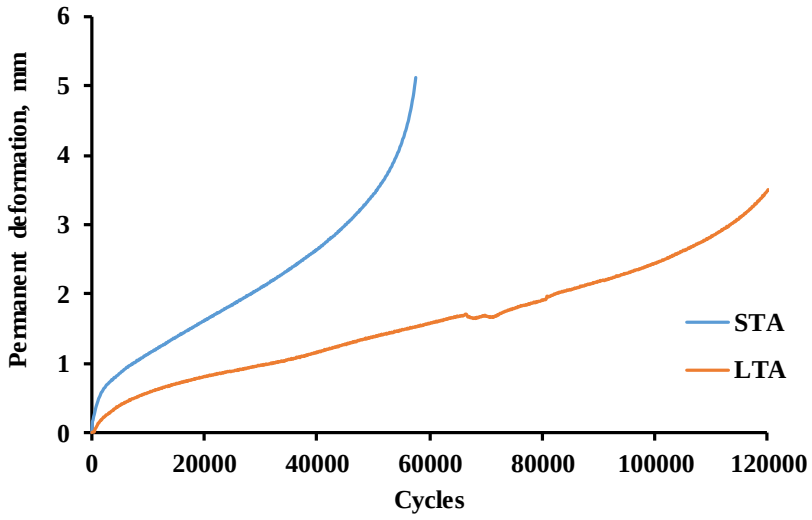

Figure 6.6 Permanent deformation of STA and LTA specimen at 400 kPa and 15 °C

Another reason behind the increment in fatigue life with aging could be the difference in stiffness modulus degradation (Perraton et al., 2015). The stiffness degradation comparison for specimen tested at STA and LTA condition at 400 kPa and 15 °C is shown in Figure 6.7.

The marked portion of the stiffness degradation curve in Figure 6.7 represents the second phase (phase II) of the stiffness degradation curve. It could be noticed from Figure 6.7 that the duration of phase II in the LTA specimen was higher than the STA specimen. Due to LTA specimens' higher stiffness, the strain experienced for the applied repeated constant stress (400 kPa at 15 °C) was relatively lower. The lower strain magnitude might have resulted in less damage and subsequently a higher number of cycles until failure in LTA specimen compared to STA specimen, as shown in Figure 6.7.

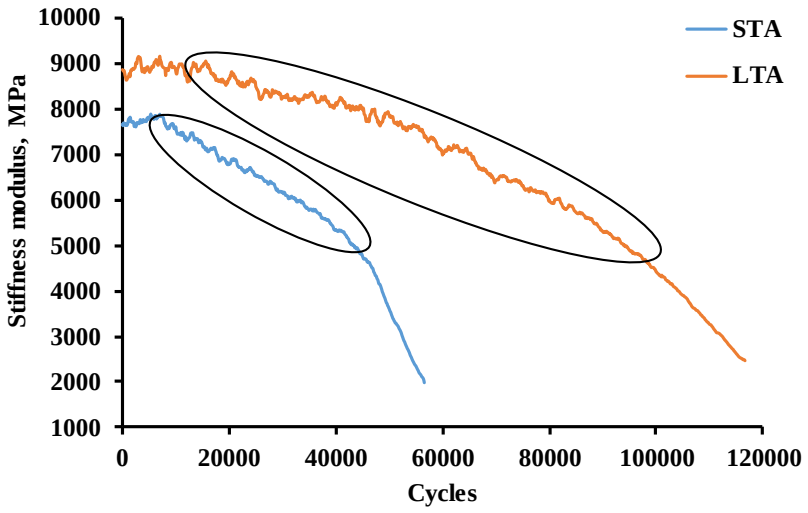

Figure 6.7 Stiffness modulus of STA and LTA specimen at 400 kPa and 15 °C

The statistical significance of the changes in the bituminous mixture's fatigue life was determined using a one-way ANOVA test at a 5 percent significance level. The effect of aging on the fatigue life of unconditioned bituminous mixtures is shown in Table 6.5. It could be noticed from Table 6.5 that aging had a significant effect on the fatigue life of bituminous mixtures at 15 °C. Whereas, at 25 °C, aging had a mixed impact on the fatigue life of bituminous mixture, with 50 percent of the mixtures showing no significant aging effect on fatigue life. Thus, the impact of aging on the fatigue behavior of a bituminous mixture might be more prominent at a lower temperature.

Table 6.5 One-way ANOVA test on fatigue life of unconditioned mixtures

Mixture	15 °C		25 °C	
	p-value	Significant	p-value	Significant
HMA-A	2.3E-04	Yes	3.7E-01	No
HMA-B	2.7E-05	Yes	0.0E+00	Yes
WMA-A	5.1E-03	Yes	1.0E+00	No

Mixture	15 °C		25 °C	
	p-value	Significant	p-value	Significant
WMA-B	4.5E-05	Yes	1.1E-06	Yes

Effect of moisture

It could be noticed from Figure 6.8 that the fatigue life of STA bituminous mixtures decreased with moisture conditioning, both at 15 °C and 25 °C. Bituminous mixtures subjected to 3FT cycles showed a higher reduction in fatigue as compared to the 1FT cycle. For example, bituminous mixtures subjected to 1FT cycles showed an average reduction of 38 percent and 32 percent at 15 °C and 25 °C. In comparison, bituminous mixtures subjected to 3FT cycles showed an average reduction of 71 percent, and 54 percent at 15 °C and 25 °C respectively. Similarly, in LTA condition, bituminous mixtures' fatigue life also reduced with moisture conditioning, as noticed in Figure 6.9. For example, bituminous mixtures subjected to 1FT cycles showed an average reduction of 63 percent and 15 percent at 15 °C and 25 °C. While bituminous mixtures subjected to 3FT cycles showed an average decrease of 80 percent and 47 percent at 15 °C and 25 °C. Interestingly, the reduction in fatigue life with moisture conditioning was relatively higher at 15 °C as compared to 25 °C. Researchers have noticed an increase in adhesive failure in a moisture-conditioned bituminous mixture with a reduction in temperature from 25 °C to 15 °C (Xie et al., 2012, Hamzah et al., 2017). Thus, adhesive failure in the bituminous mixture increases with a reduction in test temperature, which might be a reason for a higher decline in fatigue life of the bituminous mixture at 15 °C.

As noticed in the case of the unconditioned mixture in Figure 6.4, the fatigue life of moisture conditioned bituminous mixtures also reduced with the increase in test temperature from 15 °C to 25 °C (see Figure 6.8 and Figure 6.9). For example, the fatigue life of STA bituminous mixtures at 25 °C was approximately 63 percent less than the fatigue life of bituminous mixtures at 15 °C. It could be noted that in the case of unconditioned bituminous mixtures (Figure 6.4), specimens tested at 15 °C had higher fatigue life than specimens tested at 25 °C, irrespective of the type of mixture and aging condition. However, in few cases of the moisture-conditioned bituminous mixture, specimens tested at 15 °C had marginally lower fatigue life than specimens tested at 25 °C. For example, the fatigue life of STA HMA-A subjected to 3FT cycles was 10140 at 15 °C compared to 11384 at the same conditions at 25 °C. Moisture conditioning is a physical phenomenon with a different source of variability, and it might increase the overall variability of the experimental results (Fakhri & Ahmadi, 2017;

Manrique-Sanchez et al., 2020). This might be a probable reason for the higher fatigue life at 25 °C in moisture-conditioned specimens compared to 15 °C in few cases.

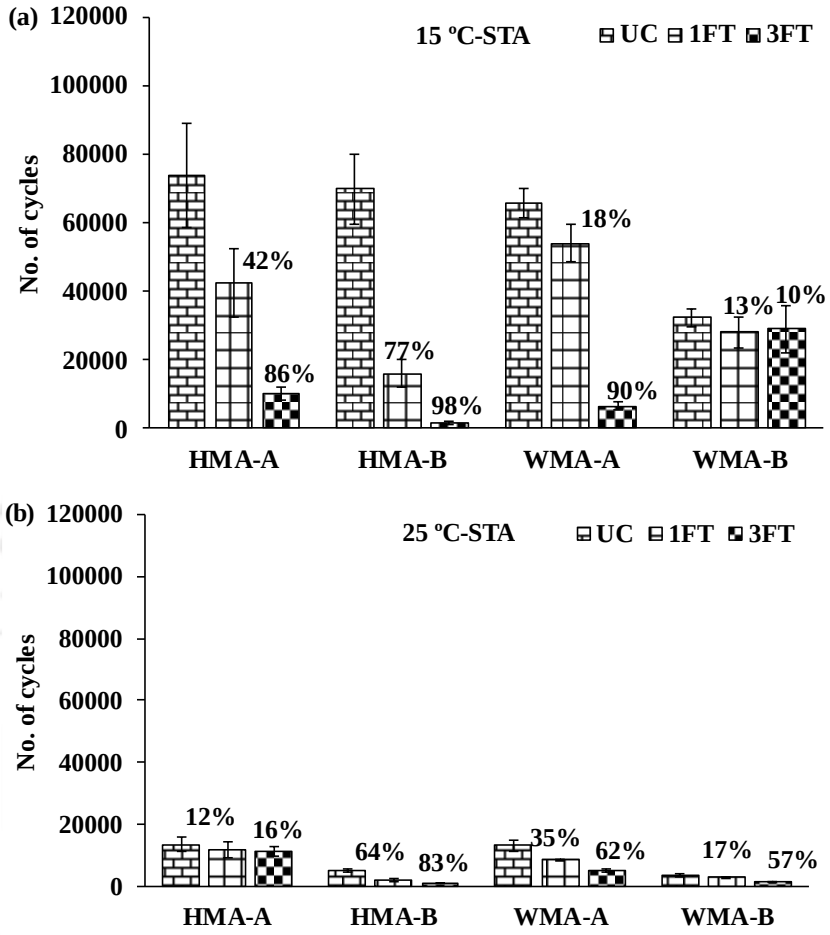

Figure 6.8 Fatigue life of MC STA bituminous mixture: (a) 15 °C; (b) 25 °C

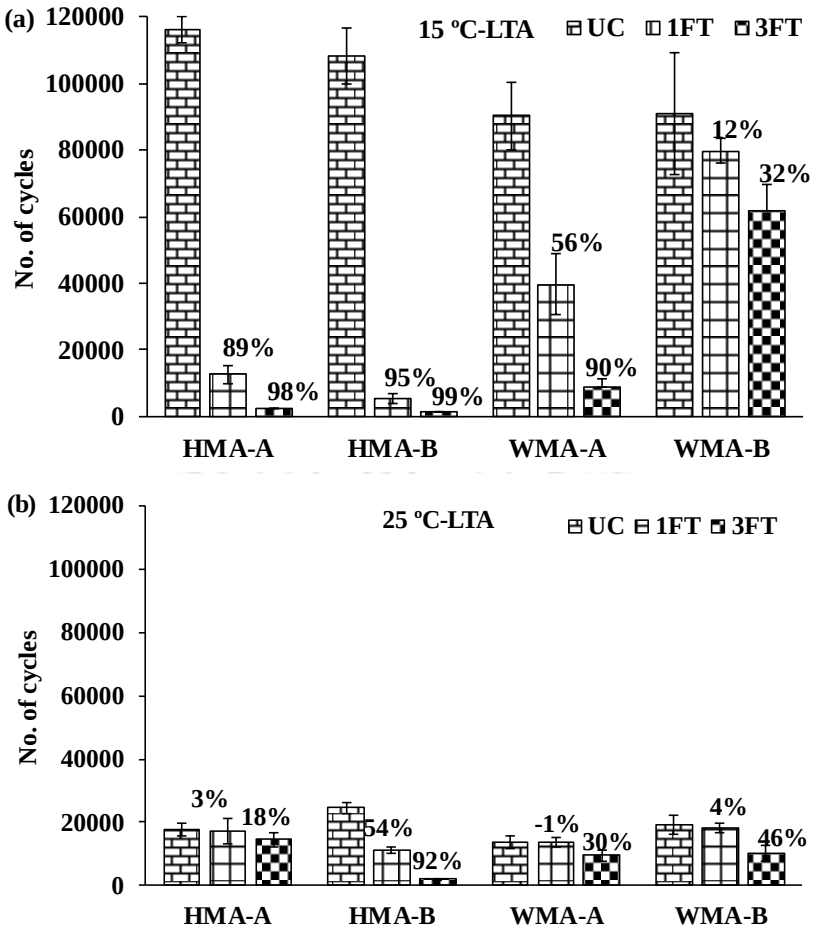

Figure 6.9 Fatigue life of MC LTA bituminous mixture: (a) 15 °C; (b) 25 °C

A one-way ANOVA (α=0.05) analysis was carried out to determine the significance of moisture on the fatigue life of STA and LTA bituminous mixtures. The effect of moisture on the STA bituminous mixture is shown in Table 6.6, and LTA bituminous mixture is shown in Table 6.7. It could be noticed from Table 6.6 and Table 6.7 that the effect of moisture on the fatigue life of the bituminous mixture was more significant at 15 °C as compared to 25 °C. Also, the effect of moisture on the fatigue life of the bituminous mixture was marginally higher in the case of LTA bituminous mixtures as compared to STA bituminous mixtures. Importantly, the inference from test results indicates that testing LTA bituminous mixture at 15 °C would be better to evaluate the effect of moisture on the fatigue life of the bituminous mixture.

Table 6.6 One-way ANOVA test on fatigue life of STA mixtures

Mixture	Condition	15 °C		25 °C	
		p-value	Significant	p-value	Significant
HMA-A	UC~1FT	3.6E-03	Yes	9.6E-01	No
	UC~3FT	3.7E-06	Yes	8.9E-01	No
	1FT~3FT	2.5E-03	Yes	1.0E+00	No
HMA-B	UC~1FT	6.7E-07	Yes	1.2E-02	Yes
	UC~3FT	2.5E-07	Yes	1.5E-03	Yes
	1FT~3FT	6.9E-02	No	7.8E-01	No
WMA-A	UC~1FT	2.7E-01	No	1.9E-02	Yes
	UC~3FT	8.4E-07	Yes	2.0E-04	Yes
	1FT~3FT	1.0E-05	Yes	1.0E-01	No
WMA-B	UC~1FT	9.9E-01	No	1.0E+00	No
	UC~3FT	1.0E+00	No	7.4E-01	No
	1FT~3FT	1.0E+00	No	9.2E-01	No

Table 6.7 One-way ANOVA test on fatigue life of LTA mixtures

Mixture	Condition	15 °C		25 °C	
		p-value	Significant	p-value	Significant
HMA-A	UC~1FT	2.4E-07	Yes	1.0E+00	No
	UC~3FT	9.8E-08	Yes	6.5E-01	No
	1FT~3FT	5.7E-01	No	7.9E-01	No
HMA-B	UC~1FT	0.0E+00	Yes	2.4E-07	Yes
	UC~3FT	0.0E+00	Yes	0.0E+00	Yes
	1FT~3FT	9.5E-01	No	4.3E-07	Yes
WMA-A	UC~1FT	5.0E-06	Yes	1.0E+00	No
	UC~3FT	9.9E-07	Yes	4.4E-02	Yes
	1FT~3FT	6.9E-04	Yes	3.6E-02	Yes
WMA-B	UC~1FT	6.5E-01	No	9.9E-01	No
	UC~3FT	1.8E-02	Yes	4.4E-04	Yes
	1FT~3FT	2.2E-01	No	1.0E-03	Yes

6.3.3 Association of cracking resistance parameter with fatigue life

The cracking resistance parameters discussed in the previous chapter (Chapter 4) were derived from the monotonic test. A repeated load test can simulate the fatigue behavior of a bituminous mixture observed in the field. Thus, the association fatigue life with ITS and FE was measured using the Pearson correlation coefficient (Montgomery & Runger, 2010). The impact of aging and moisture on the association between fatigue life and the parameters was the primary concern. Thus, different bituminous mixtures tested at 15 °C and 25 °C were

grouped at each aging and moisture conditioned state, as shown in Table 6.8. From Table 6.8, it could be noticed that both ITS and FE had a strong association with fatigue life in the unconditioned state, and the association reduced with moisture conditioning. Interestingly, FE had a better correlation with fatigue life than ITS at 3FT conditions for both STA and LTA states. Thus, FE might be better suited to assess the cracking resistance of mixtures subjected to moisture conditioning compared to ITS. Further, in mixtures that exhibit brittle-like behavior, FE might be a better parameter as it considers both peak load and post-peak behavior of the load-deformation curve.

Table 6.8 Pearson correlation coefficient of cracking parameter with fatigue life

Aging	Moisture	Pearson Correlation	
		N_f-ITS	N_f-FE
STA	UC	0.83	0.84
	1FT	0.36	0.47
	3FT	0.62	0.76
LTA	UC	0.90	0.79
	1FT	0.62	0.55
	3FT	0.29	0.65

6.3.4 Evaluating fatigue damage using stiffness degradation

In section 6.3.2, it was noticed that bituminous mixtures' fatigue life increased with aging and reduced with moisture conditioning. However, the total number of cycles to failure cannot explain the fatigue damage progression and accumulation in the bituminous mixture. In this regard, the decay in the stiffness modulus of the bituminous mixture with repeated loading cycles was used to determine the damage in the bituminous mixture. The stiffness degradation model used by Perraton et al. (2015) was used to calculate fatigue damage (D_N), as shown in Eq. (6.1) (Perraton et al., 2015). First, the raw fatigue data were fitted to an exponential model, as shown in Eq. (6.2). It was noticed that the fatigue damage in bituminous mixtures increases exponentially with load cycles, as shown in Figure 6.10. The fatigue damage of different bituminous mixtures at different conditions was compared using the fatigue damage curve shown in Figure 6.11 to Figure 6.14. The model parameters are shown in Table 6.9 and Table 6.10.

$$D_N = 1 - \frac{E_N}{E_0} \quad (6.1)$$

$$D_N = a \times exp^{(b \times N)} \quad (6.2)$$

where,

D_N= fatigue damage at Nth cycle,

E_0 = initial stiffness modulus (modulus value at 100th cycle), MPa,

E_N = stiffness modulus at Nth cycle, MPa, and

a and b = are model coefficients.

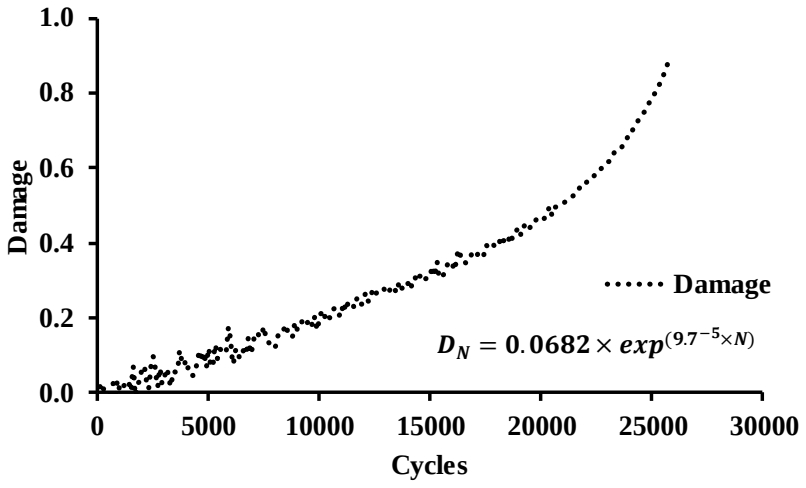

Figure 6.10 Illustration of fatigue damage propagation in the bituminous mixture

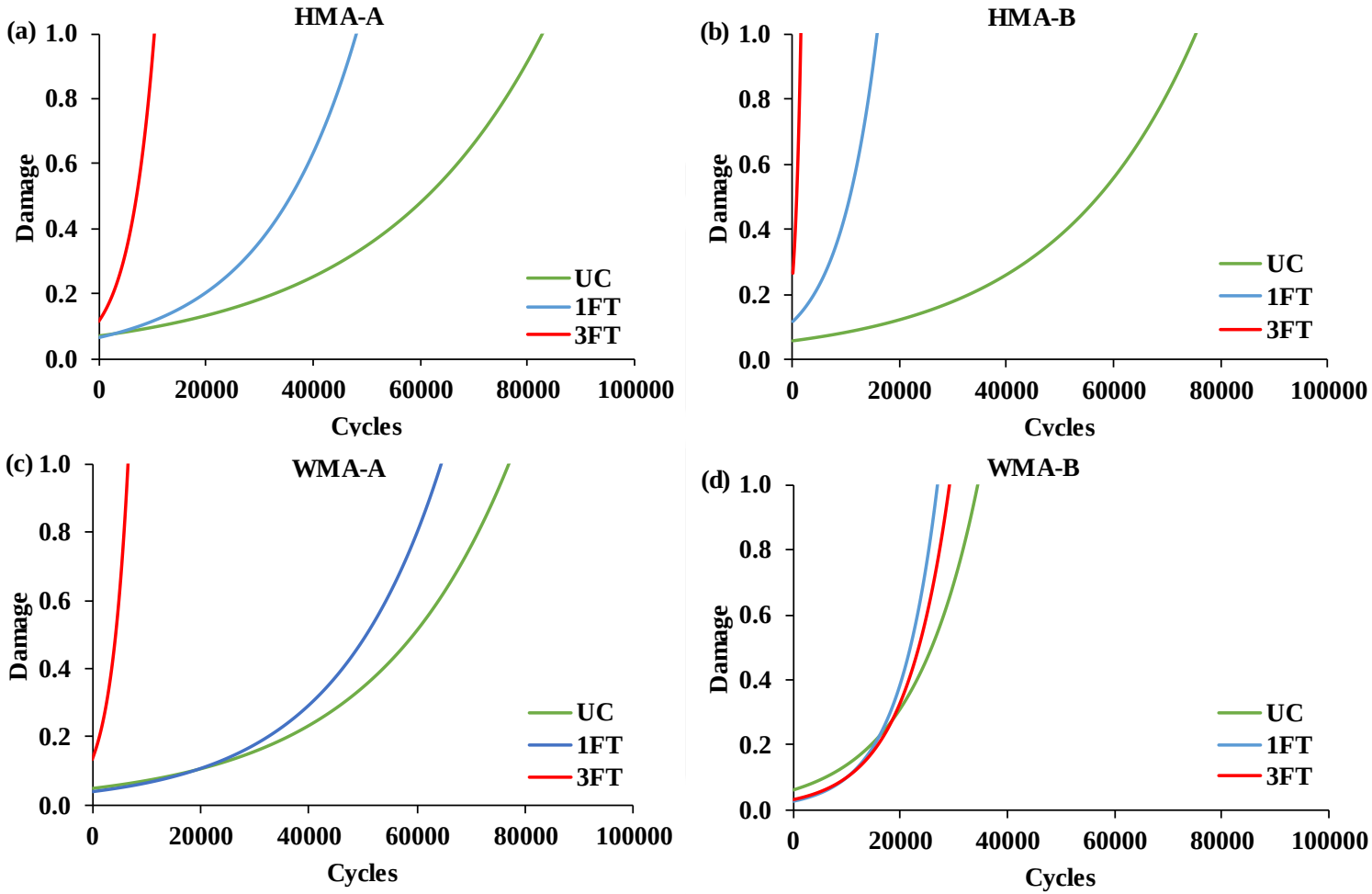

Figure 6.11 Fatigue damage curves for STA mixtures at 15 °C: (a) HMA-A; (b) HMA-B; (c) WMA-A; (d) WMA-B

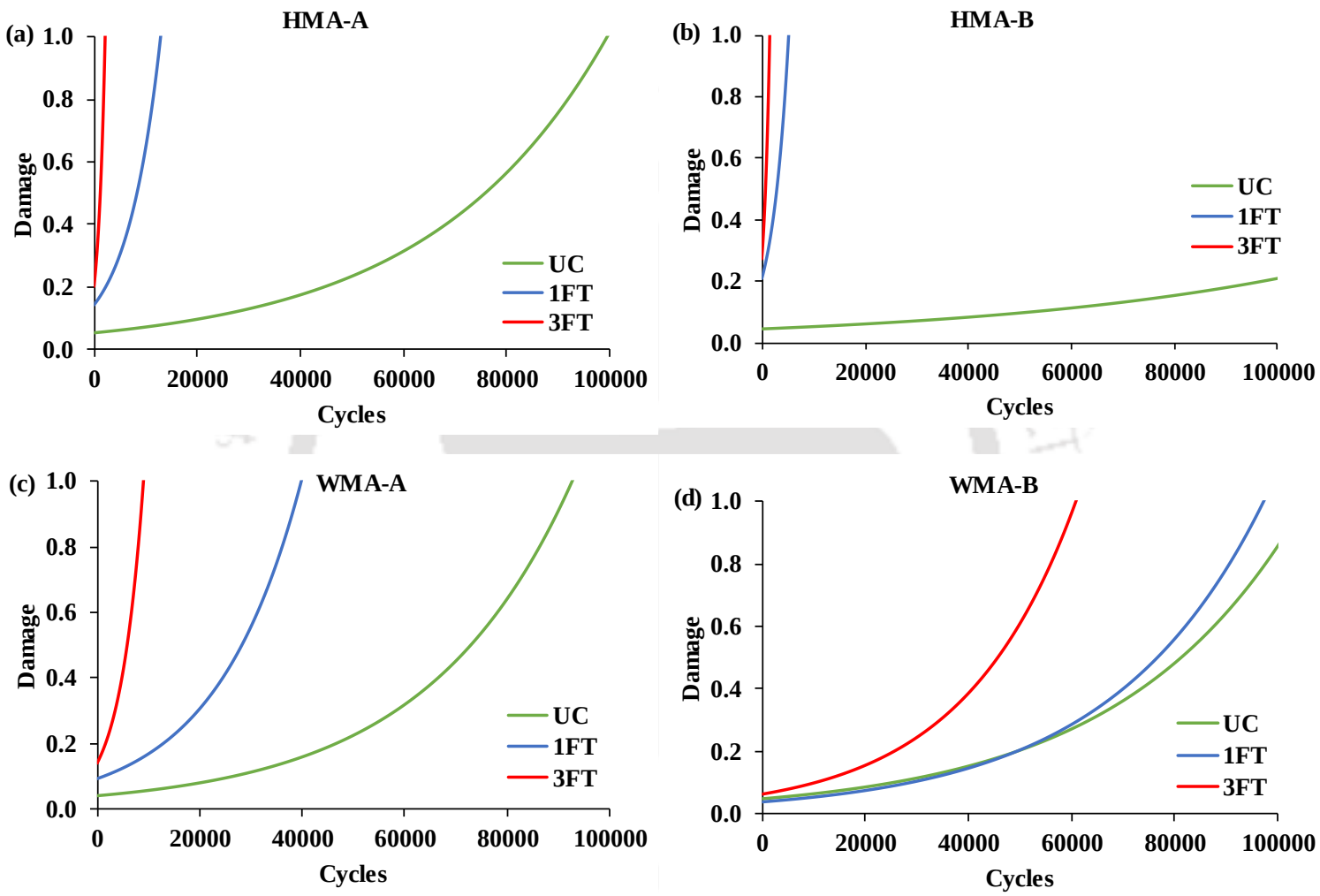

Figure 6.12 Fatigue damage curves for LTA mixtures at 15 °C: (a) HMA-A; (b) HMA-B; (c) WMA-A; (d) WMA-B

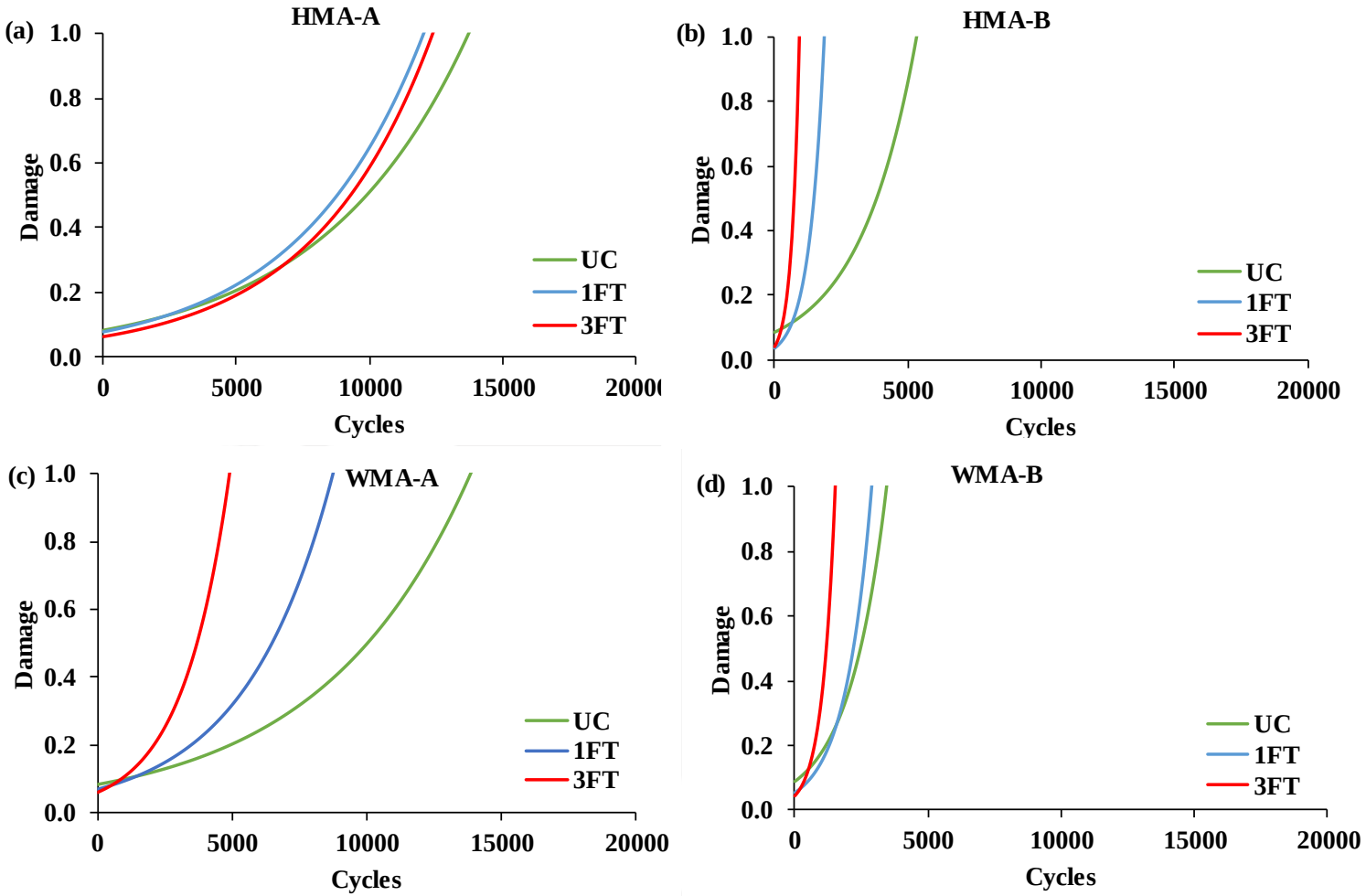

Figure 6.13 Fatigue damage curves for STA mixtures at 25 °C: (a) HMA-A; (b) HMA-B; (c) WMA-A; (d) WMA-B

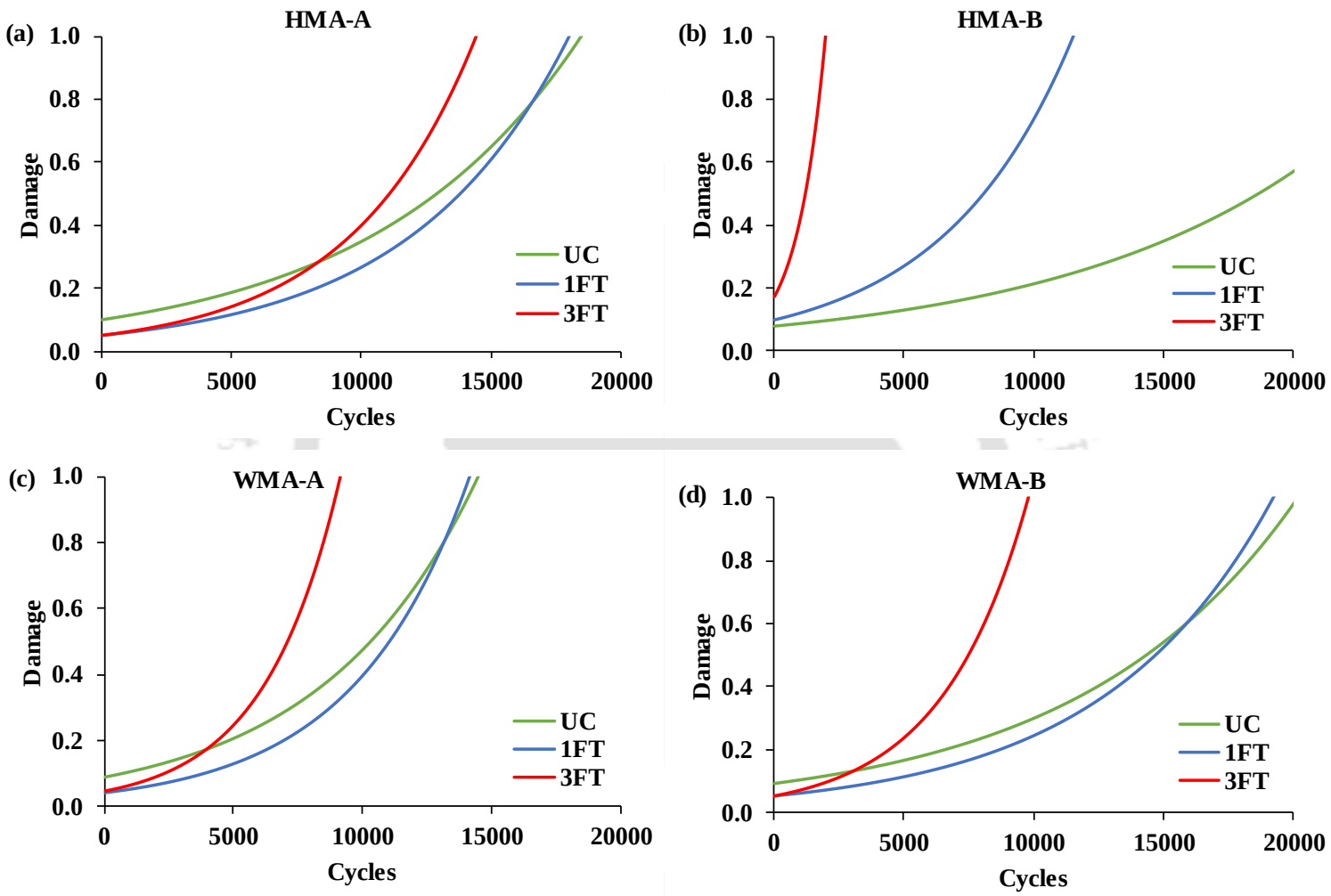

Figure 6.14 Fatigue damage curves for LTA mixtures at 25 °C: (a) HMA-A; (b) HMA-B; (c) WMA-A; (d) WMA-B

It could be noticed from Figure 6.11 to Figure 6.14 that as the loading cycles increases, the fatigue damage in the bituminous mixture also increases. As the loading cycles progress, the difference between the fatigue damage of unconditioned and moisture-conditioned bituminous mixtures also increases. Thus, the rate at which fatigue damage will progress in a bituminous mixture also depends on the dry and moisture-conditioned state of the bituminous mixture. In general, the bituminous mixture subjected to 1FT and 3FT cycles had lower fatigue life than unconditioned bituminous mixtures. From Figure 6.12 and Figure 6.14, it could be noticed that moisture conditioning had a relatively higher impact on the fatigue damage of LTA bituminous mixtures than STA bituminous mixtures. The effect of moisture on fatigue damage of the bituminous mixtures was more noticeable at 15 °C as compared to 25 °C. This is in line with Hamzah et al. (2017) findings, where the authors found that adhesive failure in bituminous mixture increased with the reduction in test temperature. Thus, moisture would have a higher impact on the fatigue damage of bituminous mixtures at lower temperatures.

According to Kringos et al. (2008), a mastic film exposed to moisture will initially have zero moisture content in the mastic film and the aggregate–mastic interface. Due to the difference in moisture concentration gradient inside the mastic, moisture will gradually infiltrate through the mastic film. The rate of moisture diffusion is controlled by diffusion coefficients of the mastic and the thickness of the mastic film. Moisture will eventually reach the aggregate–mastic interface and cause progressive debonding of the mastic from the aggregate. A numerical study conducted by Caro et al. (2010) to understand the effect of moisture diffusion on a bituminous mixture's mechanical response noticed that as the mastic diffusion coefficient increased, the maximum force resisted by the specimen also reduced (17 % to 60 %). In another study, Tong et al. (2013) noticed that the crack growth rate of FAM specimens conditioned at 100 % relative humidity (RH) was approximately 50 % higher than FAM specimens conditioned at 0 % RH. These research findings also support that a bituminous mixture might undergo more severe fatigue damage in the presence of moisture.

Table 6.9 Fatigue damage model at 15 °C

Mixture	Aging	Moisture	Model
HMA-A	STA	UC	$y = 0.069 \times exp^{(3.22E-05 \times N)}$
		1FT	$y = 0.066 \times exp^{(5.65E-05 \times N)}$
		3FT	$y = 0.113 \times exp^{(2.09E-04 \times N)}$
	LTA	UC	$y = 0.055 \times exp^{(2.92E-05 \times N)}$
		1FT	$y = 0.141 \times exp^{(1.51E-04 \times N)}$
		3FT	$y = 0.202 \times exp^{(7.37E-04 \times N)}$
HMA-B	STA	UC	$y = 0.057 \times exp^{(3.81E-05 \times N)}$
		1FT	$y = 0.117 \times exp^{(1.36E-04 \times N)}$
		3FT	$y = 0.264 \times exp^{(8.93E-04 \times N)}$
	LTA	UC	$y = 0.044 \times exp^{(1.55E-05 \times N)}$
		1FT	$y = 0.206 \times exp^{(3.03E-04 \times N)}$
		3FT	$y = 0.272 \times exp^{(8.45E-04 \times N)}$
WMA-A	STA	UC	$y = 0.048 \times exp^{(3.95E-05 \times N)}$
		1FT	$y = 0.039 \times exp^{(5.02E-05 \times N)}$
		3FT	$y = 0.134 \times exp^{(3.04E-04 \times N)}$
	LTA	UC	$y = 0.039 \times exp^{(3.51E-05 \times N)}$
		1FT	$y = 0.092 \times exp^{(5.98E-05 \times N)}$
		3FT	$y = 0.138 \times exp^{(2.18E-04 \times N)}$
WMA-B	STA	UC	$y = 0.062 \times exp^{(8.05E-05 \times N)}$
		1FT	$y = 0.025 \times exp^{(1.37E-04 \times N)}$
		3FT	$y = 0.029 \times exp^{(1.21E-04 \times N)}$
	LTA	UC	$y = 0.049 \times exp^{(2.87E-05 \times N)}$
		1FT	$y = 0.038 \times exp^{(3.36E-05 \times N)}$
		3FT	$y = 0.061 \times exp^{(4.57E-05 \times N)}$

Table 6.10 Fatigue damage model at 25 ºC

Mixture	Aging	Moisture	Model
HMA-A	STA	UC	$y = 0.084 \times exp^{(1.81E-04 \times N)}$
		1FT	$y = 0.076 \times exp^{(2.14E-04 \times N)}$
		3FT	$y = 0.062 \times exp^{(2.25E-04 \times N)}$
	LTA	UC	$y = 0.100 \times exp^{(1.24E-04 \times N)}$
		1FT	$y = 0.051 \times exp^{(1.65E-04 \times N)}$
		3FT	$y = 0.050 \times exp^{(2.08E-04 \times N)}$
HMA-B	STA	UC	$y = 0.085 \times exp^{(4.63E-04 \times N)}$
		1FT	$y = 0.036 \times exp^{(1.79E-03 \times N)}$
		3FT	$y = 0.041 \times exp^{(3.46E-03 \times N)}$
	LTA	UC	$y = 0.081 \times exp^{(9.77E-05 \times N)}$
		1FT	$y = 0.100 \times exp^{(2.00E-04 \times N)}$
		3FT	$y = 0.173 \times exp^{(8.93E-04 \times N)}$
WMA-A	STA	UC	$y = 0.080 \times exp^{(1.82E-04 \times N)}$

Mixture	Aging	Moisture	Model
WMA-B		1FT	$y = 0.069 \times exp^{(3.06E-04 \times N)}$
		3FT	$y = 0.060 \times exp^{(5.72E-04 \times N)}$
	LTA	UC	$y = 0.090 \times exp^{(1.66E-04 \times N)}$
		1FT	$y = 0.043 \times exp^{(2.23E-04 \times N)}$
		3FT	$y = 0.045 \times exp^{(3.39E-04 \times N)}$
	STA	UC	$y = 0.087 \times exp^{(7.09E-04 \times N)}$
		1FT	$y = 0.055 \times exp^{(1.01E-03 \times N)}$
		3FT	$y = 0.044 \times exp^{(2.06E-03 \times N)}$
	LTA	UC	$y = 0.091 \times exp^{(1.19E-04 \times N)}$
		1FT	$y = 0.053 \times exp^{(1.53E-04 \times N)}$
		3FT	$y = 0.053 \times exp^{(3.00E-04 \times N)}$

The fatigue damage curves shown in Figure 6.11 to Figure 6.14 presents the average value of fatigue damage in bituminous mixtures at each condition. However, high variability is associated with the fatigue damage process in a bituminous mixture. The variability further increases when bituminous mixtures are exposed to different environmental conditions. A stochastic approach is better suited to capture the randomness in fatigue damage data. Thus, a probabilistic approach was used by applying probability distribution theory to model the fatigue damage in the bituminous mixture, as discussed in the next section.

6.3.5 Probabilistic fatigue damage analysis

The effect of aging and moisture on the fatigue damage of bituminous mixtures determined in section 6.3.4 was evaluated using a probabilistic approach (Caro et al., 2008b). From section 6.3.4, it became clear that the fatigue damage (D_N) in moisture conditioned specimen was higher than unconditioned specimen at any given loading cycle. The probability (p) that the value of D_N of moisture conditioned specimen is higher than that of the unconditioned specimen at any cycles (N) is shown in Eq. (6.3) (Caro et al., 2008b). This probability value is independent of the previous loading cycle (N-1).

$$p(D_{MC} > D_{UC}|N) \tag{6.3}$$

where,

D_{MC} and D_{UC} = fatigue damage of MC and UC specimen at Nth cycle.

Different probability distribution functions were fitted to D_{MC} and D_{UC} data to determine a suitable probability distribution. The goodness of fit of normal, lognormal, and

Weibull distribution was determined using the Anderson–Darling (AD) and Kolmogorov–Smirnov (KS) test statistic value. From Table 6.11, it could be noticed that the average AD and KS statistics values were lowest in the case of lognormal distribution when compared to normal and Weibull distribution. Thus, a lognormal distribution is the best fit probability distribution for the fatigue damage data of this study (also noticed by Caro et al., 2008b).

Table 6.11 Goodness of fit statistics for fatigue damage

Sample no.	Normal		Lognormal		Weibull	
	KS	AD	KS	AD	KS	AD
1	0.19	6.27	0.11	0.87	0.14	2.75
2	0.27	8.29	0.09	0.66	0.13	1.50
3	0.21	5.29	0.07	0.34	0.07	0.45
4	0.25	3.02	0.09	0.48	0.15	0.51
5	0.27	4.54	0.08	0.41	0.13	0.94
6	0.24	5.48	0.09	0.55	0.12	1.23

Caro et al. (2008b) used Eq. (6.4) to determine the probability (p) that the D_{MC} is higher than D_{UC}, when both follow a lognormal distribution, as shown below.

$$p(D_{MC} > D_{UC}|N) = \phi\left(\frac{ln\left[\left(\frac{\mu_{D_{MC}}}{\mu_{D_{UC}}}\right)\left(\frac{1+V_{D_{UC}}^2}{1+V_{D_{MC}}^2}\right)^{1/2}\right]_N}{\left[ln\left(\left(1+V_{D_{MC}}^2\right)\left(1+V_{D_{UC}}^2\right)\right)\right]_N^{1/2}}\right) \quad (6.4)$$

where,

$\mu_{D_{MC}}$ and $\mu_{D_{MC}}$= mean value of D_{MC} and D_{UC}, and

$V_{D_{MC}}^2$ and $V_{D_{UC}}^2$= CoV of MC and UC specimen.

The distribution parameters (mean and CoV) were determined from the three replicate specimens at each cycle (N) for each condition. The $p(D_{MC} > D_{UC}|N)$ for the different conditions is shown in Figure 6.15 and Figure 6.16. For example, in Figure 6.15 (a), the STA-HMA-A-1FT/UC curve represents the probability of damage in the short-term aged HMA-A specimen subjected to 1FT being greater than short-term aged HMA-A unconditioned

specimen. The results of the first 5000 cycles were presented in Figure 6.15 and Figure 6.16, as the trend of the first 5000 cycles was sufficient for analyzing the effect of aging and moisture on the fatigue damage of bituminous mixtures. It could be noticed from Figure 6.15 and Figure 6.16 that LTA specimens had a higher probability of fatigue damage compared to STA specimens at 15 °C. While at 25 °C, STA specimens had a higher probability of fatigue damage compared to LTA specimens.

Aguiar-Moya et al. (2015) noticed that the bituminous binder's polarity with short-term aging improved the adhesive bond of the bituminous binder with aggregates. However, at LTA condition, the increase in the hardness of bituminous binder with aging counter balance the change in polarity and reduced the adhesive bond strength. Thus, the change in constituents of bituminous binder (saturate, aromatic, resin, and asphaltene fractions) will control the stiffness of bituminous mixtures, which in turn will govern the fatigue damage of bituminous mixtures. Xie et al. (2012) noticed a significant increase in adhesive failure with a reduction in test temperature from 25 °C to 15 °C. These researcher findings corroborate the higher damage seen in the case of LTA specimens at 15 °C since long-term aging increased the stiffness of bituminous mixtures, which was further supplemented by a lower test temperature of 15 °C. On the other hand, at a temperature of 25 °C, the stiffness gain with LTA might not negatively impact fatigue damage.

It could be noticed from Figure 6.15 and Figure 6.16 that the $p(D_{MC} > D_{UC}|N)$ has a non-zero value indicating that specimens subjected to moisture conditioning underwent greater fatigue damage than UC specimens. In most cases, the $p(D_{MC} > D_{UC}|N)$ of specimens subjected to 3FT cycles is higher than specimens subjected to 1FT cycles. Thus, the fatigue damage increases with the increase in moisture conditioning cycles. In the case of STA-HMA-A at 25 °C, it could be noticed from Figure 6.8 (b) that specimens subjected to UC, 1FT, and 3FT had comparable fatigue life. This might be a reason for variation in the probability of moisture damage in the case of STA-HMA-A at 25 °C.

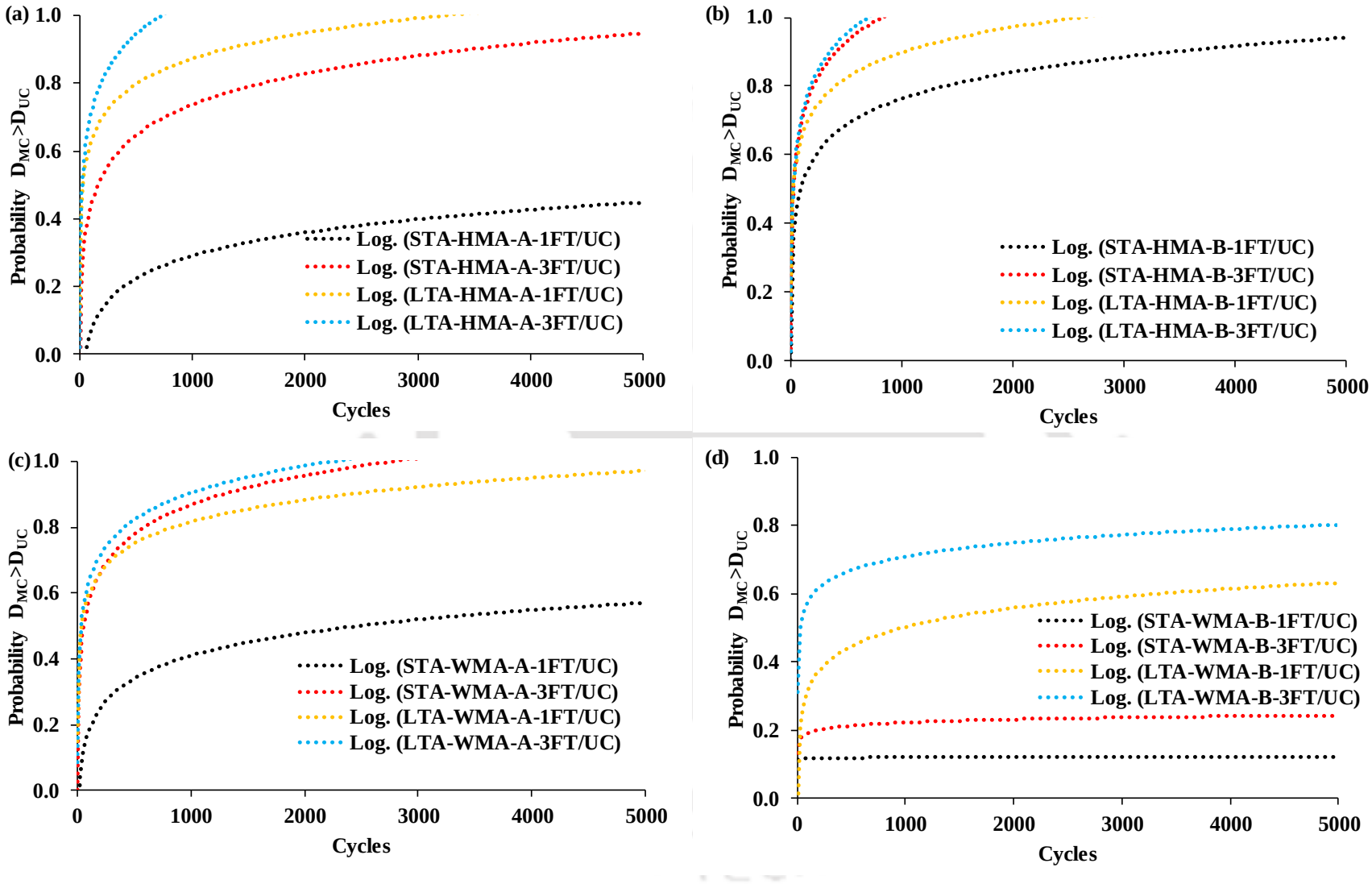

Figure 6.15 Probability of fatigue damage at 15 °C: (a) HMA-A; (b) HMA-B; (c) WMA-A; (d) WMA-B

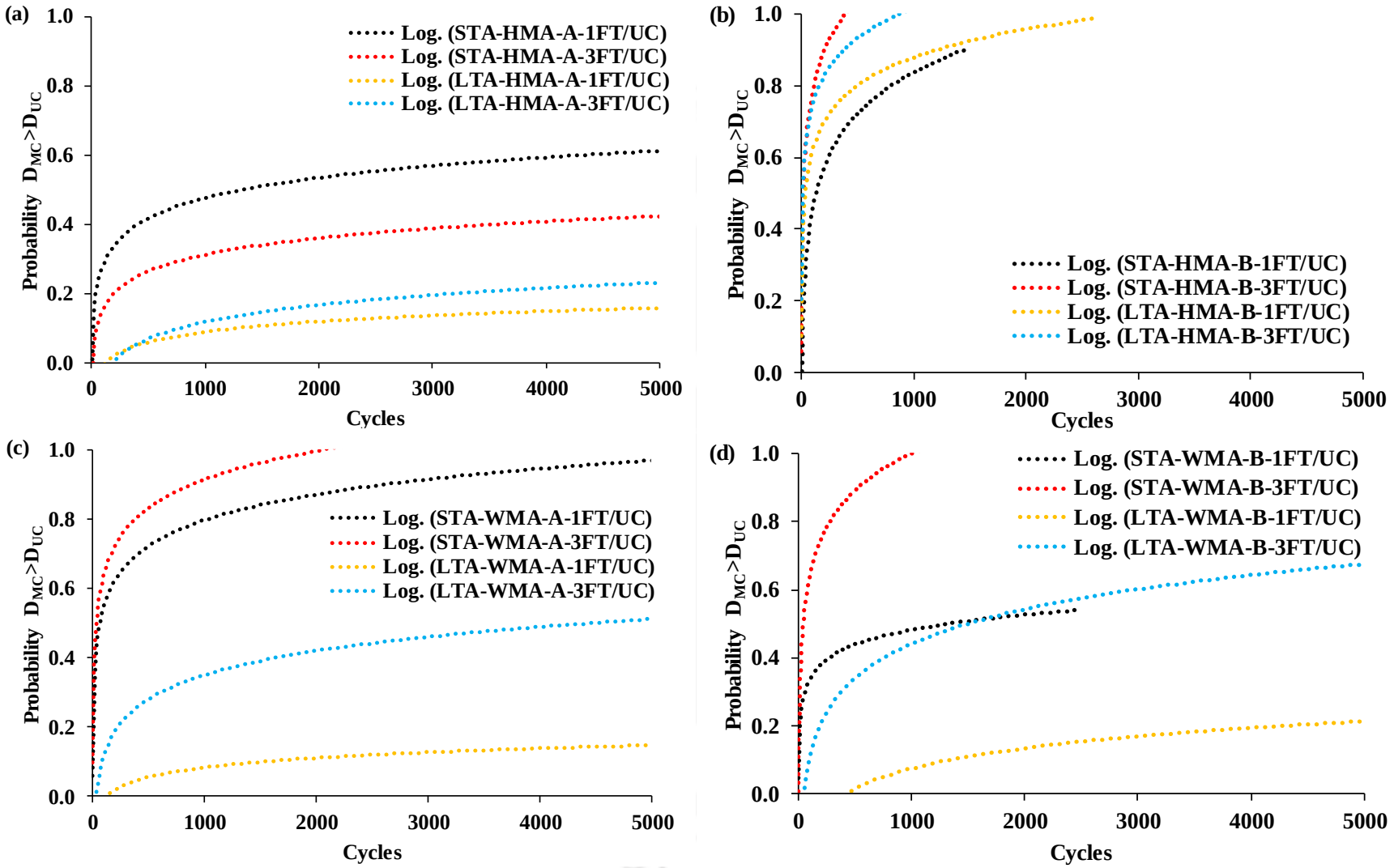

Figure 6.16 Probability of fatigue damage at 25 °C: (a) HMA-A; (b) HMA-B; (c) WMA-A; (d) WMA-B

6.3.6 Fatigue life prediction model

In general, phenomenological or regression and mechanistic approaches are used to develop fatigue life prediction models. Regression models are specific to the material property, type of test, and loading conditions used for model development, whereas mechanistic models apply to a wide range of conditions. Irrespective of the modeling approach used, fatigue damage in a bituminous mixture is stochastic, with considerable variability and randomness caused by material properties and imposed environmental conditions. A probabilistic modeling approach could account for the variability and scatter in the fatigue data and be better suited for modeling fatigue damage.

6.3.6.1 The ratio of stiffness change approach

In this study, the concept of RDEC (discussed in section 2.6.4) was carried forward into a stiffness-based formulation where the relative change in stiffness concerning initial stiffness represents the damage in the bituminous mixture, as shown in Eq. (6.5). The interval between cycles "b-a" is taken as 100 cycles. From previous research studies, it was noticed that the *PV* of bituminous mixture is independent of test conditions and material properties (Shen et al., 2006). In addition to experimental details mentioned in Table 6.1, the HMA-A mixture was subjected to additional aging and test conditions to expand the range of test conditions for model formulation. The Loose HMA-A mixture was first conditioned at 60 °C for 16 h as per AASHTO T 283 protocol and divided into three sets. The first set was aged at the compaction temperature for 90 ± 10 min before compaction. The second set was aged at 135 ± 5 °C for 4 h ± 5 min before compaction. The third set was aged at 135 ± 5 °C for 4 h ± 5 min, then compacted and placed in an oven at 85 ± 3 °C for 120 ± 0.5 h. Each specimen was tested in an unconditioned and moisture conditioned (1FT) state at 15 °C and 20 °C. Three stress levels, i.e., 450 kPa, 550 kPa, and 650 kPa (only for specimens tested at 15 °C) were applied during the ITFT.

The *PV* and the corresponding fatigue life of different mixtures and different conditions were analyzed together. From Figure 6.17, it could be noticed that bituminous mixtures with higher fatigue life had lower *PV* and vice-versa. Also, the fatigue life and inverse of *PV* followed a power-law relation, as shown in Figure 6.17. A line of equality plot of measured versus predicted fatigue life is shown in Figure 6.18. Considering the wide range of test conditions used for model formulation, the R^2 value of 0.56 could be considered fair.

$$RSC_a = \frac{S_a - S_b}{(b-a) \times S_a} \quad (6.5)$$

where,

RSC_a= ratio of stiffness changes for cycle a,

S_a and S_b= stiffness for cycle a and b, MPa.

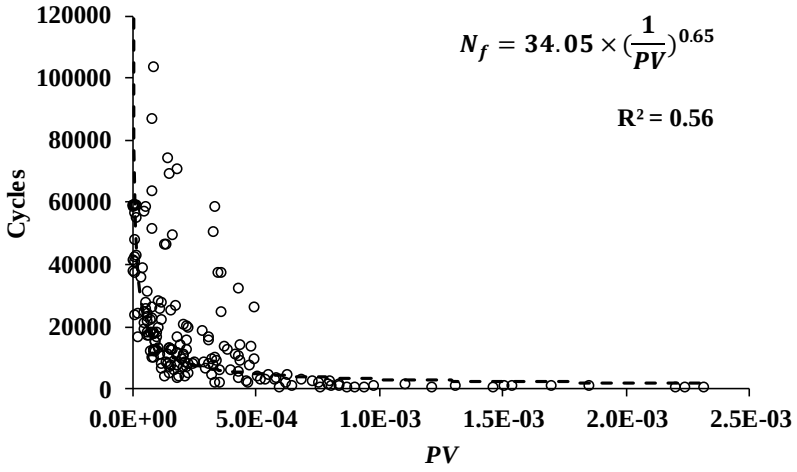

Figure 6.17 PV-N_f relation of bituminous mixtures

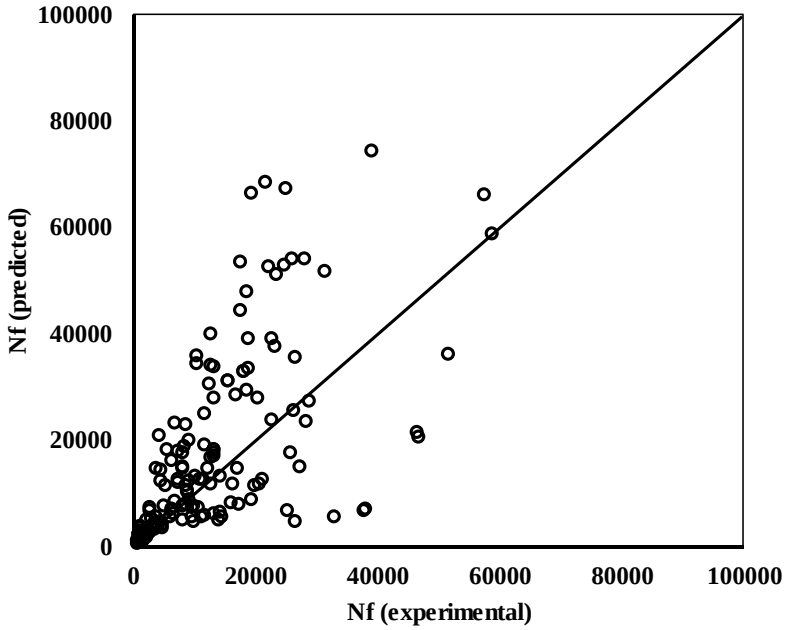

Figure 6.18 Line of equality between experimental and predicted fatigue life

6.3.6.2 Damage based approach

Regression-based fatigue life prediction models are widely used due to their simplicity and require less computational effort than the fracture mechanics approach or dissipated energy approach, or continuum damage mechanics approach. The regression models' limitation is that the models are specific to the test conditions and material properties used for development. Researchers introduced fracture energy in regression models as an appropriate material property to improve the accuracy of the models (Li et al., 2012; Bahadori et al., 2015). Fracture energy is a fundamental material property that is related to the cracking resistance of bituminous mixtures. Bahadori et al. (2015) proposed a regression model using fracture energy shown in Eq. (6.6). In this study, a concept of damage is introduced into the regression equation proposed by Bahadori et al. (2015). The model formulation is shown in Eq. (6.7). The damage ratio (DR) is the ratio of moisture conditioned fracture energy to unconditioned fracture energy, which signifies the reduction in cracking resistance of bituminous mixtures with moisture conditioning, as shown in Eq. (6.8).

$$N_f = k_1 \times \left(\frac{1}{\epsilon}\right)^{k_2} \times (FE)^{k_3} \tag{6.6}$$

$$N_f = k_1 \times \left(\frac{1}{\varepsilon}\right)^{k_2} \times (DR \times FE_{UC})^{k_3} \tag{6.7}$$

$$DR = \frac{FE_{MC}}{FE_{UC}} \tag{6.8}$$

where,

N_f= fatigue life, cycles,

ε = strain in specimen, με,

DR= damage ratio,

FE, FE_{UC} and FE_{MC}= fracture energy, fracture energy of UC, and MC specimens, MPa

k_1, k_2, and k_3= regression coefficients

The advantage of introducing the damage parameter into Eq. (6.6) is that once the model parameters were determined for a given set of conditions, the fatigue life of the bituminous mixture could be predicted for different levels of damage (either caused by moisture or by aging) by using the unconditioned fracture energy value of the mixture. Alternately, different levels of damage could be determined by determining the ratio of fracture energy ratio of

moisture conditioned to the unconditioned specimen using a monotonic test. Bituminous mixtures were divided into four groups, STA bituminous mixtures at 15 °C, LTA bituminous mixtures at 15 °C, STA bituminous mixtures at 25 °C, and LTA bituminous mixtures at 25 °C. Each group had approximately 36 data points. Model parameters were determined using the nonlinear regression function in the MATLAB program and are shown in Table 6.12. From Table 6.12, it could be noticed that the model had a good coefficient of determination, and the model is statistically significant.

Table 6.12 Regression model parameters

Condition	Coefficient	Value	Adj. R^2	Model p-value
15 °C-STA	k_1	3.00E+10	0.81	6.00E-13
	k_2	2.95E+00		
	k_3	1.04E-01		
15 °C-LTA	k_1	9.47E+08	0.88	6.15E-14
	k_2	3.09E+00		
	k_3	5.73E-01		
25 °C -STA	k_1	3.25E+06	0.89	6.73E-11
	k_2	1.65E+00		
	k_3	2.62E-01		
25 °C -LTA	k_1	5.18E+03	0.62	4.95E-46
	k_2	7.70E-01		
	k_3	5.71E-01		

6.3.7 Application of the damage-based fatigue life prediction model

There is always uncertainty associated with bituminous mixtures' behavior due to the material's inherent variation and construction variation. Aging and moisture further add to the variability. The proposed model is shown in Eq. (6.7) could be used to determine the fatigue of bituminous mixtures at different levels of damage in a deterministic manner. The variability induced by other factors will be associated with the damage ratio, strain, and fracture energy parameter. For this reason, a probabilistic-based prediction model is discussed in this section. From Figure 6.8 and Figure 6.9, it could be noticed that the HMA-B mixture had low resistance to moisture damage, while the WMA-B mixture had relatively better resistance to moisture at different levels of aging and test temperature. Thus, these two mixtures were selected for further analysis at different conditions.

The methodology adopted for prediction model formulation is shown in Figure 6.19. First, the best fit distribution for DR, ε, and FE_{UC} values was determined using AD and KS statistic. Normal and Lognormal distribution was selected. From Table 6.13, it could be noticed

that a Lognormal distribution was the best-fit distribution for each parameter. The distribution parameters for HMA-B and WMA-B at 15 °C for STA and LTA (termed as 15C-STA and 15C-LTA) and at 25 °C for STA and LTA (termed as 25C-STA and 25C-LTA) were determined. The distribution parameters were then used to create random values of DR, strain, and FE_{UC} to use in Eq. (6.7). A Monte Carlo simulation with one million iterations was carried out to predict the range of probable values of the dependent variable, i.e., the fatigue life (N_f). Cumulative probability curves were fitted to the output values (N_f) to see the distribution of predicted fatigue life, as shown in Figure 6.20.

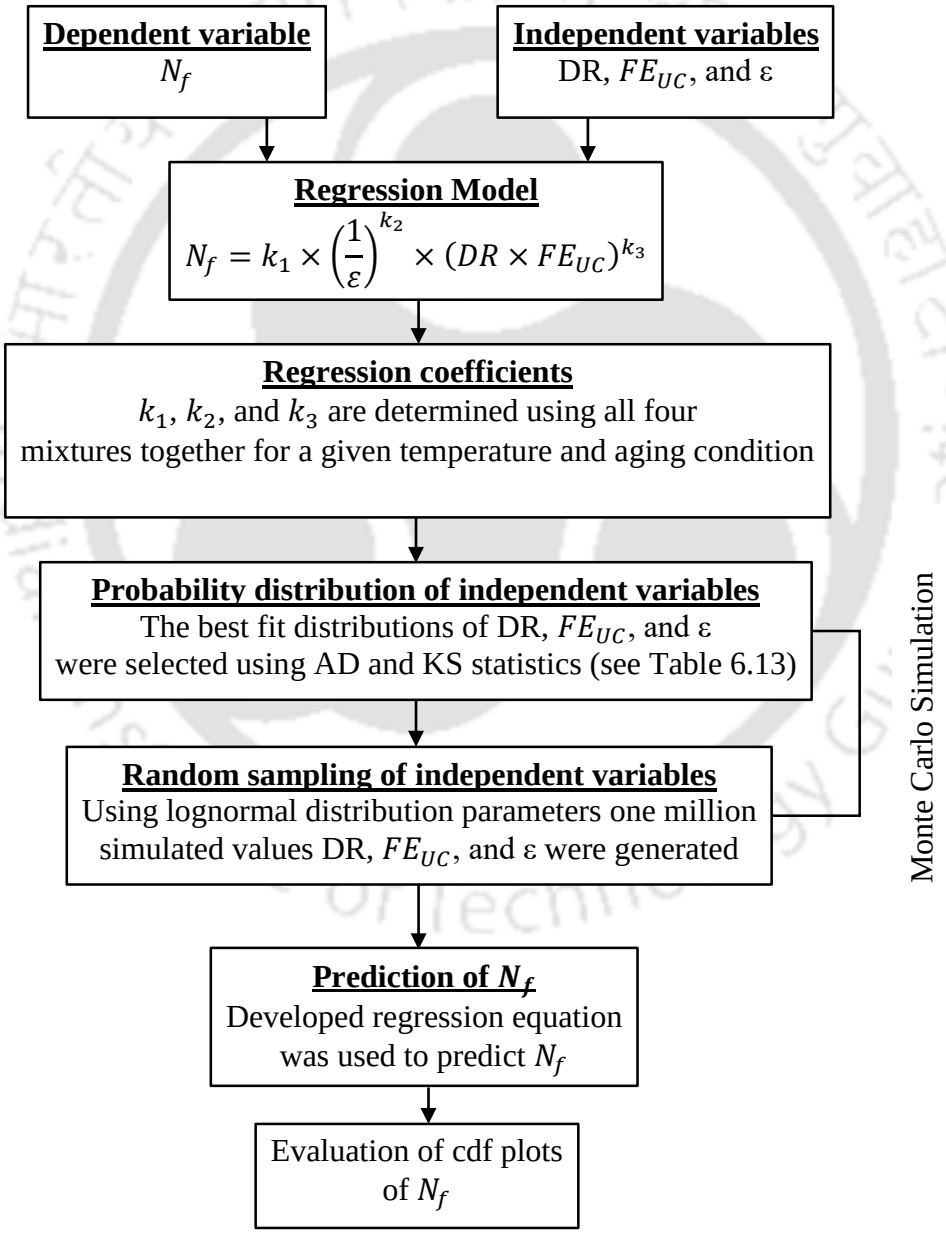

Figure 6.19 Methodology adopted for prediction model formulation

Table 6.13 Goodness of fit statistics of DR, ε, and FE_{UC}

Conditions	DR				ε				FE_{UC}			
	Normal		Log-Normal		Normal		Log-Normal		Normal		Log-Normal	
	KS	AD	KS	AD	KS	AD	KS	AD	KS	AD	KS	AD
15-STA	0.29	1.95	0.23	1.22	0.14	0.33	0.12	0.26	0.21	0.68	0.20	0.64
15-LTA	0.15	0.60	0.13	0.54	0.16	0.36	0.15	0.33	0.25	0.62	0.23	0.54
25-STA	0.19	0.65	0.18	0.82	0.13	0.18	0.13	0.18	0.13	0.12	0.11	0.11
25-LTA	0.13	0.46	0.16	0.67	0.18	0.41	0.16	0.40	0.12	0.23	0.11	0.18
Average	0.19	0.92	0.18	0.81	0.15	0.32	0.14	0.29	0.18	0.41	0.16	0.37

It could be noticed from Figure 6.20 that the variability in the fatigue life of bituminous mixtures at 15 °C was considerable as compared to 25 °C. The scatter might be due to relative variation in bituminous mixtures' high stiffness at 15 °C as compared to 25 °C. In a stress-controlled fatigue test, the bituminous mixture's fatigue life increases with the increase in stiffness (or aging). From Figure 6.20 (a) and (b), it could be noticed that at 15 °C, the STA HMA-B mixture had a higher fatigue life than the LTA HMA-B mixture for cumulative probability value lower than 0.70. The cumulative probability curves intersect at 0.70, and above a cumulative probability of 0.70, the LTA HMA-B mixture had higher fatigue life than the STA HMA-B mixture. Such behavior was not noticed in the case of the WMA-B mixture (see Figure 6.20 (c) and (d)). Thus, a probability exists that in the case of a moisture susceptible bituminous mixture, fatigue life might not increase with an increase in the aging level.

Limitations of the proposed damage-based fatigue life prediction model are listed below.

1. One of the major drawbacks of the methodology proposed in section 6.3.7 of this study is that the fatigue life prediction model is a non-linear strain and fracture energy function. Aging and moisture conditioning might increase the variability in the fracture energy of the bituminous mixture. Thus, the fatigue life prediction model might exhibit heteroscedasticity with an increase in aging and moisture conditioning levels, resulting in inconsistency in the accuracy of predicted fatigue life.
2. The proposed fatigue life prediction model is a regression-based fatigue life prediction model. The accurate prediction of the fatigue life might be confined to the specific type of materials and test combinations used in this study. The model's accuracy could be enhanced by incorporating results with different aggregate gradations, test temperatures, and types of bituminous mixtures.

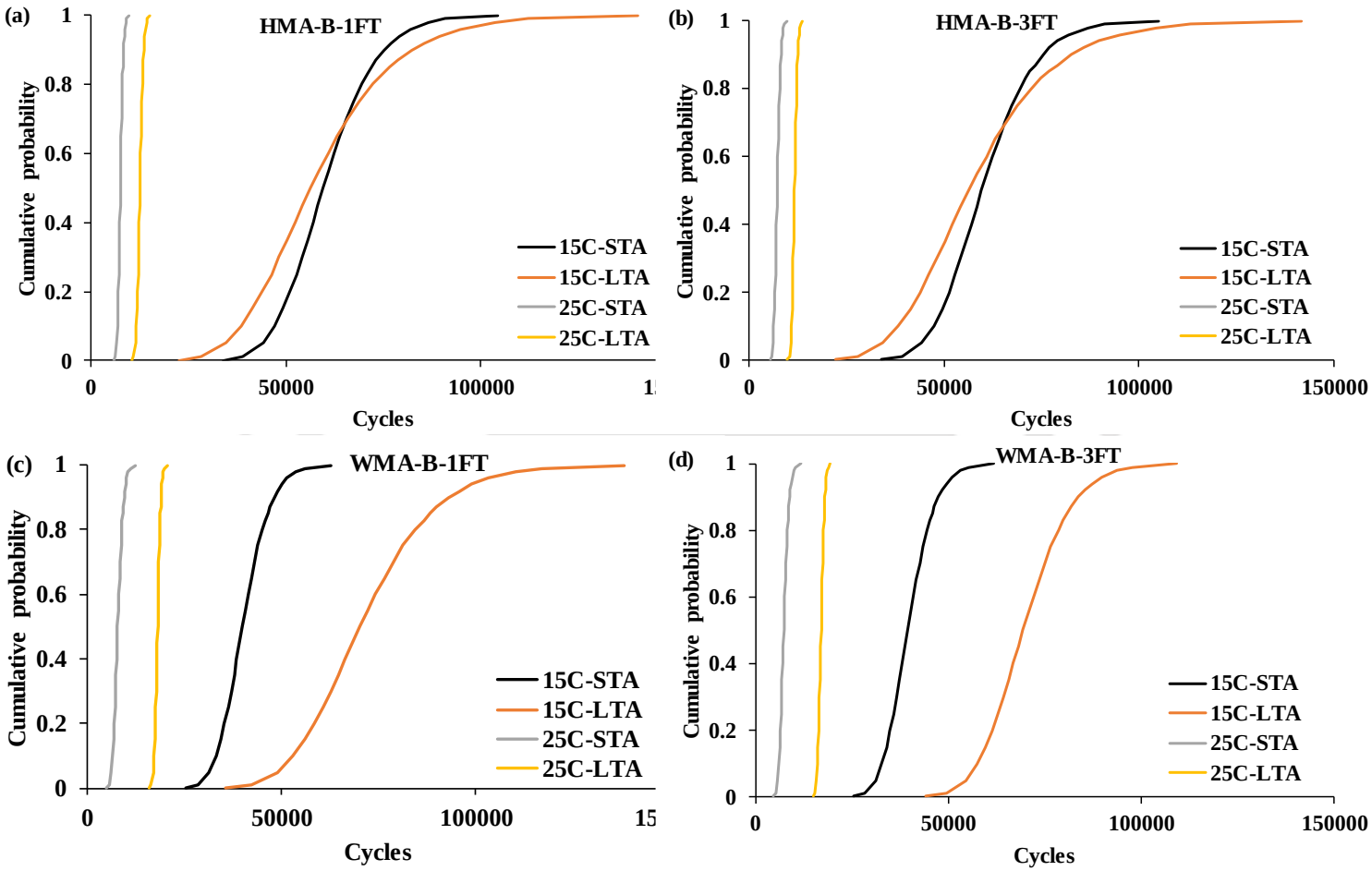

Figure 6.20 Predicted fatigue life of HMA-B and WMA-B mixture at different condition

6.3.8 Effect of warm mix additive on the fatigue life

It could be noticed from Figure 6.4 that in the case of unconditioned bituminous mixtures, HMA and WMA mixtures had comparable fatigue life. However, in the presence of moisture, it could be noticed from Figure 6.8 and Figure 6.9 that the reduction in fatigue life of HMA mixtures from UC to 1FT and from UC to 3FT was relatively higher compared to the WMA mixture. The same is depicted in Figure 6.21 and Figure 6.22, where the ratio of fatigue life of moisture conditioned (1FT and 3FT) to the unconditioned specimen in the case of WMA mixture was higher than the HMA mixture, particularly in the case of bituminous mixture with source B aggregate. The higher resistance to moisture effect might be due to adhesion promoters in warm mix additive, which increased the resistance to fatigue cracking in the presence of moisture. Further, the statistical significance testing using t-test and Cohen's d-value showed that the fatigue life of short-term aged HMA and WMA mixtures were found to be significantly different under moisture conditioned state at 15 °C. However, at 25 °C, the fatigue life was not statistically different for most cases. A similar trend was noticed in long-term aged conditions. Also, the Cohen's d-value for HMA-B and WMA-B combination compared at different conditions was relatively higher than the HMA-A and WMA-A combination, for most of the cases. This suggests that the effect of warm mix additive on the fatigue life of mixture with aggregate source B might be higher (summary tables of the statistical test are shown in Table C.9 and Table C.10 in appendix C).

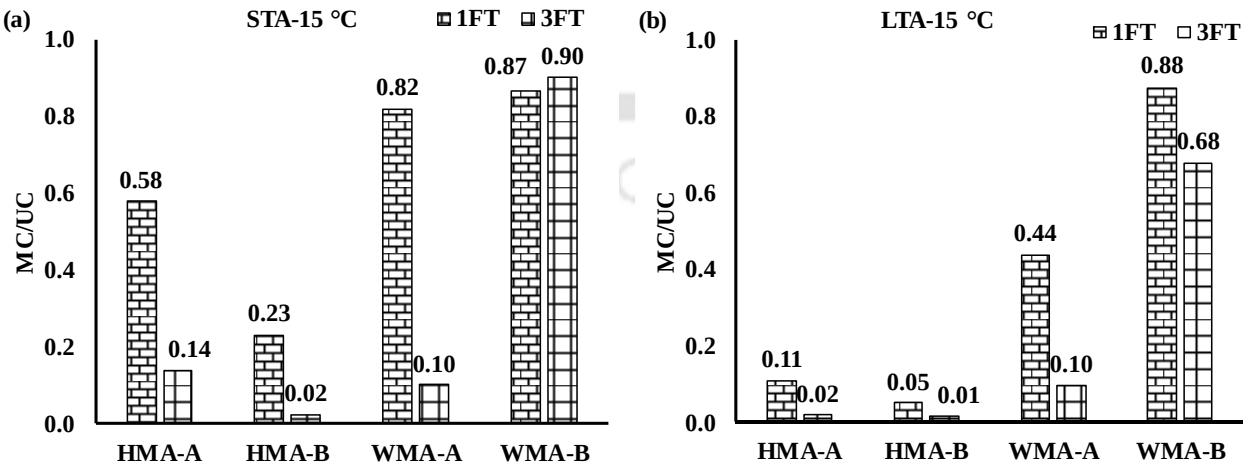

Figure 6.21 Ratio of fatigue life of UC and MC mixture at 15 °C (a) STA, (b) LTA

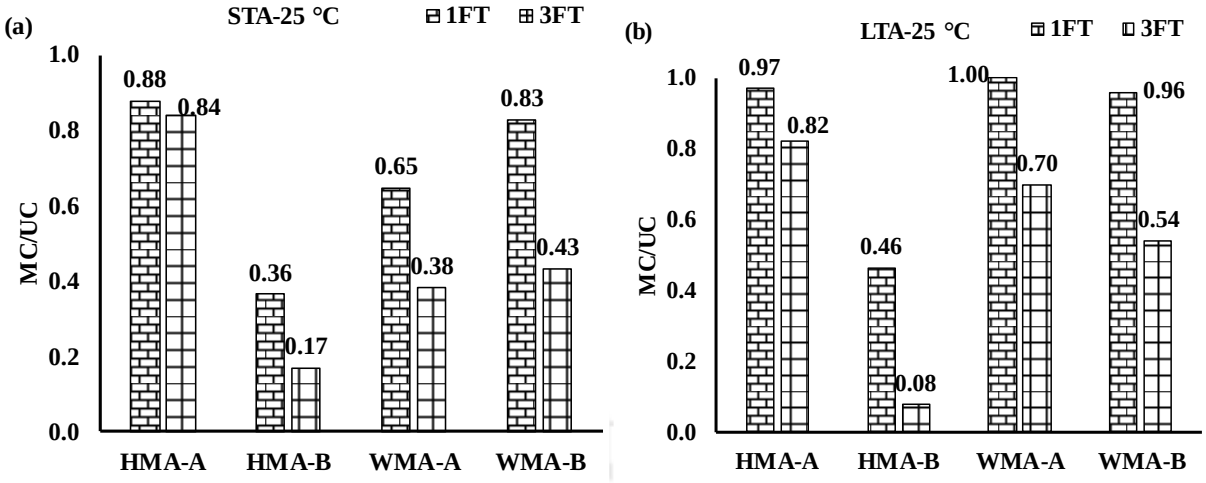

Figure 6.22 Ratio of fatigue life of UC and MC mixture at 25 °C (a) STA, (b) LTA

6.4 Summary

In this chapter, the stiffness and fatigue behavior of bituminous mixture subjected to aging and moisture conditioning were investigated at 15 °C and 25 °C. It was noticed that aging increased the stiffness modulus and moisture conditioning reduced the stiffness modulus of the bituminous mixtures. Statistical analysis showed that both aging and moisture significantly affected the bituminous mixtures' stiffness modulus. Aging also increased the fatigue life of bituminous mixtures, which endured a higher number of cycles before failure. However, the effect of aging on the fatigue life of bituminous mixtures was more significant at 15 °C as compared to 25 °C. The fatigue life of bituminous mixtures significantly decreased in the presence of moisture. As noticed in the aging case, the effect of moisture on the fatigue life of the bituminous mixture was higher at 15 °C, particularly for LTA mixtures. Pearson correlation analysis showed that in the case of bituminous mixtures subjected to 3 freeze-thaw cycles, FE better correlated with fatigue life than ITS.

The fatigue damage progression and accumulation in a bituminous mixture was studied using a stiffness degradation approach. It was noticed that the rate of damage progression was higher in moisture-conditioned mixtures as compared to unconditioned mixtures. As the loading cycles increased, the difference between the fatigue damage of unconditioned and moisture-conditioned bituminous mixtures became more apparent. The fatigue damage was captured using an exponential model. The rate of fatigue damage was quantified using the model coefficient '*b*.' It was evident from the coefficient '*b*' that fatigue damage in the 3FT conditioned bituminous mixture was approximately ten times higher than unconditioned

bituminous mixtures. A probabilistic approach used to study fatigue damage showed that the probability of fatigue damage in bituminous mixtures increased with the increase in moisture conditioning cycles. A higher likelihood of damage was noticed in the case of 3 freeze-thaw cycles than 1 freeze-thaw cycle. LTA bituminous mixtures had a higher probability of fatigue damage than short-term aged bituminous mixtures at a test temperature of 15 °C. However, no substantial impact of long-term aging on the fatigue damage of bituminous mixtures was noticed at 25 °C.

Two approaches were evaluated for fatigue life prediction models. The ratio of stiffness change approach showed that the inverse of plateau value and fatigue life followed a power-law relation with a R^2 of 0.56. The damage-based fatigue life prediction model showed a good coefficient of determination ranging from 0.62 to 0.89 for the test conditions evaluated in this study. Further, the probabilistic analysis of the damage-based fatigue life prediction model showed that the proposed damage-based model logically captured the effects of aging and moisture. Probabilistic prediction of fatigue life showed that aging (stiffness gain) might not have any substantial impact in the case of a moisture susceptible bituminous mixture. The application of the Evotherm-J1 warm mix additive might improve the fatigue life of bituminous mixtures with siliceous aggregates subjected to moisture conditioning.

Chapter 7

Effect of Moisture on Creep Behaviour of Bituminous Mixtures

7.1 Introduction

This chapter investigated the creep behavior of bituminous mixture subjected to short-term and long-term aging and moisture conditioning. First, the effect of different test conditions on the creep strain of bituminous mixtures was evaluated. Next, the flow number of the bituminous mixture was determined to understand the creep resistance at different conditions. Subsequently, the effect of stress level and test temperature on flow number of bituminous mixtures were evaluated. Finally, the effect of entrapped moisture on the creep resistance of the bituminous mixture was analyzed.

7.2 Experimental program

The experimental matrix used to understand the creep resistance of bituminous mixtures is shown in Table 7.1. Bituminous mixtures were subjected to two levels of aging, i.e., short-term and long-term aging, and three levels of moisture conditioning, i.e., UC, one, and three freeze-thaw cycles. A total of 117 specimens were tested consisting of three replicates for each test condition. An unconfined uniaxial compression was carried out at 100 kPa and 45 °C on all four mixtures as per BS DD 226 protocol. The effect of stress levels (100 kPa and 150 kPa) and test temperatures (40 °C and 45 °C) on the WMA-A mixture's creep resistance was determined. Besides, the damping effect caused by moisture entrapped on the void space of bituminous specimens was evaluated. Finally, the creep resistance at different test conditions was quantified using the flow number parameter determined using the Francken model.

Table 7.1 Experimental matrix for creep resistance study

Mixtures	Test temperature	Stress level	Aging condition	Moisture condition	Test	Parameters
HMA-A, HMA-B, WMA-A, and WMA-B	40 °C (only WMA-A) and 45 °C	100 kPa and 150 kPa (only WMA-A)	STA, LTA, and oven aged at 60 °C for 24 h (only WMA-A)	UC, freeze-thaw (1 and 3 cycles), and FT-Dry (only WMA-A)	UUC	Flow number (FN)

7.3 Results and discussion

7.3.1 Creep strain of bituminous mixtures

The effect of aging and moisture on the creep behavior of bituminous mixtures was determined at 45 °C and 100 kPa. The axial deformation of the specimen during the test was recorded. The axial strain at the end of the rest period immediately after load application was calculated using Eq. (7.1) (BS DD 226). The increment in permanent axial strain with the loading cycle for STA bituminous mixtures is shown in Figure 7.1, and for LTA mixtures is shown in Figure 7.2. It could be noticed from Figure 7.1 and Figure 7.2 that the cumulative strain of different mixtures was comparable at the beginning of the test. As the test progressed, i.e., the number of load applications increased, the differences in the axial strain undergone by different mixtures at different conditions became more noticeable. A Francken model was used to determine the cycle corresponding to the tertiary stage in the plot of cumulative strain versus cycles. The Francken model representing the relationship between creep strain and the number of cycles is shown in Eq. (7.2) (Francken, 1977). The flow number is the cycle associated with the point of inflection, i.e., where the $\frac{\partial^2 \in (p)}{\partial N^2}$ value changes from negative to positive. The flow number value was determined using Eq. (7.3) (Biligiri et al., 2007).

$$\varepsilon_{d(N,T)} = \frac{\Delta h}{h_0} \tag{7.1}$$

$$\epsilon_p(N) = AN^B + C(e^{DN} - 1) \tag{7.2}$$

$$\frac{\partial^2 \in (p)}{\partial N^2} = A \times B \times (B-1)N^{(B-2)} + (C \times D^2 \times e^{D \times N}) \tag{7.3}$$

where,

$\varepsilon_{d(N,T)}$= axial strain at T (°C) temperature after N load applications,

Δh= axial deformation of the specimen, mm,

h_0 = initial height of the sample after preloading, mm,

ϵ_p = permanent axial strain, µm, and,

A, B, C & D = are regression constants.

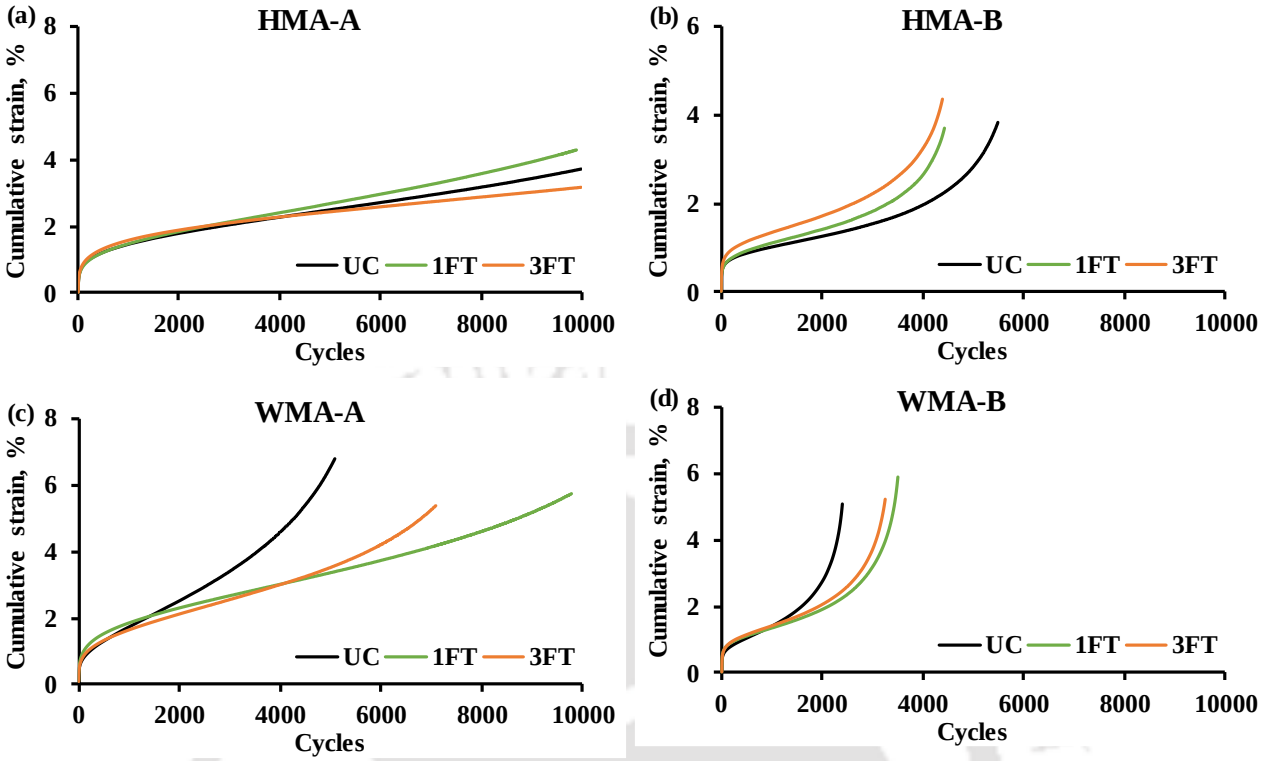

Figure 7.1 Cumulative strain of bituminous mixtures at STA conditions

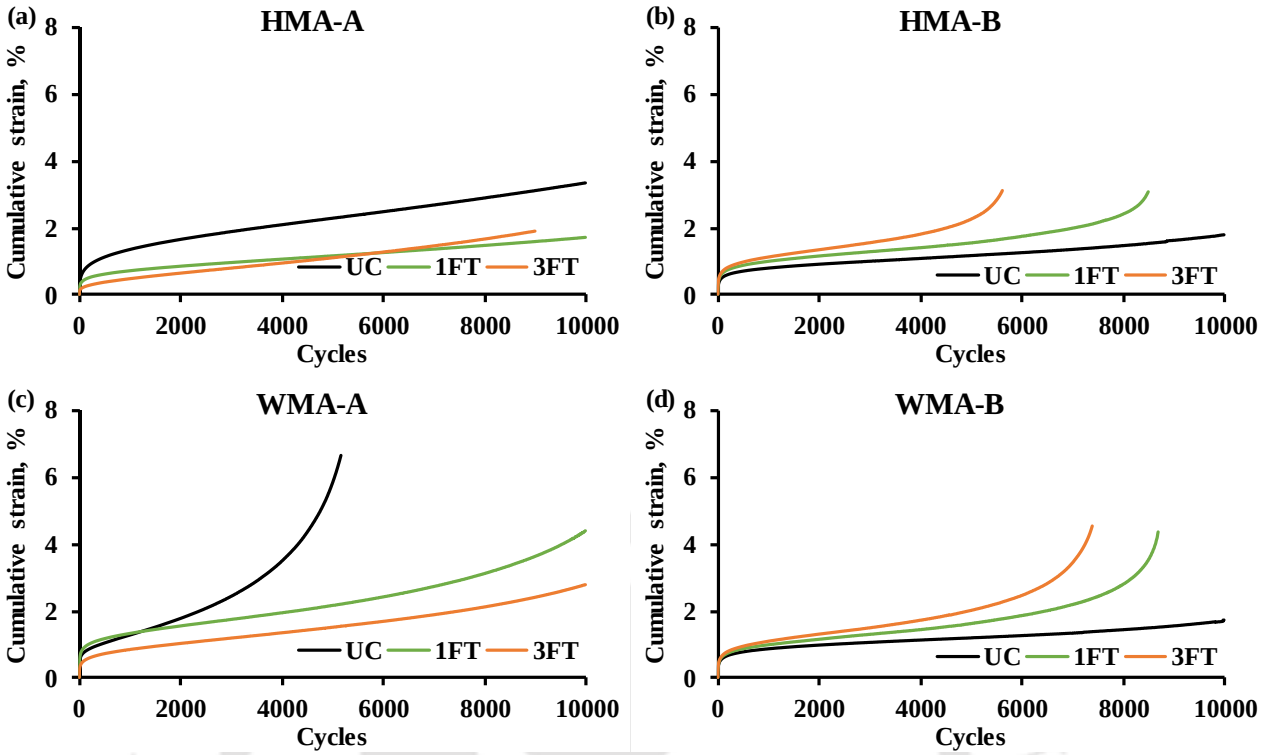

Figure 7.2 Cumulative strain of bituminous mixtures at LTA conditions

7.3.2 The creep resistance of bituminous mixtures

The flow number value determined from the Francken model was used to evaluate the creep resistance of bituminous mixtures at different conditions. The effect of aging on bituminous mixtures' creep resistance was determined by comparing unconditioned STA and LTA mixtures. The creep resistance of unconditioned STA and LTA bituminous mixtures is shown in Figure 7.3. It could be noticed from Figure 7.3 that LTA bituminous mixture had higher creep resistance compared to STA bituminous mixtures. Thus, aging increased the creep resistance of bituminous mixtures. Researchers have also noticed an increase in creep resistance of bituminous mixtures with aging (Said, 2005; Azaria & Mohseni, 2013; Othman & Omranian, 2015). The statistical significance of the changes in the bituminous mixture's creep resistance with aging was determined using a one-way ANOVA with Tukey's post-hoc test at a 5 % significance level. It could be noticed from Table 7.2 that aging did not have a significant effect on the creep resistance of bituminous mixtures for most of the cases. In addition, a paired t-test ($\alpha = 0.05$) and Cohen's d-value were used to compare the flow number of HMA and WMA mixture at different conditions (Table C.11 and Table C.12 in appendix C). A significant difference in the creep resistance of unconditioned HMA and WMA mixtures

was noticed at STA condition. However, at LTA condition, the creep resistance of unconditioned HMA and WMA mixtures was not statistically different. The effect of moisture on the creep resistance of the bituminous mixture is discussed next.

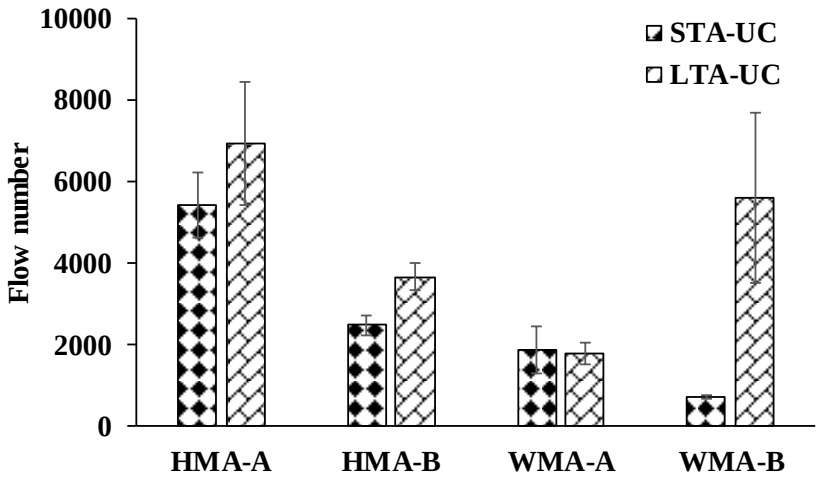

Figure 7.3 Flow number of unconditioned bituminous mixtures

Table 7.2 One-way ANOVA of flow number of UC bituminous mixtures

Mixture	Condition	p-value	Significant
HMA-A	STA-UC~LTA-UC	1.0E+00	No
HMA-B	STA-1FT~LTA-1FT	5.2E-01	No
WMA-A	STA-3FT~LTA-3FT	1.0E+00	No
WMA-B	STA-UC~LTA-UC	1.3E-03	Yes

The effect of moisture on the creep resistance of STA bituminous mixtures is shown in Figure 7.4, and LTA bituminous mixtures are shown in Figure 7.5. The impact of moisture on the creep resistance of bituminous mixtures was not straightforward. Researchers have found that moisture has a negative impact on the creep resistance of bituminous mixtures (Kanitpong & Bahia, 2005; Khattak & Kyatham, 2008). However, it could be noticed from Figure 7.4 that in the case of STA bituminous mixtures, moisture did not have a negative effect on the creep resistance of the bituminous mixtures. On the contrary, moisture-conditioned bituminous mixtures showed a higher creep resistance. One-way ANOVA test carried out at a 5 % significance level shows that the moisture conditioning had no significant effect on bituminous creep resistance (see Table 7.3). Also, a paired t-test showed that creep resistance of HMA and WMA mixture in the presence of moisture was not significantly different (Table C.11 and Table C.12 in appendix C).

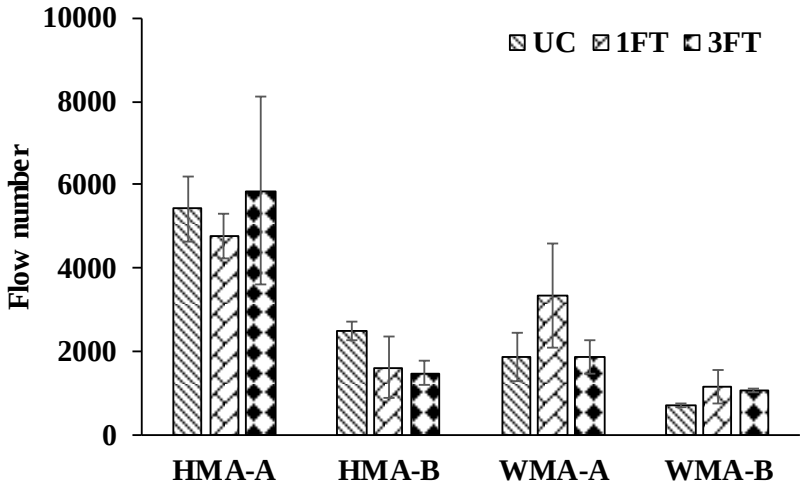

Figure 7.4 Flow number of STA bituminous mixtures

Table 7.3 One-way ANOVA of flow number of STA bituminous mixtures

Mixture	Condition	p-value	Significant
HMA-A	UC~1FT	9.6E-01	No
	UC~3FT	5.1E-02	No
	1FT~3FT	1.3E-02	Yes
HMA-B	UC~1FT	1.0E+00	No
	UC~3FT	1.0E+00	No
	1FT~3FT	1.0E+00	No
WMA-A	UC~1FT	2.4E-01	No
	UC~3FT	1.7E-01	No
	1FT~3FT	1.0E+00	No
WMA-B	UC~1FT	1.0E+00	No
	UC~3FT	1.0E+00	No
	1FT~3FT	1.0E+00	No

There might be two possibilities for the increase in creep resistance of bituminous mixtures with moisture conditioning. First, soaking bituminous mixtures in a hot water bath at 60 °C for 24 h might slightly increase the stiffness of a dense graded bituminous mixture. López-Montero & Miró (2016) noticed an increase in the stiffness and fracture energy of the unaged dense graded bituminous mixtures soaked in a water bath at 40 °C for 48 h and 72 h. Second, under the dynamic load application, the moisture entrapped in the bituminous specimen's voids space might generate hydraulic pressure and resist the applied load by acting as a damper. Mehrara & Khodaii (2011) noticed a similar increase in the creep resistance of moisture-conditioned bituminous specimens compared to dry specimens when tested at 40 °C and 100 kPa.

In the case of LTA bituminous mixtures, the bituminous mixture's creep resistance reduced with moisture conditioning for most of the cases, as noticed in Figure 7.5. The stiffness gained with hot water soaking that increased the creep resistance of bituminous mixtures might be minimal in LTA bituminous mixtures. López-Montero & Miró (2016) also noticed that hot water soaking had a negligible effect on the aged mixture's stiffness compared to the unaged mixture. Researchers have also noticed that the long-term aged bituminous mixture is more susceptible to moisture's adverse effect compared to the unaged bituminous mixture (Tong et al., 2015; Pan et al., 2018). Both factors combined might have resulted in a decrease in LTA bituminous mixtures' creep resistance with moisture conditioning. Although the creep resistance of bituminous mixtures reduced with moisture conditioning, Table 7.4 showed that the effect of moisture was not significant (also noticed in the case of STA bituminous mixtures (Table 7.3)). From the above discussion, it could be said that subjecting bituminous mixtures to long-term aging before determining the creep resistance might result in a better assessment, particularly to explore the moisture effect.

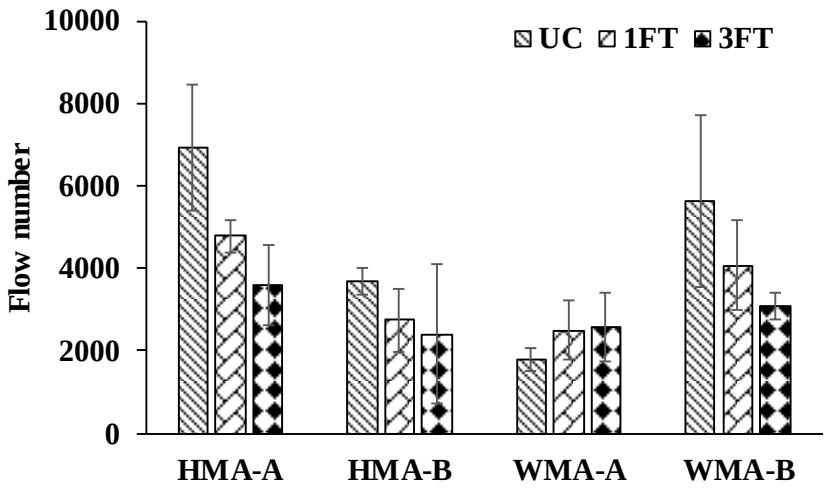

Figure 7.5 Flow number of LTA bituminous mixtures

Table 7.4 One-way ANOVA of flow number of LTA bituminous mixtures

Mixture	Condition	p-value	Significant
HMA-A	UC~1FT	9.4E-01	No
	UC~3FT	1.5E-01	No
	1FT~3FT	5.0E-01	No
HMA-B	UC~1FT	1.0E+00	No
	UC~3FT	9.4E-01	No
	1FT~3FT	9.5E-01	No
WMA-A	UC~1FT	9.7E-01	No
	UC~3FT	5.4E-01	No
	1FT~3FT	9.2E-01	No
WMA-B	UC~1FT	1.1E-01	No
	UC~3FT	2.0E-01	No
	1FT~3FT	1.0E+00	No

From the literature, it is understood that temperature and stress level influence the creep behavior of bituminous mixture (Sarkar, 2017; Pouranian et al., 2020). It would be interesting to see how the change in temperature and applied stress affect the creep resistance of bituminous mixtures subjected to different aging and moisture conditioning levels. Mehrara & Khodaii (2011) found that compared to 100 kPa, a stress level of 150 kPa was more appropriate for evaluating moisture-conditioned bituminous mixtures' creep resistance. From Figure 7.4 and Figure 7.5, it could be noticed that in the case of the WMA-A mixture, moisture had no effect, or the creep resistance increased with moisture conditioning, both at STA and LTA conditions. Thus, the effect of aging and moisture on the creep resistance of WMA-A mixture at two test temperatures and two stress levels was evaluated in the next section.

7.3.3 Effect of aging and moisture at different stress and temperature

The effect of aging and moisture on the WMA-A mixture's creep resistance was studied at a test temperature of 40 °C and 45 °C, and stress levels of 100 kPa & 150 kPa. The bituminous mixture was subjected to only one freeze-thaw cycle for moisture conditioning. The bituminous mixture's creep resistance at different conditions was determined using the flow number value (as mentioned in section 7.3.1). The flow number at different conditions is shown in Figure 7.6. It could be noticed from Figure 7.6 that the creep resistance of the bituminous mixture reduced with the increase in stress level from 100 kPa to 150 kPa at both test temperatures. The creep resistance of the bituminous mixture also reduced with an increase in the test temperature from 40 °C to 45 °C, at each stress level. In the case of an unconditioned

bituminous mixture, the creep resistance increased with the increase in aging from STA to LTA condition at each stress level and test temperature.

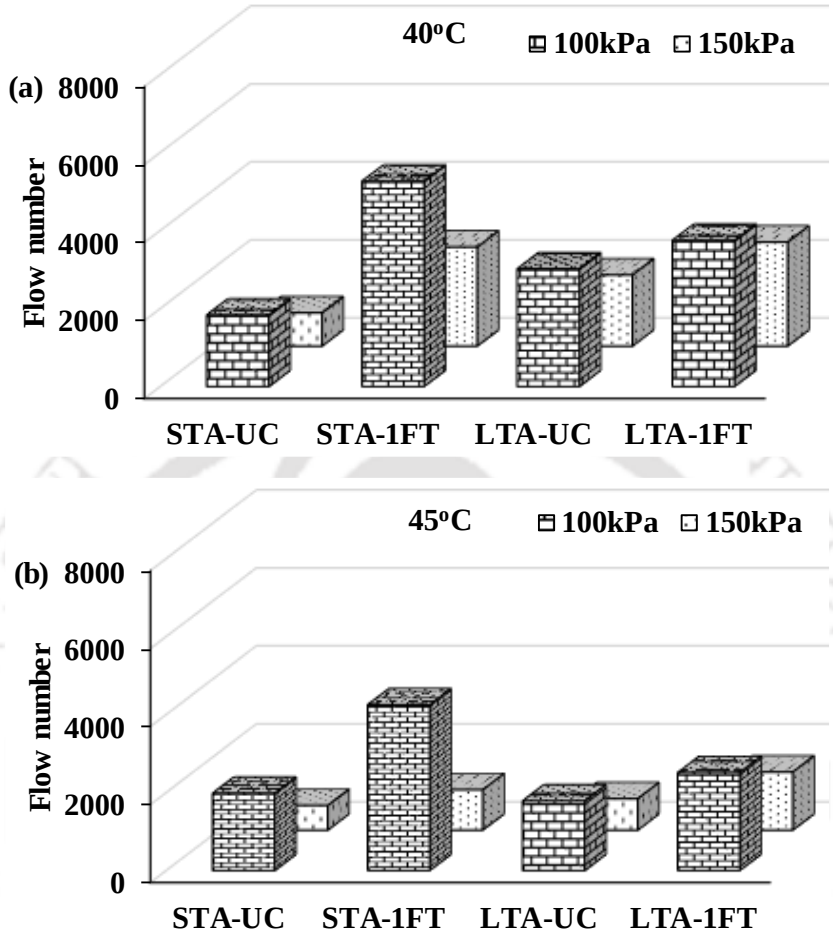

Figure 7.6 Effect of temperature and stress level on flow number: (a) 40 °C; (b) 45 °C

From Table 7.5, it could be noticed that the ratio of LTA to STA bituminous mixture was higher at 150 kPa than 100 kPa at each test temperature. For e.g., compared to STA mixture, the flow number of LTA mixture at 40 °C was 2.1 times higher at 150 kPa, and 1.6 times higher at 100 kPa. Further, it could be noticed that the ratio of LTA/STA of the bituminous mixture was relatively higher at 40 °C than 45 °C at each stress level, e.g., compared to STA mixture, the flow number of LTA mixture tested at 150 kPa was 2.1 times at 40 °C, and 1.3 times higher 45 °C. Thus, Table 7.5 suggests a relatively higher stress level and test temperature of 40 °C might be suitable to evaluate the effect of aging on the creep resistance of bituminous mixture. However, the effect of aging on the creep resistance at different stress levels and test temperatures was not significant (paired *t*-test at $\alpha = 0.05$), as shown in Table 7.6.

It could be noticed from Figure 7.6 that the creep resistance of the bituminous mixture increased with moisture conditioning at both STA and LTA conditioned, irrespective of the test temperature and stress level. However, LTA mixtures showed a lower increment in flow number with moisture conditioning than STA mixture at each test temperature and stress level (see Table 7.5). Thus, LTA bituminous mixture might be considered to evaluate the effect of moisture on creep resistance of bituminous mixture. Interestingly, the effect of stress level on creep resistance of moisture conditioned bituminous mixture was dependent on the level of aging considered.

Table 7.5 Ratio of flow number of specimens at different condition

Condition	Aging	Moisture	
	LTA/STA	1FT/UC at STA	1FT/UC at LTA
40 °C &100kPa	1.6	2.9	1.2
40 °C & 150kPa	2.1	3.0	1.5
45 °C & 100kPa	0.9	2.1	1.4
45 °C & 150kPa	1.3	1.6	1.8

Table 7.6 Paired t-test for comparing flow number of UC bituminous mixture

Temperature	Stress level	Condition	p-value	Significant
40 °C	100 kPa	STA-UC~LTA-UC	5.44E-02	No
	150 kPa	STA-UC~LTA-UC	1.25E-01	No
45 °C	100 kPa	STA-UC~LTA-UC	6.49E-01	No
	150 kPa	STA-UC~LTA-UC	2.55E-01	No

7.3.4 Damping due to entrapped moisture in the specimen

It could be noticed from Figure 7.4, Figure 7.5, and Figure 7.6 that the creep resistance of moisture-conditioned bituminous mixtures was higher than dry mixtures. This might be due to the damping effect of moisture entrapped in the void spaces of the specimen and the stiffness gained by the bituminous mixture due to soaking in hot water, as noticed in previous studies (Mehrara & Khodaii, 2011; Hernández et al., 2014; López-Montero & Miró, 2016). In this section, moisture's damping effect on the creep resistance of the bituminous mixture was determined. For this purpose, nine specimens of the STA WMA-A mixture were prepared and divided into three groups.

The first group was subjected to only oven aging at 60 °C for 24 h (termed as oven-aged). The second group was subjected to one freeze-thaw cycle (termed as 1FT). The third group was subjected to one freeze-thaw process, and then the moisture entrapped in the specimen's void space was removed using the CoreDry equipment (as shown in Figure 7.7). Specimens were then subjected to the creep test at 45 °C and 100 kPa to determine the creep resistance at different conditions. The flow number value of the above-mentioned three conditions were compared with the flow number of unconditioned WMA-A specimens (termed as UC) tested at 45 °C and 100 kPa, as shown in Figure 7.8.

Figure 7.7 CoreDry equipment

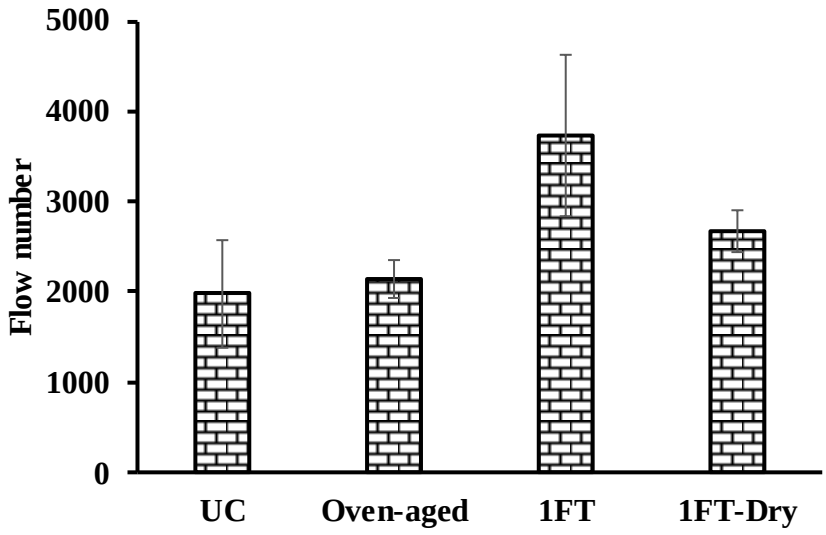

Figure 7.8 Damping effect due to entrapped moisture

From Figure 7.8, it could be noticed that oven aged specimen had higher creep resistance as compared to the UC specimen. This was due to the increase in stiffness of the bituminous mixture with oven aging, which in turn increased the creep resistance of the oven aged mixture. The bituminous mixture subjected to one freeze-thaw cycle of moisture conditioning also had higher creep resistance when compared to the UC and oven aged mixture. Upon removing the moisture entrapped in the specimen using the CoreDry equipment, i.e., the 1FT-Dry specimen offered lower creep resistance when compared to the 1FT specimen, as seen in Figure 7.8. Thus, the combination of hot water soaking at 60 °C for 24 h and the moisture entrapped in the 1FT specimen might have added to the creep resistance of the moisture conditioned specimen. One-way ANOVA at 0.05 level of significance was performed to determine the significance of different conditions on creep resistance, as shown in Table 7.7. It could be noticed from Table 7.7 that the creep resistance of 1FT specimen was significantly higher than UC and oven aged specimens. However, the creep resistance of the 1FT-Dry specimen was not significantly higher than the UC specimen. Thus, the entrapped moisture might have a significant effect on the creep resistance of the bituminous mixture. Thus, for a better assessment of the creep resistance of moisture conditioned bituminous mixture, testing should be carried out after removing the entrapped moisture in the specimen and at a higher stress level.

Table 7.7 One-way ANOVA for the damping effect

Source	p-value	Significant
UC~1FT	2.05E-02	Yes
UC~1FT-Dry	4.65E-01	No
1FT~1FT-Dry	1.73E-01	No
UC~Oven-aged	9.84E-01	No
1FT~Oven-aged	3.34E-02	Yes
1FT-Dry~Oven-aged	6.58E-01	No

7.4 Summary

In this chapter, the creep resistance of different bituminous mixtures subjected to aging and moisture conditioning was determined using the flow number obtained from the Francken model. First, the effect of aging and moisture on the creep resistance of bituminous mixtures was determined at 45 °C and 100 kPa. Next, the effect of aging and moisture on the creep resistance at different stress levels, i.e., 100 kPa and 150 kPa, and different test temperatures, i.e., 40 °C and 45 °C, were studied. Also, the effect of entrapped moisture on the creep resistance of bituminous mixtures was studied. It was noticed that aging increased the creep resistance of unconditioned bituminous mixtures. The effect of moisture on the creep resistance of the bituminous mixture was found to be dependent on the level of aging. The creep resistance of short-term aged bituminous mixtures increased with moisture conditioning. The increase in stiffness due to hot water soaking and the damping effect of the entrapped moisture might cause variation in the STA bituminous mixture's creep resistance. Whereas the creep resistance of long-term aged bituminous mixture reduced with moisture conditioning. Thus, a long-term aged bituminous mixture might be a better choice to evaluate moisture's effect on the creep resistance of bituminous mixtures. The statistical test showed that both aging and moisture conditioning did not significantly affect the creep resistance of bituminous mixtures evaluated in this study.

Further, it was noticed that the creep resistance of the bituminous mixture reduced with an increase in the stress level and test temperature. To evaluate the effect of aging and moisture on the creep resistance of bituminous mixture, a relatively higher stress level of 150 kPa applied at a lower test temperature of 40 °C might be considered. The presence of moisture might introduce a damping effect of the specimen subjected to the creep test. This, in turn, results in an increase in the creep resistance of the bituminous mixture, as noticed in this study.

Chapter 8

Summary of findings, conclusions, and future scope

8.1 Summary of findings

This study aims to understand the effect of aging and moisture conditions on the performance of bituminous mixture. In this work, hot and warm bituminous mixtures were produced with two different types of aggregates. Bituminous mixtures were subjected to different aging (short-term, long-term, and AASHTO T 283) and moisture conditioning levels (boiling water test and compacted specimens subjected to one and three freeze-thaw cycles). The indirect tensile stiffness modulus and indirect tensile strength of the bituminous mixtures were determined at 15 °C and 25 °C. Different cracking resistance parameters were evaluated and compared from the ITS test's load-deformation data. The fatigue behavior of bituminous mixtures was determined at 15 °C and 25 °C using an indirect tensile fatigue test at two stress levels (250 kPa and 400 kPa). A probabilistic analysis of fatigue life was carried out, and a damage-based fatigue life prediction model was presented. The bituminous mixture's creep resistance was determined at 40 °C and 45 °C at 100 kPa and 150 kPa. The flow number value of different mixtures was determined and compared using the Francken model. In addition, the effect of entrapped moisture on the creep resistance of the bituminous mixture was also evaluated.

It was noticed that the TSR of bituminous mixtures increases with the increase in aging level from STA (Avg. 62 %) to LTA (Avg. 69 %) and to T-283 (Avg. 84 %) aged condition. The adhesive failure in bituminous mixtures increased marginally by one percent with the increase in the aging level. Similarly, an average rise in the adhesive failure of two percent was noticed with the increase in freeze-thaw cycles. An average increase of eight percent in AF was observed with a reduction in test temperature from 25 °C to 15 °C. The fatigue life of bituminous mixtures increased with an increase in aging levels (Avg. 80 %) and reduced with an increase in moisture conditioning cycles (Avg. 50 %). The bituminous mixtures' fatigue life increased with the reduction in test temperature from 25 °C to 15 °C (Avg. 76 %). As noticed in fatigue life, aging also increased the bituminous mixture's creep resistance measured using the flow number value by approximately two times. The creep resistance of bituminous mixtures reduced with the increase in test temperature from 40 °C to 45 °C by an average of fifty percent.

8.2 Conclusions

Based on the findings of this research work, the following conclusions are drawn.

8.2.1 Cracking Resistance Parameters

- The CoV of ITS (Avg. 5 %), FWD (Avg. 10 %), FE (Avg. 10 %), and CRI (Avg. 9 %) parameters were lower compared to the CoV of CT_{Index} (Avg. 25 %) and RDCI (Avg. 22 %) parameter.
- The ITS, FWD, FE values decreased with the increase in moisture conditioning cycles, which was not noticed in CRI, CT_{Index}, and RDCI parameters.
- Statistical analysis showed that a change in the aging level and moisture conditioning cycles significantly affect the ITS, FE, and FWD values of different mixtures. Considering that FE utilizes both peak load and post-peak behavior of bituminous mixture, FE might be better suited to evaluate the mixtures cracking resistance of which exhibit brittle like behavior due to aging.

8.2.2 Adhesion Failure

- The AF values of different mixtures ranged from 4 % to 33 %, with moisture susceptible HMA-B mixture having an average AF value of 19 %. A bituminous mixture's resistance to moisture damage was divided into three zones using TSR in conjunction with AF. A bituminous mixture with TSR > 80 % and AF < 10 % was designated as highly resistant to moisture damage. Likewise, a bituminous mixture with TSR between 80 % to 70 % and AF between 10 % to 15 % was termed as moderate, and a bituminous mixture with TSR < 70 % and AF > 15 % was termed as low resistance against moisture intrusion.
- The fracture energy associated with these three zones served as a measure of high (FE > 5200 J/m^2), moderate (5200 J/m^2 < FE < 3300 J/m^2), and low cracking (FE < 3300 J/m^2) resistance of bituminous mixtures in the presence of moisture.
- The AF and percent loss measured from loose bituminous mixtures were comparable and had a fair association. Thus, AF quantified using image analysis will help understand the extent of detachment and displacement mechanism of moisture damage evaluated using a freeze-thaw process.

8.2.3 Fatigue Behaviour

- The adverse effect of moisture on bituminous mixtures' fatigue life was higher at 15 °C (63 % average reduction in fatigue life) than 25 °C (37 % average reduction in fatigue life).
- Probabilistic fatigue damage analysis at 15 °C showed that LTA bituminous mixtures had a higher probability of fatigue damage than the STA mixtures. However, long-term aging had no substantial impact on the fatigue damage of bituminous mixtures at 25 °C. The likelihood of fatigue damage in bituminous mixtures increased with the increase in moisture conditioning cycles.
- The damage-based fatigue life prediction model had a good coefficient of determination ($0.62 \leq R^2 \leq 0.89$) at different test conditions used in this study. The simulated fatigue life of the damage-based fatigue life prediction model using Monte Carlo simulation showed that aging might not substantially affect the fatigue life of moisture susceptible bituminous mixtures.

8.2.4 Creep Behaviour

- The LTA bituminous mixture flow number increased by at least 25 percent for most cases than STA, indicating an increase in creep resistance with aging.
- Inconsistency in the results was noticed due to entrapped moisture in the specimen. Statistically, the UC mixture's creep resistance was comparable with the creep resistance of the specimen after the removal of entrapped moisture.
- Study highlight that long-term aged mixture might be a better choice to evaluate moisture's effect on the creep resistance of mixtures.

8.3 Significance of the study findings

Overall, the study results pointed out that aging and moisture substantially affect the performance of bituminous mixtures. Table 8.1 presents the agreement of different mixture properties with the aging conditions. The aging index is computed as the ratio of LTA and STA for each test parameter. The average index values are presented in Table 8.1, highlighted aging conditions had highest effect of fatigue life, and creep resistance of bituminous mixtures. It is interesting to notice from Table 8.2, that moisture had a negative effect on all parameters studied. It is important to note that moisture had highest effect on tensile strength, fracture energy, and fatigue life. This highlights that moisture damage predominantly influences the cracking resistance of bituminous mixtures. However, the effect of moisture on the creep behaviour was found to be marginal. Hence, along with tensile strength, it is important to consider the moisture effect while evaluating bituminous mixtures' fracture energy and fatigue behavior. This will help control the effect of environmental factors, i.e., aging and moisture, on the durability issues of bituminous mixtures. In this regard, the future scope of the work that can be explored to gain more specific information is presented in section 8.5.

Table 8.1 Agreement of mixture properties at different aging conditions

Test	Parameter	Aging Index	
		Effect	LTA/STA
ITS	ITS	Increment	1.09
	FE	Comparable	0.99
ITSM	Stiffness modulus	Increment	1.38
ITFT	Fatigue life	Increment	1.75
Creep	Flow number	Increment	1.91

Table 8.2 Agreement of mixture properties at different moisture conditions

Test	Parameter	Moisture Index		
		Effect	1FT/UC	3FT/UC
ITS	ITS	Reduction	0.60	0.47
	FE	Reduction	0.56	0.45
ITSM	Stiffness modulus	Reduction	0.70	0.53
ITFT	Fatigue life	Reduction	0.51	0.25
Creep	Flow number	Reduction	0.99	0.88

8.4 Research implementation

It is well understood that moisture and aging have a substantial effect on the behaviour of bituminous mixtures. Even though the mixture resistance to moisture is assessed during the mix design, specifications seldom considered the effect of moisture on the mechanical behaviour of bituminous mixtures. This study showed that aging and moisture conditioning significantly affected the mechanical properties (fatigue and creep). Hence it is proposed to consider both aging and moisture conditioning during the mixture design and performance testing. A preliminary framework is proposed in Figure 8.1 to implement and fine-tune the research findings. The limits of tensile strength ratio, fracture energy, adhesive failure, and fatigue life ratio proposed in this framework need further refinement and validation with field studies.

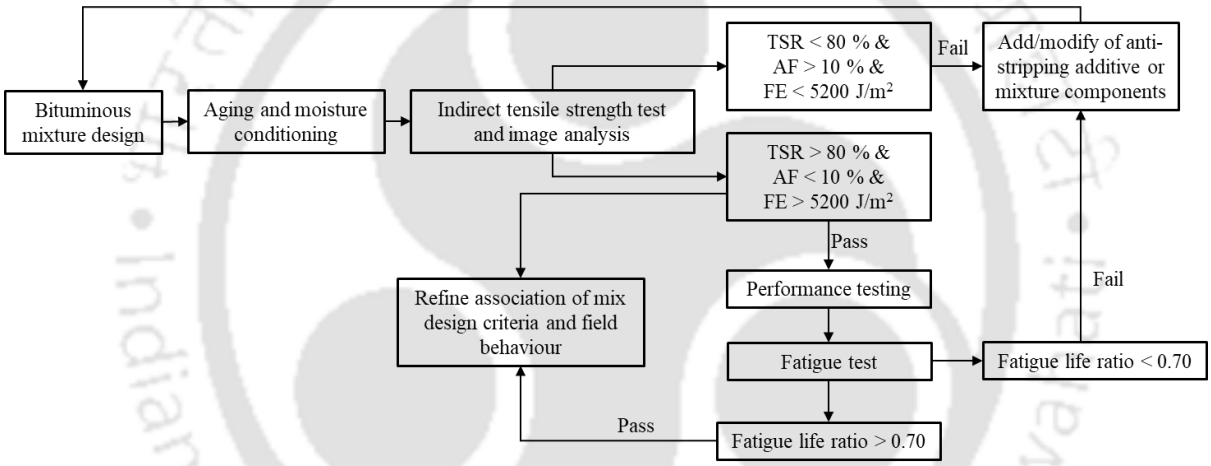

Figure 8.1 Implementation plan of this research work

8.5 Future scope

Based on the framework and findings of this study, the following future scopes are proposed.

1. The strength and the mechanical behavior evaluated in this study suggest that bituminous mixture exposed to varying aging and moisture conditions must be evaluated and related to field cores behavior. This would help to improve the traditional protocols to design durable bituminous mixtures.
2. Most importantly, different aging and moisture damage mechanisms should be studied to highlight the critical mechanisms and address the durability issues.

3. Studies are also required to corroborate specific conclusion made in this study, like the CoV of 10 % to determine the suitability of a parameter, limits on adhesive failure (less than 10 %, 10 % to 15 %, and more than 15 %), limits on fracture energy (5200 J/m^2 and 3300 J/m^2). Furthermore, the information on the association of adhesive failure with fundamental mixture properties must be explored further.
4. Validating the laboratory findings with field cores is important. Particularly, the adhesive failure values associated with the field cores and the corresponding cracking resistance parameter values could be used to establish threshold limits to screen moisture susceptible bituminous mixtures.

Publications

Journal

1. Das, B., & Siddagangaiah, A. (2021). Moisture Damage Analysis Based on Adhesive Failure in Asphalt Mixtures. *International Journal of Pavement Engineering*. https://doi.org/10.1080/10298436.2020.1862840.
2. Das, B., Babar, P., & Siddagangaiah, A. (2021). Impact of Aging and Moisture on Fatigue Life of Asphalt Mixture. *Advances in Civil Engineering Materials*, 10 (1), 1–15. https://doi.org/10.1520/ACEM20190211.
3. Das, B., & Siddagangaiah, A. (2021). Identification of Parameter to Assess Cracking Resistance of Asphalt Mixtures Subjected to Aging and Moisture Conditioning. *Journal of Traffic and Transportation Engineering (English Edition)*. (***Accepted***).
4. Das, B., Das, S., & Siddagangaiah, A. (2020). Probabilistic Modeling of Fatigue damage in Asphalt Mixture. *Construction and Building Materials. 269*,121300 *https://doi.org/10.1016/j.conbuildmat.2020.121300.*
5. Das, B., Bhargava, N., & Siddagangaiah, A. (2018). Influence of Environmental Conditions on the Performance of Bituminous Mixtures. *Advances in Civil Engineering Materials*, 7(2), 163-180. https://doi.org/10.1520/ACEM20170091
6. Bhargava, N., Das, B., & Siddagangaiah, A. (2018). Synergistic influence of aging and moisture on performance of warm mix asphalt. *International Journal of Pavement Research and Technology*, 11, 789-799. https://doi.org/10.1016/j.ijprt.2018.06.002

International conference

1. Das, B., Bhargava, N., & Siddagangaiah, A. (2017). Influence of aging and moisture conditioning on the tensile strength characteristics of bituminous mixtures. *71st RILEM annual week & ICACMS 2017*, Chennai, India, 3rd to 8th September 2017.

References

AASHTO R30. (2002). *Standard Practice for Mixture Conditioning of Hot Mix Asphalt (HMA)*, American Association of State Highway and Transportation Officials, Washington, DC.

AASHTO T 283. (2014). *Standard Method of Test for Resistance of Compacted Asphalt Mixtures to Moisture-Induced Damage*, American Association of State Highway and Transportation Officials, Washington, DC.

AASHTO T324. (2019). *Standard Method of Test for Hamburg Wheel-Track Testing of Compacted Asphalt Mixtures*, American Association of State Highway and Transportation Officials, Washington, DC.

Abd El-Hakim, R. T., Epps, J., Epps Martin, A., & Arámbula-Mercado, E. (2019). "Laboratory and field investigation of moisture susceptibility of hot and warm mix asphalts." *International Journal of Pavement Engineering*, 1-10.

Abo-Qudais, S., & Al-Shweily, H. (2007). "Effect of aggregate properties on asphalt mixtures stripping and creep behavior." *Construction and Building Materials*, *21*(9), 1886–1898.

Aguiar-Moya, J. P., Salazar-Delgado, J., Baldi-Sevilla, A., Leiva-Villacorta, F., & Loria-Salazar, L. (2015). "Effect of aging on adhesion properties of asphalt mixtures with the use of bitumen bond strength and surface energy measurement tests." *Transportation Research Record*, *2505*, 57–65.

Airey, G. D., Collop, A. C., Zoorob, S. E., & Elliott, R. C. (2008). "The influence of aggregate, filler and bitumen on asphalt mixture moisture damage." *Construction and Building Materials*, *22*(9), 2015–2024.

Airey, Gordon D, Choi, Y. K., Collop, A. C., Moore, A. J. V, & Elliott, R. C. (2005). "Combined Laboratory Ageing/Moisture Sensitivity Assessment of High Modulus Base Asphalt Mixtures (With Discussion)." *Association of Asphalt Paving TechnologistsTechnologists*, *74*, 307–346.

Akentuna, M., Mohammad, L. N., Kim, M., Cooper III, S. B., & Cooper Jr, S. B. (2020).

"Improving Durability of Asphalt Pavements in Louisiana through Increased In-Place Field Density." *Transportation Research Record*, 2674(10), 806-816.

Akpolat, M., Vural Kök, B., & Yilmaz, M. (2020). "Performance and Aging Characteristics of Hot Mixture Asphalt with Crumb Rubber and Warm Mix Asphalt Additives." *Journal of Materials in Civil Engineering*, 32(8), 04020226.

Al-Asi, A., & Asi, I. (2021). "Using Cement Kiln Dust in Asphalt Concrete Mixes in Jordan." *Journal of Materials in Civil Engineering*, 33(3), 04021010.

Alataş, T., & Yilmaz, M. (2013). "Effects of different polymers on mechanical properties of bituminous binders and hot mixtures." *Construction and Building Materials*, *42*, 161–167.

Al-Khateeb, G. G., & Ghuzlan, K. A. (2014). "The combined effect of loading frequency, temperature, and stress level on the fatigue life of asphalt paving mixtures using the IDT test configuration." *International Journal of Fatigue*, *59*, 254–261.

Al-Qadi, I. L., Wang, H., Baek, J., Leng, Z., Doyen, M., & Gillen, S. (2012). "Effects of curing time and reheating on performance of warm stone-matrix asphalt." *Journal of Materials in Civil Engineering*, *24*(11), 1422–1428.

Amani, S., Kavussi, A., & Karimi, M. M. (2020). "Effects of aging level on induced heating-healing properties of asphalt mixes." *Construction and Building Materials*, 263, 120105.

Amelian, S., Abtahi, S. M., & Hejazi, S. M. (2014). "Moisture susceptibility evaluation of asphalt mixes based on image analysis." *Construction and Building Materials*, *63*, 294–302.

Anderson, T. L. (2017). *Fracture mechanics: fundamentals and applications*, Taylor & Francis Group, CRC Press, 6000 Broken Sound Parkway NW, Suite 300.

Apeagyei, A. K., Grenfell, J. R. A., & Airey, G. D. (2014). "Moisture-induced strength degradation of aggregate-asphalt mastic bonds." *Asphalt Paving Technology: Association of Asphalt Paving Technologists-Proceedings of the Technical Sessions*, *83*(January), 549–582.

Apeagyei, A. K., Grenfell, J. R. A., & Airey, G. D. (2015). "Influence of aggregate absorption and diffusion properties on moisture damage in asphalt mixtures." *Road Materials and Pavement Design*, *16*(August 2016), 404–422.

Arega, Z. A., Bhasin, A., & De Kesel, T. (2013). "Influence of extended aging on the properties of asphalt composites produced using hot and warm mix methods." *Construction and Building Materials*, *44*, 168–174.

Asphalt Institute. (1982). *Research and Development of Asphalt Institute's Thickness Design Manual*, 9th Ed., Research Report 82-2.

Asphalt Institute. (2014). *Mix design methods for asphalt concrete and other hot-mix types,* Manual Series No. 2 (MS-2), 7th ed. Lexington, KY, USA.

ASTM D1075. (2011). *Standard Test Method for Effect of Water on Compressive Strength of Compacted Bituminous Mixtures (Withdrawn),* ASTM International, West Conshohocken, PA.

ASTM D1559. (1989). *Test method for resistance of plastic flow of bituminous mixtures using marshall apparatus (Withdrawn),* ASTM International, West Conshohocken, PA.

ASTM D1754. (2014). *Standard Test Method for Effects of Heat and Air on Asphaltic Materials (Thin-Film Oven Test),* ASTM International, West Conshohocken, PA.

ASTM D2872. (2019). *Standard Test Method for Effect of Heat and Air on a Moving Film of Asphalt (Rolling Thin-Film Oven Test),* ASTM International, West Conshohocken, PA.

ASTM D3625. (2012). *Standard Practice for Effect of Water on Bituminous-Coated Aggregate Using Boiling Water*, ASTM International, West Conshohocken, PA.

ASTM D4402. (2015). *Standard Test Method for Viscosity Determination of Asphalt at Elevated Temperatures Using a Rotational Viscometer,* ASTM International, West Conshohocken, PA.

ASTM D4867. (2014). *Standard Test Method for Effect of Moisture on Asphalt Concrete Paving Mixtures*, ASTM International, West Conshohocken, PA.

ASTM D6521. (2019). *Standard Practice for Accelerated Aging of Asphalt Binder Using a Pressurized Aging Vessel (PAV),* ASTM International, West Conshohocken, PA

ASTM D6931. (2017). *Standard Test Method for Indirect Tensile (IDT) Strength of Asphalt Mixtures*, ASTM International, West Conshohocken, PA.

ASTM D7175. (2015). *Standard Test Method for Determining the Rheological Properties of*

Asphalt Binder Using a Dynamic Shear Rheometer, ASTM International, West Conshohocken, PA.

ASTM D7870. (2013). *Moisture Conditioning Compacted Asphalt Mixture Specimens by Using Hydrostatic Pore Pressure*, ASTM International, West Conshohocken, PA.

ASTM D8044. (2016). *Standard Test Method for Evaluation of Asphalt Mixture Cracking Resistance using the Semi-Circular Bend Test (SCB) at Intermediate Temperatures*, ASTM International, West Conshohocken, PA.

ASTM D8225. (2019). *Standard Test Method for Determination of Cracking Tolerance Index of Asphalt Mixture Using the Indirect Tensile Cracking Test at Intermediate Temperature*, ASTM International, West Conshohocken, PA.

Azaria, H., & Mohseni, A. (2013). "Effect of short-term conditioning and long-term ageing on permanent deformation characteristics of asphalt mixtures." *Road Materials and Pavement Design*, *14*(November), 79–91.

Baaj, H., Di Benedetto, H., & Chaverot, P. (2005). "Effect of binder characteristics on fatigue of asphalt pavement using an intrinsic damage approach." *Road Materials and Pavement Design*, *6*(2), 147–174.

Baek, C., Underwood, B., & Kim, Y. (2012). "Effects of oxidative aging on asphalt mixture properties." *Transportation Research Record*, *2296*, 77–85.

Bahadori, A. M., Mansourkhaki, A., & Ameri, M. (2015). "A Phenomenological Fatigue Performance Model of Asphalt Mixtures Based on Fracture Energy Density." *Journal of Testing and Evaluation*, *43*(1), 20130057.

Bala, N., & Napiah, M. (2020). "Fatigue life and rutting performance modelling of nanosilica / polymer composite modified asphalt mixtures using Weibull distribution." *International Journal of Pavement Engineering*, *21*(4), 497–506.

Barksdale, R. D. (1972). "Laboratory evaluation of rutting in base course materials." *Proc., 3rd Int. Conf. on Structure Design of Asphalt Pavements*, Univ. of Michigan, Mich. 161–174.

Batioja-Alvarez, D., Lee, J., & Haddock, J. E. (2019). "Understanding the Illinois Flexibility Index Test (I-FIT) using Indiana Asphalt Mixtures." *Transportation Research Record*,

2673(6), 337–346.

Bayekolaei, M. D., Naderi, K., & Nejad, F. M. (2016). "A statistical analysis on the mechanical properties of nanocomposite modified asphalt mixtures." *Petroleum Science and Technology*, 34(16), 1439-1446.

Bennert, T., Maher, A., & Sauber, R. (2011). "Influence of production temperature and aggregate moisture content on the initial performance of warm-mix asphalt." *Transportation Research Record, 2208,* 97–107.

Bharath, G., Reddy, K. S., Tandon, V., & Reddy, M. A. (2021). "Aggregate gradation effect on the fatigue performance of recycled asphalt mixtures." *Road Materials and Pavement Design*, 22(1), 165-184.

Bhasin, A., Howson, J., Masad, E., Little, D. N., & Lytton, R. L. (2007). "Effect of Modification Processes on Bond Energy of Asphalt Binders." *Transportation Research Record, 1998*(1), 29–37.

Biligiri, K. P., Kaloush, K. E., Mamlouk, M. S., & Witczak, M. W. (2007). "Rational modeling of tertiary flow for asphalt mixtures." *Transportation Research Record, 2001*, 63–72.

Botella, R., Pérez-Jiménez, F. E., Miro, R., & Martínez, A. H. (2017). "New methodology to estimate the fatigue behavior of bituminous mixtures using a strain sweep test." *Construction and Building Materials*, *135*, 233–240.

Brown, S. F., and C. A. Bell. (1979). "The Prediction of Permanent Deformation in Asphalt Pavements." *Journal of the Association of Asphalt Paving Technologies*, Vol. 48, pp. 438–476.

BS DD226. (1996). *Method for Determining Resistance to Permanent Deformation of Bituminous Mixtures Subject to Unconfined Dynamic Loading*, British Standards Institution, London, UK.

BS EN 12697-11. (2020). *Test methods -Determination of the affinity between aggregate and bitumen*, British Standard Institute, UK.

BS EN 12697-24. (2004). *Bituminous mixtures – Test methods for hot mix asphalt – Part 24: Resistance to fatigue*, British Standard Institute, UK.

BS EN 12697-26. (2012). *Bituminous mixtures - Test methods for hot mix asphalt – Part 26: Stiffness*, British Standard Institute, UK.

BS EN 12697-45. (2020). *Bituminous mixtures - Test methods Part 45: Saturation Ageing Tensile Stiffness (SATS) conditioning test*, British Standard Institute, UK.

Canestrari, F., Cardone, F., Graziani, A., Santagata, F. A., & Bahia, H. U. (2010). "Adhesive and Cohesive Properties of Asphalt-Aggregate Systems Subjected to Moisture Damage." *Road Materials and Pavement Design*, *11*(sup1), 11–32.

Cao, W., Mohammad, L. N., Barghabany, P., & Cooper, S. B. (2019). "Relationship between laboratory and full-scale fatigue performance of asphalt mixtures containing recycled materials." *Materials and Structures*, 52(1), 1-15.

Caro, S., Masad, E., Bhasin, A., & Little, D. N. (2008a). "Moisture susceptibility of asphalt mixtures, Part 1: Mechanisms." *International Journal of Pavement Engineering*, *9*(2), 81–98.

Caro, Silvia, Masad, E., Airey, G., Bhasin, A., & Little, D. (2008b). "Probabilistic Analysis of Fracture in Asphalt Mixtures Caused by Moisture Damage." *Transportation Research Record*, *2057*(1), 28–36.

Caro, Silvia, Masad, E., Bhasin, A., & Little, D. (2010). "Micromechanical modeling of the influence of material properties on moisture-induced damage in asphalt mixtures." *Construction and Building Materials*, *24*(7), 1184–1192.

Chen, Xingwei, & Huang, B. (2008). "Evaluation of moisture damage in hot mix asphalt using simple performance and superpave indirect tensile tests." *Construction and Building Materials*, *22*(9), 1950–1962.

Chen, Xuan, & Solaimanian, M. (2020). "Simple Indexes to Identify Fatigue Performance of Asphalt Concrete." *Journal of Testing and Evaluation*, *48*(5), 20170722.

Cheng, D. X., Little, D. N., Lytton, R. L., & Holste, J. C. (2003). "Moisture Damage Evaluation of Asphalt Mixtures by Considering Both Moisture Diffusion and Repeated-Load Conditions." *Transportation Research Record*, *1832*, 42–49.

Cong, L., Ren, M., Shi, J., Yang, F., & Guo, G. (2020). "Experimental investigation on performance deterioration of asphalt mixture under freeze–thaw cycles." *International Journal*

of Transportation Science and Technology.

Corradini, A., & Cerni, G. (2020). "A new analytical approach for stiffness loss modelling of asphalt mixtures under cyclic indirect tensile loadings." *International Journal of Fatigue*, 135, 105535.

Crucho, J., Picado-Santos, L., Neves, J., Capitão, S., & Al-Qadi, I. L. (2020). "Tecnico accelerated ageing (TEAGE)–a new laboratory approach for bituminous mixture ageing simulation." *International Journal of Pavement Engineering*, 21(6), 753-765.

Cucalon, L. G., Yin, F., Martin, A. E., Arambula, E., Estakhri, C., & Park, E. S. (2016). "Evaluation of moisture susceptibility minimization strategies for warm-mix asphalt: Case study." *Journal of Materials in Civil Engineering*, 28(2), 05015002.

Cui, S., Blackman, B. R. K., Kinloch, A. J., & Taylor, A. C. (2014). "Durability of asphalt mixtures: Effect of aggregate type and adhesion promoters." *International Journal of Adhesion and Adhesives*, *54*, 100–111.

Curtis C. W., Ensley K., & Epps J. (1993). *Fundamental Properties of Asphalt– Aggregate Interactions Including Adhesion and Adsorption*, Strategic Highway Research Program, National Research Council, Washington, DC, USA, Report SHRP-A-341.

Daryaee, D., Ameri, M., & Mansourkhaki, A. (2020). "Utilizing of waste polymer modified bitumen in combination with rejuvenator in high reclaimed asphalt pavement mixtures." *Construction and Building Materials*, 235, 117516.

Das, P. K., Baaj, H., Kringos, N., & Tighe, S. (2015). "Coupling of oxidative ageing and moisture damage in asphalt mixtures." *Road Materials and Pavement Design*, *16*, 265–279.

Di Benedetto, H., De La Roche, C., Baaj, H., Pronk, A., & Lundström, R. (2004). "Fatigue of bituminous mixtures." *Materials and structures*, 37(3), 202-216.

Diab, A., Enieb, M., & Singh, D. (2019). "Influence of aging on properties of polymer-modified asphalt." *Construction and Building Materials*, 196, 54–65.

Enieb, M., Diab, A., & Yang, X. (2021). "Short-and long-term properties of glass fiber reinforced asphalt mixtures." *International Journal of Pavement Engineering*, 22(1), 64-76.

Fakhri, M., & Ahmadi, A. (2017). "Evaluation of fracture resistance of asphalt mixes involving steel slag and RAP: Susceptibility to aging level and freeze and thaw cycles." *Construction and Building Materials*, 157, 748–756.

Fan, Z., Xu, H., Xiao, J., & Tan, Y. (2020). "Effects of freeze-thaw cycles on fatigue performance of asphalt mixture and development of fatigue-freeze-thaw (FFT) uniform equation." *Construction and Building Materials*, 242, 118043.

Fang, H., Liu, Q., Mo, L., Javilla, B., Shu, B., & Wu, S. (2017). "Characterization of three-stage rutting development of asphalt mixtures." *Construction and Building Materials*, 154, 340–348. https://doi.org/10.1016/j.conbuildmat.2017.07.222

Fattah, M. Y., Ibrahim Al Helo, K. H., & Qasim, Z. I. (2016). "Prediction models for fatigue resistance of local hot mix asphalt." *Road Materials and Pavement Design*, 17(4), 793-809.

Fernández-Gómez, W. D., Vides-Berdugo, A. C., Roncallo-Contreras, S. P., Bautista-Rondón, F., Rondón-Quintana, H. A., & Reyes-Lizcano, F. A. (2016). "Effects of environmental aging and ultra violet radiation on asphalt mixture dynamic modulus, permanent deformation and fatigue life." *Revista Facultad de Ingenieria*, 2016(80), 89–96.

Francken, L. (1977). "Pavement Deformation Law of Bituminous Road Mixes in Repeated Load Triaxial Compression." *Proc., 4th International Conference on the Structural Design of Asphalt Pavements*, Vol. 1, University of Michigan, Ann Arbor, pp. 483–496

Gao, Y., Geng, D., Huang, X., & Li, G. (2017). "Degradation evaluation index of asphalt pavement based on mechanical performance of asphalt mixture." *Construction and Building Materials*, 140, 75–81.

Garcia Cucalon, L., Kassem, E., Little, D. N., & Masad, E. (2017). "Fundamental evaluation of moisture damage in warm-mix asphalts." *Road Materials and Pavement Design*, *18*(January), 258–283.

Ghabchi, R., Singh, D., Zaman, M., & Tian, Q. (2013). "Mechanistic evaluation of the effect of WMA additives on wettability and moisture susceptibility properties of asphalt mixes." *Journal of Testing and Evaluation*, 41(6), 933-942.

Goli, H., & Latifi, M. (2020). “Evaluation of the effect of moisture on behavior of warm mix asphalt (WMA) mixtures containing recycled asphalt pavement (RAP).” *Construction and Building Materials*, 247, 118526.

Gupta, A., Castro-Fresno, D., Lastra-Gonzalez, P., & Rodriguez-Hernandez, J. (2021). “Selection of fibers to improve porous asphalt mixtures using multi-criteria analysis.” *Construction and Building Materials*, 266, 121198.

Haggag, M. M., Mogawer, W. S., & Bonaquist, R. (2011). “Fatigue evaluation of warm-mix asphalt mixtures: Use of uniaxial, cyclic, direct tension compression test.” *Transportation research record*, 2208(1), 26-32.

Hajj, E. Y., Morian, N., Tannoury, G. A. E., Manoharan, S., & Sebaaly, P. E. (2011). “Impact of lime application method on ravelling and moisture sensitivity in HMA mixtures.” *International Journal of Pavement Engineering*, 12(2), 149–160.

Hamzah, M. O., Kakar, M. R., Quadri, S. A., & Valentin, J. (2014). “Quantification of moisture sensitivity of warm mix asphalt using image analysis technique.” *Journal of Cleaner Production*, 68, 200–208.

Hamzah, M. O., Teh, S. Y., Golchin, B., & Voskuilen, J. (2017). “Use of imaging technique and direct tensile test to evaluate moisture damage properties of warm mix asphalt using response surface method.” *Construction and Building Materials*, 132, 323–334.

Hasan, Z., Hamid, B., Amir, I., & Danial, N. (2013). “Long term performance of warm mix asphalt versus hot mix asphalt.” *Journal of Central South University*, 20(1), 256–266.

Hernández Noguera, J. A., Rondón Quintana, H. A., & Fernández Gómez, W. D. (2014). “The influence of water on the oxidation of asphalt cements.” *Construction and Building Materials*, 71, 451–455.

Hill, B., Behnia, B., Buttlar, W. G., & Reis, H. (2013). “Evaluation of warm mix asphalt mixtures containing reclaimed asphalt pavement through mechanical performance tests and an acoustic emission approach.” *Journal of Materials in Civil Engineering*, 25(12), 1887-1897.

Huang, B., Shu, X., Dong, Q., & Shen, J. (2010). “Laboratory evaluation of moisture susceptibility of hot-mix asphalt containing cementitious fillers.” *Journal of Materials in Civil*

Engineering, 22(7), 667–673.

Hunter, R. N., Self, A., & Read, J. (2015). *The shell bitumen handbook*, ICE Publishing.

Hurley, G. C., & Prowell, B. D. (2006). *Evaluation of Evotherm for use in warm mix asphalt*, NCAT report, 6(02).

Huschek, S. (1985). "The Deformation Behavior of Asphalt Concrete under Triaxial Compression." *Journal of the Association of Asphalt Paving Technologists*, Vol. 54, pp. 407–431.

Ingevity Corporation. Evother-J1, 5255 Virginia Avenue, North Charleston, SC. http://www.ingevity.com/sustainability/product-benefits. (Last accessed 10 November 2018).

IRC: 111. (2009). *Specifications for dense graded bituminous mixes*, Indian Roads Congress (IRC), New Delhi, India.

IRC: SP 101. (2014). *Interim guidelines for warm mix asphalt*, Indian Roads Congress, New Delhi, India.

IS 1202. (1978). *Methods for Testing Tar and Bituminous Materials: Determination of Specific Gravity*, Bureau of Indian Standards, New Delhi, India.

IS 1203. (1978). *Methods for Testing Tar and Bituminous Materials: Determination of Penetration*, Bureau of Indian Standards, New Delhi, India.

IS 1205. (1978). *Methods for Testing Tar and Bituminous Materials: Determination of Softening point*, Bureau of Indian Standards, New Delhi, India.

IS 1208. (1978). *Methods for Testing Tar and Bituminous Materials: Determination of Ductility*, Bureau of Indian Standards, New Delhi, India.

IS 2386 -Part I. (1963). *Methods of Test for Aggregates for Concrete: Particle Size and Shape*, Bureau of Indian Standards, New Delhi, India.

IS 2386 -Part III. (1963). *Methods of Test for Aggregates for Concrete: Specific Gravity, Density, Voids, Absorption and Bulking*, New Delhi, India.

IS 2386 -Part IV. (1963). *Methods of Test for Aggregates for Concrete: Mechanical Properties*,

New Delhi, India.

IS 6241. (2003). *Method of test for determination of stripping value of road aggregates*, Bureau of Indian Standards, New Delhi, India.

Islam, M. R., & Tarefder, R. A. (2015). "Study of Asphalt Aging through Beam Fatigue Test." *Transportation Research Record*, 2505(1), 115–120.

Izadi, A., Motamedi, M., Alimi, R., & Nafar, M. (2018). "Effect of aging conditions on the fatigue behavior of hot and warm mix asphalt." *Construction and Building Materials*, 188, 119–129.

Jahanbakhsh, H., Karimi, M. M., Naseri, H., & Nejad, F. M. (2020). "Sustainable asphalt concrete containing high reclaimed asphalt pavements and recycling agents: Performance assessment, cost analysis, and environmental impact." *Journal of Cleaner Production*, 244, 118837.

Júnior, J. L. O. L., Babadopulos, L. F. A. L., & Soares, J. B. (2019). "Moisture-induced damage resistance, stiffness and fatigue life of asphalt mixtures with different aggregate-binder adhesion properties." *Construction and Building Materials*, 216, 166–175.

Kakade, V. B., Reddy, M. A., & Reddy, K. S. (2016). "Effect of aging on fatigue performance of hydrated lime modified bituminous mixes." *Construction and Building Materials*, 113, 1034-1043.

Kandhal, Prithvi S. (1992). *Moisture susceptibility of HMA mixes: identification of problem and recommended solutions*, Report No. 92-1, Auburn University, National Center for Asphalt Technology.

Kanitpong, K., & Bahia, H. (2005). "Relating adhesion and cohesion of asphalts to the effect of moisture on laboratory performance of asphalt mixtures." *Transportation Research Record*, 1901, 33–43.

Kaseer, F., Yin, F., Arámbula-Mercado, E., Epps Martin, A., Daniel, J. S., & Salari, S. (2018). "Development of an index to evaluate the cracking potential of asphalt mixtures using the semi-circular bending test." *Construction and Building Materials*, 167(February), 286–298.

Kassem, E., Garcia Cucalon, L., Masad, E., & Little, D. (2018). "Effect of warm mix additives on the interfacial bonding characteristics of asphalt binders." *International Journal of Pavement Engineering*, 19(12), 1111-1124.

Kenis, W. J. (1977). *Predictive design procedures, VESYS users manual*, Rep. No. FHWA-RD-77-154, Federal Highway Administration, McLean, Va.

Khattak, M. J., & Kyatham, V. (2008). "Viscoelastic behavior of hydrated lime-modified asphalt matrix and hot-mix asphalt under moisture damage conditions." *Transportation Research Record*, 2057, 64–74.

Khedr, S. A. (1986). "Deformation Mechanism in Asphaltic Concrete." *Journal of Transportation Engineering*, ASCE, Vol. 112, No. 1, pp. 29–45.

Kiggundu, Badru M., and Freddy L. Roberts. (1988). *Stripping in HMA mixtures: State-of-the-art and critical review of test methods*, Report No. 88-2, Auburn University, National Center for Asphalt Technology.

Kim, Y. R., Little, D. N., & Lytton, R. L. (2004). "Effect of moisture damage on material properties and fatigue resistance of asphalt mixtures." *Transportation Research Record*, 1891, 48–54.

Kim, Y.-R., Zhang, J., & Ban, H. (2012). "Moisture damage characterization of warm-mix asphalt mixtures based on laboratory-field evaluation." *Construction and Building Materials*, 204-211

Kringos, Niki, Scarpas, T., Kasbergen, C., & Selvadurai, P. (2008). "Modelling of combined physical-mechanical moisture-induced damage in asphaltic mixes, Part 1: Governing processes and formulations." *International Journal of Pavement Engineering*, 9(2), 115–128.

Lee, J. S., & Kim, Y. R. (2014). "Performance-based moisture susceptibility evaluation of warm-mix asphalt concrete through laboratory tests." *Transportation Research Record*, 2446, 17–28.

Lee, J. S., Lee, J. J., Kwon, S. A., & Kim, Y. (2013). "Use of cyclic direct tension tests and digital imaging analysis to evaluate moisture susceptibility of warm-mix asphalt concrete." *Transportation Research Record*, 2372, 61–71.

Leng, Z., Gamez, A., & Al-Qadi, I. L. (2014). “Mechanical property characterization of warm-mix asphalt prepared with chemical additives.” *Journal of Materials in Civil Engineering*, 26(2), 304-311

Li, Q., Lee, H. J., & Kim, T. W. (2012). “A simple fatigue performance model of asphalt mixtures based on fracture energy.” *Construction and Building Materials*, 27(1), 605–611.

Liang, Y., Wu, R., Harvey, J. T., Jones, D., & Alavi, M. Z. (2019). “Investigation into the Oxidative Aging of Asphalt Binders.” *Transportation Research Record*, 2673(6), 368–378.

Ling, C., Swiertz, D., Mandal, T., Teymourpour, P., & Bahia, H. (2017). “Sensitivity of the Illinois flexibility index test to mixture design factors.” *Transportation Research Record*, 2631,

Little, D. N., & Jones, I. V. (2003). *Chemical and mechanical processes of moisture damage in hot-mix asphalt pavements. Moisture Sensitivity of Asphalt Pavements,* A National SeminarCalifornia Department of Transportation; Federal Highway Administration*;* National Asphalt Pavement Association; California Asphalt Pavement Alliance; and Transportation Research Board.

Liu, G., Yang, T., Li, J., Jia, Y., Zhao, Y., & Zhang, J. (2018). “Effects of aging on rheological properties of asphalt materials and asphalt-filler interaction ability.” *Construction and Building Materials*, 168, 501–511.

Lopes, M., Zhao, D., Chailleux, E., Kane, M., Gabet, T., Petiteau, C., & Soares, J. (2014). “Characterisation of ageing processes on the asphalt mixture surface.” *Road Materials and Pavement Design*, 15(3), 477–487.

López-Montero, T., & Miró, R. (2016). “Differences in cracking resistance of asphalt mixtures due to ageing and moisture damage.” *Construction and Building Materials*, 112, 299–306.

Lu, D. X. & Saleh, M. (2016). “Laboratory evaluation of warm mix asphalt incorporating high RAP proportion by using evotherm and sylvaroad additives.” *Construction and Building Materials*, 114, 580-587.

Lu, X., & Isacsson, U. (2002). “Effect of ageing on bitumen chemistry and rheology.” *Construction and Building Materials*, 16(1), 15–22.

Lytton, R. L., et al. (1993). *Development and validation of performance prediction models and*

specifications for asphalt binders and paving mixes, Rep. No. SHRP-A-357, Strategic Highway Research Program, National Research Council, Washington, D.C.

Maggiore, C., Airey, G., & Marsac, P. (2014). "A dissipated energy comparison to evaluate fatigue resistance using 2-point bending." *Journal of Traffic and Transportation Engineering (English Edition)*, 1(1), 49-54.

Majidzadeh, K., Aly, M., Bayomy, F., and El-Laithy, A. (1980). *Implementation of a pavement design system, Vol. 1 and 2,* Final Rep. No. EES 578, The Ohio State Univ. Engineering Experiment Station, Columbus, Ohio.

Manrique-Sanchez, L., Caro, S., & Kim, Y.-R. (2020). "Coupled effects of ageing and moisture on the fracture properties of Permeable Friction Courses (PFC)." *International Journal of Pavement Engineering*, 1–13.

Meena, P. K., Saha, G., & Biligiri, K. P. (2016). "Estimation of Fatigue Life Using Resilient Moduli of Asphalt Mixtures." *Journal of Testing and Evaluation*, 44(1), 20140373.

Mehrara, A., & Khodaii, A. (2011). "Evaluation of asphalt mixtures' moisture sensitivity by dynamic creep test." *Journal of Materials in Civil Engineering*, 23(2), 212–219.

Mehrara, A., & Khodaii, A. (2017). "Moisture damage evaluation using energy based responses." *Journal of Civil Engineering and Management*, 23(1), 47–58.

Merusi, F., Caruso, A., Roncella, R., & Giuliani, F. (2010). "Moisture susceptibility and stripping resistance of asphalt mixtures modified with different synthetic waxes." *Transportation Research Record*, 2180, 110–120.

Miner, M. A. (1945). "Cumulative Damage in Fatigue." *Journal of Applied Mechanics.* Vol. 12 (9), pp. A159–A164.

Mirhosseini, A. F., Tahami, S. A., Hoff, I., Dessouky, S., & Ho, C. H. (2019). "Performance evaluation of asphalt mixtures containing high-RAP binder content and bio-oil rejuvenator." *Construction and Building Materials*, 227, 116465.

Modarres, A., & Aloogar, A. (2017). "Comparison between the fatigue response of hot and warm mix asphalts based on the dissipated energy approach." *International Journal of Pavement Engineering*, 18(1), 60–72.

Mogawer, W. S., Austerman, A. J., & Bahia, H. U. (2011). "Evaluating the effect of warm-mix asphalt technologies on moisture characteristics of asphalt binders and mixtures." *Transportation Research Record*, 2209(1), 52-60.

Moghadas Nejad, F., Azarhoosh, A., & Hamedi, G. H. (2014). "Effect of high density polyethylene on the fatigue and rutting performance of hot mix asphalt – a laboratory study." *Road Materials and Pavement Design*, 15(3), 746–756.

Mohammad, L., Hassan, M., & Cooper, S. (2012). "Mechanical characteristics of asphaltic mixtures containing titanium-dioxide photocatalyst." *Journal of Testing and Evaluation*, 40(6), 998-1005.

Monismith, C. L., Ogawa, N., and Freeme, C. R. (1975). "Permanent deformation characterization of subgrade soils due to repeated loading." *Transportation Research Record*, 537, Transportation Research Board, Washington, D.C., 1–17.

Monismith, C. L., R. G. Hicks, F. N. Finn, J. Sousa, J. Harvey, S. Weissman, J. Deacon, J. Coplantz, and G. Paulsen. (1994). *Permanent Deformation Response of Asphalt Aggregate Mixes*, SHRP-A-415. TRB, National Research Council, Washington, D.C.

Montgomery, D. C., & Runger, G. C. (2010). *Applied statistics and probability for engineers*, John Wiley & Sons, New Jersey, US

Moreno-Navarro, Fernando, Sol-Sánchez, M., García-Travé, G., & Rubio-Gámez, M. C. (2018). "Fatigue cracking in asphalt mixtures: the effects of ageing and temperature." *Road Materials and Pavement Design*, 19(3), 561–570.

MORTH. (2001). *Specifications for road and bridge works (fourth revision)*, Indian Roads Congress, New Delhi, India.

MORTH. (2013). *Specifications for road and bridge works (fifth revision)*, Indian Roads Congress, New Delhi, India.

Nazzal, M. D., Sargand, S., & Al-Rawashdeh, A. (2011). "Evaluation of warm mix asphalt mixtures containing RAP using accelerated loading tests." *Journal of Testing and Evaluation*, 39(3), 305-312

Nejad, F. M., Aflaki, E., & Mohammadi, M. A. (2010). "Fatigue behavior of SMA and HMA

mixtures." *Construction and Building Materials*, 24(7), 1158-1165.

Nejad, F. M., Azarhoosh, A., Hamedi, G. H., & Roshani, H. (2014). "Rutting performance prediction of warm mix asphalt containing reclaimed asphalt pavements." *Road Materials and Pavement Design*, 15, 207–219.

Nemati, R., Haslett, K., Dave, E. V., & Sias, J. E. (2019). "Development of a rate-dependent cumulative work and instantaneous power-based asphalt cracking performance index." *Road Materials and Pavement Design*, 20(1), S315–S331.

Newcomb, D., Martin, A.E., Yin, F., Arambula, E., Park, E.S., Chowdhury, A., Brown, R., Rodezno, C., Tran, N., Coleri, E., Jones, D., Harvey, J.T., and Signore, J.M. (2015). *Short-Term Laboratory Conditioning of Asphalt Mixtures*, Washington, DC: The National Academies Press.

Othman, M. H., & Omranian, S. R. (2015). "Effects of short term aging on dynamic creep properties of asphalt mixtures." *Jurnal Teknologi (Sciences and Engineering)*, 14, 91–97.

Pakenari, M. M., & Hamedi, G. H. (2021). "Investigating the Effective Laboratory Parameters on the Stiffness Modulus and Fatigue Cracking of Warm Mix Asphalt." *International Journal of Civil Engineering*, 1-14.

Pan, P., Kuang, Y., Hu, X., & Zhang, X. (2018). "A Comprehensive Evaluation of Rejuvenator on Mechanical Properties, Durability, and Dynamic Characteristics of Artificially Aged Asphalt Mixture." *Materials (Basel, Switzerland)*, 11(9), 1554.

Perraton, D., Touhara, R., Di Benedetto, H., & Carter, A. (2015). "Ability of the classical fatigue criterion to be associated with macro-crack growth." *Materials and Structures/Materiaux et Constructions*, 48(8), 2383–2395. https://doi.org/10.1617/s11527-014-0321-8

Petersen, J. (1984). "Chemical composition of asphalt as related to asphalt durability: state of the art." *Transportation research Board*, Washington, D. C., pp 13-30.

Petersen, J. C. (2000). "Chapter 14 Chemical Composition of Asphalt as Related to Asphalt Durability." *Developments in Petroleum Science,* Vol. 40, (B).

Petersen, J. C. (2009). "A review of the fundamentals of asphalt oxidation: chemical,

physicochemical, physical property, and durability relationships." *Transportation Research Board,* E-Circular, E-C140.

Phan, T. M., Nguyen, S. N., Seo, C. B., & Park, D. W. (2021). "Effect of treated fibers on performance of asphalt mixture." *Construction and Building Materials*, 274, 122051.

Pouranian, M. R., Imaninasab, R., & Shishehbor, M. (2020). "The effect of temperature and stress level on the rutting performance of modified stone matrix asphalt." *Road Materials and Pavement Design*, 21(5), 1386–1398.

Praveen, K., & P., A. (2012). "Laboratory Study on Moisture Susceptibility of Dense Graded Mixes." *Journal of Transportation Engineering*, 138(1), 105–113.

Prowell, B. D., Brown, E. R., Anderson, R. M., Daniel, J. S., Swamy, A. K., Quintus, H. V., Shen, S., Carpenter, S. H., Bhattacharjee, S., & Maghsoodloo, S. (2010). *Validating the Fatigue Endurance Limit for Hot Mix Asphalt*, Washington, DC: The National Academies Press.

Punith, V. S., Xiao, F., & Amirkhanian, S. N. (2012). "Effects of lime content on moisture susceptibility of rubberized stone matrix asphalt mixtures using warm mix additives in terms of statistical analysis." *Journal of materials in civil engineering*, 24(12), 1431-1440.

Radhakrishnan, V., Sri, M.R., and Reddy, K.S. (2020). "Sensitivity of rutting and moisture resistance of asphalt mixes to gradation and design air void content." *International Journal of Pavement Engineering*, *21*(9), 1035–1043.

Rahman, M. M., Airey, G. D., & Collop, A. C. (2010). "Moisture Susceptibility of High and Low Compaction Dry Process Crumb Rubber–Modified Asphalt Mixtures." *Transportation Research Record,* 2180(1), 121–129.

Rodezno, M. C., West, R., & Taylor, A. (2015). "Flow Number Test and Assessment of AASHTO TP 79-13 Rutting Criteria: Comparison of rutting performance of hot-mix and warm-mix asphalt mixtures." *Transportation Research Record: Journal of the Transportation Research Board,* 100-107.

Roque, R., Birgisson, B., Sangpetngam, B., & Zhang, Z. (2002). "Hot mix asphalt fracture mechanics: a fundamental crack growth law for asphalt mixtures." *Journal of the Association of Asphalt Paving Technologists,* 71, 957–1064.

Rowe, G. M., & Bouldin, M. G. (2000). "Improved techniques to evaluate the fatigue resistance of asphaltic mixtures." *2nd Eurasphalt & Eurobitume Congress*, Barcelona, Vol. 2000.

Saeidi, H., & Aghayan, I. (2016). "Investigating the effects of aging and loading rate on low-temperature cracking resistance of core-based asphalt samples using semi-circular bending test." *Construction and Building Materials*, 126, 682–690.

Safaei, F., & Castorena, C. (2016). "Temperature Effects of Linear Amplitude Sweep Testing and Analysis." *Transportation Research Record*, 2574(1), 92–100.

Saha, G., & Biligiri, K. P. (2019). "Investigation of Crack Initiation Behavior of Asphalt Mixtures: Fatigue through Dynamic Semicircular Bending Test." *Journal of Testing and Evaluation*, 47(5), 20180668.

Said, S. F. (2005). "Aging Effect on Mechanical Characteristics of Bituminous Mixtures." *Transportation Research Record, Journal of the Transportation Research Board*, 1901(1), 1–9.

Sarkar, A. (2017). "Combined effect of loading pattern, pulse duration, and stress level on the cyclic creep test of asphalt mixture." *Journal of Materials in Civil Engineering*, 29(1), 1–8.

Sebaaly, P. E., Hajj, E. Y., & Piratheepan, M. (2015). "Evaluation of selected warm mix asphalt technologies." *Road Materials and Pavement Design*, 16(1), 475-486.

Sebaaly, P. E., Hajj, E. Y., Sathanathan, T., & Shivakolunthar, S. (2017). "A comprehensive evaluation of moisture damage of asphalt concrete mixtures." *International Journal of Pavement Engineering*, 18(2), 171–184.

Shell Pavement Design Manual. (1978). *Asphalt Pavements and Overlays for Road Traffic*, Shell International Petroleum Company Limited, London, England.

Shen, S., Airey, G. D., Carpenter, S. H., & Huang, H. (2006). "A dissipated energy approach to fatigue evaluation." *Road Materials and Pavement Design*, 7(1), 47–69.

Shu, X., Huang, B., & Vukosavljevic, D. (2008). Laboratory evaluation of fatigue characteristics of recycled asphalt mixture. *Construction and Building Materials*, 22(7), 1323–1330.

Singh, P., & Swamy, A. K. (2017). "Probabilistic characterisation of damage characteristic curve of asphalt concrete mixtures." *International Journal of Pavement Engineering*, 20(6), 659-668.

Smith, B. T., & Howard, I. L. (2019). "Comparing laboratory conditioning protocols to longer-term aging of asphalt mixtures in the southeast United States." *Journal of Materials in Civil Engineering*, 31(1).

Sreedhar, S., & Coleri, E. (2020). "The effect of long-term aging on fatigue cracking resistance of asphalt mixtures." *International Journal of Pavement Engineering*, 1–13.

Stuart, Kevin D. (1990). *Moisture damage in asphalt mixtures-a state-of-the-art report*, FHWA-RD-90-019, United States, Federal Highway Administration.

Taherkhani, H., & Noorian, F. (2020). "Comparing the effects of waste engine and cooking oil on the properties of asphalt concrete containing reclaimed asphalt pavement (RAP)." *Road Materials and Pavement Design*, 21(5), 1238-1257.

Tangella, S. R., Craus, J., Deacon, J. A., & Monismith, C. L. (1990). *Summary report on fatigue response of asphalt mixtures,* Strategic Highway Research Program, No. SHRP-A-312, Washington, DC.

Tanzadeh, J., Gamasaei, R.S., and Gilani, F.R., (2020). "Laboratory Evaluation on the Performance Comparison between OGFC Asphalt Reinforcement with Fibers and Modified with Nanosilica."

Tapsoba, N., Sauzéat, C., & Di Benedetto, H. (2013). "Analysis of fatigue test for bituminous mixtures." *Journal of Materials in Civil Engineering*, 25(6), 701–710.

Tayebali, A. A., Deacon, J. A., Coplantz, J. S., Harvey, J. T., and Monismith, C. L. (1994) *Fatigue Response of Asphalt-Aggregate Mixes*, SHRP A-404, TRB, National Research Council, Washington, D.C.

Tayebali, A. A., Kusam, A., & Bacchi, C. (2018). "An Innovative Method for Interpretation of Asphalt Boil Test." *Journal of Testing and Evaluation*, 46(4), 20160383.

Tong, Y., Luo, R., & Lytton, R. L. (2013). "Modeling water vapor diffusion in pavement and its influence on fatigue crack growth of fine aggregate mixture." *Transportation Research*

Record, 2373, 71–80.

Tong, Y., Luo, R., & Lytton, R. L. (2015). "Moisture and aging damage evaluation of asphalt mixtures using the repeated direct tensional test method." *International Journal of Pavement Engineering*, 16(5), 397–410.

Traxler RN. (1963). "Durability of asphalt cements." *Proceedings of the Association of Asphalt Paving Technologists*, 32: 44–63.

Tseng, K. H., and R. L. Lytton. (1989). "Prediction of Permanent Deformation in Flexible Pavement Materials." *Implication of Aggregate in Design, Construction and Performance of Flexible Pavements,* ASTM STP 1016, ASTM, Philadelphia, pp. 154–172.

Vargas-Nordcbeck, A., Leiva-Villacorta, F., Aguiar-Moya, J. P., & Loria-Salazar, L. (2016). "Evaluating moisture susceptibility of asphalt concrete mixtures through simple performance tests." *Transportation Research Record*, 2575(2575), 70–78.

Vuorinen, M., & Hartikainen, O. P. (2001). "A New Ultrasonic Method for Measuring Stripping Resistance of Bitumen on Aggregate." *Road Materials and Pavement Design*, 2(3), 297–309.

Walubita, L. F., Faruk, A. N., Alvarez, A. E., & Scullion, T. (2013). "The Overlay Tester (OT): Using the Fracture Energy Index concept to analyze the OT monotonic loading test data." *Construction and Building Materials*, 40, 802-811.

Wang, C., Hao, P., Ruan, F., Zhang, X., & Adhikari, S. (2013). "Determination of the production temperature of warm mix asphalt by workability test." *Construction and Building Materials*, 48, 1165-1170.

Wang, D., Falchetto, A. C., Moon, K. H., Riccardi, C., Pei, J., & Wen, Y. (2019). "Artificially prepared Reclaimed Asphalt Pavement (RAP)—an experimental investigation on re-recycling." *Environmental Science and Pollution Research*, 26(35), 35620-35628.

Wang, X., Gu, X., Ni, F., Deng, H., & Dong, Q. (2018). "Rutting resistance of porous asphalt mixture under coupled conditions of high temperature and rainfall." *Construction and Building Materials*, 174, 293–301.

Wen, H. (2013). "Use of fracture work density obtained from indirect tensile testing for the

mix design and development of a fatigue model." *International Journal of Pavement Engineering*, 14(6), 561–568.

Wen, H., & Kim, Y. R. (2002). "Simple performance test for fatigue cracking and validation with WesTrack mixtures." *Transportation Research Record*, 1789, 66–72.

Witczak, M. W., K. Kaloush, T. Pellinen, M. El-Basyouny, and H. Von Quintus. (2002). *NCHRP Report 465: Simple Performance Test for SuperpaveMix Design*, TRB, National Research Council, Washington, D.C.

Wu, H., Huang, B., & Shu, X. (2014). "Characterizing fatigue behavior of asphalt mixtures utilizing loaded wheel tester." *Journal of materials in civil engineering*, 26(1), 152-159.

Wu, S., Pang, L., Liu, G., & Zhu, J. (2010). "Laboratory study on ultraviolet radiation aging of bitumen." *Journal of Materials in Civil Engineering*, 22(8), 767–772.

Xie, J., Xiao, Y., Wu, S., & Huang, J. (2012). "Research on fracture characteristic of gneiss prepared asphalt mixture with direct tensile test." *Construction and Building Materials*, 28(1), 476–481.

Xie, Z., Shen, J., Fan, W., & Wang, L. (2014). "Laboratory investigation of the effect of warm mix asphalt (WMA) additives on the properties of WMA used in China." *Journal of Testing and Evaluation*, 42(5), 1165-1172.

Yilmaz, M., Kök, B. V., & Kuloğu, N. (2013). "Investigation of mechanical properties of short- and long-term aged asphaltite modified asphalt mixtures." *Journal of Materials in Civil Engineering*, 25(5), 563–572.

Yin, F., Arámbula-Mercado, E., Epps Martin, A., Newcomb, D., & Tran, N. (2017). "Long-term ageing of asphalt mixtures." *Road Materials and Pavement Design*, 18(1), 2–27.

Yongli, X., Enhao, Z., & Liyan, S. (2019). "Effect of SARA on Rheological Properties of Asphalt Binders." *Journal of Materials in Civil Engineering*, 31(6), 4019086.

Yousif, R. A., Muniandy, R., Hassim, S., & Jakarni, F. (2018). "Effect of steam aging on performance-related properties of hot asphalt mixture." *Journal of Materials in Civil Engineering*, 30(3), 1–8.

Yuan, Y., Zhu, X., & Chen, L. (2020). “Relationship among cohesion, adhesion, and bond strength: From multi-scale investigation of asphalt-based composites subjected to laboratory-simulated aging.” *Materials & Design*, 185, 108272.

Zhang, J., Airey, G. D., Grenfell, J., & Apeagyei, A. K. (2017). “Moisture damage evaluation of aggregate–bitumen bonds with the respect of moisture absorption, tensile strength and failure surface.” *Road Materials and Pavement Design*, 18(4), 833–848.

Zhang, J., Apeagyei, A. K., Airey, G. D., & Grenfell, J. R. A. (2015). “Influence of aggregate mineralogical composition on water resistance of aggregate-bitumen adhesion.” *International Journal of Adhesion and Adhesives*, 62, 45–54.

Zhang, Z., Roque, R., & Birgisson, B. (2001). “Evaluation of laboratory-measured crack growth rate for asphalt mixtures.” *Transportation Research Record*, 1767(1), 67-75.4

Zhou, F., & Scullion, T. (2002). “Discussion: Three Stages of Permanent Deformation Curve and Rutting Model.” *International Journal of Pavement Engineering*, 3(4), 251–260.

Zhou, F., Im, S., Sun, L., & Scullion, T. (2017). “Development of an IDEAL cracking test for asphalt mix design and QC/QA.” *Asphalt Paving Technology: Association of Asphalt Paving Technologists-Proceedings of the Technical Sessions*, 86(0), 549–577.

Zhou, F., Scullion, T., & Sun, L. (2004). “Verification and modeling of three-stage permanent deformation behavior of asphalt mixes.” *Journal of Transportation Engineering*, 130(4), 486–494.

Zhu, G. J., Wu, S. P., Liu, R., & Zhou, L. (2009). “Study on the Fatigue Property for Aged Asphalt Mixtures by Using Four Point Bending Tests.” *Materials Science Forum*, 614, 289–294.

Ziari, H., Amini, A., & Goli, A. (2020). “The effect of different aging conditions and strain levels on relationship between fatigue life of asphalt binders and mixtures.” *Construction and Building Materials*, 244, 118345.

Zou, J., Isola, M., Roque, R., Chun, S., Koh, C., & Lopp, G. (2013). “Effect of hydrated lime on fracture performance of asphalt mixture.” *Construction and Building Materials*, 44, 302–308.

Appendix A

Statistical Analysis of test results: Chapter 6

Table A.1 One-way ANOVA of ITSM of HMA-A mixture at 15 °C

Factor	DF	Sum of squares	Mean square	F value	Prob>F
Between groups	5	2.0E+07	4.1E+06	7.4E+01	1.3E-08
Within groups	12	6.6E+05	5.5E+04		
Total	17	2.1E+07			

Table A.2 Tukey's post-hoc test of ITSM of HMA-A mixture at 15 °C

Condition	Mean difference	Std. error	q Value	p-value	95% confidence interval	
					Lower bound	Upper bound
STA-1FT~STA-UC	-1239	191	9.17	3.3E-04	-1880	-597
STA-3FT~STA-UC	-2113	191	15.65	1.3E-06	-2755	-1471
STA-3FT~STA-1FT	-874	191	6.47	6.5E-03	-1516	-233
LTA-UC~STA-UC	823	191	6.09	1.0E-02	181	1465
LTA-UC~STA-1FT	2062	191	15.27	1.8E-06	1420	2703
LTA-UC~STA-3FT	2936	191	21.74	9.6E-07	2294	3578
LTA-1FT~STA-UC	-251	191	1.86	7.7E-01	-893	390
LTA-1FT~STA-1FT	987	191	7.31	2.5E-03	346	1629
LTA-1FT~STA-3FT	1862	191	13.79	5.5E-06	1220	2503
LTA-1FT~LTA-UC	-1074	191	7.96	1.2E-03	-1716	-433
LTA-3FT~STA-UC	-1938	191	14.35	3.5E-06	-2579	-1296
LTA-3FT~STA-1FT	-699	191	5.18	3.0E-02	-1341	-57
LTA-3FT~STA-3FT	175	191	1.30	9.3E-01	-466	817
LTA-3FT~LTA-UC	-2761	191	20.44	2.5E-07	-3402	-2119
LTA-3FT~LTA-1FT	-1686	191	12.49	1.6E-05	-2328	-1045

Table A.3 One-way ANOVA of ITSM of HMA-B mixture at 15 °C

Factor	DF	Sum of squares	Mean square	F value	Prob>F
Between groups	5	3.8E+07	7.5E+06	1.4E+02	3.9E-10
Within groups	12	6.6E+05	5.5E+04		
Total	17	3.8E+07			

Table A.4 Tukey's post-hoc test of ITSM of HMA-B mixture at 15 °C

Condition	Mean difference	Std. error	q Value	p-value	95% confidence interval	
					Lower bound	Upper bound
STA-1FT~STA-UC	-2285	192	16.82	5.6E-07	-2931	-1640
STA-3FT~STA-UC	-2883	192	21.21	2.6E-07	-3529	-2237
STA-3FT~STA-1FT	-598	192	4.40	7.6E-02	-1243	48
LTA-UC~STA-UC	1347	192	9.91	1.6E-04	701	1992
LTA-UC~STA-1FT	3632	192	26.72	0.0E+00	2986	4278
LTA-UC~STA-3FT	4230	192	31.12	0.0E+00	3584	4875
LTA-1FT~STA-UC	-1159	192	8.53	6.5E-04	-1805	-513
LTA-1FT~STA-1FT	1126	192	8.29	8.4E-04	481	1772
LTA-1FT~STA-3FT	1724	192	12.69	1.3E-05	1078	2370
LTA-1FT~LTA-UC	-2506	192	18.44	2.4E-07	-3151	-1860
LTA-3FT~STA-UC	-1992	192	14.66	2.8E-06	-2638	-1346
LTA-3FT~STA-1FT	293	192	2.16	6.6E-01	-352	939
LTA-3FT~STA-3FT	891	192	6.56	5.9E-03	245	1537
LTA-3FT~LTA-UC	-3339	192	24.57	2.4E-07	-3984	-2693
LTA-3FT~LTA-1FT	-833	192	6.13	9.7E-03	-1479	-187

Table A.5 One-way ANOVA of ITSM of WMA-A mixture at 15 °C

Factor	DF	Sum of squares	Mean square	F value	Prob>F
Between groups	5	1.9E+07	3.8E+06	4.4E+01	2.7E-07
Within groups	12	1.1E+06	8.8E+04		
Total	17	2.0E+07			

Table A.6 Tukey's post-hoc test of ITSM of WMA-A mixture at 15 °C

Condition	Mean difference	Std. error	q Value	p-value	95% confidence interval	
					Lower bound	Upper bound
STA-1FT~STA-UC	-496	242	2.90	3.7E-01	-1308	317
STA-3FT~STA-UC	-1423	242	8.32	8.1E-04	-2235	-610
STA-3FT~STA-1FT	-927	242	5.42	2.3E-02	-1739	-115
LTA-UC~STA-UC	1645	242	9.62	2.1E-04	833	2458
LTA-UC~STA-1FT	2141	242	12.52	1.5E-05	1329	2953
LTA-UC~STA-3FT	3068	242	17.94	3.2E-07	2256	3880
LTA-1FT~STA-UC	1208	242	7.06	3.3E-03	396	2021
LTA-1FT~STA-1FT	1704	242	9.96	1.5E-04	892	2516
LTA-1FT~STA-3FT	2631	242	15.38	1.6E-06	1819	3443
LTA-1FT~LTA-UC	-437	242	2.55	5.0E-01	-1249	375

Condition	Mean difference	Std. error	q Value	p-value	95% confidence interval	
					Lower bound	Upper bound
LTA-3FT~STA-UC	614	242	3.59	1.9E-01	-198	1427
LTA-3FT~STA-1FT	1110	242	6.49	6.3E-03	298	1922
LTA-3FT~STA-3FT	2037	242	11.91	2.6E-05	1225	2849
LTA-3FT~LTA-UC	-1031	242	6.03	1.1E-02	-1843	-219
LTA-3FT~LTA-1FT	-594	242	3.47	2.1E-01	-1406	218

Table A.7 One-way ANOVA of ITSM of WMA-B mixture at 15°C

Factor	DF	Sum of squares	Mean square	F value	Prob>F
Between groups	5	1.4E+07	2.8E+06	4.2E+01	3.4E-07
Within groups	12	8.0E+05	6.7E+04		
Total	17	1.5E+07			

Table A.8 Tukey's post-hoc test of ITSM of WMA-B mixture at 15 °C

Condition	Mean difference	Std. error	q Value	p-value	95% confidence interval	
					Lower bound	Upper bound
STA-1FT~STA-UC	-1437	211	9.64	2.1E-04	-2145	-729
STA-3FT~STA-UC	-1842	211	12.36	1.7E-05	-2550	-1135
STA-3FT~STA-1FT	-405	211	2.72	4.3E-01	-1113	302
LTA-UC~STA-UC	822	211	5.52	2.0E-02	114	1530
LTA-UC~STA-1FT	2259	211	15.16	1.9E-06	1551	2967
LTA-UC~STA-3FT	2664	211	17.88	3.3E-07	1957	3372
LTA-1FT~STA-UC	-497	211	3.34	2.4E-01	-1205	210
LTA-1FT~STA-1FT	940	211	6.31	7.9E-03	232	1647
LTA-1FT~STA-3FT	1345	211	9.03	3.9E-04	637	2053
LTA-1FT~LTA-UC	-1319	211	8.85	4.6E-04	-2027	-612
LTA-3FT~STA-UC	-738	211	4.95	3.9E-02	-1446	-30
LTA-3FT~STA-1FT	699	211	4.69	5.4E-02	-9	1407
LTA-3FT~STA-3FT	1104	211	7.41	2.2E-03	397	1812
LTA-3FT~LTA-UC	-1560	211	10.47	9.4E-05	-2268	-852
LTA-3FT~LTA-1FT	-241	211	1.62	8.5E-01	-948	467

Table A.9 One-way ANOVA of ITSM of HMA-A mixture at 25 °C

Factor	DF	Sum of squares	Mean square	F value	Prob>F
Between groups	5	2.39E+07	4.77E+06	132.73	4.50E-10
Within groups	12	4.32E+05	3.60E+04		
Total	17	2.43E+07			

Table A.10 Tukey's post-hoc test of ITSM of HMA-A mixture at 25 °C

Condition	Mean difference	Std. error	q Value	p-value	95% confidence interval	
					Lower bound	Upper bound
STA-1FT~STA-UC	-924	155	8.44	7.2E-04	-1444	-404
STA-3FT~STA-UC	-2479	155	22.64	1.0E-06	-2999	-1959
STA-3FT~STA-1FT	-1555	155	14.20	4.0E-06	-2075	-1035
LTA-UC~STA-UC	1327	155	12.12	2.1E-05	807	1847
LTA-UC~STA-1FT	2251	155	20.56	2.5E-07	1731	2771
LTA-UC~STA-3FT	3806	155	34.76	0.0E+00	3286	4326
LTA-1FT~STA-UC	-25	155	0.23	1.0E+00	-545	495
LTA-1FT~STA-1FT	899	155	8.21	9.2E-04	379	1419
LTA-1FT~STA-3FT	2454	155	22.41	9.9E-07	1934	2974
LTA-1FT~LTA-UC	-1352	155	12.35	1.8E-05	-1872	-832
LTA-3FT~STA-UC	-727	155	6.64	5.3E-03	-1247	-207
LTA-3FT~STA-1FT	196	155	1.79	8.0E-01	-324	716
LTA-3FT~STA-3FT	1751	155	16.00	1.0E-06	1231	2271
LTA-3FT~LTA-UC	-2055	155	18.77	2.0E-07	-2575	-1535
LTA-3FT~LTA-1FT	-702	155	6.41	6.9E-03	-1222	-182

Table A.11 One-way ANOVA of ITSM of HMA-B mixture at 25 °C

Factor	DF	Sum of squares	Mean square	F value	Prob>F
Between groups	5	4.11E+07	8.23E+06	269.05	6.92E-12
Within groups	12	3.67E+05	3.06E+04		
Total	17	4.15E+07			

Table A.12 Tukey's post-hoc test of ITSM of HMA-B mixture at 25 °C

Condition	Mean difference	Std. error	q Value	p-value	95% confidence interval	
					Lower bound	Upper bound
STA-1FT~STA-UC	-1276	143	12.64	1.4E-05	-1756	-797
STA-3FT~STA-UC	-2168	143	21.48	9.6E-07	-2648	-1689
STA-3FT~STA-1FT	-892	143	8.84	4.7E-04	-1372	-412
LTA-UC~STA-UC	2514	143	24.91	2.4E-07	2035	2994
LTA-UC~STA-1FT	3791	143	37.55	0.0E+00	3311	4270
LTA-UC~STA-3FT	4683	143	46.38	0.0E+00	4203	5162
LTA-1FT~STA-UC	-550	143	5.45	2.2E-02	-1030	-71
LTA-1FT~STA-1FT	726	143	7.19	2.8E-03	246	1206
LTA-1FT~STA-3FT	1618	143	16.03	1.0E-06	1138	2098
LTA-1FT~LTA-UC	-3065	143	30.36	0.0E+00	-3544	-2585
LTA-3FT~STA-UC	-1493	143	14.79	2.5E-06	-1973	-1013
LTA-3FT~STA-1FT	-217	143	2.15	6.6E-01	-696	263
LTA-3FT~STA-3FT	675	143	6.69	5.0E-03	196	1155
LTA-3FT~LTA-UC	-4007	143	39.69	0.0E+00	-4487	-3528
LTA-3FT~LTA-1FT	-943	143	9.34	2.8E-04	-1422	-463

Table A.13 One-way ANOVA of ITSM of WMA-A mixture at 25 °C

Factor	DF	Sum of squares	Mean square	F value	Prob>F
Between groups	5	9.50E+06	1.90E+06	85.13	6.01E-09
Within groups	12	2.68E+05	2.23E+04		
Total	17	9.77E+06			

Table A.14 Tukey's post-hoc test of ITSM of WMA-A mixture at 25 °C

Condition	Mean difference	Std. error	q Value	p-value	95% confidence interval	
					Lower bound	Upper bound
STA-1FT~STA-UC	-678	122	7.86	1.3E-03	-1088	-268
STA-3FT~STA-UC	-1358	122	15.74	1.2E-06	-1767	-948
STA-3FT~STA-1FT	-680	122	7.88	1.3E-03	-1089	-270
LTA-UC~STA-UC	1040	122	12.05	2.3E-05	630	1449
LTA-UC~STA-1FT	1718	122	19.91	1.1E-07	1308	2127
LTA-UC~STA-3FT	2397	122	27.79	0.0E+00	1988	2807
LTA-1FT~STA-UC	-104	122	1.21	9.5E-01	-514	306
LTA-1FT~STA-1FT	574	122	6.65	5.2E-03	164	984
LTA-1FT~STA-3FT	1254	122	14.53	3.1E-06	844	1663
LTA-1FT~LTA-UC	-1144	122	13.26	8.3E-06	-1553	-734
LTA-3FT~STA-UC	-91	122	1.05	9.7E-01	-500	319

Condition	Mean difference	Std. error	q Value	p-value	95% confidence interval	
					Lower bound	Upper bound
LTA-3FT~STA-1FT	587	122	6.81	4.4E-03	178	997
LTA-3FT~STA-3FT	1267	122	14.69	2.7E-06	857	1677
LTA-3FT~LTA-UC	-1130	122	13.11	9.4E-06	-1540	-721
LTA-3FT~LTA-1FT	13	122	0.15	1.0E+00	-396	423

Table A.15 One-way ANOVA of ITSM of WMA-B mixture at 25 °C

Factor	DF	Sum of squares	Mean square	F value	Prob>F
Between groups	5	2.52E+07	5.04E+06	192.68	5.00E-11
Within groups	12	3.14E+05	2.61E+04		
Total	17	2.55E+07			

Table A.16 Tukey's post-hoc test of ITSM of WMA-B mixture at 25 °C

Condition	Mean difference	Std. error	q Value	p-value	95% confidence interval	
					Lower bound	Upper bound
STA-1FT~STA-UC	-956	132	10.24	1.2E-04	-1400	-513
STA-3FT~STA-UC	-1743	132	18.67	2.1E-07	-2187	-1300
STA-3FT~STA-1FT	-787	132	8.43	7.2E-04	-1230	-344
LTA-UC~STA-UC	2059	132	22.06	9.8E-07	1616	2503
LTA-UC~STA-1FT	3016	132	32.30	0.0E+00	2572	3459
LTA-UC~STA-3FT	3803	132	40.73	0.0E+00	3359	4246
LTA-1FT~STA-UC	351	132	3.76	1.6E-01	-92	795
LTA-1FT~STA-1FT	1308	132	14.01	4.6E-06	864	1751
LTA-1FT~STA-3FT	2095	132	22.44	9.9E-07	1651	2538
LTA-1FT~LTA-UC	-1708	132	18.30	2.6E-07	-2151	-1265
LTA-3FT~STA-UC	-395	132	4.23	9.1E-02	-839	48
LTA-3FT~STA-1FT	561	132	6.01	1.1E-02	118	1004
LTA-3FT~STA-3FT	1348	132	14.44	3.3E-06	905	1791
LTA-3FT~LTA-UC	-2455	132	26.29	0.0E+00	-2898	-2011
LTA-3FT~LTA-1FT	-747	132	8.00	1.2E-03	-1190	-303

Table A.17 One-way ANOVA of ITFT of HMA-A mixture at 15 °C

Factor	DF	Sum of squares	Mean square	F value	Prob>F
Between groups	5	2.99E+10	5.97E+09	100.64	2.27E-09
Within groups	12	7.12E+08	5.93E+07		
Total	17	3.06E+10			

Table A.18 Tukey's post-hoc test of ITFT of HMA-A mixture at 15 °C

Condition	Mean difference	Std. error	q Value	p-value	95% confidence interval	
					Lower bound	Upper bound
STA-1FT~STA-UC	-31045	6289	6.98	3.6E-03	-52169	-9921
STA-3FT~STA-UC	-63544	6289	14.29	3.7E-06	-84668	-42420
STA-3FT~STA-1FT	-32498	6289	7.31	2.5E-03	-53622	-11374
LTA-UC~STA-UC	42393	6289	9.53	2.3E-04	21269	63517
LTA-UC~STA-1FT	73438	6289	16.51	7.0E-07	52314	94562
LTA-UC~STA-3FT	105937	6289	23.82	2.4E-07	84813	127061
LTA-1FT~STA-UC	-61034	6289	13.72	5.7E-06	-82158	-39910
LTA-1FT~STA-1FT	-29989	6289	6.74	4.7E-03	-51113	-8865
LTA-1FT~STA-3FT	2510	6289	0.56	1.0E+00	-18614	23634
LTA-1FT~LTA-UC	-103427	6289	23.26	2.4E-07	-124551	-82303
LTA-3FT~STA-UC	-71524	6289	16.08	9.6E-07	-92648	-50400
LTA-3FT~STA-1FT	-40479	6289	9.10	3.6E-04	-61603	-19355
LTA-3FT~STA-3FT	-7981	6289	1.79	8.0E-01	-29105	13143
LTA-3FT~LTA-UC	-113917	6289	25.62	9.8E-08	-135041	-92793
LTA-3FT~LTA-1FT	-10490	6289	2.36	5.7E-01	-31614	10634

Table A.19 One-way ANOVA of ITFT of HMA-B mixture at 15 °C

Factor	DF	Sum of squares	Mean square	F value	Prob>F
Between groups	5	3.01E+10	6.01E+09	190.99	5.27E-11
Within groups	12	3.78E+08	3.15E+07		
Total	17	3.04E+10			

Table A.20 Tukey's post-hoc test of ITFT of HMA-B mixture at 15 °C

Condition	Mean difference	Std. error	q Value	p-value	95% confidence interval	
					Lower bound	Upper bound
STA-1FT~STA-UC	-53669	4580	16.57	6.7E-07	-69054	-38283
STA-3FT~STA-UC	-68165	4580	21.05	2.5E-07	-83551	-52780
STA-3FT~STA-1FT	-14497	4580	4.48	6.9E-02	-29882	889
LTA-UC~STA-UC	38373	4580	11.85	2.7E-05	22987	53758
LTA-UC~STA-1FT	92041	4580	28.42	0.0E+00	76656	107427
LTA-UC~STA-3FT	106538	4580	32.89	0.0E+00	91153	121923
LTA-1FT~STA-UC	-64389	4580	19.88	1.1E-07	-79774	-49004
LTA-1FT~STA-1FT	-10720	4580	3.31	2.5E-01	-26106	4665
LTA-1FT~STA-3FT	3776	4580	1.17	9.6E-01	-11609	19162
LTA-1FT~LTA-UC	-102762	4580	31.73	0.0E+00	-118147	-87376
LTA-3FT~STA-UC	-68212	4580	21.06	2.5E-07	-83598	-52827
LTA-3FT~STA-1FT	-14544	4580	4.49	6.8E-02	-29929	842
LTA-3FT~STA-3FT	-47	4580	0.01	1.0E+00	-15432	15338
LTA-3FT~LTA-UC	-106585	4580	32.91	0.0E+00	-121970	-91200
LTA-3FT~LTA-1FT	-3823	4580	1.18	9.5E-01	-19209	11562

Table A.21 One-way ANOVA of ITFT of WMA-A mixture at 15 °C

Factor	DF	Sum of squares	Mean square	F value	Prob>F
Between groups	5	1.62E+10	3.23E+09	80.99	8.03E-09
Within groups	12	4.79E+08	3.99E+07		
Total	17	1.66E+10			

Table A.22 Tukey's post-hoc test of ITFT of WMA-A mixture at 15 °C

Condition	Mean difference	Std. error	q Value	p-value	95% confidence interval	
					Lower bound	Upper bound
STA-1FT~STA-UC	-11836	5157	3.25	2.7E-01	-29157	5485
STA-3FT~STA-UC	-59304	5157	16.26	8.4E-07	-76625	-41983
STA-3FT~STA-1FT	-47468	5157	13.02	1.0E-05	-64789	-30147
LTA-UC~STA-UC	24315	5157	6.67	5.1E-03	6994	41636
LTA-UC~STA-1FT	36151	5157	9.91	1.6E-04	18830	53472
LTA-UC~STA-3FT	83619	5157	22.93	2.4E-07	66298	100940
LTA-1FT~STA-UC	-26336	5157	7.22	2.7E-03	-43657	-9015
LTA-1FT~STA-1FT	-14501	5157	3.98	1.2E-01	-31822	2820
LTA-1FT~STA-3FT	32967	5157	9.04	3.8E-04	15646	50288
LTA-1FT~LTA-UC	-50652	5157	13.89	5.0E-06	-67973	-33331
LTA-3FT~STA-UC	-57240	5157	15.70	1.3E-06	-74561	-39919

Condition	Mean difference	Std. error	q Value	p-value	95% confidence interval	
					Lower bound	Upper bound
LTA-3FT~STA-1FT	-45404	5157	12.45	1.6E-05	-62725	-28083
LTA-3FT~STA-3FT	2064	5157	0.57	1.0E+00	-15257	19385
LTA-3FT~LTA-UC	-81555	5157	22.37	9.9E-07	-98876	-64234
LTA-3FT~LTA-1FT	-30904	5157	8.48	6.9E-04	-48225	-13583

Table A.23 One-way ANOVA of ITFT of WMA-B mixture at 15 °C

Factor	DF	Sum of squares	Mean square	F value	Prob>F
Between groups	5	1.16E+10	2.32E+09	28.34	2.99E-06
Within groups	12	9.83E+08	8.19E+07		
Total	17	1.26E+10			

Table A.24 Tukey's post-hoc test of ITFT of WMA-B mixture at 15 °C

Condition	Mean difference	Std. error	q Value	p-value	95% confidence interval	
					Lower bound	Upper bound
STA-1FT~STA-UC	-4225	7391	0.81	9.9E-01	-29050	20600
STA-3FT~STA-UC	-3174	7391	0.61	1.0E+00	-27999	21651
STA-3FT~STA-1FT	1051	7391	0.20	1.0E+00	-23774	25876
LTA-UC~STA-UC	58841	7391	11.26	4.5E-05	34016	83666
LTA-UC~STA-1FT	63066	7391	12.07	2.2E-05	38241	87891
LTA-UC~STA-3FT	62015	7391	11.87	2.7E-05	37190	86840
LTA-1FT~STA-UC	47548	7391	9.10	3.6E-04	22723	72373
LTA-1FT~STA-1FT	51773	7391	9.91	1.6E-04	26948	76598
LTA-1FT~STA-3FT	50721	7391	9.71	2.0E-04	25896	75546
LTA-1FT~LTA-UC	-11293	7391	2.16	6.5E-01	-36118	13532
LTA-3FT~STA-UC	29548	7391	5.65	1.7E-02	4723	54373
LTA-3FT~STA-1FT	33773	7391	6.46	6.5E-03	8948	58598
LTA-3FT~STA-3FT	32722	7391	6.26	8.3E-03	7897	57547
LTA-3FT~LTA-UC	-29293	7391	5.61	1.8E-02	-54118	-4468
LTA-3FT~LTA-1FT	-18000	7391	3.44	2.2E-01	-42825	6825

Table A.25 One-way ANOVA of ITFT of HMA-A mixture at 25 °C

Factor	DF	Sum of squares	Mean square	F value	Prob>F
Between groups	5	1.06E+08	2.12E+07	3.34	4.05E-02
Within groups	12	7.61E+07	6.35E+06		
Total	17	1.82E+08			

Table A.26 Tukey's post-hoc test of ITFT of HMA-A mixture at 25 °C

Condition	Mean difference	Std. error	q Value	p-value	95% confidence interval	
					Lower bound	Upper bound
STA-1FT~STA-UC	-1652	2057	1.14	9.6E-01	-8561	5256
STA-3FT~STA-UC	-2149	2057	1.48	8.9E-01	-9058	4759
STA-3FT~STA-1FT	-497	2057	0.34	1.0E+00	-7405	6411
LTA-UC~STA-UC	4216	2057	2.90	3.7E-01	-2692	11124
LTA-UC~STA-1FT	5868	2057	4.04	1.1E-01	-1040	12777
LTA-UC~STA-3FT	6365	2057	4.38	7.8E-02	-543	13274
LTA-1FT~STA-UC	3669	2057	2.52	5.1E-01	-3239	10578
LTA-1FT~STA-1FT	5322	2057	3.66	1.7E-01	-1587	12230
LTA-1FT~STA-3FT	5819	2057	4.00	1.2E-01	-1090	12727
LTA-1FT~LTA-UC	-547	2057	0.38	1.0E+00	-7455	6362
LTA-3FT~STA-UC	1043	2057	0.72	9.9E-01	-5865	7951
LTA-3FT~STA-1FT	2695	2057	1.85	7.7E-01	-4213	9604
LTA-3FT~STA-3FT	3192	2057	2.20	6.4E-01	-3716	10101
LTA-3FT~LTA-UC	-3173	2057	2.18	6.5E-01	-10081	3735
LTA-3FT~LTA-1FT	-2626	2057	1.81	7.9E-01	-9535	4282

Table A.27 One-way ANOVA of ITFT of HMA-B mixture at 25 °C

Factor	DF	Sum of squares	Mean square	F value	Prob>F
Between groups	5	1.25E+09	2.50E+08	283.05	5.12E-12
Within groups	12	1.06E+07	8.84E+05		
Total	17	1.26E+09			

Table A.28 Tukey's post-hoc test of ITFT of HMA-B mixture at 25 °C

Condition	Mean difference	Std. error	q Value	p-value	95% confidence interval	
					Lower bound	Upper bound
STA-1FT~STA-UC	-3235	768	5.96	1.2E-02	-5813	-656
STA-3FT~STA-UC	-4227	768	7.79	1.5E-03	-6805	-1649
STA-3FT~STA-1FT	-992	768	1.83	7.8E-01	-3571	1586
LTA-UC~STA-UC	19414	768	35.77	0.0E+00	16835	21992
LTA-UC~STA-1FT	22648	768	41.73	0.0E+00	20070	25227
LTA-UC~STA-3FT	23641	768	43.55	0.0E+00	21062	26219
LTA-1FT~STA-UC	6282	768	11.57	3.4E-05	3704	8860
LTA-1FT~STA-1FT	9517	768	17.53	4.0E-07	6938	12095
LTA-1FT~STA-3FT	10509	768	19.36	1.4E-07	7931	13087
LTA-1FT~LTA-UC	-13132	768	24.19	2.4E-07	-15710	-10553
LTA-3FT~STA-UC	-3173	768	5.85	1.4E-02	-5752	-595
LTA-3FT~STA-1FT	61	768	0.11	1.0E+00	-2517	2640
LTA-3FT~STA-3FT	1054	768	1.94	7.4E-01	-1525	3632
LTA-3FT~LTA-UC	-22587	768	41.61	0.0E+00	-25165	-20009
LTA-3FT~LTA-1FT	-9455	768	17.42	4.3E-07	-12034	-6877

Table A.29 One-way ANOVA of ITFT of WMA-A mixture at 25 °C

Factor	DF	Sum of squares	Mean square	F value	Prob>F
Between groups	5	1.84E+08	3.67E+07	17.32	4.04E-05
Within groups	12	2.54E+07	2.12E+06		
Total	17	2.09E+08			

Table A.30 Tukey's post-hoc test of ITFT of WMA-A mixture at 25 °C

Condition	Mean difference	Std. error	q Value	p-value	95% confidence interval	
					Lower bound	Upper bound
STA-1FT~STA-UC	-4657	1189	5.54	1.9E-02	-8651	-664
STA-3FT~STA-UC	-8151	1189	9.70	2.0E-04	-12145	-4158
STA-3FT~STA-1FT	-3494	1189	4.16	1.0E-01	-7487	499
LTA-UC~STA-UC	340	1189	0.40	1.0E+00	-3654	4333
LTA-UC~STA-1FT	4997	1189	5.94	1.2E-02	1004	8990
LTA-UC~STA-3FT	8491	1189	10.10	1.3E-04	4498	12484
LTA-1FT~STA-UC	469	1189	0.56	1.0E+00	-3524	4463
LTA-1FT~STA-1FT	5127	1189	6.10	1.0E-02	1133	9120
LTA-1FT~STA-3FT	8621	1189	10.25	1.1E-04	4627	12614

Condition	Mean difference	Std. error	q Value	p-value	95% confidence interval	
					Lower bound	Upper bound
LTA-1FT~LTA-UC	130	1189	0.15	1.0E+00	-3864	4123
LTA-3FT~STA-UC	-3750	1189	4.46	7.0E-02	-7743	244
LTA-3FT~STA-1FT	908	1189	1.08	9.7E-01	-3086	4901
LTA-3FT~STA-3FT	4402	1189	5.24	2.8E-02	408	8395
LTA-3FT~LTA-UC	-4089	1189	4.86	4.4E-02	-8083	-96
LTA-3FT~LTA-1FT	-4219	1189	5.02	3.6E-02	-8212	-226

Table A.31 One-way ANOVA of ITFT of WMA-B mixture at 25 °C

Factor	DF	Sum of squares	Mean square	F value	Prob>F
Between groups	5	9.47E+08	1.89E+08	65.11	2.82E-08
Within groups	12	3.49E+07	2.91E+06		
Total	17	9.82E+08			

Table A.32 Tukey's post-hoc test of ITFT of WMA-B mixture at 25 °C

Condition	Mean difference	Std. error	q Value	p-value	95% confidence interval	
					Lower bound	Upper bound
STA-1FT~STA-UC	-587	1393	0.60	1.0E+00	-5265	4091
STA-3FT~STA-UC	-1916	1393	1.95	7.4E-01	-6594	2762
STA-3FT~STA-1FT	-1330	1393	1.35	9.2E-01	-6008	3348
LTA-UC~STA-UC	15681	1393	15.92	1.1E-06	11003	20359
LTA-UC~STA-1FT	16268	1393	16.52	7.0E-07	11590	20946
LTA-UC~STA-3FT	17598	1393	17.87	3.3E-07	12920	22276
LTA-1FT~STA-UC	14905	1393	15.13	2.0E-06	10227	19583
LTA-1FT~STA-1FT	15491	1393	15.73	1.3E-06	10813	20169
LTA-1FT~STA-3FT	16821	1393	17.08	4.5E-07	12143	21499
LTA-1FT~LTA-UC	-777	1393	0.79	9.9E-01	-5455	3901
LTA-3FT~STA-UC	6920	1393	7.03	3.4E-03	2242	11598
LTA-3FT~STA-1FT	7507	1393	7.62	1.7E-03	2829	12185
LTA-3FT~STA-3FT	8836	1393	8.97	4.1E-04	4158	13514
LTA-3FT~LTA-UC	-8761	1393	8.90	4.4E-04	-13439	-4083
LTA-3FT~LTA-1FT	-7985	1393	8.11	1.0E-03	-12663	-3307

Table B.1 One-way ANOVA of flow number of HMA-A mixture at 45 °C and 100 kPa

Factor	DF	Sum of squares	Mean square	F value	Prob>F
Between groups	5	5.71E+07	1.14E+07	7.28	2.39E-03
Within groups	12	1.88E+07	1.57E+06		
Total	17	7.59E+07			

Table B.2 Tukey's post-hoc test of HMA-A mixture at 45 °C and 100 kPa

Condition	Mean difference	Std. error	q Value	p-value	95% confidence interval	
					Lower bound	Upper bound
STA-1FT~STA-UC	-826	1022	1.14	0.96	-4260	2608
STA-3FT~STA-UC	3427	1022	4.74	0.05	-7	6861
STA-3FT~STA-1FT	4253	1022	5.88	0.01	819	7687
LTA-UC~STA-UC	271	1022	0.37	1.00	-3164	3705
LTA-UC~STA-1FT	1097	1022	1.52	0.88	-2338	4531
LTA-UC~STA-3FT	-3156	1022	4.37	0.08	-6591	278
LTA-1FT~STA-UC	-631	1022	0.87	0.99	-4065	2804
LTA-1FT~STA-1FT	195	1022	0.27	1.00	-3239	3630
LTA-1FT~STA-3FT	-4058	1022	5.61	0.02	-7492	-623
LTA-1FT~LTA-UC	-901	1022	1.25	0.94	-4336	2533
LTA-3FT~STA-UC	-2476	1022	3.42	0.22	-5910	959
LTA-3FT~STA-1FT	-1650	1022	2.28	0.61	-5084	1785
LTA-3FT~STA-3FT	-5903	1022	8.16	0.00	-9337	-2468
LTA-3FT~LTA-UC	-2746	1022	3.80	0.15	-6181	688
LTA-3FT~LTA-1FT	-1845	1022	2.55	0.50	-5279	1589

Table B.3 One-way ANOVA of flow number of HMA-B mixture at 45 °C and 100 kPa

Factor	DF	Sum of squares	Mean square	F value	Prob>F
Between groups	5	4.72E+07	9.45E+06	1.71	2.07E-01
Within groups	12	6.64E+07	5.53E+06		
Total	17	1.14E+08			

Table B.4 Tukey's post-hoc test of HMA-B mixture at 45 °C and 100 kPa

Condition	Mean difference	Std. error	q Value	p-value	95% confidence interval	
					Lower bound	Upper bound
STA-1FT~STA-UC	-306	1920	0.23	1.00	-6756	6144
STA-3FT~STA-UC	-454	1920	0.33	1.00	-6904	5996
STA-3FT~STA-1FT	-148	1920	0.11	1.00	-6598	6302
LTA-UC~STA-UC	3384	1920	2.49	0.52	-3066	9834
LTA-UC~STA-1FT	3690	1920	2.72	0.43	-2760	10140
LTA-UC~STA-3FT	3839	1920	2.83	0.40	-2611	10289
LTA-1FT~STA-UC	3285	1920	2.42	0.55	-3165	9735
LTA-1FT~STA-1FT	3591	1920	2.64	0.46	-2859	10041
LTA-1FT~STA-3FT	3740	1920	2.75	0.42	-2710	10190
LTA-1FT~LTA-UC	-99	1920	0.07	1.00	-6549	6351
LTA-3FT~STA-UC	1646	1920	1.21	0.95	-4804	8096
LTA-3FT~STA-1FT	1952	1920	1.44	0.90	-4498	8402
LTA-3FT~STA-3FT	2101	1920	1.55	0.87	-4349	8551
LTA-3FT~LTA-UC	-1738	1920	1.28	0.94	-8188	4712
LTA-3FT~LTA-1FT	-1639	1920	1.21	0.95	-8089	4811

Table B.5 One-way ANOVA of flow number of WMA-A mixture at 45 °C and 100 kPa

Factor	DF	Sum of squares	Mean square	F value	Prob>F
Between groups	5	1.98E+07	3.96E+06	2.88	6.18E-02
Within groups	12	1.65E+07	1.38E+06		
Total	17	3.63E+07			

Table B.6 Tukey's post-hoc test of WMA-A mixture at 45 °C and 100 kPa

Condition	Mean difference	Std. error	q Value	p-value	95% confidence interval	
					Lower bound	Upper bound
STA-1FT~STA-UC	2268	958	3.35	0.24	-949	5485
STA-3FT~STA-UC	2477	958	3.66	0.17	-740	5694
STA-3FT~STA-1FT	209	958	0.31	1.00	-3008	3426
LTA-UC~STA-UC	-197	958	0.29	1.00	-3414	3020
LTA-UC~STA-1FT	-2465	958	3.64	0.18	-5682	752
LTA-UC~STA-3FT	-2673	958	3.95	0.13	-5890	544
LTA-1FT~STA-UC	527	958	0.78	0.99	-2690	3744
LTA-1FT~STA-1FT	-1741	958	2.57	0.49	-4958	1476
LTA-1FT~STA-3FT	-1950	958	2.88	0.38	-5167	1267
LTA-1FT~LTA-UC	723	958	1.07	0.97	-2494	3940

Condition	Mean difference	Std. error	q Value	p-value	95% confidence interval	
					Lower bound	Upper bound
LTA-3FT~STA-UC	1458	958	2.15	0.66	-1759	4675
LTA-3FT~STA-1FT	-810	958	1.20	0.95	-4027	2407
LTA-3FT~STA-3FT	-1019	958	1.50	0.89	-4236	2198
LTA-3FT~LTA-UC	1654	958	2.44	0.54	-1563	4871
LTA-3FT~LTA-1FT	931	958	1.37	0.92	-2286	4148

Table B.7 One-way ANOVA of flow number of WMA-B mixture at 45 °C and 100 kPa

Factor	DF	Sum of squares	Mean square	F value	Prob>F
Between groups	5	4.56E+07	9.13E+06	9.44	7.66E-04
Within groups	12	1.16E+07	9.68E+05		
Total	17	5.73E+07			

Table B.8 Tukey's post-hoc test of of WMA-B mixture at 45 °C and 100 kPa

Condition	Mean difference	Std. error	q Value	p-value	95% confidence interval	
					Lower bound	Upper bound
STA-1FT~STA-UC	240	803	0.42	1.00	-2457	2938
STA-3FT~STA-UC	373	803	0.66	1.00	-2324	3071
STA-3FT~STA-1FT	133	803	0.23	1.00	-2565	2831
LTA-UC~STA-UC	4470	803	7.87	0.00	1773	7168
LTA-UC~STA-1FT	4230	803	7.45	0.00	1532	6928
LTA-UC~STA-3FT	4097	803	7.21	0.00	1399	6795
LTA-1FT~STA-UC	2173	803	3.83	0.14	-524	4871
LTA-1FT~STA-1FT	1933	803	3.40	0.23	-765	4631
LTA-1FT~STA-3FT	1800	803	3.17	0.29	-898	4498
LTA-1FT~LTA-UC	-2297	803	4.04	0.11	-4995	401
LTA-3FT~STA-UC	2459	803	4.33	0.08	-239	5156
LTA-3FT~STA-1FT	2218	803	3.91	0.13	-479	4916
LTA-3FT~STA-3FT	2085	803	3.67	0.17	-612	4783
LTA-3FT~LTA-UC	-2012	803	3.54	0.20	-4709	686
LTA-3FT~LTA-1FT	285	803	0.50	1.00	-2412	2983

Appendix C

Paired *t*-test and Cohen's d test to compare HMA and WMA mixtures

Table C.1 Comparison of ITS values of STA HMA and WMA mixture

Temperature	Moisture	Mixture	p-value	Significant	Cohen's d
15 °C	UC	HMA-A~WMA-A	0.03	Yes	3.61
		HMA-B~WMA-B	0.13	No	2.77
	1FT	HMA-A~WMA-A	0.03	Yes	4.52
		HMA-B~WMA-B	0.05	No	2.44
	3FT	HMA-A~WMA-A	0.01	Yes	5.88
		HMA-B~WMA-B	0.05	No	3.57
25 °C	UC	HMA-A~WMA-A	0.00	Yes	13.06
		HMA-B~WMA-B	0.29	No	1.47
	1FT	HMA-A~WMA-A	0.02	Yes	7.81
		HMA-B~WMA-B	0.02	Yes	5.30
	3FT	HMA-A~WMA-A	0.78	No	0.16
		HMA-B~WMA-B	0.02	Yes	6.31

Table C.2 Comparison of ITS values of LTA HMA and WMA mixture

Temperature	Moisture	Mixture	p-value	Significant	Cohen's d
15 °C	UC	HMA-A~WMA-A	0.89	No	0.14
		HMA-B~WMA-B	0.12	No	2.61
	1FT	HMA-A~WMA-A	0.27	No	0.85
		HMA-B~WMA-B	0.01	Yes	6.25
	3FT	HMA-A~WMA-A	0.03	Yes	3.53
		HMA-B~WMA-B	0.00	Yes	12.44
25 °C	UC	HMA-A~WMA-A	0.10	No	2.93
		HMA-B~WMA-B	0.14	No	2.61
	1FT	HMA-A~WMA-A	0.10	No	2.20
		HMA-B~WMA-B	0.02	Yes	6.15
	3FT	HMA-A~WMA-A	0.21	No	1.48
		HMA-B~WMA-B	0.01	Yes	9.06

Table C.3 Comparison of FE values of STA HMA and WMA mixture

Temperature	Moisture	Mixture	p-value	Significant	Cohen's d
15 °C	UC	HMA-A~WMA-A	0.05	Yes	2.00
		HMA-B~WMA-B	0.39	No	0.84
	1FT	HMA-A~WMA-A	0.65	No	0.60
		HMA-B~WMA-B	0.04	Yes	4.03
	3FT	HMA-A~WMA-A	0.47	No	0.18
		HMA-B~WMA-B	0.02	Yes	7.76
25 °C	UC	HMA-A~WMA-A	0.06	No	4.48
		HMA-B~WMA-B	0.31	No	1.24
	1FT	HMA-A~WMA-A	0.16	No	2.11
		HMA-B~WMA-B	0.01	Yes	8.95
	3FT	HMA-A~WMA-A	0.25	No	1.37
		HMA-B~WMA-B	0.02	Yes	4.62

Table C.4 Comparison of FE values of LTA HMA and WMA mixture

Temperature	Moisture	Mixture	p-value	Significant	Cohen's d
15 °C	UC	HMA-A~WMA-A	0.21	No	1.54
		HMA-B~WMA-B	0.17	No	1.15
	1FT	HMA-A~WMA-A	0.03	Yes	2.75
		HMA-B~WMA-B	0.14	No	1.72
	3FT	HMA-A~WMA-A	0.07	No	2.07
		HMA-B~WMA-B	0.02	Yes	4.97
25 °C	UC	HMA-A~WMA-A	0.07	No	0.86
		HMA-B~WMA-B	0.11	No	2.34
	1FT	HMA-A~WMA-A	0.86	No	0.14
		HMA-B~WMA-B	0.00	Yes	7.37
	3FT	HMA-A~WMA-A	0.76	No	0.33
		HMA-B~WMA-B	0.01	Yes	7.99

Table C.5 Comparison of adhesive failure values of STA HMA and WMA mixture

Temperature	Moisture	Mixture	p-value	Significant	Cohen's d
15 °C	1FT	HMA-A~WMA-A	0.96	No	0.03
		HMA-B~WMA-B	0.62	No	0.18
	3FT	HMA-A~WMA-A	0.32	No	1.45
		HMA-B~WMA-B	0.23	No	1.22
25 °C	1FT	HMA-A~WMA-A	0.64	No	0.41
		HMA-B~WMA-B	0.48	No	0.82
	3FT	HMA-A~WMA-A	0.22	No	1.48
		HMA-B~WMA-B	0.57	No	0.60

Table C.6 Comparison of adhesive failure values of LTA HMA and WMA mixture

Temperature	Moisture	Mixture	p-value	Significant	Cohen's d
15 °C	1FT	HMA-A~WMA-A	0.41	No	0.09
		HMA-B~WMA-B	0.58	No	0.66
	3FT	HMA-A~WMA-A	0.06	No	1.60
		HMA-B~WMA-B	0.64	No	0.40
25 °C	1FT	HMA-A~WMA-A	0.26	No	4.22
		HMA-B~WMA-B	0.41	No	0.62
	3FT	HMA-A~WMA-A	0.48	No	0.96
		HMA-B~WMA-B	0.93	No	0.12

Table C.7 Comparison of stiffness modulus of STA HMA and WMA mixture

Temperature	Moisture	Mixture	p-value	Significant	Cohen's d
15 °C	UC	HMA-A~WMA-A	0.04	Yes	3.64
		HMA-B~WMA-B	0.18	No	1.91
	1FT	HMA-A~WMA-A	0.61	No	0.32
		HMA-B~WMA-B	0.06	No	1.42
	3FT	HMA-A~WMA-A	0.74	No	0.29
		HMA-B~WMA-B	0.08	No	3.04
25 °C	UC	HMA-A~WMA-A	0.01	Yes	9.63
		HMA-B~WMA-B	0.17	No	1.81
	1FT	HMA-A~WMA-A	0.01	Yes	9.18
		HMA-B~WMA-B	0.87	No	0.19
	3FT	HMA-A~WMA-A	0.19	No	1.19
		HMA-B~WMA-B	0.48	No	0.81

Table C.8 Comparison of stiffness modulus of LTA HMA and WMA mixture

Temperature	Moisture	Mixture	p-value	Significant	Cohen's d
15 °C	UC	HMA-A~WMA-A	0.37	No	0.69
		HMA-B~WMA-B	0.00	Yes	4.05
	1FT	HMA-A~WMA-A	0.06	No	2.93
		HMA-B~WMA-B	0.58	No	0.58
	3FT	HMA-A~WMA-A	0.00	Yes	7.53
		HMA-B~WMA-B	0.05	No	2.92
25 °C	UC	HMA-A~WMA-A	0.01	Yes	7.04
		HMA-B~WMA-B	0.00	Yes	5.96
	1FT	HMA-A~WMA-A	0.02	Yes	4.77
		HMA-B~WMA-B	0.01	Yes	4.19
	3FT	HMA-A~WMA-A	0.02	Yes	4.32
		HMA-B~WMA-B	0.02	Yes	3.80

Table C.9 Comparison of fatigue life of STA HMA and WMA mixture

Temperature	Moisture	Mixture	p-value	Significant	Cohen's d
15 °C	UC	HMA-A~WMA-A	0.55	No	0.70
		HMA-B~WMA-B	0.02	Yes	5.10
	1FT	HMA-A~WMA-A	0.26	No	1.41
		HMA-B~WMA-B	0.00	Yes	2.86
	3FT	HMA-A~WMA-A	0.01	Yes	2.20
		HMA-B~WMA-B	0.02	Yes	5.59
25 °C	UC	HMA-A~WMA-A	0.91	No	0.14
		HMA-B~WMA-B	0.08	No	2.87
	1FT	HMA-A~WMA-A	0.12	No	1.90
		HMA-B~WMA-B	0.15	No	2.48
	3FT	HMA-A~WMA-A	0.03	Yes	5.69
		HMA-B~WMA-B	0.06	No	4.48

Table C.10 Comparison of fatigue life of LTA HMA and WMA mixture

Temperature	Moisture	Mixture	p-value	Significant	Cohen's d
15 °C	UC	HMA-A~WMA-A	0.03	Yes	3.41
		HMA-B~WMA-B	0.23	No	1.19
	1FT	HMA-A~WMA-A	0.04	Yes	3.99
		HMA-B~WMA-B	0.00	Yes	26.18
	3FT	HMA-A~WMA-A	0.05	Yes	3.70
		HMA-B~WMA-B	0.01	Yes	10.50
25 °C	UC	HMA-A~WMA-A	0.23	No	1.94
		HMA-B~WMA-B	0.17	No	2.19
	1FT	HMA-A~WMA-A	0.33	No	1.18
		HMA-B~WMA-B	0.00	Yes	5.76
	3FT	HMA-A~WMA-A	0.13	No	2.60
		HMA-B~WMA-B	0.04	Yes	4.66

Table C.11 Comparison of flow number of STA HMA and WMA mixture

Temperature	Moisture	Mixture	p-value	Significant	Cohen's d
45 °C	UC	HMA-A~WMA-A	0.02	Yes	5.18
		HMA-B~WMA-B	0.01	Yes	8.99
	1FT	HMA-A~WMA-A	0.94	No	0.08
		HMA-B~WMA-B	0.08	No	1.22
	3FT	HMA-A~WMA-A	0.01	Yes	1.77
		HMA-B~WMA-B	0.05	No	3.48

Table C.12 Comparison of flow number of LTA HMA and WMA mixture

Temperature	Moisture	Mixture	p-value	Significant	Cohen's d
45 °C	UC	HMA-A~WMA-A	0.08	No	4.54
		HMA-B~WMA-B	0.90	No	1.00
	1FT	HMA-A~WMA-A	0.04	Yes	3.21
		HMA-B~WMA-B	0.26	No	0.02
	3FT	HMA-A~WMA-A	0.47	No	1.01
		HMA-B~WMA-B	0.47	No	0.17

Appendix D
List of permission for reuse of figure

Figure 2.1

Thesis/Dissertation Reuse Request:

"Taylor & Francis is pleased to offer reuses of its content for a thesis or dissertation free of charge contingent on resubmission of permission request if work is published (accessed 28/06/2021)."

Figure 2.2

Gratis Reuse:

"*Permission is granted at no cost for use of content in a Master's Thesis and/or Doctoral Dissertation, subject to the following limitations. You may use a single excerpt or up to 3 figures tables. If you use more than those limits, or intend to distribute or sell your Master's Thesis/Doctoral Dissertation to the general public through print or website publication, please return to the previous page and select 'Republish in a Book/Journal' or 'Post on intranet/password-protected website' to complete your request (accessed 28/06/2021).*"

Figure 2.3

Thesis/Dissertation Reuse Request:

"*Taylor & Francis is pleased to offer reuses of its content for a thesis or dissertation free of charge contingent on resubmission of permission request if work is published (accessed 28/06/2021).*"

Figure 2.4

Gratis Reuse:

"*Permission is granted at no cost for use of content in a Master's Thesis and/or Doctoral Dissertation, subject to the following limitations. You may use a single excerpt or up to 3 figures tables. If you use more than those limits, or intend to distribute or sell your Master's Thesis/Doctoral Dissertation to the general public through print or website publication, please return to the previous page and select 'Republish in a Book/Journal' or 'Post on intranet/password-protected website' to complete your request (accessed 28/06/2021)."*

Figure 2.5

Thesis/Dissertation Reuse Request:

"Taylor & Francis is pleased to offer reuses of its content for a thesis or dissertation free of charge contingent on resubmission of permission request if work is published (accessed 28/06/2021)."

Figure 2.6

Reuse in a thesis/dissertation:

"*No royalties will be charged for this reuse request although you are required to obtain a license and comply with the license terms and conditions. To obtain the license, click the Accept button below*."

License purchased on 21/06/2021 (License no. 5093540486730)

Figure 2.7

Thesis/Dissertation Reuse Request:

"*No royalties will be charged for this reuse request although you are required to obtain a license and comply with the license terms and conditions. To obtain the license, click the Accept button below*."

License purchased on 21/06/2021 (License no. 5093541030207)

Figure 2.8

Thesis/Dissertation Reuse Request:

"*Taylor & Francis is pleased to offer reuses of its content for a thesis or dissertation free of charge contingent on resubmission of permission request if work is published (accessed 28/06/2021).*"